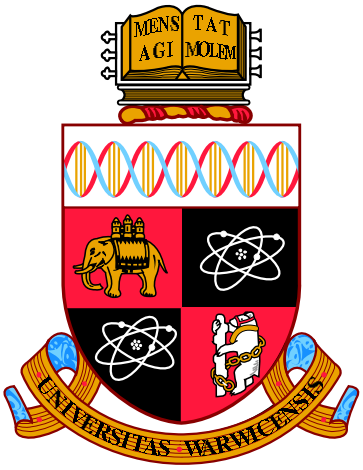

Structural and Ligand Binding Investigation of VanS, a Protein Involved in Antibiotic Resistance

by

Christine Lockey

Thesis

Submitted to the University of Warwick

for the degree of

Doctor of Philosophy

Department of Chemistry

September 2017

THE UNIVERSITY OF
WARWICK

Contents

List of Tables

List of Figures

Acknowledgments

I thank my supervisors, Ann Dixon and Dave Roper, for taking me on as a student and for their support, patience and guidance over the last four years. I am forever grateful to both of you, for the opportunity and the experience.

I am also so grateful to members of the Dixon and Roper research groups, and of the Chemical Biology and Structural Biology research clusters. I owe particular thanks to Rich, who got me started in this project, and to Rachael and Dom, who sent me home when it was finally done. That "one last gel" wouldn't have done me any good in the end, you were right.

Chris, Leo, Muhammad, Dhadchi, Amy, Nicola, Adrian, Julie and Anita - you have been kinder and more supportive of me in the last four years than I had any right to expect. Thank you for everything.

Many thanks to Cerith, Phil, Lijiang, and especially Ivan, for their instruction and support, and for accommodating my self-inflicted crises on numerous occasions.

I owe a debt of thanks to Alison Rodger, who founded MOAC, to Nikola Chmel, who offered me a place, and to Hugo van den Berg, who was on sabbatical at the time of my interview. MOAC gave me the opportunity to come to Warwick and provided the funding to allow me to complete this work, but just as importantly, MOAC is a family, and that's because of you.

Liam, thank you for keeping me laughing through this crazy time, and for your support and friendship. It means a lot.

Mum and Dad, your blind faith that I would eventually pull this off has been alternately reassuring and maddening. I guess you were right; thank you for believing in me. Catherine, thank you for constantly checking in and reminding me to eat vegetables and go to bed. You'll be a great (honorary) doctor.

Finally - Luke. I don't know how we did it, but I think we've pulled this off. The cats are furious, the laundry isn't done, and we both have more coffee than blood in our veins. Let's make better decisions in the future. I love you.

Declarations

The work in this thesis is original, and was conducted by the author, unless otherwise stated, under the supervision of Dr Ann M. Dixon (Department of Chemistry) and Professor David I. Roper (School of Life Sciences).

The work was funded by the EPSRC, through the Molecular Organisation and Assembly in Cells (MOAC) Doctoral Training Centre.

This work has not previously been presented for another degree.

Funding was provided by an EPSRC studentship.

All sources of information have been acknowledged by means of reference.

Abstract

VanS is an integral membrane protein, and a receptor histidine kinase representing one half of the VanSR two component system. In the presence of vancomycin, as well as certain other antibiotics, VanS undergoes autophosphorylation at a conserved histidine residue and then transfers this phosphoryl group to a conserved aspartate on VanR. The phosphorylated form of VanR binds to the promoter region of the *vanHAX* operon, inducing expression of these genes, which confer glycopeptide antibiotic resistance to the cell.

Although the vancomycin resistance mechanism is mostly well-characterised, questions surrounding the structure and mode of activation of VanS remain unanswered. This thesis describes work towards the structural and ligand-binding characterisation of the extracellular "sensor" domain of VanS. Little is known of the structure of this domain, and while there exists evidence in the literature to support numerous theories surrounding the identity of the VanS ligand, no report has yet been made of a direct observation of a binding event involving any VanS protein and its ligand.

To identify the ligand to VanS, the catalytically active, full-length VanS proteins of *Enterococcus faecium* (VanS_A) and *Streptomyces coelicolor* (VanS_{SC}) were heterologously expressed, solubilised and purified, and binding studies were carried out by solution-state NMR. We present evidence of interactions between vancomycin and both VanS proteins, indicating that direct binding of vancomycin may be the mechanism by which both proteins are activated. The VanS_{SC} extracellular domain was isolated as a synthetic peptide, its structure characterised, and the binding interface between this domain and vancomycin was investigated. Evidence of binding at the N-terminal end of the extracellular domain, in agreement with the findings of Koteva et al. (2010), is presented here. An interaction between vancomycin and DPC detergent micelles was also observed and characterised, and the biological significance of such an interaction is discussed.

Chapter 1

Introduction

1.1 The Emerging Problem of Antibiotic Resistance

The first penicillin antibiotic, benzylpenicillin, was discovered by Alexander Fleming in 1929, ushering in the "Antibiotic Era". Penicillins are members of the methicillin class of β-lactam antibiotics. Penicillin was first applied topically in 1930 (Wainwright and Swan, 1986), and first applied intravenously in 1943 (Lyons, 1943) following industrialisation of the production process. Resistance to penicillin was first reported in *Pneumococcus* in 1943 (Schmidt and Sesler, 1943), and in *Staphylococcus* in the mid-1940s (Chambers and DeLeo, 2010).

Genes encoding β-lactamase enzymes, conferring resistance to β-lactam antibiotics including penicillin, have since been demonstrated to far predate the discovery of this class of antibiotics (D'Costa et al., 2011). Many of the world's antibiotics are biological in origin (Walsh, 2003), giving pathogens a head start in developing resistance to these drugs before they are even put into use in the clinic. The Antibiotic Era has been, since its inception, an "arms race" between mankind and pathogenic infections. Novel antibiotics are discovered, and resistance quickly emerges.

Pathogenic resistance to antibiotics continues to develop and spread, and poses a major risk to human health and industry (Bush et al., 2011). Pathogens resistant to one antibiotic must be treated with a different antibiotic; the emergence of multi-drug resistance, alongside factors such as antibiotic allergies in individual patients, and local availability of different medicines, means that we move ever-closer to a reality in which bacterial infections cannot reliably be treated.

Resistance to antibiotics is achieved by bacteria via three main routes, as outlined in Figure 1.1: the molecular targets of antibiotics may be changed, as in the emergence of

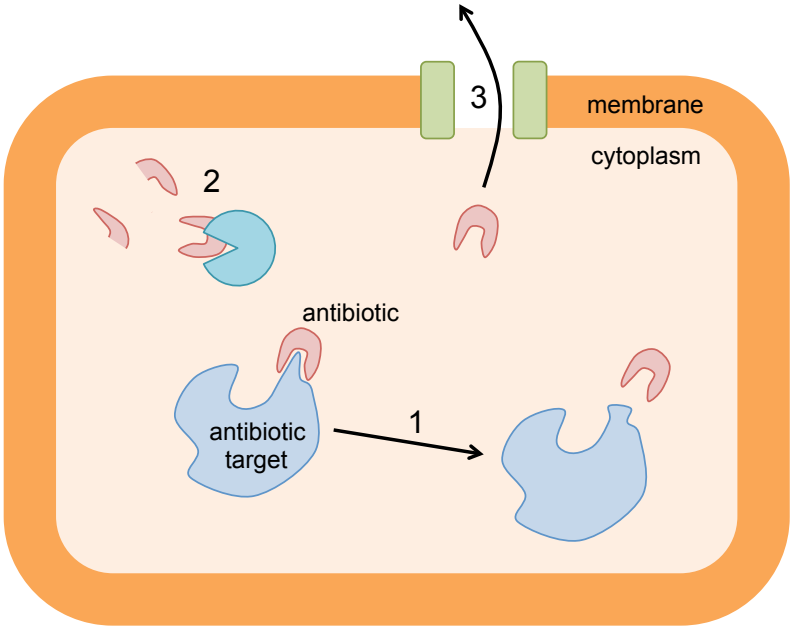

Figure 1.1: Three routes by which antibiotic resistance may develop. The presence of the antibiotic may be tolerated, if the molecular target is mutated such that the antibiotic can no longer bind (1). Alternatively, accumulation of the antibiotic may be prevented, either by enzymatic digestion (2) or by active transport of the antibiotic through the cell membrane (3).

mutant penicillin binding proteins, so that antibiotics can no longer bind to their targets; enzymes may be developed or modified to hydrolyse antibiotics, as in the emergence of β-lactamase enzymes, so that antibiotics are degraded by the target cell; or efflux pumps that are part of the normal bacterial membrane proteome may become overexpressed, such as the MtrCDE efflux pump in *Neisseria gonorrheae*, so that antibiotic molecules are actively removed from the cell (Piddock, 2016). The problem of antibiotic resistance is compounded by the occurrence of horizontal gene transfer, and resistance genes have been identified in one species following intergeneric transfer from a resistant co-isolate (Chambers and DeLeo, 2010).

Another contributing factor to the rate at which antibiotic resistance continues to emerge is the misuse and overuse of antibiotics. The development of resistance in bacteria exposed to sub-lethal doses of antibiotic was observed and reported by Alexander Fleming

over 70 years ago (Fleming, 1945), yet antibiotics have routinely been used in agriculture both prophylactically against infection, and to promote the growth of livestock (Boeckel et al., 2015). In the clinic, antibiotics have often been erroneously prescribed for the treatment of viral infections (Bertino, 2003), against which they are ineffective. The widespread misuse and overuse of antibiotics leads pathogens to be exposed unnecessarily, providing avoidable opportunities for resistance to develop. There is mounting pressure from scientists to limit the use of antibiotics, to slow this process. It remains the case, however, that antibiotic resistance will continue to develop even if human use of antibiotics is stopped altogether (D'Costa et al., 2011). It is not enough, therefore, to control the administration of existing antibiotics.

In order to undermine a bacterium's resistance mechanism, it must first be properly characterised. While many antibiotic resistance mechanisms are broadly understood, and some fully characterised, many details remain to be elucidated. It is essential that these mechanisms be fully described and characterised in order that they should be successfully undermined, to restore the efficacy of existing antibiotics, or bypassed, to allow the development of novel antibiotics to which pathogens are susceptible.

1.2 The Bacterial Cell Wall

Bacterial cells are encased within a cell wall composed of peptidoglyan, a matrix of carbohydrate chains crosslinked by short peptides (Lazar and Walker, 2002). The primary function of this cell wall is to withstand osmotic pressure, maintaining the integrity of the cell membrane and preventing lysis by osmotic stress (van Heijenoort, 2001). In Gram-positive bacteria, the cell wall is exposed to the environment, and responds to Gram staining. In Gram-negative bacteria, the cell wall is itself enveloped in a second plasma membrane, preventing Gram staining from taking place. Examples of clinically relevant Gram-positive bacteria include *Streptococcus*, *Staphylococcus*, and *Bacillus*, and there is significant interest in characterising the antibiotic resistance mechanisms displayed by these genera.

The importance of the cell wall is reflected in its popularity as a target for antibiotics. Peptidoglycan is composed of subunits which are synthesised inside the cell as the molecule lipid II (Barreteau et al., 2008), exported through the membrane (Breukink and de Kruijff, 2006), and assembled extracellularly by penicillin binding proteins (PBPs) which catalyse bond formation between the sugars that make up the backbone, and the amino acids which form cross-links between chains (Sauvage et al., 2004). These steps are outlined in Figure 1.2. The lipid chain anchoring the subunit to the cell membrane is cleaved following transglycosylation of the sugar moieties (Baptista et al., 1996). The crosslinking reaction between lipid II pentapeptides is shown in detail in Figure 1.3; γ-D-Lysine (or diaminopimelic acid) at the third position of one peptide is crosslinked to the penultimate D-Alanine of another peptide, connecting the two molecules.

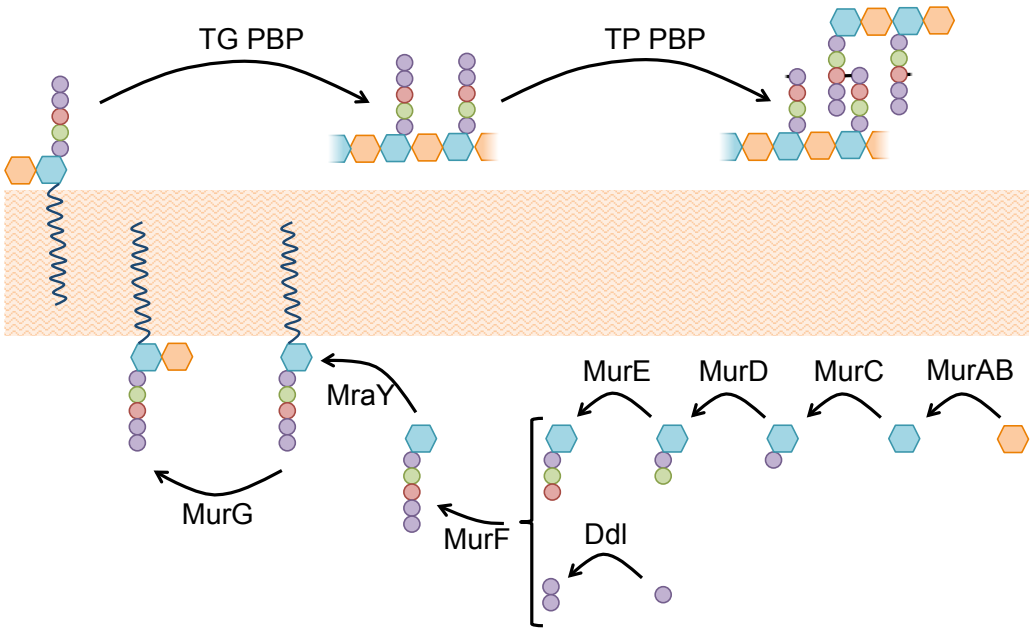

Figure 1.2: Schematic outlining the steps of peptidoglycan biosynthesis. Blue hexagon, *N*-acetylmuramic acid. Orange hexagon, *N*-acetylglucosamine. Purple circle, alanine. Green circle, glutamate. Red circle, lysine or diaminopimelic acid. Meandering line, undecaprenol.

The synthesis of lipid II and its incorporation into the peptidoglycan cell wall is a complex process which is disrupted at a number of stages by a range of clinically relevant antibiotics. Fosfomycin is an inhibitor of MurA, the enzyme which forms UDP-GlcNAc-

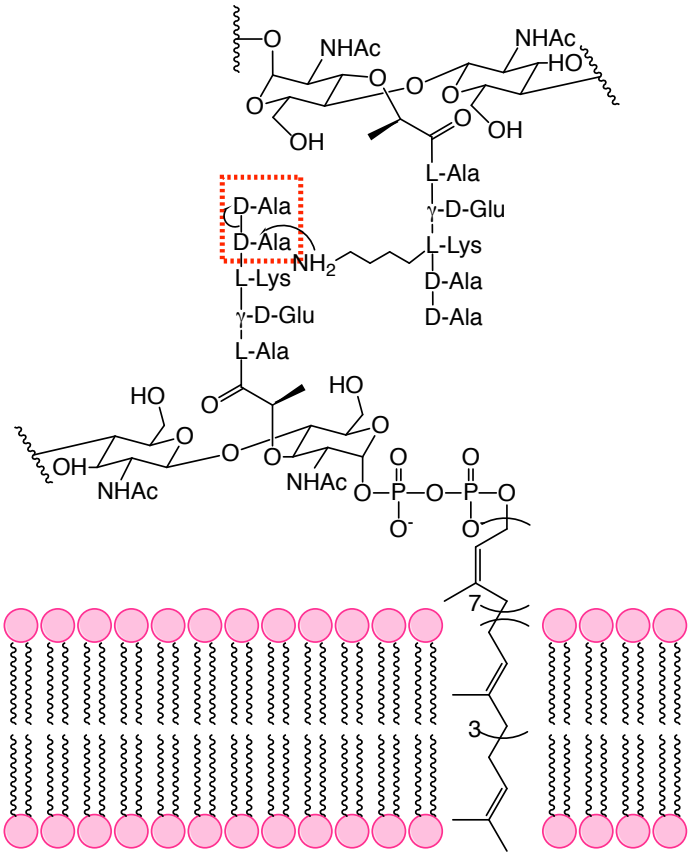

Figure 1.3: The formation of crosslinks between pentapeptide and disaccharide components of lipid II leads to the synthesis of a peptidoglycan matrix, of which the bacterial cell wall is composed. Adapted from Lazar and Walker (2002). Outlined in red is the terminal D-Alanyl-D-Alanine; binding of antibiotics to this region of the lipid II molecule prevents incorporation into the peptidoglycan matrix, leading to cell death.

enolpyruvate from UDP-GlcNAc and phosphoenol pyruvate (Kahan et al., 1974). Bacitracin binds to undecaprenol pyrophosphate (Stone and Strominger, 1971), preventing its incorporation into lipid I by MraY (van Heijenoort, 2001). β-lactam antibiotics (methicillins and cephalosporins) are structural analogues of the D-Alanyl-D-Alanine component of lipid II, and act as inhibitors to the penicillin binding proteins which catalyse crosslinking reactions. Glycopeptide antibiotics bind to D-Alanyl-D-Alanine-terminating peptides, including those of lipid II, and prevent binding of PBPs and subsequent incorporation into the matrix.

The incorporation of lipid II into peptidoglycan is the target of several other classes of antibiotic, beyond that of glycopeptides (Breukink and de Kruijff, 2006). B-type lantibiotics including mersacidin (Brotz et al., 1997), lipoglycodepsipeptides ramoplanin and enduracidin (Fang et al., 2006), and mannopeptimycins (Ruzin et al., 2004) all bind to lipid II by different mechanisms, and inhibit its transglycosylation by penicillin binding proteins. It is estimated that only 2000 lipid II molecules contribute to cell wall biosynthesis in a given Gram-positive cell (Breukink and de Kruijff, 2006), and these molecules are turned over at a rate of 1-3 cycles per second. Since this cycle is critical for peptidoglycan biosynthesis and comprises such a small number of molecules, its disruption is both devastating to the cell and relatively easy to achieve. It is therefore a common target for antibiotic activity.

1.3 The Glycopeptide Antibiotic Vancomycin

1.3.1 The Structure and Function of Vancomycin

Vancomycin (Figure 1.4) was the first glycopeptide to be identified, having been isolated from *Amycolatopsis orientalis* in 1956 (McCormick et al., 1956; Dutton and Elmes, 1959). In common with all glycopeptide antibiotics, it is composed of a saccharide and a heptapeptide. The heptapeptide is comprised of a number of nonproteinogenic amino acids, many of which contain bulky hydrocarbon rings in their sidechains. Vancomycin is glycosylated on the sidechain of residue 4; the sugar is a disaccharide composed of glucose (proximally) and vancosamine (distally) (Barna and Williams, 1984).

The hydrocarbon rings in the heptapeptide sidechains which confer structural rigidity to the peptide component, also confer hydrophobicity to the molecule. Glycosylation is therefore an essential step in maintaining the aqueous solubility of the antibiotic. Glycosylation also contributes to the propensity for glycopeptide antibiotics to form back-to-back dimers (Beauregard et al., 1995), enhancing their substrate-binding capacity.

The mode of action of glycopeptide antibiotics is mediated by the heptapeptide component. Crosslinking between aromatic sidechains increases the rigidity of the heptapeptide, such that the backbone is shaped into a binding pocket (Beauregard et al., 1995). Atoms within the peptide backbone, particularly amide protons, form hydrogen bonds with D-Alanyl-D-Alanine, the C-terminus of the pentapeptide component of lipid II (Figure 1.4). In binding lipid II, vancomycin blocks interactions between lipid II and PBPs which catalyse crosslinking reactions to integrate lipid II into the peptidoglycan matrix. In the presence of vancomycin, therefore, the cell wall cannot be expanded or maintained, and cells become susceptible to osmotic stress (van Heijenoort, 2001).

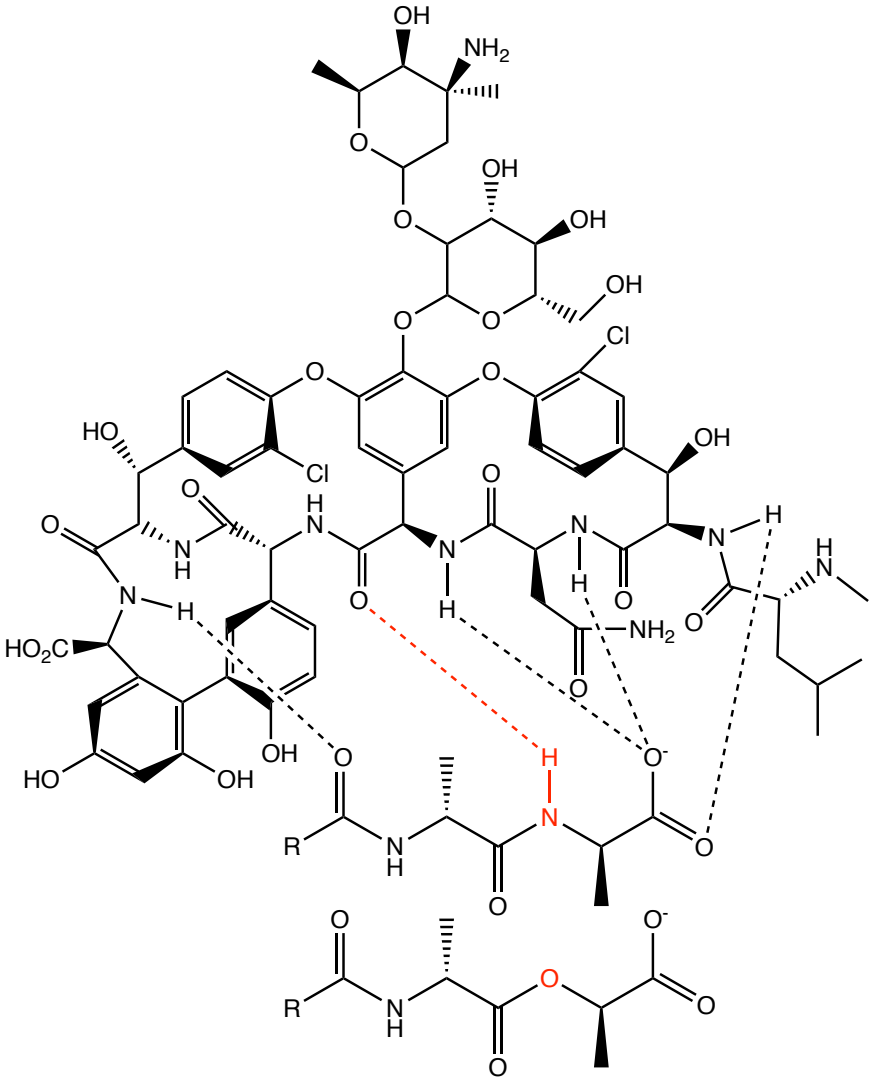

Figure 1.4: The interaction between vancomycin (top) and the D-Alanyl-D-Alanine terminus of the peptide component of lipid II (middle) (Barna and Williams, 1984). In D-Alanyl-D-Lactate (bottom), the absence of a single hydrogen atom prevents the formation of a crucial hydrogen bond with vancomycin (shown in red), significantly lowering vancomycin's affinity for this peptidoglycan precursor (Bugg et al., 1991).

1.3.2 The Clinical Significance of Vancomycin

Vancomycin has been widely used in the clinical treatment of antibiotic-resistant Gram-positive pathogenic bacteria, including methicillin-resistant *S. aureus* (MRSA) (Steinkraus et al., 2007). In many cases, methicillin-resistant bacteria are only susceptible to glycopeptide antibiotics (Enright et al., 2000); there is therefore significant clinical reliance on vancomycin as a last line of defence against MRSA.

There are several routes by which resistance to an antibiotic may be achieved; a common route, and one by which methicillin resistance has been accomplished, is through modification of the antibiotic target. Methicillins bind penicillin binding proteins, preventing them from binding their target D-Alanyl-D-Alanine-terminating peptides of lipid II. PBP2a is a modified penicillin binding protein encoded by the *mecA* gene, which displays a reduced affinity for β-lactam antibiotics while maintaining an affinity for D-Alanyl-D-Alanine. The *mecA* gene is thought to have first mutated in *S. sciuri*, and is now spread via horizontal gene transfer as part of staphylococcal cassette chromosome (SCC)*mec* (Lambert, 2005).

While methicillins bind PBPs by mimicking D-Alanyl-D-Alanine, vancomycin directly binds D-Alanyl-D-Alanine-terminating peptides. The target molecule of vancomycin is not a protein, but the peptide component of a large and complex molecule, the assembly of which is coordinated by a large number of enzymes (van Heijenoort, 2001). It was therefore hoped that vancomycin resistance would be slow to emerge, as there is no single target protein in which a random mutation would undermine vancomycin's mode of action. Nevertheless, vancomycin resistance was first reported in Enterococci in 1988 (Leclercq et al., 1988; Uttley et al., 1988), and vancomycin resistance in MRSA was first reported in 1997 (Hiramatsu et al., 1997).

1.4 The Mechanism of Vancomycin Resistance

Vancomycin was first isolated from the soil bacterium *Amycolatopsis orientalis*, and it is not surprising that resistance to the antibiotic should be observed in other Actinomycete species including in *Streptomyces coelicolor* which does not produce its own glycopeptide antibiotic but does share an environment with actinomycetes which do (Hong et al., 2008). A-type resistance in *Enterococci*, mediated by transposon Tn*1546* (Courvalin, 2006), spread intergenerically to *Staphylococcus aureus*, resulting in the first strains of vancomycin- and methicillin-resistant *S. aureus* (VRSA) (Weigel et al., 2003).

VanS proteins from different species are responsive to different antibiotics (Table 1.1). VanS from *Enterococci* displaying A-type vancomycin resistance is sensitive to vancomycin, moenomycin - an antibiotic which is markedly dissimilar to vancomycin - and teicoplanin, a lipidated glycopeptide antibiotic with significant structural similarities to vancomycin and which functions similarly (Baptista et al., 1999). However, VanS from B-type Enterococci is sensitive to only vancomycin (Baptista et al., 1996), and is not activated by either teicoplanin or moenomycin.

	Vancomycin	Teicoplanin	Moenomycin
E. faecium	✓	✓	✓
E. faecalis	✓		
S. coelicolor	✓		

Table 1.1: In some species, VanS can confer resistance to a number of other antibiotics as well as vancomycin. In clinically significant *Enterococci*, VanS proteins are typically classed as either A-type (*e.g.* VanS from *E. faecium*), conferring resistance to vancomycin, teicoplanin, and moenomycin, or B-type (*e.g.* VanS from *E. faecalis*), conferring resistance to vancomycin but leaving the cell vulnerable to teicoplanin and moenomycin. The biological source of glycopeptide antibiotics is actinomycetes, for which *Streptomyces coelicolor* is a model organism. VanS from this species confers resistance to vancomycin only, and may be described as B-type-like for this reason.

Comparison of the amino acid sequences of A-type and B-type VanS indicates that

while the proteins are similar in terms of their gross structures and catalytic activities, they are evolutionarily distantly related (Table 1.2); there is little sequence homology in the putative ligand binding sites (extracellular loop domains) of VanS from *E. faecium* ($VanS_A$) and *E. faecalis* ($VanS_B$) (Hong et al., 2008). Several Actinomycete species display resistance to vancomycin which may be described as B-type-like in nature. Though VanS proteins from actinomycetes display more significant sequence homology than in *Enterococci*, this is not true for the putative ligand binding sites (Hong et al., 2008).

	E. faecium	*E. faecalis*	*S. coelicolor*	*S. toyocaensis*
E. faecium		21.55 (16.67)	20.18 (17.14)	22.16 (11.76)
E. faecalis	21.55 (16.67)		24.21 (17.86)	25.57 (23.08)
S. coelicolor	20.18 (17.14)	24.21 (17.86)		65.84 (27.27)
S. toyocaensis	22.16 (11.76)	25.57 (23.08)	65.84 (27.27)	

Table 1.2: Sequence homology identity matrix from Clustal2.1, comparing pairwise full-length (and putative ligand-binding domain) sequence identity percentages of four VanS proteins. $VanS_A$ from *E. faecium* and $VanS_B$ from *E. faecalis*, which exhibit different antibiotic sensitivity profiles, share 21.55% sequence homology, but only 16.67% homology in the putative ligand binding regions (extracellular domains, predicted by TMHMM). VanS from two *Streptomyces* species, with similar antibiotic sensitivity profiles, share 65.84% overall sequence homology, but only 27.27% in the putative ligand binding regions.

Vancomycin resistance is achieved by the production of modified peptidoglycan precursors, to which vancomycin cannot bind. To achieve this, the D-Alanyl-D-Alanine-terminating pentapeptide in lipid II is replaced by one terminating in D-Alanyl-D-Lactate (Figure 1.4) (Bugg et al., 1991), removing a hydrogen atom which is crucial for the formation of hydrogen bonds which stabilise the vancomycin/pentapeptide complex (Figure 1.4) (McComas et al., 2003). The affinity of vancomycin for this alternative precursor is approximately 1000-fold lower than for wildtype lipid II (Bugg et al., 1991); therefore cells producing D-Alanyl-D-Lactate-terminating precursors are better able to survive exposure to vancomycin.

1.4.1 The *van* Gene Cluster

The production of the D-Alanyl-D-Lactate-containing precursor is controlled by genes within the *van* cluster, and primarily by three genes which form the *vanHAX* operon. The interference of these proteins in peptidoglycan biosynthesis is outlined in Figure 1.5. VanH is a D-specific α-keto acid dehydrogenase (Bugg et al., 1991), which converts pyruvate to lactate, ensuring sufficient lactate is available for the production of D-Alanyl-D-Lactate-terminating precursors. VanA is a D-Alanyl-D-Lactate ligase which catalyses the formation of ester bonds between D-Alanine and D-Lactate generated by VanH (Bugg et al., 1991). VanX is a D-, D-dipeptidase (Reynolds et al., 1994) which hydrolyses free D-Alanyl-D-Alanine - but not D-Alanyl-D-Lactate (Wu et al., 1995) - preventing assembly of the wildtype pentapeptide (Hutchings et al., 2006). The combined actions of these three enzymes leads to a scarcity of D-Alanyl-D-Alanine and a coinciding increase in availability of D-Alanyl-D-Lactate, which is incorporated into lipid II by MurF, a component of the existing peptidoglycan synthesis machinery (Duncan et al., 1990).

The exact content of the *van* gene cluster varies between vancomycin-resistant pathogens, but must at a minimum contain the *vanHAX* operon, and the two genes *vanS* and *vanR*, encoding the proteins VanS and VanR respectively, which are constitutively expressed at low levels. VanS is an integral transmembrane protein exhibiting both kinase and phosphatase activities. When activated, VanS undergoes homodimerisation, followed by autophosphorylation at a conserved histidine residue. The acquired phosphate group is then transferred to an aspartate on VanR. Phosphorylated VanR binds to the promoter regions upstream of *vanHAX* and *vanSR* and enhances the ability of RNA polymerase to bind at these positions, upregulating expression of all five genes (Depardieu et al., 2005). The regulatory role of VanSR on *vanHAX* expression is shown in Figure 1.6.

Other genes appear within the *van* clusters of various vancomycin-resistant species. In *S. coelicolor*, the cluster includes genes encoding VanJ and VanK. A glycine branch crucial for crosslink formation is added to the D-Alanyl-D-Alanine-terminating pentapeptide of lipid II in *S. coelicolor* by FemX; however, FemX cannot perform this action when the

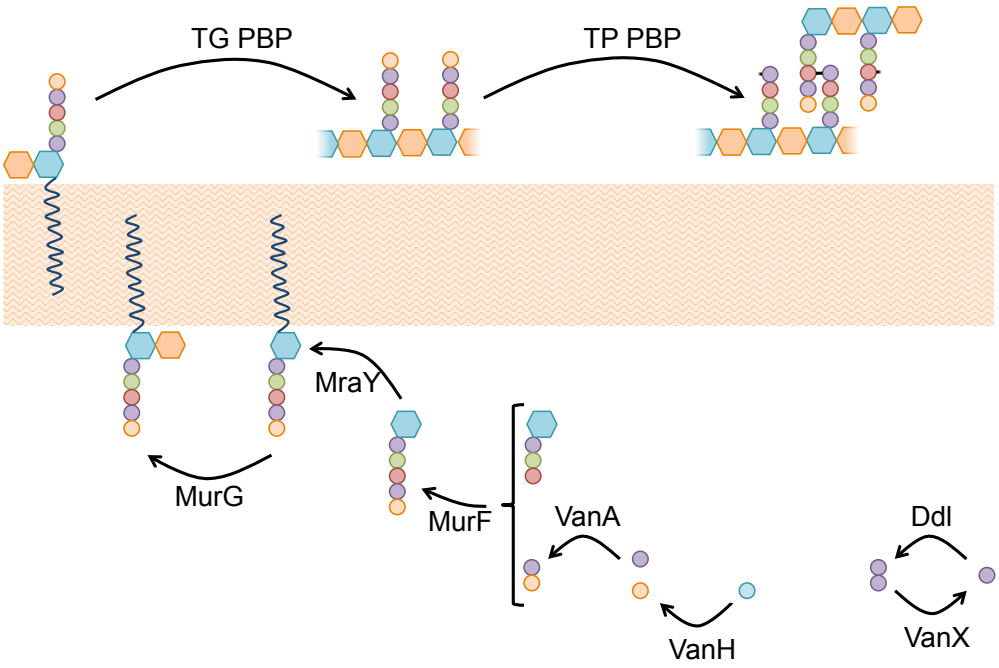

Figure 1.5: Schematic outlining the interference of proteins encoded in the *vanHAX* operon in peptidoglycan biosynthesis (see Figure 1.2 for an overview of the process of wildtype peptidoglycan biosynthesis). Orange circle, D-Lactate. Blue circle, pyruvate. The D-, D-dipeptidase VanX hydrolyses free D-alanyl-D-alanine, preventing its incorporation into peptidoglycan precursors by MurF. In its place, MurF incorporates D-alanyl-D-lactate, which is generated through the combined activities of VanH, an α-keto acid dehydrogenase synthesising D-lactate from pyruvate, and VanA, a D-alanyl-D-lactate ligase.

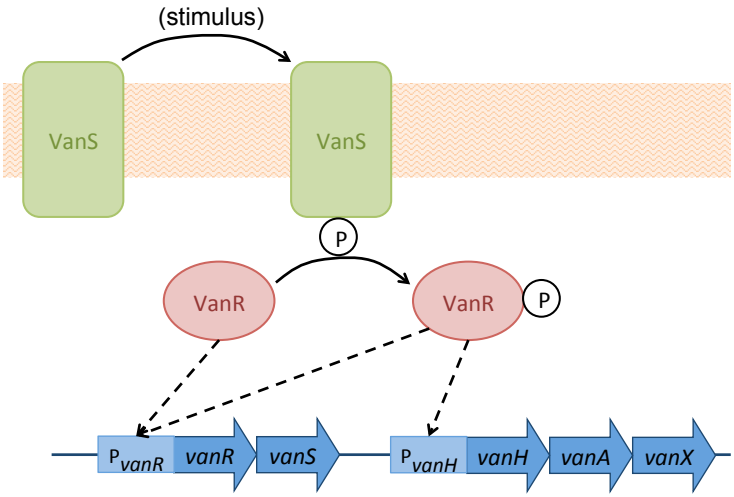

Figure 1.6: The regulatory role of VanSR on *vanHAX* transcription. VanS is stimulated, in the presence of vancomycin, to undergo autophosphorylation and subsequent phosphotransfer to VanR. Compared to VanR, Phospho-VanR has an increased binding affinity for the promoter region of *vanH*. In the absence of vancomycin, VanR remains dephosphorylated, and binds only to the promoter region of *vanR* to maintain low-level expression of VanSR.

pentapeptide terminates D-Alanyl-D-Lactate. VanK is therefore expressed in *S. coelicolor* to add this glycine branch to the modified pentapeptide (Hong et al., 2004). VanJ is unlike other genes within the *S. coelicolor van* cluster in that it is not involved in conferring resistance to vancomycin, but instead, confers teicoplanin resistance to the cell (Novotna et al., 2012), which is not conferred by *S. coelicolor* VanS ($VanS_{SC}$).

In A-type *Enterococci*, the *van* cluster includes *vanY* and *vanZ*. VanY, like VanX, is a D-, d-dipeptidase, but rather than hydrolysing free D-Alanyl-D-Alanine in the cytoplasm, VanY cleaves the terminal D-Alanine from bulkier peptidoglycan precursors, such as UDP-MurNAc-pentapeptide, into which D-Alanyl-D-Alanine has already been incorporated (Arthur et al., 1998). VanZ confers teicoplanin resistance to the cell via a poorly understood mechanism which does not involve substitution of D-Alanyl-D-Alanine for a related dipeptide (Arthur et al., 1995).

The *van* gene cluster in B-type *Enterococci* also encodes *vanY*, but not *vanZ*. In its place is the gene *vanW*. The exact function of VanW remains to be elucidated; it contains a G5 domain, which is understood to bind to GlcNAc, one of the sugar moieties in lipid II.

VanW has therefore been proposed to mediate interactions between lipid II and other Van proteins (Bateman et al., 2005). Since all genes within the B-type *van* cluster are encoded on the sense strand (Hong et al., 2008), disruption of the transcription terminator between B-type *vanS* and *vanY* leads to constitutive expression of Van proteins in the absence of antibiotic (Millan et al., 2009).

1.5 VanS: A Histidine Kinase Controlling Inducible Vancomycin Resistance

Transcription of *vanHAX* and of other genes within the *van* gene cluster is controlled by the VanSR two component system. Two component systems such as this one, comprised of a sensor kinase and a response regulator protein, are widely prevalent among bacteria, with 67 such systems having been identified in *S. coelicolor* (Hutchings et al., 2004). Two component systems control a huge range of cellular activities, and can be regulated by stimuli as diverse as temperature, ion concentration, and ligand binding (Wilke et al., 2012).

In the VanSR two component system, VanS is an integral membrane protein and sensor histidine kinase (Hutchings et al., 2006), the function of which is to detect the presence of vancomycin in the cellular environment. When vancomycin is detected, VanS dimerises, undergoes autophosphorylation, and then transfers the acquired phosphate group to VanR, the response regulator. Phospho-VanR binds upstream of the *vanSR* and *vanHAX* transcription elements, and induces expression of these proteins, leading to vancomycin resistance.

1.5.1 Predicted Structural Features of VanS

A complete structure of VanS has not been obtained experimentally. However, the structures of a number of histidine kinases have been solved, and the general structure of a canonical two-component system sensor histidine kinase has been published (Bhate et al., 2015) and is shown in Figure 1.7. Through sequence homology analysis of VanS with ref-

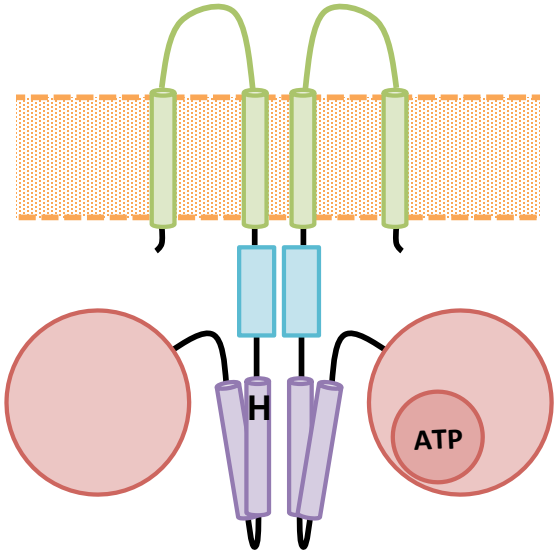

Figure 1.7: The predicted structure of VanS, based on homology modelling: extracellular "sensor" domain flanked by two transmembrane helices (green), followed by an intracellular HAMP domain (blue), DHp domain (purple) with conserved histidine residue which is the site of autophosphorylation, and ATPase domain (red). Adapted from Bhate et al. (2015). When active, VanS is expected to form a rotationally symmetric homodimer, bringing the autophosphorylation site of one monomer into close proximity with the ATP binding site of the other, and *vice versa*.

erence to this canonical structure, VanS has been determined to consist of an extracellular sensor domain flanked by two transmembrane domains, and intracellular HAMP, DHp, and ATPase domains (Arthur and Jr., 2001; Bhate et al., 2015).

The transmembrane domains integrate the protein into the cell membrane, orienting it such that the short section connecting the two transmembrane domains is external to the cell, and the much larger, catalytic domain of the protein is held within the cytoplasm. The extracellular domain is believed to act as a receptor to a ligand, the identity of which will be discussed shortly, to detect (or "sense") the presence of vancomycin in the environment. Hence this region is also referred to as the "sensor domain".

HAMP domains derive their name from the fact that they are found in **h**istidine kinases, **a**denylyl cyclases, methyl-accepting chemotaxis proteins, and **p**hosphatases (Aravind and Ponting, 1999). They connect extracellular sensor and intracellular catalytic domains and form coiled-coil structures, and are understood to be involved in signal transduction (Hulko et al., 2006).

Dimerisation and Histidine phosphorylation (DHp) domains form the catalytic core of receptor histidine kinases. This domain is responsible for initial dimerisation of VanS, which brings together the HAMP domains of two proteins to allow signal transduction

to occur. A conserved histidine residue within the DHp domain of each protein is trans-phosphorylated, with each ATPase domain bringing a molecule of ATP into close proximity with the histidine residue of the other protein within the dimer. Phosphoryl groups are then transferred from histidine to conserved aspartate residues within VanR, enabling VanR to upregulate expression of *van* genes.

Although the structure of VanS has not been solved, it is possible to predict the structures of many regions of the protein by analysis of the sequence and comparison to homologous receptor histidine kinases. Certainly, the enzymatic activities of many domains of VanS are well-characterised (Section 1.5.2). One region of the protein for which minimal information is available is the extracellular "sensor" domain, believed to serve as a receptor to the as-yet unidentified VanS ligand.

1.5.2 Enzymatic Activities of VanS

The role of the VanSR two component signalling system is to recognise and respond to the presence of vancomycin (and related antibiotics) in the cellular environment, and upregulate the expression of various enzymes from the *van* gene cluster, which limit the manufacture of wildtype peptidoglycan precursors and induce the manufacture of a modified precursor to which vancomycin cannot bind. The mechanism by which VanSR controls the upregulation of other *van* genes is well-documented. Both VanS and VanR are expressed at low levels in the absence of vancomycin; under exposure to the antibiotic, the VanSR two-component system upregulates transcription of the *vanS* and *vanR* genes alongside other genes on the *van* gene cluster (Hong et al., 2004).

In the absence of vancomycin, VanR is phosphorylated by acetyl phosphate and dephosphorylated by VanS. This has been demonstrated for A-type VanR from *E. faecium* (VanR_A) in an experiment in which detection of β-galactosidase indicated that a *vanH*$_A$-*lacZ* fusion gene was transcribed in an *ackA* strain of *E. coli* under heterologous expression of VanR_A (Haldimann et al., 1997). The strain overproduces acetyl phosphate, resulting in phosphorylation of VanR and upregulation of the VanH_A-LacZ fusion protein, and con-

sequently high levels of β-galactosidase. Thus, as a result of phosphorylation by acetyl phosphate, VanR from *E. faecium* is constitutively active in the absence of VanS.

Phosphorylation of VanR by acetyl phosphate has also been observed in *S. coelicolor*. Deletion of the *vanS* gene in *S. coelicolor* resulted in constitutive activity of VanR, suggesting that VanS negatively controls VanR in the absence of antibiotic. However, deletion of *vanS* and both *pta* and *ackA*, which together regulate the synthesis and degradation of acetyl phosphate, did not result in constitutive activity of VanR, suggesting the presence of acetyl phosphate is necessary for constitutive activity of VanR (Hutchings et al., 2006).

The role of VanS as an active phosphatase, rather than as a VanR phosphorylation inhibitor, has also been demonstrated (Wright et al., 1993). A fusion protein of maltose binding protein (MBP) and the cytosolic domain of VanS from *E. faecium* (VanS_A) destabilised phosphorylated VanR, leading to an approximately 6-fold acceleration in VanR dephosphorylation in the presence of the fusion protein.

VanS acts as a VanR kinase in the presence of vancomycin (Wright et al., 1993). A *pta ackA* double mutant of *S. coelicolor* survived vancomycin exposure (*i.e.* in the absence of acetyl phosphate, VanR was phosphorylated on exposure to vancomycin), but vancomycin was lethal to a *vanS pta ackA* triple mutant (*i.e.* VanR was not phosphorylated in the absence of VanS). γ-^{32}P was observed to be taken up by the cytosolic domain of VanS from [γ-^{32}P]-ATP, and subsequently transferred to VanR, in the absence of vancomycin (Wright et al., 1993).

1.6 VanS: A Sensor to Vancomycin in the Cellular Environment

VanS switches from a phosphatase to a kinase activity mode in the presence of vancomycin (Wright et al., 1993). It is believed that vancomycin is detected, either directly or indirectly, by the extracellular domain of VanS, but the mechanism by which this detection is achieved is the matter of some debate.

A compounding factor to the debate surrounding this issue is the varying antibiotic sensitivity profiles displayed by VanS proteins originating in different species. All known glycopeptide antibiotics originate in Actinomycetes; Actinomycetes producing a glycopeptide antibiotic are typically resistant to that antibiotic. *Amycolatopsis orientalis*, the bacterium which produces vancomycin, is itself resistant to vancomycin (Xu et al., 2015); *Streptomyces toyocaensis* produces and is resistant to the glycopeptide antibiotic A47934, but is sensitive to vancomycin (Pootoolal et al., 2002). *Actinoplanes teichomyceticus* produces teicoplanin, and is resistant to teicoplanin and a broad range of other glycopeptide antibiotics. However, the vancomycin resistance machinery has been shown to be constitutively expressed in *A. teichomyceticus* (Beltrametti et al., 2007), so its broad resistance profile does not necessarily indicate a broad binding profile for VanS.

Kinase activity in Enterococcal VanS ($VanS_A$) is induced by a number of glycopeptide antibiotics (Lai and Kirsch, 1996), including both vancomycin and teicoplanin (Baptista et al., 1996), as well as by the nonglycopeptide antibiotic moenomycin (Handwerger and Kolokathis, 1990; Figure 1.8). Moenomycin is structurally unrelated to glycopeptide antibiotics; its capacity to activate $VanS_A$ suggests that activation may not be a result of direct binding of the antibiotic to the protein, since there is no conserved motif between antibiotics at which VanS might bind in each case. It has been suggested that $VanS_A$ could be activated by binding of a product of antibiotic activity, such as accumulated lipid II, common to moenomycin as well as glycopeptide antibiotics.

Enterococcal B-type VanS ($VanS_B$) is activated by vancomycin, but not by nongly-

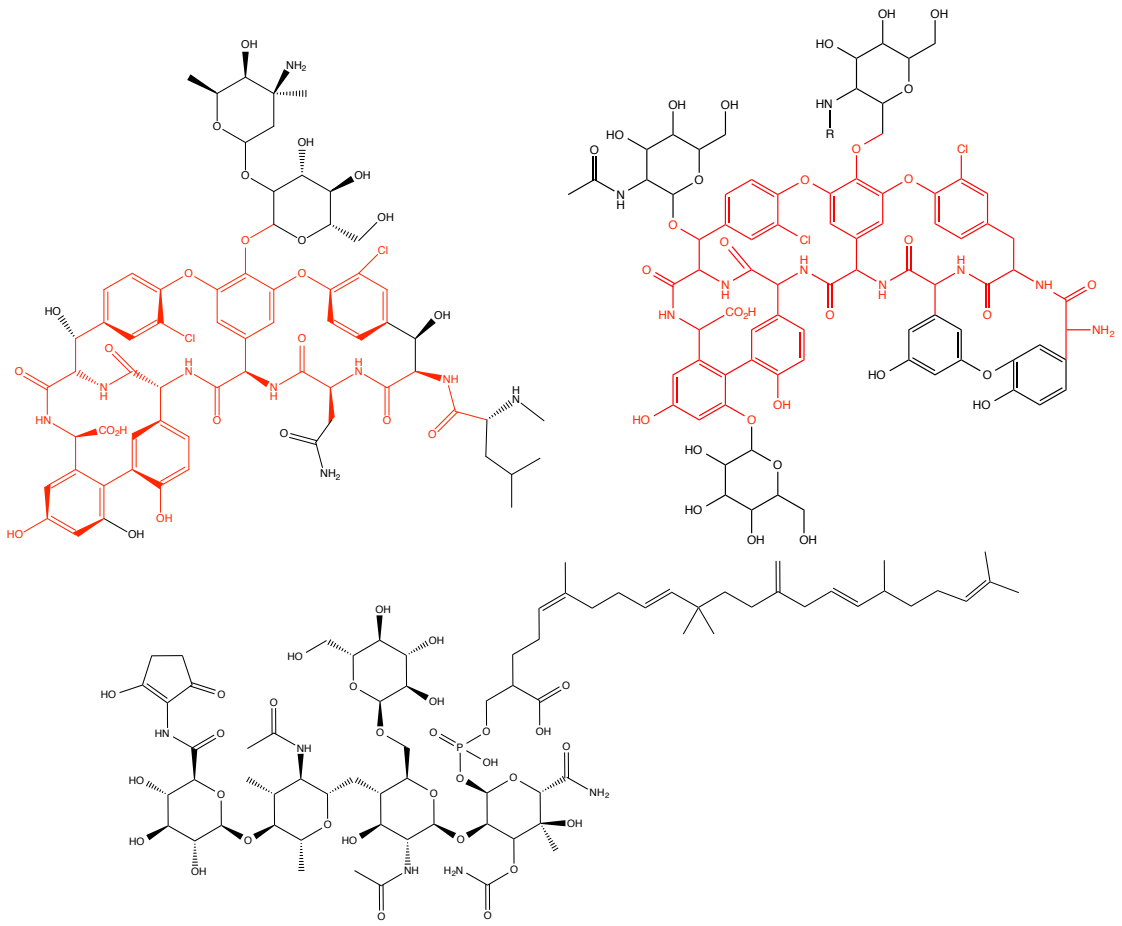

Figure 1.8: The atomic structures of three antibiotics, which trigger resistance in some or all vancomycin-resistant bacteria. Top left: vancomycin Clardy and Walsh (2004). Top right: the glycopeptide portion of teicoplanin Reynolds (1989), where R denotes one of a number of lipid chains. Bottom: moenomycin A Ostash et al. (2007). Structural elements that are conserved between vancomycin and teicoplanin are highlighted in red.

copeptide antibiotics or by teicoplanin (Baptista et al., 1996, 1997, 1999), although vancomycin and teicoplanin possess significant structural homology (Figure 1.8) and both act identically, by binding to D-Alanyl-D-Alanine-terminating lipid II pentapeptides. Specificity of induction of VanS$_B$ may indicate that it is activated by direct binding of vancomycin, rather than by a product of vancomycin activity.

1.6.1 Evidence Supporting Glycopeptide Antibiotics as Ligands to VanS

A number of studies have reported evidence that $VanS_B$, and VanS from actinomycetes, is activated by direct binding of vancomycin or other antibiotics to which the cell is resistant. The organisms producing these proteins are generally resistant to vancomycin, but not to other glycopeptide or non-glycopeptide antibiotics. $VanS_B$ is normally activated by vancomycin but not by teicoplanin; A30G and D168Y mutations in the sensor domain of $VanS_B$ confer resistance to teicoplanin (Baptista et al., 1997). Because the activities of vancomycin and teicoplanin both result in the accumulation of free lipid II (Nicolaou et al., 1999) and degradation of the cell wall, but wildtype $VanS_B$ is not activated in the presence of teicoplanin, this suggests that $VanS_B$ is activated by direct binding of antibiotic to the protein, and that ligand specificity is modulated by mutations at these residues.

$VanS_B$ from six inducibly teicoplanin-resistant mutants of B-type *Enterococcus faecalis* were found to have mutations upstream of the DHp domain; two of these mutations were in the extracellular domain, with the remaining four falling within the HAMP domain which is understood to transmit signals between the extracellular sensor and intracellular catalytic domains (Hulko et al., 2006). These results suggest that $VanS_B$ may possess some capacity to bind teicoplanin, and that this capacity is enhanced by mutations in the extracellular domain - while mutations in the HAMP domain allow propagation of a signal resulting from binding in the wildtype extracellular domain.

A modified vancomycin photoprobe has been shown to bind to $VanS_{SC}$ from *S. coelicolor* (Figure 1.9), and particularly, to the N-terminal product of tryptic digestion of $VanS_{SC}$, which comprises the N-terminal intracellular peptide, the first transmembrane domain, and a fragment of the extracellular domain of sequence LLDQGW (Koteva et al., 2010). VanS of *S. toyocaensis*, which is not resistant to vancomycin, did not bind this photoprobe, supporting the hypothesis that direct binding of specific glycopeptides to VanS proteins induces kinase activity.

Recently, evidence has emerged in the literature for an *in vitro* interaction between A-type VanS and glycopeptide antibiotics. $VanS_A$ from *E. faecium*, which is resistant to

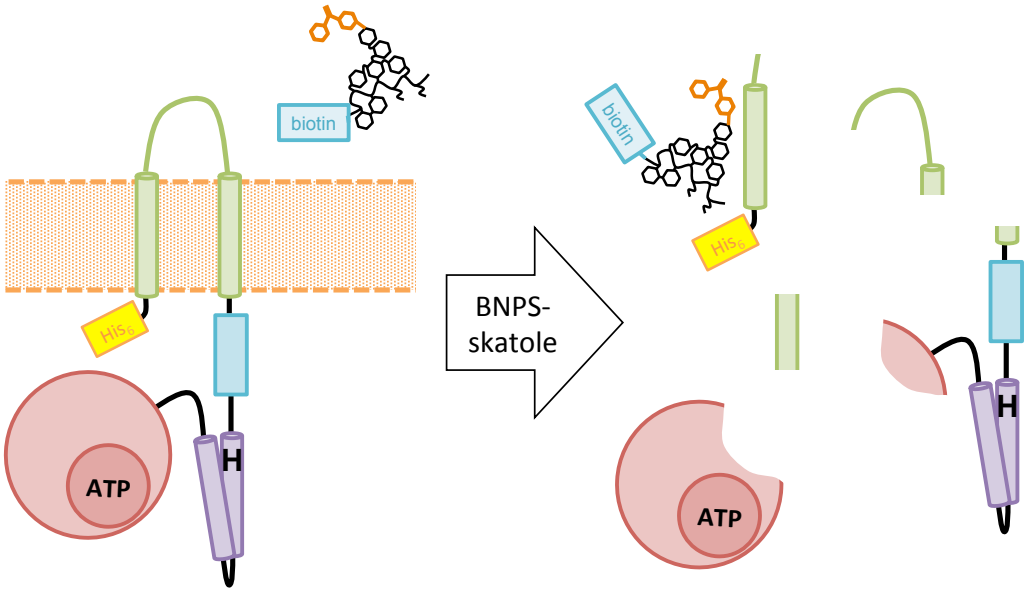

Figure 1.9: From Koteva et al. (2010). *E. coli* cell membranes containing heterologously expressed His_6-$VanS_{SC}$ were incubated with a modified vancomycin-benzophenone photoprobe, and irradiated so that benzophenone covalently bound with proteins to which it was near. After this, the mixture was treated chemically with 3-bromo-3-methyl-2-(2-nitrophenyl) thiol-3H-indole (BNPS-skatole) to cleave proteins at WXxx junctions. There are four such junctions in $VanS_{SC}$, yielding five cleavage products, illustrated. Analysis of the products by SDS-PAGE revealed a 9 kDa band colabelled with His_6 and biotin, indicating that the photoprobe interacted only with the cleavage product corresponding to the first transmembrane domain of $VanS_{SC}$. Since the only region of this cleavage product exposed to the extracellular environment is the short region of the extracellular domain with sequence LLDQGW, this is proposed to be the binding site of $VanS_{SC}$ for vancomycin.

a range of antibiotics including vancomycin, teicoplanin, and moenomycin, was found by analytical ultracentrifugation to undergo either dimerisation or a significant conformational change in aqueous solution, in the presence of vancomycin. The thermal stability of $VanS_A$ in 0.025% DM is reported to increase significantly in the presence of vancomycin, but not teicoplanin or a number of lipid II components (Hughes et al., 2017). Circular dichroism data acquired in the 260 - 320 nm range indicates a change in tertiary structure of $VanS_A$ in the presence of vancomycin, teicoplanin, and a mixture of vancomycin and lipid II pentapeptide, but not in the presence of lipid II components alone. Fluorescence spectroscopy also indicates a change in the polar environment of $VanS_A$ tryptophan residues in the presence of vancomycin and teicoplanin.

1.6.2 Evidence Supporting Lipid II as the Ligand to VanS

Some evidence in the literature indicates that, rather than directly binding antibiotics, VanS binds a cell wall intermediate which accumulates as a result of antibiotic activity. This mechanism would neatly explain the sensitivity of A-type VanS to a range of glycopeptide and non-glycopeptide antibiotics. The function of moenomycin, to which A-type VanS is sensitive, is to inhibit the transglycosylation activity of penicillin binding proteins (van Heijenoort et al., 1978), so that lipid II is not integrated into the peptidoglycan matrix (Figure 1.2). Thus, moenomycin activity may lead to an accumulation of lipid II.

E. faecalis BM4110, exhibiting A-type vancomycin resistance, was exposed to a range of peptidoglycan-targetting antibiotics. Resistance was induced by vancomycin, teicoplanin, and moenomycin, all of which disrupt transglycosylation of lipid II, but not by any other antibiotics tested, which disrupt various stages of the assembly of lipid II or, in the case of penicillin, the final transpeptidation reaction that forms peptidoglycan (Baptista et al., 1996). If a peptidoglycan precursor is the ligand to $VanS_A$, then, this suggests that the transglycosylation step limits interactions between lipid II and $VanS_A$.

S. coelicolor strains were constructed which synthesised variable ratio of D-Alanyl-D-Alanine to D-Alanyl-D-Lactate in the absence of vancomycin. The expression of *van* genes

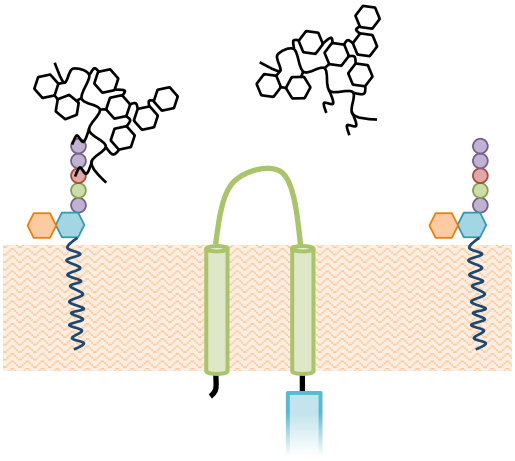

Figure 1.10: The activity of vancomycin leads to an accumulation of lipid II, to which PBPs cannot bind to catalyse transglycosylation. There is therefore a high concentration of vancomycin, lipid II, and lipid II-vancomycin complex, any of which might represent the ligand to VanS.

following exposure of these strains to vancomycin was quantified, and found to correlate positively with the relative abundance of D-Alanyl-D-Alanine (Kwun et al., 2013), indicating that the presence of D-Alanyl-D-Alanine-terminating lipid II is vital for VanS_{SC} activation. *S. coelicolor* is not resistant to teicoplanin. Exposure of wildtype *S. coelicolor* to teicoplanin blocked the cell's normal response to a subsequent application of vancomycin, possibly due to a saturation effect in which D-Alanyl-D-Alanine termini are occupied by teicoplanin such that vancomycin cannot bind (Kwun et al., 2013). This suggests that the ligand to VanS_{SC} is neither vancomycin nor lipid II, but a complex of the two molecules (Figure 1.10).

While several models have been proposed describing the ligand(s) and mechanisms responsible for induction of kinase activity in VanS, a consensus has not yet been reached. This is due to the fact that direct observation of a binding event between any unmodified ligand and a VanS protein has not been reported. In the absence of such an observation, these models remain speculative and open to interpretation. Indisputable identification of the VanS ligand might lead to the development of novel drugs, either to bypass VanS binding (in the case that glycopeptide antibiotics serve as ligands to VanS), or to inhibit binding (in the case that peptidoglycan precursors serve as ligands). For these reasons, the biophysical investigation of VanS-ligand interactions is the focus of work described in this thesis.

1.7 Aims and Outline of This Thesis

1.7.1 Aims

Antibiotic resistance is a major and ongoing problem facing modern medicine. The emergence of multiple-resistant strains, including vancomycin- and methicillin-resistant *Staphylococcus aureus* (MRSA), represents a significant threat to human health. Antibiotic resistance might be overcome by the creation of novel antibiotics, to which pathogens are not resistant, or by the design of novel inhibitors to prevent interactions between existing antibiotics and bacterial sensor proteins. In either case, detailed characterisation of the sensors involved, and of the mechanisms by which they operate, is an essential first step towards successful treatment in the future.

Vancomycin is a glycopeptide antibiotic effective against Gram-positive infections, including *Staphylococcus aureus*. Resistance to this antibiotic is induced by the kinase activity of the integral membrane protein VanS. As has been discussed in Section 1.5.1, complete structural characterisation of VanS proteins has yet to be achieved. In particular, little is known of the structure of the extracellular domain, in which the ligand binding site is most likely located.

The mechanism by which kinase activity in VanS is induced remains to be elucidated. There exists a wealth of circumstancial evidence in the literature to support multiple theories describing the activation of VanS (Section 1.6); there remains the possibility that VanS proteins of different bacterial origins are activated by different mechanisms. Though numerous techniques have been utilised in the search for the ligand of VanS, there is no documentation in the literature describing the observation of direct binding of any unmodified ligand to a VanS protein.

Here we have identified several unknowns surrounding the structural and functional details of VanS. The work of this thesis was conducted with three questions in mind:

1. What are the structural features of the extracellular domain of VanS? In what ways do these features facilitate activation of VanS in the presence of vancomycin?

Characterisation of the VanS extracellular domain, and in particular, a detailed understanding of how the different structural features of this domain allow kinase activity in the intracellular domain to become active, is a vital first step towards the rational design of novel inhibitors to signal transduction.

2. By what mechanism is kinase activity in VanS induced? If this is achieved by ligand binding, what is the identity of the ligand?

Sensor kinases are known to be regulated by stimuli as diverse as temperature, ion concentration, and ligand binding (Wilke et al., 2012). As direct binding of a ligand to VanS has not yet been reported, it remains possible that VanS is activated by some other mechanism. The activity of vancomycin leads to accumulation of lipid II; as this remains anchored in the membrane by undecaprenol, this could conceivably affect the fluidity of the cell membrane, such that the structure of VanS is altered and kinase activity is induced.

3. If there is a ligand to which VanS must bind to induce kinase activity, what are the characteristics of the binding site on this ligand? How might these characteristics be mimicked, in the design of an effective inihibitor?

The ultimate goal of characterising the VanS activation system is that it may eventually be disrupted. If a ligand exists, identification of that ligand is a crucial first step towards this intervention. Following identification, characterisation of the binding site would facilitate the design of inhibitors to the interaction, or of novel antibiotics in which the required binding site is not present.

Definitive answers to these questions would allow for the design of novel inhibitors to prevent induction of kinase activity in VanS; alternatively, it may be possible to design

novel glycopeptide antibiotics which circumvent the VanS activation mechanism. This would facilitate treatment of vancomycin-resistant pathogens, including VRSA.

Hoping to contribute to the body of knowledge surrounding the questions enumerated above, the work of this thesis has focused on the structural and ligand-binding characterisation of VanS proteins derived from *Enterococcus faecium* ($VanS_A$) and *Streptomyces coelicolor* ($VanS_{SC}$).

1.7.2 Outline

Chapter 3 discusses the heterologous expression and chromatographic purification of hexahistidine-tagged (His_6-) $VanS_A$ and $VanS_{SC}$. Preliminary structural characterisation of the proteins is achieved by circular dichroism spectroscopy. The constitutive ATPase activity of both proteins is measured by a coupled enzymatic assay, indicating that the proteins are properly folded and active in the detergent micelles in which they are encapsulated.

In Chapter 4, the hexahistidine tag in His_6-$VanS_A$ is substituted with a StrepII tag by site-directed mutagenesis, to facilitate purification of a VanS protein to which no metal ion affinity is conferred. Vancomycin is applied to a Cu^{2+} affinity column and demonstrated to be retained until eluted with imidazole. Steps are taken towards the purification of StrepII-$VanS_A$, with the aim of applying this protein to the Cu^{2+} column previously charged with vancomycin. Retention of the protein by the column would indicate an interaction between $VanS_A$ and vancomycin.

Chapter 5 describes a binding study between His_6-$VanS_A$ and His_6-$VanS_{SC}$, and vancomycin and lipid II pentapeptides. This study is conducted by saturation transfer difference solution-state NMR, allowing for the identification of protons within those ligands which come into close contact with protons of the proteins.

In Chapter 6, the extracellular domain of $VanS_{SC}$ (extracted as a synthetic peptide) is structurally characterised by circular dichroism spectroscopy and solution-state NMR, and found to adopt a partially helical conformation. Titration experiments of this peptide

and vancomycin identify residues within the peptide in which NMR signals are attenuated by vancomycin. Simultaneously, protons within vancomycin are identified which experience chemical shift perturbations in the presence of the peptide.

Chapter 7 describes a study made of interactions between vancomycin and the membrane mimetics used in this thesis, to investigate the possibility that the presence of membrane mimetics in protein samples interferes with binding studies. We show that vancomycin interacts with DPC micelles, but not with LMPG micelles, and that the vancomycin/protein interactions reported thus far are sustained when the vancomycin/DPC interaction is accounted for.

Chapter 2

Materials and Methods

2.1 Materials for Microbiology

2.1.1 Provided Constructs

N-terminally hexahistidine-tagged VanS proteins from *Enterococcus faecium* ($VanS_A$) and *Streptomyces coelicolor* ($VanS_{SC}$) were expressed using plasmids kindly provided by Dr Richard Edwards (2014); modifications to these constructs were made by site-directed mutagenesis. Plasmids used in this study are listed in Table 2.1.

Plasmid Name	Description	Antibiotic Resistance	Source or Template
pProEx::His_6-$VanS_A$	pProEx vector containing VanS from *E. faecium* with N-terminal hexahistidine tag	Ampicillin	Edwards (2014)
pProEx::His_6-$VanS_{SC}$	pProEx vector containing wild-type VanS from *S. coelicolor* with N-terminal hexahistidine tag	Ampicillin	Edwards (2014)
pProEx::His_6-$VanS_A$-3C	pProEx vector containing VanS from *E. faecium*, with N-terminal hexahistidine tag and inserted 3C cleavage site	Ampicillin	Edwards (2014)
pProEx::His_6-$VanS_{SC}$-3C	pProEx vector containing VanS from *S. coelicolor*, with N-terminal hexahistidine tag and inserted 3C cleavage site	Ampicillin	Edwards (2014)
pProEx::Strep-$VanS_A$	pProEx vector containing VanS from *E. faecium* with N-terminal StrepII tag	Ampicillin	pProEx::His_6-$VanS_A$
pProEx::Strep-$VanS_{SC}$	pProEx vector containing VanS from *S. coelicolor* with N-terminal StrepII tag	Ampicillin	pProEx::His_6-$VanS_{SC}$

Table 2.1: Plasmids used in this study; the source of previously-generated plasmids is given, as are the templates of plasmids generated in this study.

2.1.2 Site-Directed Mutagenesis

Site-directed mutagenesis was employed in order to substitute a Strep-tag II (sequence WSHPQFEK) in place of the hexahistadine tag (sequence HHHHHH) initially in place on the N-terminus of the His_6-$VanS_A$ construct (Figure 2.1). The primers were manufactured by Integrated DNA Technologies (Iowa); their sequences are described in Table 2.2.

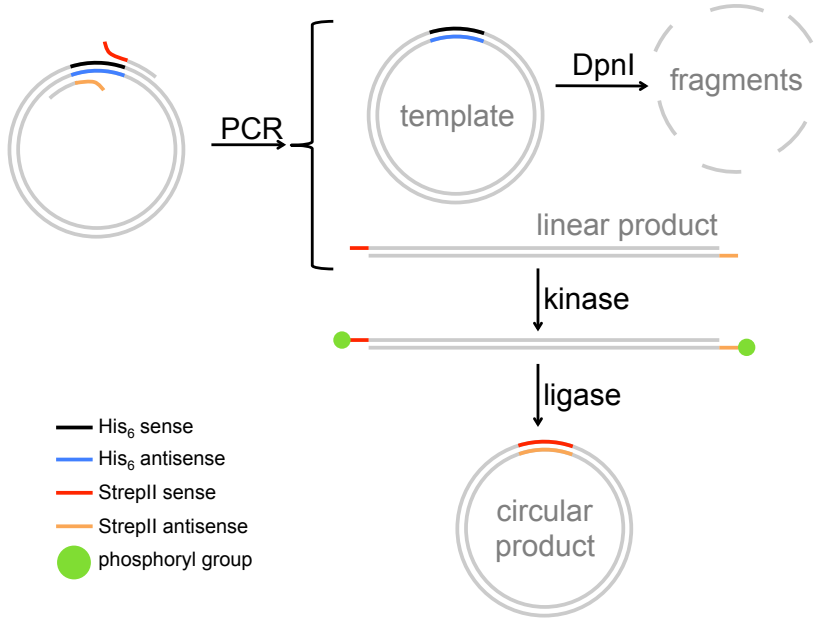

Figure 2.1: Site-directed mutagenesis was used to replace the existing N-terminal His_6 tag on $VanS_A$ with a StrepII tag. The TEV cleavage site between the tag and the protein was retained.

Primer name	Sequence	Length	Tm (°C)
forward	CAGTTCGAAAAGGATTACGATATCCCAACG	30	55
reverse	CGGGTGGCTCCAGTAGTACGACATGGTCTG	30	57

Table 2.2: Primers for site-directed mutagenesis. Colours correspond to those in Figure 2.1.

These primers complement the template DNA either side of the resident hexahistidine (His_6) tag, and encode a Strep-tag II in place of the His_6 tag. The primers were added to a final concentration of 0.5 μM, to 25 μL PCR reaction mix consisting of template DNA

(25 ng) and 1× Q5 Hot Start High-Fidelity Master Mix (New England Biolabs, Ipswich). A PCR reaction was carried out, using the parameters shown in Table 2.3.

Step	Temperature (°C)	Time (seconds)
Initial Denaturation	98	30
25 Cycles	98	10
	58	30
	72	180
Final Extension	72	120
Hold	4	

Table 2.3: Cycling conditions for site-directed mutagenesis PCR reaction.

With the addition of a proprietary KLD reaction mixture (New England Biolabs, Ipswich), linear strands of modified DNA are phosphorylated by a kinase and then circularised by a ligase. The restriction enzyme DpnI digests methylated DNA, *i.e.* the template DNA which was propagated in *E. coli*, and not the modified DNA, which is not methylated during PCR amplification.

2.1.3 Plasmid Purification

Plasmids were purified using the GeneJET MiniPrep Kit (Thermo Fisher Scientific) as per manufacturers' instructions, yielding 50 μL aliquots in dH_2O to be stored at -20 °C.

To confirm successful mutagenesis of the affinity tag, Sanger sequencing was carried out by GATC Biotech using the M13 pUC Rev primer (24mer); sequences were analysed using A Plasmid Editor (ApE; M. Wayne Davis, University of Utah).

2.1.4 *Escherichia coli* Strains

The strains of *E. coli* used in this study are outlined in Table 2.4.

Strain	Genotype	Reference or Source
Top10	F$^-$ *araDJ39* Δ(*ara,leu*)7697 Δ*lacX74 galU galK rpsL deoR* ϕ80d*lac*ZΔM15 *endAI nupG recAl mcrA* Δ(*mrr hsdRMS mcrBC*)	Grant et al. (1990)
BL21 (DE3)	F$^-$ *ompT gal dcm lon hsdS$_B$*($r_B{}^-$ $m_B{}^-$) λ(DE3 [*lacI lacUV5-T7p07 ind1 sam7 nin5*]) [*malB*$^+$]$_{K-12}$(λ^S)	Moffat and Studier (1987)
BL21 (DE3) Star.pRosetta	F- *ompT hsd*S$_B$ ($r_B{}^-$, $m_B{}^-$) *galdcmrne*131 (DE3) pRARE (Cam^R)	Addinall et al. (2005)
C41 (DE3) pRIL	F$^-$ *ompT hsd*S$_B$($r_B{}^-$ $m_B{}^-$) *gal dcm* (DE3), contains pRIL plasmid for rare codon optimisation	Miroux and Walker (1996)

Table 2.4: *E. coli* strains used in this study.

2.1.5 Bacterial Growth Media

Lysogeny Broth (LB; Bertani (2004)) is a popular medium for the culturing of *E. coli*, consisting of 0.1% bacto-tryptone, 0.05% yeast extract, and 0.1% sodium chloride. In this study, LB was prepared in deionised water and autoclaved prior to use. Antibiotics were added to final concentrations described in Table 2.5.

Antibiotic	Concentration (μg mL^{-1})
Carbenicillin	100
Chloramphenicol	35

Table 2.5: Concentrations of antibiotics included in bacterial growth media.

LB/agar plates were prepared by dissolving bacto-agar into LB to a concentration of 0.15%. The mixture was allowed to cool slightly before appropriate antibiotics were added as described in Table 2.5, and the mixture was poured into sterile Petri dishes and allowed to cool before being sealed with parafilm and stored at 4 °C.

Super-Optimal Broth with Catabolites (SOC Media; Hanahan (1983)) consists of

2% bacto-tryptone, 0.5% yeast extract, 10 mM NaCl, 2.5 mM KCl, 10 mM $MgCl_2$, 10 mM $MgSO_4$, and 20 mM glucose. $MgCl_2$, $MgSO_4$, and glucose are filter-sterilised as concentrated stocks, and added to the autoclaved medium. This medium was used during transformation as it is more nutrient-rich than LB.

2.1.6 Preparation of Chemically Competent Cells for DNA Transformation

2.5 mL of LB (Section 2.1.5) with appropriate antibiotics was innoculated with 100 μL of the required *Escherichia coli* strain (from glycerol stock, stored at -80°C) and incubated overnight at 37 °C with agitation at 180 rpm.

250 mL of LB with appropriate antibiotics and 20 mM $MgSO_4$ was innoculated with the overnight culture and incubated at 37 °C, 180 rpm until an OD_{600} of 0.5 was reached. Cells were pelleted from this culture by centrifugation at 4,000 × g, 4 °C, for 10 minutes. Pelleted cells were resuspended in 10 mL of TFB1 buffer (30 mM potassium acetate, 10 mM calcium chloride, 50 mM manganese chloride, 100 mM rubidium chloride, 15% (v/v) glycerol, pH 5.8), incubated on ice for 5 minutes and then pelleted by centrifugation at 4,000 × g, 4 °C, for 10 minutes. The cells were then resuspended in 10 mL of TFB2 buffer (10 mM MOPS pH 6.5, 75 mM calcium chloride, 10 mM rubidium chloride, 15% (v/v) glycerol), incubated on ice for 30 minutes, and then snap-frozen in liquid nitrogen in 100 μL aliquots and stored at -80 °C.

2.2 DNA Transformation of Competent *E. coli* Cells

10-100 ng of required plasmid was added to a 100 μL aliquot of competent cells (the preparation of which is described in Section 2.2.4) and incubated on ice for 20 minutes. Cells were heat-shocked for 45 seconds at 42 °C and then returned to ice for 2 minutes. 300 μL sterile super-optimal broth with catabolites (SOC; Section 2.1.5) was added and cells were incubated at 37 °C, 180 rpm, for 45 minutes. Cells were then spread onto LB/agar plates with appropriate antibiotics, and incubated at 37 °C overnight.

2.3 Expression and Purification of the Integral Membrane Protein VanS

2.3.1 Membrane Protein Overexpression

10 mL of LB with appropriate antibiotics was innoculated with a single colony picked from a plate of appropriately transformed *E. coli* cells and incubated overnight at 37 °C with agitation at 180 rpm.

This starter culture was used to innoculate 1 L of LB, appropriate antibiotics, and 0.2% (w/v) glucose, which was incubated at 37 °C, 180 rpm, until the culture reached an optical density at 600 nm (OD_{600}) of 0.5. Isopropyl β-D-1-thiogalactopyranoside (IPTG) was added to a concentration of 200 μM and the culture was incubated at 25 °C (for cultures expressing $VanS_A$), or 16 °C (for cultures expressing $VanS_{SC}$), and 180 rpm, overnight.

Cells were harvested by centrifugation at 8,000 × g, 4 °C, for 20 minutes using a Beckmann JA 8.1000 rotor. Cells were resuspended in 20-30 mL 25 mM sodium phosphate pH buffer (pH 6.8), 300 mM NaCl, 10% (v/v) glycerol. 2 μM Leupeptin, 2 μM pepstatin, and 20 μM PMSF were added to prevent protein degradation.

2.3.2 Preparation of Native Cell Membranes

20 μg/mL DNAse I, 100 μg/mL magnesium chloride, and 2.5 mg/mL hen egg lysozyme were added to thawed *E. coli* cell pellets (Section 2.3.1), which were rocked at room temperature for 30 minutes before being lysed using a continuous cell disruptor (Constant Cell Disruption Systems), with 2 passes at 30 kpsi, 4 °C.

Lysate was centrifuged at 20,000 × g, 4 °C for 30 minutes to pellet cell debris, and supernatant was further centrifuged at 200,000 × g, 4 °C, for 2 hours to pellet cell membranes.

Membranes were resuspended in 25 mM sodium phosphate pH buffer (pH 6.8), 300 mM NaCl, 10% (v/v) glycerol, using a hand held homogeniser, to a volume of 20 mL buffer per litre of overnight cell culture. Membrane pellets were stored at -20 °C.

2.3.3 Membrane Protein Solubilisation From Native Membranes

Membrane proteins were solubilised from membranes using 10.0 mM dodecylphosphocholine (DPC) (CMC 1.5 mM, aggregation number ∼70 (Patel, 2012); equivalent to 120 μM DPC micelles) or 6.7 mM 1-myristoyl-2-hydroxy-sn-glycero-3-phospho-(1'-rac-glycerol) (LMPG) (CMC 0.21 mM (Yildiz et al., 2013), aggregation number 55 (Sigalov and Hendricks, 2009); equivalent to 120 μM LMPG micelles). Membranes were rocked with detergent for 2 hours at 4 °C, and then centrifuged at 200,000 × g, 4 °C, for 40 minutes to pellet the residual membranes. Proteins were retained in solution, solubilised into the detergent micelles.

2.3.4 Detergent Screening

2% (w/v) of each screened detergent (Figure 3.4) was added to 1.5 mL of prepared native membranes. The mixtures were rocked at 4 °C for 2 hours, except in the case of SDS, which crystallises at low temperatures; this sample was rocked at room temperature. After this incubation step, membranes were pelleted by ultracentrifugation at 60,000 × g, 4 °C, for 40 minutes. Pellets were resuspended in 1.5 mL 25 mM sodium phosphate buffer (pH 6.8), 300 mM NaCl, 10% (v/v) glycerol, using a hand held homogeniser. Supernatants, consisting

of detergent micelles and solubilised membrane proteins, and membrane pellets, containing proteins that were not solubilised into detergent micelles, were analysed by SDS-PAGE and Western blotting to assess the ability of each detergent to solubilise the target proteins.

2.3.5 Immobilised Metal-Ion Affinity Chromatography

In solubilising the target protein into detergent micelles, many other membrane proteins are also solubilised. It is necessary to separate the target protein from other unwanted proteins; this was achieved by immobilised metal-ion affinity chromatography (IMAC).

VanS was expressed with an N-terminal hexahistidine tag, which has an affinity for various metal ions, noteably nickel. A HisTrap High Pressure (HP) 5 mL prepacked nickel-sepharose column was pre-equilibrated with 5 column volumes (CV) of distilled water, followed by 5 CV of wash buffer (25 mM sodium phosphate buffer (pH 6.8), 50 mM NaCl, 2 μM leupeptin, 2 μM pepstatin, and appropriate detergent at a concentration just above its CMC).

The mixture of detergent-solubilised membrane proteins was then applied to the column, at a flow rate of 2 mL/min, at 4 °C for 1 hour. After this time, the flowthrough was collected. The column was then washed with 5 CV of wash buffer, 5 CV of wash buffer with 500 mM NaCl, and 5 CV of wash buffer with 20 mM imidazole. The protein was then eluted from the column in 3 $\times$ 2.5 mL of wash buffer with 300 mM imidazole. Eluates were desalted using PD10 columns to 3 $\times$ 3.5 mL fractions in wash buffer. These fractions were then pooled and concentrated with a Vivaspin 2 ®5,000 MWCO PES centrifugal concentrator (Vivaproducts, Massachussets) to a volume of approximately 200 μL.

2.3.6 Size Exclusion Chromatography

In the absence of the protease inhibitors leupeptin and pepstatin (2 μM), VanS$_{SC}$ was observed by SDS-PAGE analysis (Section 2.6.1) to degrade in a matter of hours, including following purification by IMAC (Section 2.3.5). Speculating that a protease co-elutes from the IMAC column along with the target protein, a further purification step of size exclusion

chromatography was introduced to allow for the removal of protease inhibitors from final $VanS_{SC}$ samples.

IMAC eluates containing the target protein were pooled and concentrated to a total volume of 150 - 200 μL (Section 2.3.5). This was loaded onto a Superdex 200 Increase 10/300 GL gel filtration column (GE Healthcare Life Sciences, Pittsburgh, USA) equilibrated in wash buffer at 4 °C. Proteins were then eluted in wash buffer lacking protease inhibitors, at a flow rate of 0.5 mL/min and maintaining a pressure of below 1.5 MPa.

Degradation of $VanS_{SC}$ was not observed following purification by size exclusion chromatography, supporting the hypothesis that a protease had co-eluted with the target protein from the IMAC column.

2.4 Buffer Exchange

Protease inhibitors interfere with the BCA protein concentration assay, and are therefore undesirable in purified protein samples. Additionally, saturation transfer difference (STD) NMR experiments were conducted in 100% deuterated buffer. The cost of deuterating purification buffers throughout IMAC and size exclusion chromatography steps was prohibitive. It was therefore necessary to exchange proteins into more appropriate buffers following purification, prior to study.

Buffer exchange was carried out using a Vivaspin 2 ®5,000 MWCO PES centrifugal concentrator (Vivaproducts, Massachussets). Purified protein samples were concentrated to a volume of 200 μL, then diluted to 2 mL in the desired buffer (25 mM sodium phosphate buffer (pH 6.8), 50 mM NaCl, appropriate detergent, and 100% D_2O in the case of STD-NMR experiments), to result in a protein sample in 90% desired buffer. This cycle of concentration and dilution was repeated a further three times, resulting in a protein sample in 99.99% desired buffer, 0.2 nM protease inhibitors, and 0.01% protonated water in deuterated STD-NMR samples.

2.5 Purification of Synthetic Peptides

Synthetic peptides with sequences corresponding to different portions of the $VanS_{SC}$ extracellular loop were purchased in either crude or purified forms from Insight Biotechnology (Middlesex, UK); purification by high pressure liquid chromatography (HPLC) was occasionally required.

Purification was performed using a Luna 5u C5 100 A HPLC column (Phenomenex) and an HPLC Isocratic Pump unit (Jasco), run with ChromNav software. The column has a bed volume of approximately 20 mL, and a void volume of approximately 13 mL (Kazakevich and Lobrutto, 2007). The solvent mixtures used were based on those recommended by Ortega-Roldan et al. (2015) and are outlined in Table 2.6.

Solvent mixture	% H2O	% ACN	% IPA	% TFA
A	95	5	0	0.1
B	5	38	57	0.1

Table 2.6: Components of buffers A and B used in the purification of synthetic peptides by HPLC, as recommended by Ortega-Roldan et al. (2015). Components used are of HPLC grade.

The HPLC column and system was equilibrated in 30:70 B:A at a flow rate of 1 mL/min. Lyophilised synthetic peptide was solubilised in 30:70 B:A and loaded onto the column. The system proceeded to run at 30:70 for 10 minutes. The B:A ratio then increased to 70:0 at a rate of 1% min^{-1}, and then to 100:0 at a rate of 6$\hat{m}in^{-1}$, causing the system to apply 100% solvent B to the column starting 75 minutes after application of the peptide. 100% solvent B was applied for a further 20 minutes to ensure elution of all materials from the column. Elution of the peptide was monitored at 280 nm. Fractions were collected every minute, and fractions corresponding to peaks in the 280 nm spectrum were assessed by MALDI-TOF (2.6.5) for the presence of peptide.

2.6 Detection and Analysis of Purified Proteins and Peptides

2.6.1 Sodium Dodecyl Sulfate Polyacrylamide Gel Electrophoresis

Resolving and stacking layers of the SDS-PAGE gel were prepared as described in Table 2.7. Protein samples were standardised to a concentration of 20 μg/mL, unless the purpose of the study was to compare protein concentrations between samples. Appropriately diluted protein samples were combined with 4× loading buffer (0.25 mM Tris-HCl pH 6.8, 10% (w/v) SDS, 0.008% (w/v) bromophenol blue, 40% (w/v) glycerol, 2.86 M β-mercaptoethanol) at a ratio of 3:1. The gel comb was removed and wells washed with SDS-PAGE running buffer (25 mM tris pH 8.3, 250 mM glycine, 0.1% (w/v) SDS) before samples were loaded into the wells. Gels were run at 180 V until the gel front reached the resolving layer (approximately 15 minutes) and then 160 V thereafter until the gel front reached the end of the gel.

Component	Resolving gel	Stacking gel
distilled water	1.1 mL	1.4 mL
30% acrylamide (37.5:0.8)	2.5 mL	266 μL
1.5 mM Tris-HCl pH 8.8	1.3 mL	-
0.5 mM Tris-HCl pH 6.8	-	260 μL
10% SDS	40 μL	20 μL
10% APS	40 μL	20 μL
TEMED	4 μL	2 μL

Table 2.7: Volumes of components necessary to produce 1 × 15%-polyacrylamide gel for SDS-PAGE.

2.6.2 Visualisation of Proteins by Coomassie Staining

Following electrophoresis (Section 2.6.1), gels were stained by rocking at room temperature in Coomassie blue stain (20 mg coomassie brilliant blue, 40 mL 10% acetic acid), for several hours or overnight. To improve contrast, gels were destained by rocking at room temperature in Coomassie destain (20% methanol, 7% acetic acid) for several hours.

Depending on availability, InstantBlue ^{TM}Ultrafast Protein Stain was sometimes used in place of Coomassie blue stain. This is a fast-acting coomassie-based stain which does not require the use of a destain, and allows for the visualisation of proteins on an SDS-PAGE gel after 30 minutes.

2.6.3 Western Blotting

Following electrophoresis (Section 2.6.1), gels were applied to a Trans-Blot®Turbo^{TM} (Bio-Rad, Hertfordshire) Mini PVDF membrane and sandwiched between two layers of filter paper stacks that are pre-saturated in buffer by the manufacturer. Assembled stacks were loaded into a Trans-Blot® Turbo^{TM} cassette, and proteins were transferred from the SDS-PAGE gel to the PVDF membrane by the application of a 1.3 A, 25 V charge for 7 minutes.

The membrane was blocked in 20 mL of 5% milk powder in TBS-T (50 mM tris pH 7.6, 150 mM NaCl, 0.05% Tween-20) overnight at 4 °C, then washed 3 times for 10 minutes in TBS-T. Mouse anti-His antibody (Roche) was applied at 0.2 μg mL^{-1} in 10 mL of 5% milk powder in TBS-T for 2 hours at room temperature, and again the membrane was washed 3 times for 10 minutes in TBS-T. Goat anti-mouse antibody conjugated to horseradish peroxidase (Sigma) was applied at 0.4 μg mL^{-1} in 10 mL of 5% milk powder in TBS-T for an hour, and the membrane was washed in TBS-T. 2 mL of Immobilon Western Chemiluminescent HRP Substrate (Millipore, Hertfordshire) was then applied to the membrane, and chemiluminescence was visualised using the ImageQuant LAS4000 Blot Imaging System (GE Healthcare Life Sciences, Pittsburgh USA).

2.6.4 BCA Assay for Protein Concentration

Several commercially-available assay kits are available for the accurate measurement of protein concentration. The bicinchoninic acid (BCA) assay is a colorimetric assay which has the advantages of being detergent-compatible, and covering a broad range of protein concentrations (20 μg to 2 mg per mL). It is therefore well-suited to assaying the concentration of purified membrane proteins which are solubilised in detergent micelles.

The basis of the assay is the formation of a complex of Cu^{+} and BCA, which exhibits absorbance at 562 nm. The limiting factor in the formation of this complex is the abundance of Cu^{+} ions, which are formed by the reduction of Cu^{2+} ions in the Biuret reaction, which is itself limited by the concentration of protein (more accurately, the abundance of peptide bones).

In the Biuret reaction, peptides at least 3 residues in length undergo chelation with Cu^{2+} ions in an alkaline environment, reducing the copper to Cu^{+} and releasing an electron. This reaction can also be used to assay protein concentration, as the formed chelate absorbs light at 540 nm.

The BCA assay relies not on the Cu^{2+} chelate, but on the complex of Cu^{+} and BCA, which absorbs light at 562 nm. The formation of this complex is influenced, both by the presence of cysteine, cystine, tryptophan and tyrosine residues (Wiechelman et al. (1988)), and at higher temperatures, by the peptide bond. Thus, incubation at higher temperatures results in a measurable output which is less dependent on the amino acid composition of the protein in question; this allows for a more direct comparison between standard measurements (e.g. of known concentrations bovine serum albumin, BSA) and sample measurements, resulting in a more accurate estimate of concentration.

BCA assays were carried out following manufacturer's guidelines (Thermo Scientific). Protein samples (both BSA standards, and purified samples of VanS) were incubated at 60 °C for 30 minutes with a proprietary mixture of BCA reagents. Samples were cooled to room temperature, and their absorbance at 562 nm measured against a blank containing only the proprietary mixture (also appropriately incubated). A standard curve is constructed using

the values from the BSA standards, and this is used to estimate the concentration of VanS from the absorbance value measured.

2.6.5 Mass Spectrometry

To assess the purity of synthetic peptides prepared by HPLC, a saturated solution of the matrix sinapic acid was prepared in 80% ACN, and mixed with peptide samples in 1:1, 1:10, and 1:100 peptide:matrix ratios before being applied to a Bruker Daltonics ground steel MALDI plate, and allowed to dry. Samples were analysed using an Autoflex Speed MALDI-TOF Spectrometer (Bruker).

2.7 Circular Dichroism Spectroscopy

Circular dichroism (CD) spectroscopy was employed to investigate the secondary structure of proteins and peptides, in different membrane mimetic environments and in the presence of different potential ligands.

CD spectroscopy measures the difference in absorbance exhibited by a sample exposed to left- vs right-handed circularly-polarised light (A_L and A_R, respectively). At a given wavelength, this is calculated from Equation 2.1:

$$\Delta A = \Delta A_L - \Delta A_R \tag{2.1}$$

CD spectropolarimeters typically output this difference in absorption in units of millidegrees (θ). In order to normalise CD spectra with respect to sample concentration, protein chain length, and cuvette pathlength, units are converted from millidegrees to mean residue ellipticity (MRE; Θ), using Equation 2.2,

$$\Theta = \frac{\theta \times 0.1 \times M_r}{c \times l \times N_A} \tag{2.2}$$

where M_r is the mean residue weight, c is the protein concentration in mg mL^{-1}, l is the pathlength in cm and N_A is the residue length of the protein. MRE is reported in units of mdeg cm^2 $dmol^{-1}$.

CD spectra were recorded using a Jasco J-1500 spectropolarimeter (Jasco UK, Essex, UK), with acquisition parameters outlined in Table 2.8. Quartz cuvettes were used, with pathlength 0.1 cm for detergent-solubilised protein samples, and pathlength 0.02 cm for lipid-solubilised protein samples, to minimise the effect of light scattering by lipid vesicles.

Protein samples for CD were typically of a concentration of approximately 10 μM, in minimal detergent as required for solution state NMR (2 mM DPC or 1.15 mM LMPG).

2-3 mg mL^{-1} stocks of peptides were prepared in 25 mM sodium phosphate buffer (pH 6.8), 25 mM NaCl, and exact concentrations accurately calculated from absorbance at

Parameter	Value
Measurement range	300 - 180 nm
Data pitch	0.2 nm
CD scale	200 mdeg/1.0 dOD
FL scale	200 mdeg/1.0 dOD
D.I.T.	2 sec
Bandwidth	2.00 nm
Start mode	Immediately
Scanning speed	100 nm/min
Baseline correction	None
Shutter control	Auto
Accumulations	32

Table 2.8: Acquisition parameters for the Jasco J-1500 circular dichroism spectropolarimeter.

280 nm. CD samples consisting 0.5 mg mL^{-1} peptide and either 100 mM detergent, or 3 mg mL^{-1} lipid, were prepared from concentrated stocks. Peptide CD spectra were acquired in a 0.02 cm pathlength cuvette, to minimise the effect of scattering from lipid molecules on high tension voltage.

For all CD samples, baseline spectra were acquired of the relevant buffer/membrane mimetic solution, and baseline spectra were subtracted from protein or peptide spectra prior to conversion of the signal from units of millidegree to mean residue elipticity.

CD datasets were analysed via the CD fitting server DichroWeb (Whitemore and Wallace, 2007), using the analysis programme CDSSTR and reference set 4 (Sreerama and Woody, 2000). These processing parameters resulted in accurate reconstruction of data, indicating a high level of accuracy in estimations of protein structure.

2.8 Continuous ADP Release Assay

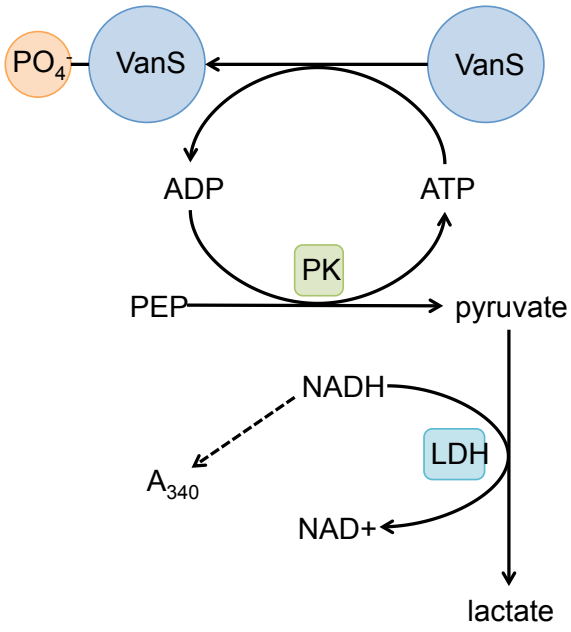

Figure 2.2: Schematic breakdown of reactions taking place during a continuous ADP release assay. The target protein VanS undergoes autophosphorylation, releasing ADP to which another phosphate group is transferred by pyruvate kinase (PK). This results in the conversion of phosphoenol pyruvate (PEP) to pyruvate. Lactate dehydrogenase (LDH) catalyses the oxidation of NADH to NAD+, converting pyruvate to lactate. The concentration of NADH can be measured spectrophotomerically at 340 nm; a reduction in absorbance at this wavelength corresponds to an increase in ADP concentration, and thus indicates autophosphorylation by VanS.

The ADP release assay is a coupled enzymatic assay which allows for the continuous proxy measurement of kinase activity. During phosphorylation, a phosphate group is transferred from ATP to the target protein (*i.e.* VanS), resulting in the release of an ADP molecule (Figure 2.2). ADP is a substrate for the enzyme pyruvate kinase (PK), which transfers a phosphate group from phosphoenol pyruvate (PEK) to this free ADP, producing ATP and pyruvate. Pyruvate, in turn, is converted to lactate by the enzyme lactate dehydrogenase (LDH), which also catalyses the oxidation of NADH to NAD+. The conversion of NADH and NAD+ may be measured spectrophotomerically, as NADH absorbs light at 340 nm while NAD+ does not. Therefore, the release of ADP may be measured by proxy, through the change in absorbance at 340 nm. A reduction in absorbance translates to an increase in concentration of ADP, and thus the autophosphorylation of VanS.

The reaction mixture was assembled as shown in Table 2.9, and mixed in a 1 mm pathlength quartz cuvette (Hellma). The assay was performed at room temperature, with measurements taken every 5 seconds. The cuvette was blanked against water, and measurements began immediately after reaction components were combined. Reaction rates were

Component stock	Volume (μL)	Final concentration
5 × buffer	40	1 ×
2 M KCl	5	50 mM
0.1 M DTT	2	1 mM
0.2 M PEP	2	2 mM
PK/LDH mixture (Sigma)	6	3.6-6.0 units PK 5.4-8.4 units LDH
10 mM NADH	2	100 μM
Water	101	-
20 mM ATP	10	1 mM
VanS	10	-

Table 2.9: Components for the continuous ADP release assay. 5 × buffer consisted of 125 mM sodium phosphate buffer (pH 6.8), 125 mM NaCl, 5.75 mM LMPG. VanS had been purified into 1.15 mM LMPG, 25 mM sodium phosphate buffer (pH 6.8), 25 mM NaCl. The pH of each component was confirmed to be 6.8 prior to mixing.

calculated in units of μmol ADP released per mg VanS, per minute.

2.9 ^{1}H Solution State NMR Spectroscopy

Solution-state NMR is a high resolution biophysical technique which allows the electrical environments of individual atoms within a molecule to be monitored. It is therefore well-suited to both structural characterisation and ligand-binding studies, in which the electrical environments of atoms are descriptive of the chemical environment. A change in chemical environment, such as a binding event, is detected as a change in electrical environment. The fundamental principles upon which solution-state NMR operates are described here, to provide a basic overview of the technique.

2.9.1 Spin Angular Momentum

Protons and neutrons within atomic nuclei possess a property known as "spin", an intrinsic quantum mechanical property with no classical physical analogue, but units of angular momentum. The spins of protons and neutrons contribute to the net spin of the atomic nucleus; if the spins are paired, as in ^{12}C, then S = 0, and the atom is NMR inactive. If spins are unpaired, as in ^{1}H (S = $\frac{1}{2}$), then the atom possesses a net spin, and may be studied by NMR.

Spin in atoms with unpaired nucleons produces a magnetic dipole moment, μ, according to Equation 2.3:

$$\mu = \gamma\hbar\sqrt{\mathrm{S(S+1)}} \tag{2.3}$$

where $\hbar$ is Planck's constant divided by 2π, and γ is the gyromagnetic ratio unique to each NMR-active isotope. Since γ varies between nuclei, so do the strengths of the magnetic dipole moments and therefore their NMR frequencies.

When a magnetic field B_0 is applied to a sample containing nuclei of S = $\frac{1}{2}$, the spin of each nucleus aligns either with or against the magnetic field. The ratio of populations aligning with or against the field is described by the Boltzmann distribution; at thermal equilibrium, there is a slight preference for spins to align with rather than against the applied

magnetic field. This results in a small net magnetisation (M_0), which can be measured.

2.9.2 The Larmor Frequency

The direction in which B_0 is applied is by convention designated the z axis. While aligned in this direction, the magnetic moment precesses around this axis (Figure 2.3). The rate at which this occurs is known as the Larmor frequency (ω_0), which may be calculated for each isotope using Equation 2.4:

$$\omega_0 = -\gamma B_0 \tag{2.4}$$

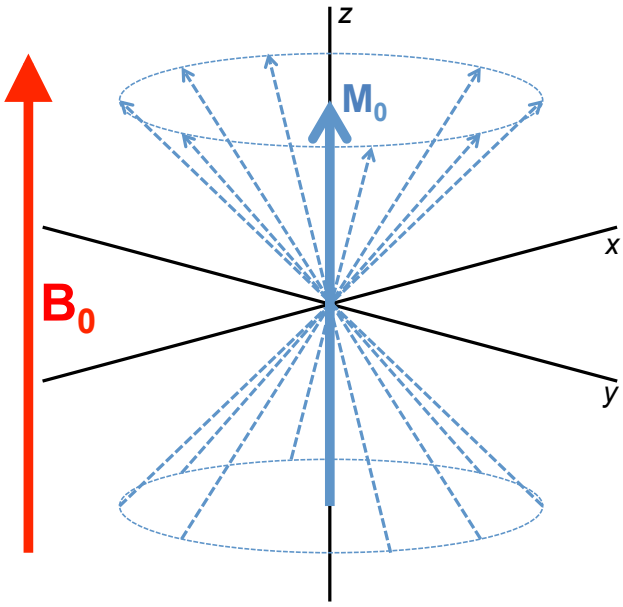

Figure 2.3: Precession of a spin around magnetic field B_0, applied in the z axis. The radius of the circle traced by the spin vector is 0, and net magnetisation M_0 is parallel to the applied magnetic field.

When M_0 is aligned along the z axis, the radius of precession is 0. The frequency with which precession occurs cannot be measured, and an NMR signal is not generated. In order to generate an NMR signal, this radius must be increased, so M_0 must be perturbed away from the z axis. This is achieved by the application of a radio frequency (RF) pulse at the Larmor frequency of the studied nucleus, applied along the x axis. This moves the magnetic moment away from the z axis into the xy plane (Figure 2.4). Magnetisation now processes with radius >0 in the xy plane, generating an electrical current which is detected

by a receiver coil within an NMR spectrometer.

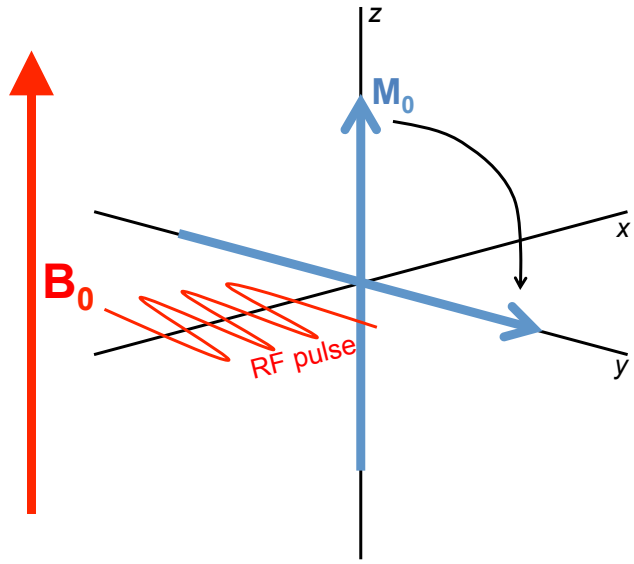

Figure 2.4: Application of a radio frequency pulse in the x axis moves the net magnetisation away from the z axis and into the xy plane. Net magnetisation will continue to precess, now tracing a circle with radius >0. Then the RF pulse ceases, net magnetisation will relax towards the z axis, and the radius will decrease to 0 as precession continues.

2.9.3 Free Induction Decay

When application of the RF pulse is terminated, the magnetic moment relaxes back towards the z axis. The rate at which this occurs depends on the longitudinal and transverse relaxation rates, R1 and R2. R1 describes the return of magnetisation to equilibrium as a result of interactions between spins and the surrounding lattice; R2 describes the return to equilibrium as a result of interactions between spins. Precession continues during relaxation, so that the radius of precession continuously shortens as M_0 approaches the z axis. The amplitude of the detected NMR signal therefore decays over time following termination of the RF pulse. The free induction decay (FID) plots NMR signal intensity with respect to time. The FID is composed of overlapping sine curves, with each sine curve mapping the decaying signal of a different nucleus within the sample. Fourier transformation of the FID resolves these sine curves, yielding a frequency domain spectrum in which each peak represents the Larmor frequency of a distinct nucleus (Figure 2.5).

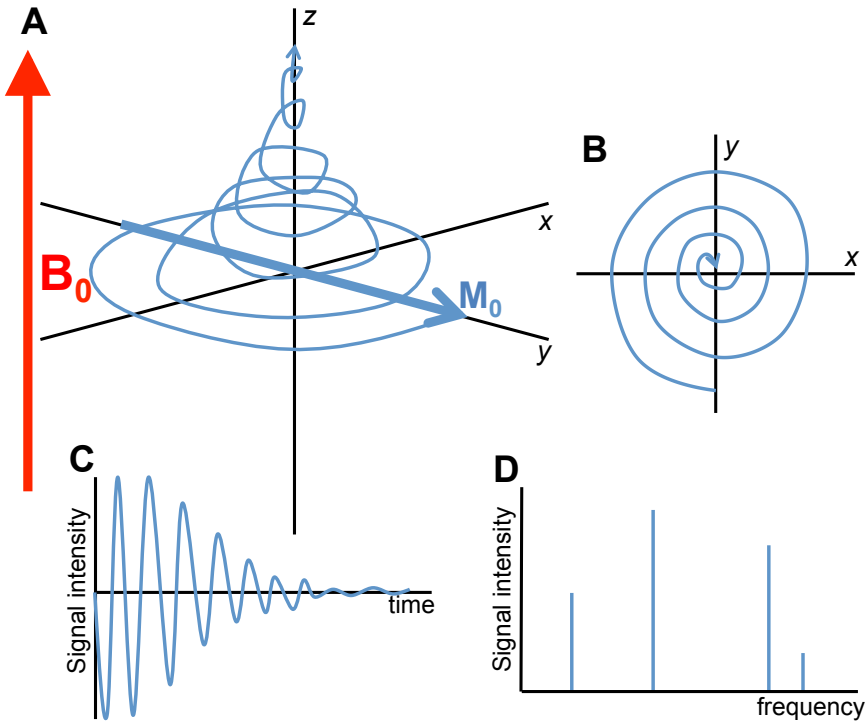

Figure 2.5: Relaxation of net magnetisation M_0 towards the z axis (A) results in a signal of decaying intensity in the xy plane (B). Plotting signal decay with respect to time yields the FID (C), and Fourier transformation of this results in a frequency spectrum (D) in which each peak describes a nucleus with a distinct Larmor frequency, ω_0.

2.9.4 Chemical Shift

Each NMR-active nucleus within the magnetic field acts as an electromagnet in its own right. This means that each nucleus imposes its own local magnetic field, which may oppose the applied field B_0. Nuclei within electropositive groups are shielded from the magnetic field; the frequencies of these nuclei are lower (Equation 2.4) than expected. Conversely, nuclei within electronegative groups are deshielded and experience a greater level of magnetisation than expected, with corresponding higher frequencies. The exact magnetic field of each nucleus is different, so each nucleus has a different precession frequency. Frequencies are described with reference to the frequency of a chosen standard, usually 4,4-dimethyl-4-silapentane-1-sulfonic acid when protons are studied in aqueous solution. The low electronegativity of the Si results in the nine methyl protons adopting identical, very upfield, Larmor frequencies.

Frequencies of studied protons are normalised with respect to this standard frequency, and with respect to the field strength of the NMR spectrometer, by Equation 2.5:

$$\delta_{ppm} = \frac{\omega_0 - \omega_{ref}}{\omega_{ref}} \times 10^6 \tag{2.5}$$

where ω_{ref} is the Larmor frequency of the methyl protons in 4,4-dimethyl-4-silapentane-1-sulfonic acid, in this case.

The chemical shifts of nuclei within a sample are descriptive of the chemical structures within that sample. A disperse set of chemical shifts indicates that nuclei within the sample experience a number of different chemical environments. A spectrum such as this might indicate, for example, that a protein of interest has adopted a range of secondary structure motifs, providing a range of chemical environments for nuclei. In an unstructured or aggregated protein, a narrower range of chemical environments is available to nuclei, and a less disperse set of chemical shifts would be expected in the NMR spectrum.

In NMR spectra acquired of samples containing many NMR-active nuclei, for instance ^{1}H NMR spectra acquired of large biomolecules such as proteins, it is often impossible to distinguish between NMR signals arising from each nucleus individually; NMR

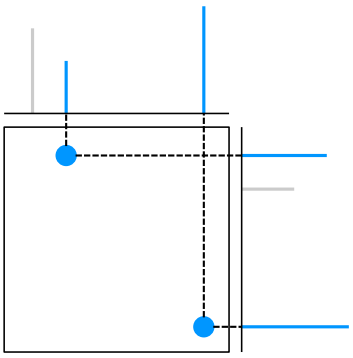

Figure 2.6: A 2D NMR experiment correlating signals from two 1D spectra. Crosspeaks resolve when an NMR signal in one spectrum correlates with a signal in a second spectrum; uncorrelated signals (shown in grey) are lost.

signals overlap, particularly those arising from nuclei in similar chemica environments, and cannot be resolved. In these circumstances, two-dimensional NMR spectrometry is often utilised. In 2D NMR, signals from two 1D NMR spectra are correlated; these signals are resolved as crosspeaks in a 2-dimensional spectrum (Figure 2.6). An example of this is **To**tal **C**orrelation **S**pectroscop**y** (TOCSY), in which the signal arising from nucleus A correlates with signals arising from nuclei to which nucleus A is covalently bound; another is **N**uclear **O**verhauser **E**ffect **S**pectroscop**y** (NOESY), in which which the signal arising from nucleus A correlates with signals arising from nuclei within approximately 5 Å of nucleus A. Strategic use of 2D NMR experiments can facilitate full assignment of all NMR signals arising from nuclei within a large biomolecule, even when the 1D spectrum is crowded.

2.9.5 ^{1}H 1D NMR Experiments

All NMR experiments were conducted at 298 K on a 700 MHz Bruker Avance spectrometer equipped with a cryoprobe, housed at the University of Warwick. Recorded spectra were referenced to residual water.

200 μL samples of 1 mM synthetic peptide or glycopeptide antibiotic were prepared in 25 mM sodium phosphate buffer (pH 6.8), 25 mM NaCl, 10% D_2O. Water suppression was achieved using the WATERGATE method (Liu et al., 1998). Spectra were acquired of 32k complex data points in 64 scans. Data were zero-filled to 64k and processed using a squared sine window function.

2.9.6 ^{1}H Saturation Transfer Difference NMR Experiments

Saturation transfer difference (STD) NMR is a solution-state NMR method for the study of protein-ligand interactions. STD NMR is especially well-suited to interactions between small ligands and large proteins, because NMR signals from protons in larger molecules (*e.g.* proteins >40 kDa) will tend to be broader and less intense than those from smaller molecules. This is because the chemical shift of a proton depends on its environment, which is anisotropic; the observable chemical shift of a nucleus therefore changes depending on the orientation of the nucleus with respect to the magnetic field of the NMR spectrometer (Rule and Hitchens, 2006). For small molecules, this is not a problem. Due to Brownian motion, small molecules in solution "tumble" at a rate that is sufficiently fast that every orientation with respect to the magnetic field is occupied in a very short space of time. These anisotropic chemical shifts therefore cancel one another out, leaving only the isotropic chemical shifts to be recorded. This results in a high signal:noise ratio for smaller molecules.

As the size of a molecule increases, the benefits of tumbling are reduced. Larger molecules tumble more slowly, so that all possible orientations with respect to the magnetic field are not occupied within the necessary timeframe. This means that NMR signals from large molecules will tend to be broad, with a poor signal:noise ratio.

STD NMR takes advantage of this difference in signal intensity, allowing one to

preferentially observe the signals of a small molecule (*i.e.* a ligand) as it binds to a large molecule (a protein) in a sample containing both components. The low-intensity signals from the large protein are selectively irradiated by a saturation pulse. Over time, this irradiation spreads throughout the entire protein. This irradiation can also spread, via the nuclear Overhauser effect, to protons that are within 5 Å of the protein. If a ligand molecule is bound to a protein, protons on the ligand that come within 5 Å of the protein will become irradiated (Viegas et al., 2011). As the ligand molecule dissociates from the protein, it carries this saturation with it, and protons that have come into close proximity of the protein will display signal attenuation in a ^{1}H 1D spectrum. This approach is illustrated in Figure 2.7.

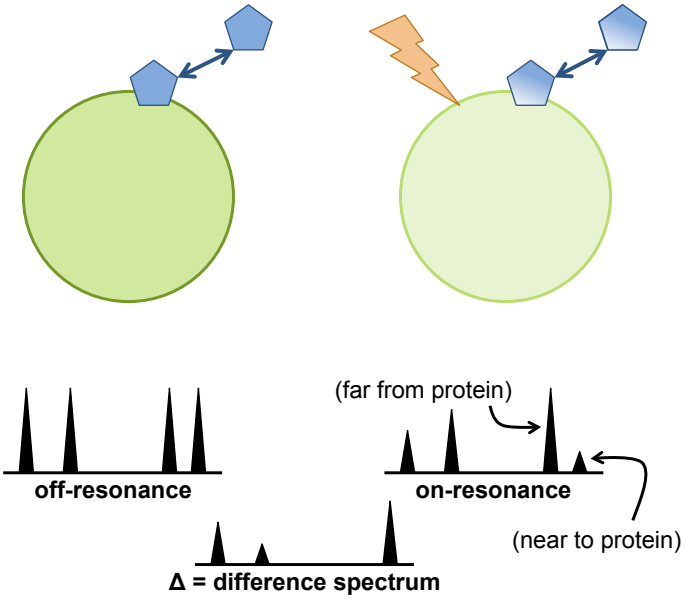

Figure 2.7: Protons in the receptor (green) are irradiated by a selective saturation pulse (orange) which does not directly irradiate protons in the ligand (blue). If binding occurs, saturation transfers through the nuclear Overhauser effect, resulting in proximity-dependent irradiation of protons in the ligand. Adapted from Viegas et al. (2011).

The ^{1}H spectrum acquired for a mixed sample of protein and ligand, in which protons in the protein are selectively saturated, is called the "on-resonance" spectrum. In STD-NMR, the on-resonance spectrum is subtracted from a ^{1}H spectrum in which a saturation pulse is applied at a frequency far from any protons in the sample (the "off-resonance"

spectrum). Subtraction yields a 1D difference spectrum in which "signal intensity" is proportional to the level of signal attenuation of a proton, due to the accumulation of saturation from the protein (Figure 2.8). By comparing the saturation transfer difference spectrum to an assigned ^{1}H 1D spectrum of the ligand, protons physically close to the protein at the time of a binding event may be identified. The relative proximity of individual protons in the ligand to the protein may be assessed by normalising signal intensities in the difference spectrum with respect to signal intensities in the off-resonance spectrum.

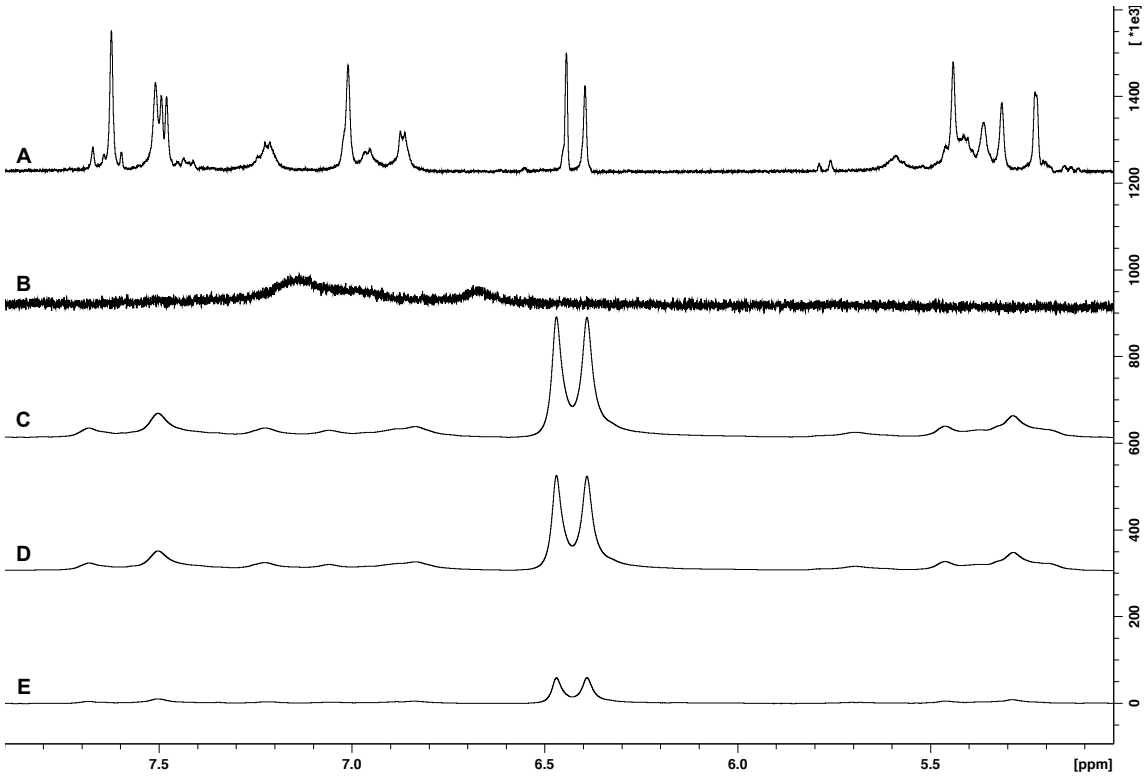

Figure 2.8: ^{1}H 1D NMR spectra, each recorded at 298 K in 25 mM sodium phosphate buffer (pD 6.8), 25 mM NaCl, 100% D_2O. **A**, 1 mM vancomycin hydrochloride; **B**, 10 μM His_6-$VanS_{SC}$ with expected broad and low-intensity peaks; **C**, off-resonance spectrum of 10 μM His_6-$VanS_{SC}$ and 4 mM vancomycin hydrochloride, with a saturation pulse applied at 40 ppm; **D**, on-resonance spectrum as in C, with saturation applied at -2 ppm saturating His_6-$VanS_{SC}$; **E**, the difference spectrum resulting in subtraction of **D** from **C**. Relative signal intensity is manually reduced in **A** and increased in **B** to allow peaks to be visualised concurrently; relative signal intensity is consistent between spectra **C**, **D** and *E*. The presence of peaks in **E** corresponding to protons in vancomycin indicates saturation transfer to vancomycin from His_6-$VanS_{SC}$.

300 μL samples of 10 μM VanS were prepared in 25 mM sodium phosphate buffer (pD 6.8), 25 mM NaCl, 1.15 mM LMPG, 100% D_2O. A concentrated stock of appropriate ligand was prepared in the same buffer lacking detergent, and two dilutions of this stock were also prepared so that appropriate titrations could be made. As ligand was titrated in, the concentration of VanS in the sample was recalculated to account for dilution. Ligand was titrated into the protein sample from the prepared stock solutions in order to achieve, as closely as possible, ligand:protein ratios of 0.5, 1, 2, 5, 10, 20, 50, 100, 200, and 400.

At each titration point, a pseudo-2D STD-NMR experiment was executed, consisting of four ^{1}H 1D spectra. Spectra were acquired with 4 increments in the t_1 dimension and 32k data points in the t_2 dimension, as 16 loops of 8 scans, with on- and off-resonance spectra acquired in an interleaved fashion. The spectral width was 14 ppm in t_2 and 2 ppm in t_1. Water suppression was achieved using excitation sculpting (Hwang and Shaka, 1995). Data were zero-filled to 64k in t_2 and processed using an exponential multiplication window function and quadratic baseline correction in t_2, and sine window function and linear baseline correction in t_1.

An off-resonance frequency of 40 ppm (24718 Hz) was used for all STD-NMR experiments. A range of on-resonance frequencies was trialed for each ligand; for vancomycin, an on-resonance frequency of -2 ppm (-4692 Hz) was selected. For the lipid II pentapeptide, an on-resonance frequency of -1.2 ppm (-4131 Hz) was selected.

Once a 100-fold molar excess of ligand was reached, a series of experiments were run in which the saturation time ranged between 0.5 and 5 s. This allows for the binding epitope of the ligand to be mapped, as ligand protons spatially proximal to the protein will experience more extreme signal attenuation as saturation time increases. Titration of ligand was then resumed until a 400-fold molar excess was achieved.

The dissociation constant (K_D) for the interaction between a protein and its ligand may be estimated from STD data by comparing the signal intensities of ligand protons in on- and off-resonance spectra. For each proton, on- and off-resonance signal intensities are measured at each titration point, for which accurate ligand and protein concentrations

are known. We designate these I_{sat} and I_0, respectively. The extent to which a signal is attentuated is calculated by subtracting I_{sat} from I_0, as in Equation 2.6:

$$I_{STD} = I_0 - I_{sat} \tag{2.6}$$

This value is then normalised using Equation 2.7, with respect to the off-resonance signal intensity, and the ligand and protein concentrations of the sample, to give an STD amplification factor (A_{STD}) by which signal attentuation at different titration points may be compared.

$$A_{STD} = \frac{I_{STD}}{I_0} \times \frac{[L]}{[P]} \tag{2.7}$$

A_{STD} may then be plotted against ligand:protein ratio (EL; molar excess of ligand), giving a curve resembling a Michaelis Menten saturation curve, from which the dissociation constant may straightforwardly be estimated (Viegas et al., 2011).

2.9.7 Diffusion Ordered Spectroscopy

In DOSY spectra, pulsed field gradients of equal magnitude and opposite sign are used to spatially encode and decode signals from protons within the sample on either side of a diffusion delay time. The intensity of signals from protons that diffuse quickly along the length of the sample will be attenuated, while the intensity of signals from slowly diffusing protons will not. In this way, integration of signals from every resolvable proton in a sample can be used to calculate individual tracer diffusion coefficients for that proton. Averaging the diffusion coefficients for protons within one molecule provides an estimate of the diffusion coefficient for the entire molecule or assembly. Larger molecules exhibit smaller diffusion coefficients as they tumble more slowly in solution and thus have slower correlation times than smaller molecules.

2.9.8 ^{1}H 2D NMR Experiments

200 μL samples of 1 mM synthetic peptide or glycopeptide antibiotic were prepared in 25 mM sodium phosphate buffer (pH 6.8), 25 mM NaCl, 10% D_2O. Spectra were acquired with 256 data points in the t_1 dimension and 8k data points in the t_2 dimension, with 64 scans. Water suppression was achieved using excitation sculpting (Hwang and Shaka, 1995). The spectral width was 14 ppm in both dimensions. Data were zero-filled to 16k in t_2 and 512 in t_1 processed using a Gaussian multiplication window function in t_2 and shifted sine window function in t_1, and quadratic baseline corrections in both dimensions.

In TOCSY experiments, the pulse program dipsi2esgpph was used, with 40, 80, and 140 ms mixing times.

In NOESY experiments, the pulse program noesyesgpph was used, with 40, 80, and 140 ms mixing times.

Chapter 3

Expression, Purification and Preliminary Characterisation of VanS From *Streptomyces coelicolor* and *Enterococcus faecium*

3.1 Introduction

In recent years at the University of Warwick, significant time and resources have been invested in the study of full-length VanS proteins by either solution-state NMR or X-ray crystallography. VanS is an approximately 45 kDa, integral membrane protein understood to dimerise when active; significant difficulties have been noted in the expression and purification of these proteins, particularly to the high concentrations required for study by these techniques. It was decided that alternative approaches should be considered, particularly with respect to the final required concentration of protein for any investigation. Techniques were identified in which low concentrations of protein were preferable, and alternative approaches to the structural characterisation of the extracellular domain of VanS were considered. Proteins were then expressed and purified into conditions amenable to investigation by these techniques. To validate these experiments, the structural integrity of the proteins under these new conditions had first to be confirmed.

VanS is an integral membrane protein, the function of which is to detect the presence of vancomycin (and similar antibiotics) in the environment and initiate a process leading to the expression of resistance genes which allow the bacterial cell to survive antibiotic exposure. Induction is regulated by VanR, a cytosolic protein which when phosphorylated, selectively binds the promoter to the *vanHAX* operon with a 500-fold greater affinity than unphosphorylated VanR (Holman et al., 1994), leading to transcription of *van* genes.

Phosphorylation of VanR is regulated by VanS, which is capable of both kinase and phosphatase activity (Wright et al., 1993). In its capacity as a kinase, VanS undergoes autophosphorylation in its cytosolic domain in an ATP-dependent manner before transferring this phosphoryl group to VanR (Figure 3.1).

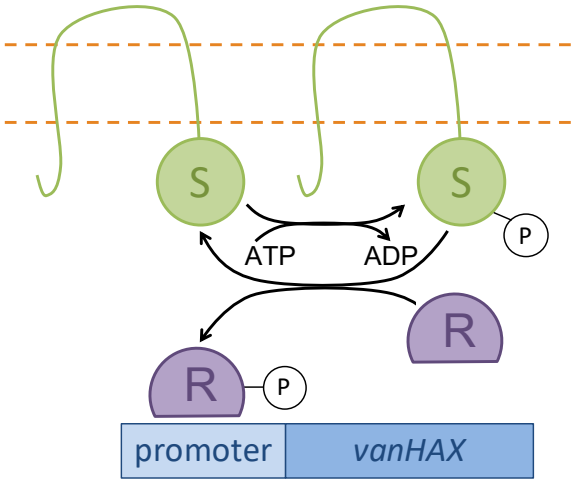

Figure 3.1: Schematic outlining the autophosphorylation and kinase activities of the receptor histidine kinase, VanS. Phosphorylation of VanR increases its binding affinity for the *vanHAX* promoter region 500-fold.

Though the process by which vancomycin resistance is induced is generally well-characterised, the mechanism of activation of VanS has yet to be elucidated. One complicating factor is that VanS proteins from different species are responsive to different antibiotics (Table 1.2). B-type VanS is sensitive to vancomycin, but insensitive to moenomycin and teicoplanin. This suggests that the ligand to $VanS_B$ may be vancomycin itself. However, A-type VanS is sensitive to all three of these antibiotics (Baptista et al., 1996), suggesting the ligand may be a downstream product of antibiotic activity such as bacterial cell wall degradation products. Comparison of the amino acid sequences of A-type and B-type VanS supports the hypothesis that the two proteins may respond to different ligands (Table 1.2); there is little sequence homology in the putative ligand binding sites (extracellular loop domains) of VanS from *Enterococcus faecium* ($VanS_A$) and *Enterococcus faecalis* ($VanS_B$) (Hong et al., 2008). Vancomycin is a glycopeptide originally derived from Actinomycetes, and several species within this order display resistance to vancomycin which may be described as B-type-like. Though VanS from actinomycetes display significant sequence homology, this is not true for the putative ligand binding sites (Hong et al., 2008).

Questions remain in this area of antibiotic resistance, because direct observation of ligand binding has never been achieved for VanS of any type; it is therefore desirable that VanS proteins exhibiting a range of sensitivities should be studied in order that further data describing their ligand binding profiles may be gathered.

In this study, VanS from *Enterococcus faecium* ($VanS_A$) and *Streptomyces coelicolor* ($VanS_{SC}$; a B-type-like VanS from an actinomycete) were selected for study. They are both represented in the literature (Hutchings et al., 2006; Hughes et al., 2017), their antibiotic sensitivities are established, and they have previously been demonstrated to be constitutively active in detergent micelles (Edwards, 2014). To investigate the ligand-binding characteristics of these two proteins, they were heterologously expressed in *E. coli*, extracted from bacterial cell membranes into an appropriate membrane mimetic, and purified by appropriate chromatography techniques. The folds and specific activities of each protein will be invesigated, to determine whether their native folds have been maintained over the course of extraction and purification.

VanS autophosphorylation is constitutive. An appropriate activity assay was used to provide an indication of the condition of the protein under experimental conditions. An ADP-release assay will be utilised in this study to assess the condition of heterologously expressed VanS in detergent micelles, prior to further study of the protein by solution-state NMR to investigate its ligand-binding characteristics.

3.2 Aims

1. To express $VanS_A$ and $VanS_{SC}$ in *E. coli* in such a way that it is inserted into the bacterial cell membrane in a manner that maintains the proteins' native fold;

2. To efficiently solubilise $VanS_A$ and $VanS_{SC}$ into appropriate membrane mimetics, such that a sufficient yield of protein is achieved after solubilisation;

3. To obtain pure, natively folded and active $VanS_A$ and $VanS_{SC}$ after purification by immobilised ion affinity chromatography and size exclusion chromatography;

4. To demonstrate the constitutive activity and appropriate fold of $VanS_A$ and $VanS_{SC}$ through the use of an ADP release kinase activity assay, and circular dichroism spectroscopy.

3.3 Heterologous Overexpression of VanS in *E. coli*

Previous work by Dr Richard Edwards (2014) indicated that expression of His_6-$VanS_A$ from the pProEx::His_6-$VanS_A$ plasmid could be achieved in the C41 (DE3) pRIL cell line. His_6-$VanS_A$ was overexpressed in this cell line as described in Section 2.3.1. Following purification by immobilised ion affinity chromatography (Section 2.3.5), an average protein yield of 1.4 mg His_6-$VanS_A$ per litre of cell culture was obtained.

Attempts to express His_6-$VanS_{SC}$ from the pProEx::His_6-$VanS_{SC}$ plasmid in the C41 (DE3) pRIL cell line under the conditions optimised for His_6-$VanS_A$ were unsuccessful. A trial was performed comparing His_6-$VanS_{SC}$ expression in C41 (DE3) pRIL, BL21 (DE3), and BL21 (DE3) Star.pRosetta cell lines (Section 2.1.4). Competent cells were transformed with the pProEx::His_6-$VanS_{SC}$ plasmid and starter cultures were grown overnight at 37 °C and 180 rpm. LB was innoculated with these starter cultures and incubated at 37 °C and 180 rpm to an optical density at 600 nm (OD_{600}) of 0.6. Expression of His_6-$VanS_{SC}$ was induced with 0.1, 0.5, and 1 mM IPTG, and cultures were incubated overnight at 16 and 37 °C. The results of this trial are shown in Figure 3.2, a Western blot testing for the presence

of a His_6-tagged protein of appropriate size in the cell lysates; expression of His_6-$VanS_{SC}$ was only observed in BL21 (DE3) Star.pRosetta cells incubated overnight at 16 °C. Protein yield did not vary noticeably with respect to IPTG concentration; a concentration of 0.2 mM IPTG was selected, to align more closely with the His_6-$VanS_A$ expression protocol.

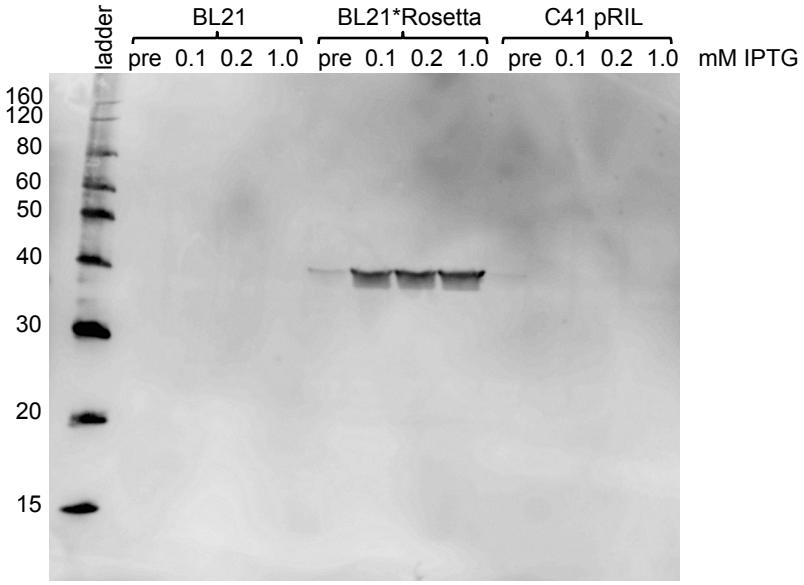

Figure 3.2: Western blot probing for the presence of His_6. Samples of cell culture acquired immediately before, and 12 hours after induction with varying concentrations of IPTG are compared. Expression of His_6-$VanS_{SC}$, a 42 kDa protein, is observed in the BL21 (DE3) Star.pRosetta cell line following overnight incubation at 16 °C, with no obvious difference in yield with respect to IPTG concentration.

3.4 Selection of an Appropriate Buffering System

Initial work by Dr Richard Edwards (2014) demonstrated that His_6-$VanS_A$ is soluble in DPC detergent micelles and may be purified by immobilised metal ion affinity chromatography (IMAC) in 20 mM HEPES buffer, pH 7.8. However, HEPES buffer is known to absorb circularly polarised light strongly at 180-200 nm (Kelly et al. (2005)) and is therefore not suitable for CD spectroscopy. Sodium phosphate is readily available, buffers in the pH range 5.7 - 8.0, similar to HEPES' pH range of 6.8 - 8.2, and is not known to be problematic for either CD or NMR. Sodium phosphate buffer was therefore selected as an appropriate buffer for CD and NMR experiments.

In selection of a buffer pH, consideration is given to the theoretical isoelectric point (pI) of the protein - the pH at which the protein has a net neutral charge and is least soluble - and to the biological relevance of the selected pH. The theoretical pI of $VanS_A$ is 5.7 (Gasteiger et al., 2005), so a buffer pH of 6.8 was selected in the first instance to support solubility of the protein. Later, the same pH was utilised in the purification of $VanS_{SC}$, though this protein has a theoretical pI of 7.2. The protein was observed to be soluble at pH 6.8 (Figure 3.6), so this pH was maintained throughout the study in order to maintain consistency between results obtained for the two proteins.

3.5 Solubilisation of VanS from *E. coli* Cell Membranes into Detergent Micelles

Membrane proteins are embedded in native cell membranes; complex mixtures of lipids and other hydrophobic molecules which form large raft-like structures and impede analysis of the proteins. It is therefore sometimes necessary to extract membrane proteins from their native environment, to facilitate their study by solution-phase methods.

Membrane proteins were solubilised from their native membranes by exposure to high concentrations of detergents. Detergents are amphipathic molecules, with a polar head group and a single non-polar tail, similar in structure to lipids (which typically have two non-polar tails). By virtue of this single tail, a detergent molecule can be approximately considered to be conical in shape, while lipid molecules are approximately cylindrical (Figure 3.3). While lipids pack into flat layers (e.g. cell membranes, lipid vesicles), detergents pack into small spheres, known as micelles, with the polar head groups on the surface and the single lipid tails contained within.

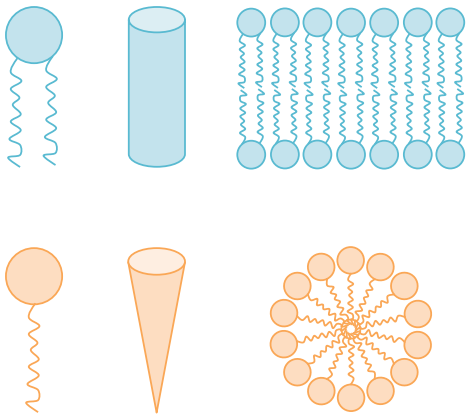

Figure 3.3: Schematic illustrating the basic 3-dimensional shapes of lipids (blue) and detergents (orange). Detergents, having only one non-polar tail, are approximately conical, and pack into spherical micelles with the non-polar tails shielded within a polar shell. Lipids, with two non-polar tails, are approximately cylindrical, and typically pack into bilayers.

Micelles form when the concentration of detergent is above the detergent's critical micellar concentration (CMC), a value which varies for each detergent depending on conditions such as temperature and pH. The number of detergent molecules that will assemble into a micelle - the aggregation number - also varies with respect to these conditions. The number of micelles in a detergent solution can be approximated using Equation 3.1:

$$[\text{micelle}] = \frac{[\text{detergent}] - \text{CMC}}{\text{aggregation number}} \tag{3.1}$$

The qualities of a detergent can lead it to be well-suited to one biophysical technique, and incompatible with another. Therefore it was necessary to screen a wide range of detergents for their ability to solubilise and support the native fold of VanS during purification, in order to identify a number of detergents which may be utilised in different experiments. Previous work by Dr Richard Edwards (2014) indicated that His_6-$VanS_A$ is highly soluble in DPC detergent micelles. However, this detergent is not ideal for saturation transfer difference (STD) NMR experiments due to its relatively high CMC, resulting in a high concentration of detergent monomers in solution. It was desirable to identify a detergent of low CMC into which His_6-$VanS_A$ is similarly soluble.

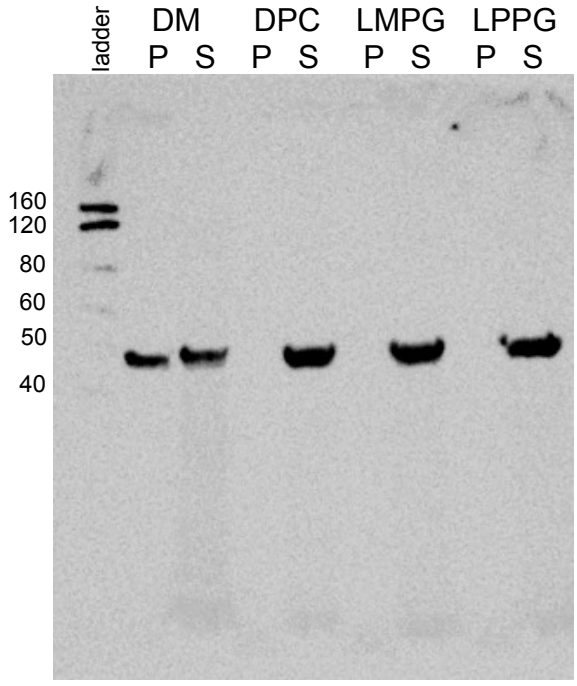

Figure 3.4: Western blot probing for His_6, comparing pellets (P) and supernatants (S) following incubation of cell membranes with various detergents. His_6-$VanS_A$ is highly soluble in DPC, LMPG, and LPPG, but only partially solubilised by DM.

To screen the solubility of His_6-$VanS_A$ in a range of detergents with low CMC, 2

mL samples of cell membranes containing His_6-$VanS_A$, suspended in sodium phosphate buffer as described in 2.3.2, were incubated with 2% (w/v) *n*-decyl-β-D-maltopyranoside (DM, CMC 0.13 mM; Chung et al. (2012)), *n*-dodecylphosphocholine (DPC, CMC 1.5 mM; Patel (2012)), 1-myristoyl-2-hydroxy-*sn*-glycero-3-phospho-(1'-rac-glycerol) (LMPG, CMC 0.21 mM; Yildiz et al. (2013)), and 1-palmitoyl-2-hydroxy-*sn*-glycero-3-phospho-(1'-rac-glycerol) (LPPG, CMC 0.018 mM; Stafford et al. (1989)) for 2 hours at 4 °C. This concentration of detergent was selected because when screening detergents for membrane protein solubility, it is important that a large excess of detergent is provided so that solubility is not limited by the availability of micelles. 1% or 2% (w/v) detergent is common (Drew et al., 2006). The samples were then centrifuged at 60,000 × g, 4 °C, for 40 minutes to pellet the cell membranes. Membrane pellets were resuspended in buffer, and the relative amounts of His_6-$VanS_A$ in the membrane pellet and supernatant (*i.e.* solubilised in detergent micelles) were assessed by Western blot (Figure 3.4). The solubility of His_6-$VanS_A$ in LMPG and LPPG was found to be similar to that in DPC. In consideration of detergent cost and availability, LMPG was selected as a low-CMC detergent appropriate for STD-NMR experiments.

Once an appropriate low-CMC detergent had been identified, in the interest of cost, it was preferable to reduce the concentration of detergent used when solubilising proteins from cell membranes. 2% (w/v) LMPG is equivalent to 42 mM detergent, and 759 μM micelles (Yildiz et al., 2013; Sigalov and Hendricks, 2009). 2% DPC is equivalent to 57 mM detergent, and 792 μM micelles (Patel, 2012). 10 mM DPC was demonstrated by Edwards (2014) to be sufficient to solubilise VanS from membranes; this is equivalent to 120 μM micelles. 120 μM LMPG micelles, *i.e.* 6.7 mM detergent, was found to be sufficient to solubilise membrane proteins without resulting in a loss of yield of His_6-$VanS_A$.

3.6 Purification of VanS by Immobilised Metal Ion Affinity Chromatography

His_6-$VanS_A$ was solubilised from prepared *E. coli* bacterial membranes in 10 mM DPC or 6.7 mM LMPG, and purified in 2 mM DPC or 1.15 mM LMPG as described in Section 2.3.5. Protease inhibitors were excluded from the elution buffer, to facilitate assaying of protein concentration in these samples. The majority of His_6-$VanS_A$ was observed to elute in fractions E2 and E3 (Figure 3.5). These two fractions were pooled, concentrated and exchanged into appropriate buffers for further analysis as described in Section 2.4.

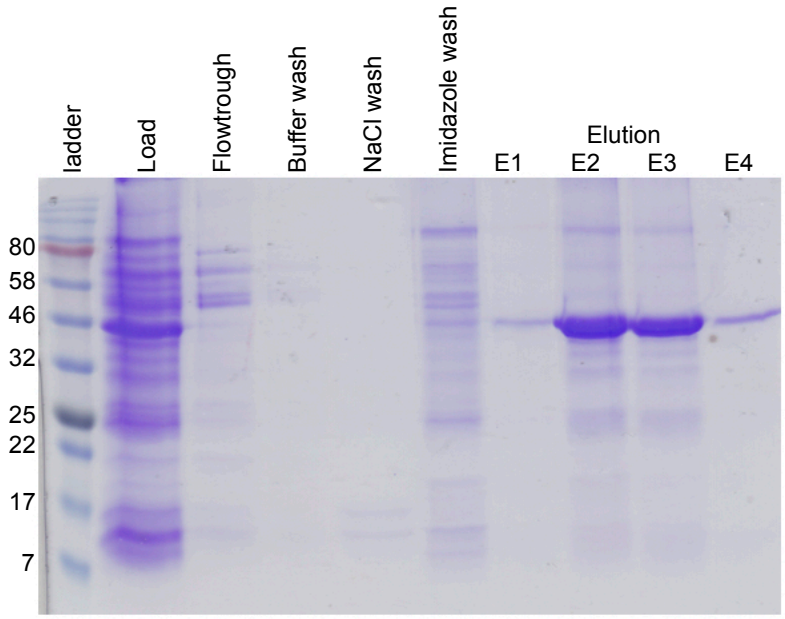

Figure 3.5: Coomassie-stained polyacrylamide gel. His_6-$VanS_A$ is solubilised from 1 litre of *E. coli* cell membranes into 10 mM DPC, and purified in 2 mM DPC as described in 2.3.5. Eluate fractions E2 and E3 contain the majority of the target protein; these fractions are pooled, concentrated, and exchanged into appropriate buffers for later experiments as described in Section 2.4.

His_6-$VanS_{SC}$ was solubilised and purified as described above, but significant degradation of the target protein was observed after elution (Figure 3.6). This degradation was not observed when protease inhibitors were included in the elution buffer, suggesting the presence of a protease which co-elutes from the IMAC column along with $VanS_{SC}$. The issue of

degradation was resolved by the inclusion of 2 μM leupeptin and pepstatin protease inhibitors throughout IMAC purification, and the addition of a size exclusion chromatography purification step to remove this contaminant protease (Figure 3.8).

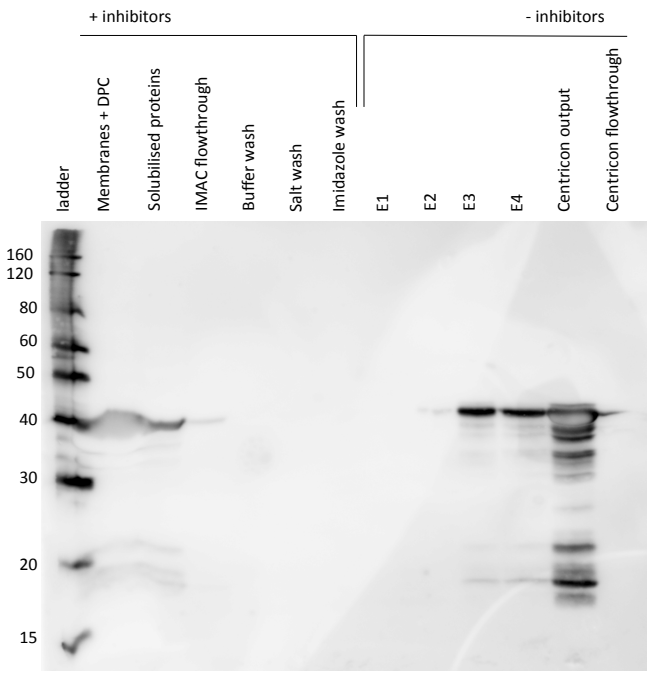

Figure 3.6: Western blot probing for His_6. His_6-$VanS_{SC}$ is solubilised from 1 litre of *E. coli* cell membranes into 10 mM DPC, and purified in 2 mM DPC as described in 2.3.5. Eluate fractions E3 and E4 contain the majority of the target protein; these fractions are pooled and concentrated, at which point degradation of the target protein is observed. This is later avoided by the inclusion of protease inhibitors leupeptin and pepstatin (both 2 μM) in IMAC elution buffers, and the addition of a size exclusion chromatography step to remove a contaminant protease.

3.7 Purification of VanS by Size Exclusion Chromatography

His_6-$VanS_{SC}$ IMAC eluates 3 and 4 (Figure 3.6) were pooled and concentrated to a volume of 200 μL and loaded onto a Superdex 200 Increase 10/300 GL gel filtration column (GE Healthcare Life Sciences, Pittsburgh USA) equilibrated in wash buffer lacking protease inhibitors. Proteins were eluted from the column in the same buffer, at 4 °C at a flow rate of 0.5 mL min^{-1}.

Superdex 200 gel filtration resin has a fractionation range of 10 to 600 kDa; His_6-$VanS_{SC}$ is 41.8 kDa and the molecular weight of an LMPG micelle is approximately 26.3 kDa (mw 478.23, aggregation number 55 (Sigalov and Hendricks (2009))), giving the LMPG-solubilised target protein an effective molecular weight of 68.1 kDa. Protein was observed to elute after approximately 10 mL of buffer had been applied to the column (Figure 3.7). The eluate was collected in 2 mL fractions and analysed by Western blot (Figure 3.8).

The target protein was observed in fraction 2. Degradation products are visible in the sample which was applied to the column, but do not appear in the eluted fractions. Further degradation is not observed following purification by size exclusion chromatography, allowing for the safe removal of protease inhibitors from purified protein samples. Following solubilisation, IMAC, and size exclusion chromatography steps, a typical yield for His_6-$VanS_{SC}$ was 10 μg protein per litre of expression culture.

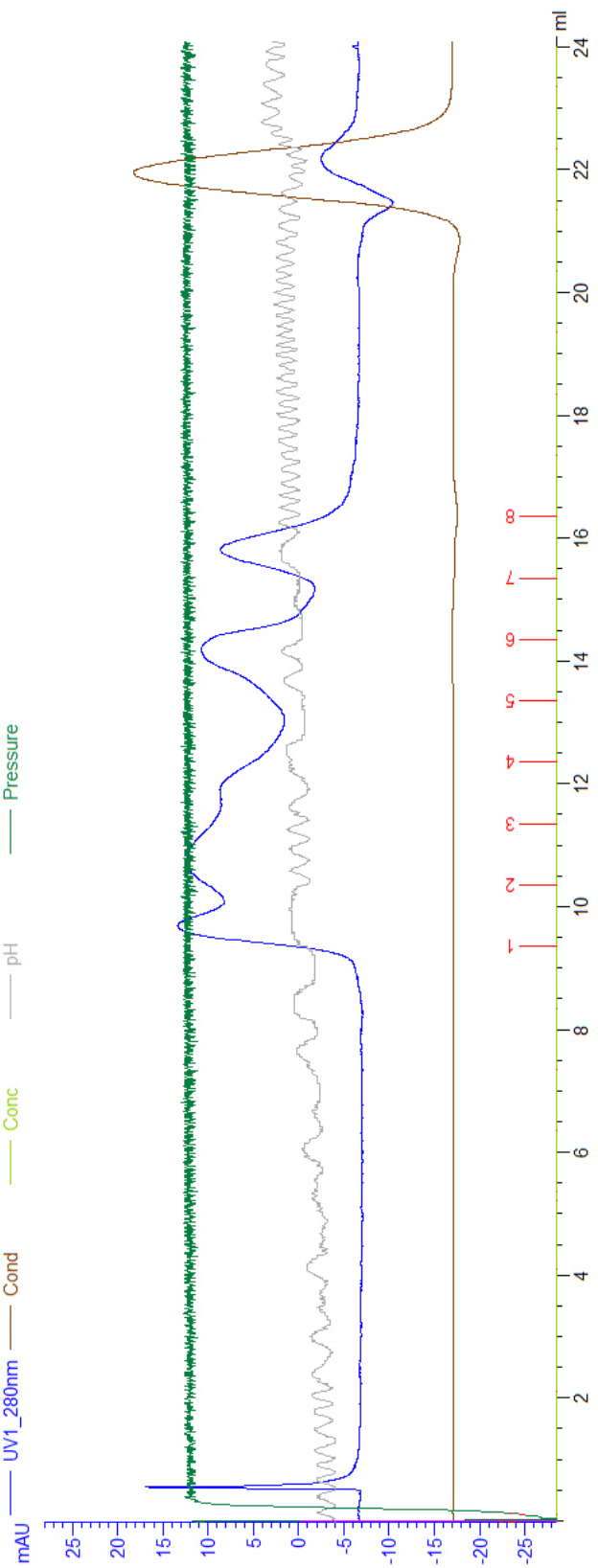

Figure 3.7: FPLC chromatogram showing absorbance at 280 nm (blue) as proteins are eluted from a Superdex 200 Increase 10/300 GL gel filtration column. His_6-$VanS_{SC}$ IMAC eluate was pooled, concentrated, applied to and eluted from the column to remove a contaminant protease. Fractions 1-8 were analysed by SDS-PAGE and Western blot, and VanS found in Fraction 2 (Figure 3.8).

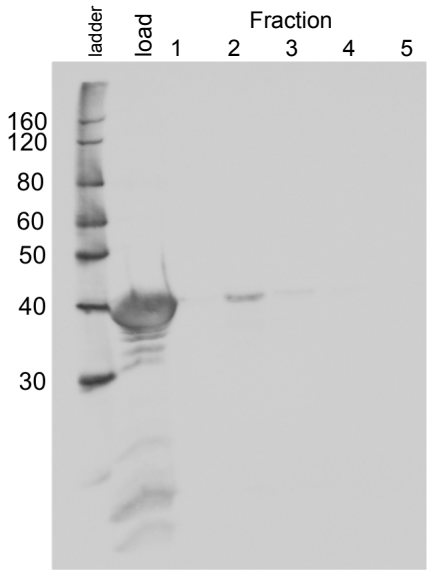

Figure 3.8: Western blot probing for His_6. His_6-$VanS_{SC}$ was observed only in size exclusion chromatography fraction 2. Degradation of the protein is seen in the sample loaded onto the column, but not in eluted fractions.

3.8 Analysis of Secondary Structure by Circular Dichroism (CD) Spectroscopy

CD spectra were acquired from His_6-$VanS_A$ and His_6-$VanS_{SC}$ (Figure 3.9) in 25 mM sodium phosphate buffer (pH 6.8), 25 mM NaCl, and either 2 mM DPC or 1.15 mM LMPG. Circular dichroism data were recorded in millidegrees and converted to mean residue elipticity as described in Section 2.7. Converted data files were processed as described in Section 2.7. His_6-$VanS_A$ was estimated to be 36% α-helical, with 17% β-strands and 20% turns in 1.15 mM LMPG (NRMSD = 0.047), and 38% α-helical, with 14% β-strands and 20% turns in 2 mM DPC (NRMSD = 0.021). His_6-$VanS_{SC}$ was estimated to be 18% α-helical, 32% β-strand, and 25% turns in 1.15 mM LMPG (NRMSD = 0.013), and 52% α-helical, with 18% β-strands and 10% turns in 2 mM DPC (NRMSD = 0.009).

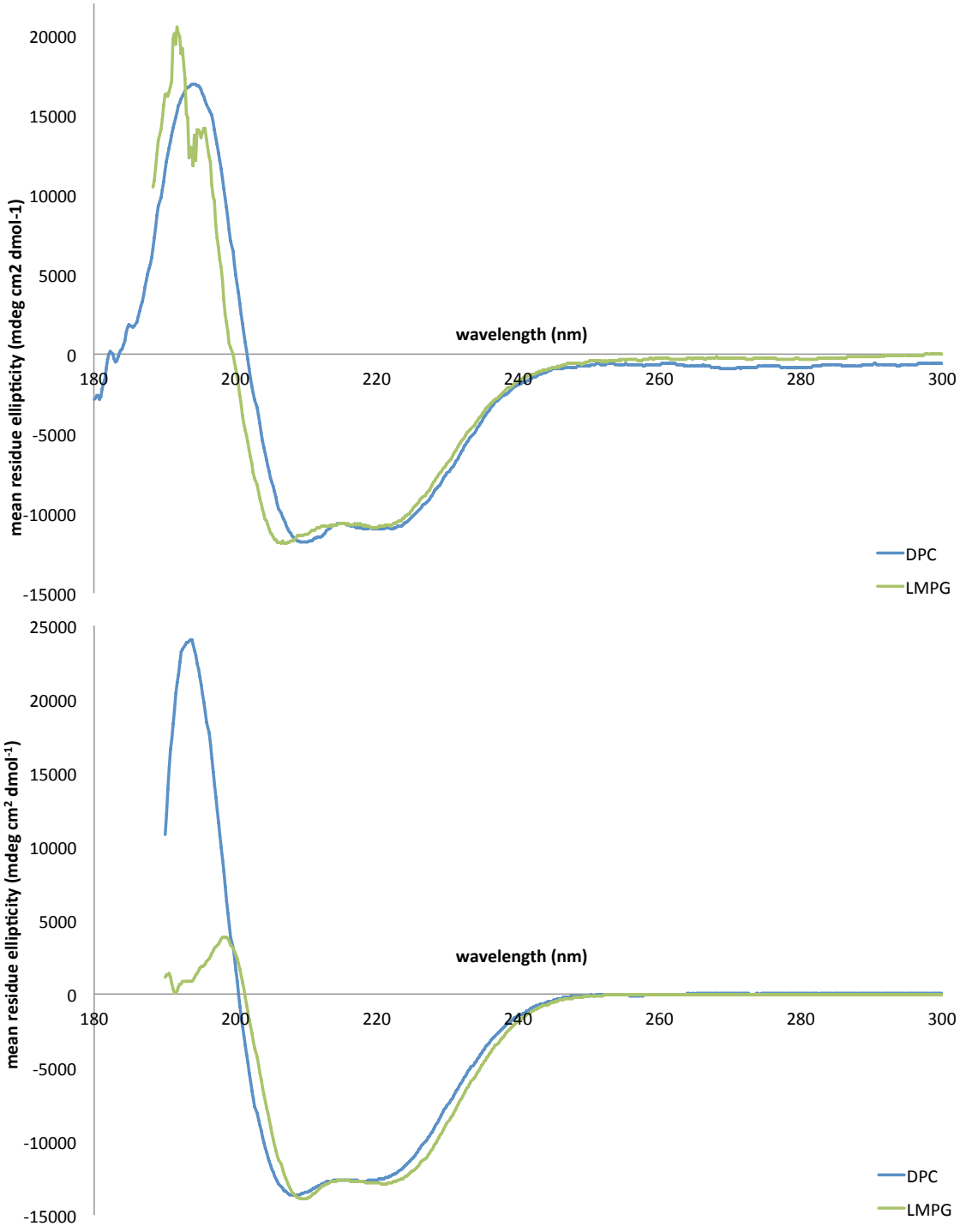

Figure 3.9: CD spectra of His_6-$VanS_A$ (top) and His_6-$VanS_{SC}$ (bottom) in 25 mM sodium phosphate buffer (pH 6.8), 25 mM NaCl, and 2 mM DPC (blue) or 1.15 mM LMPG (green). Visual assessment of the spectra suggest that both proteins adopt similar conformations in either detergent.

When acquiring data for both His$_6$-VanS$_{SC}$ and His$_6$-VanS$_A$, the presence of LMPG in the sample caused high tension to exceed 600 V at low wavelengths. Where high tension exceeds 600 V, the signal:noise ratio is typically deemed too low to be reliable, so data is truncated to prevent interference of the noise in structural calculations. In the His$_6$-VanS$_A$ spectrum, truncation at 190 nm was sufficient to remove data acquired when high tension exceeded 600 V; however, high tension exceeded this level in the His$_6$-VanS$_{SC}$ dataset at 200 nm. Analysis by CDSSTR requires a dataset at least covering the range 190-240 nm, so data in the range 190-200 nm had to be included although the signal:noise ratio is problematic.

In His$_6$-VanS$_A$, estimated % helicities in DPC and LMPG are in good agreement with one another. In His$_6$-VanS$_{SC}$, estimated % helicities are significantly different. In LMPG, HT(V) exceeded 600 at 200 nm, so the positive peak expected at 190 nm was not resolved. The loss of this peak appears to have caused an underestimation in % helicity of His$_6$-VanS$_{SC}$ in LMPG micelles. Above 200 nm, CD data acquired of His$_6$-VanS$_{SC}$ in DPC and LMPG look quite similar.

The Sequence Annotated by Structure (SAS) tool of EMBL-EBI (Milburn et al., 1998) was used to predict the percentage helicity of His$_6$-VanS$_A$ and His$_6$-VanS$_{SC}$ from their amino acid sequences. The tool uses FASTA alignment to compare inputted amino acid sequences against the sequences of all proteins of known structure in the Protein Data Bank. The tool estimates that His$_6$-VanS$_A$ is 42% helical, and that His$_6$-VanS$_{SC}$ is 36% helical, when properly folded. There is good agreement between the SAS prediction and the CDSSTR analyses for His$_6$-VanS$_A$ in both detergents, but poor agreement for His$_6$-VanS$_{SC}$; the SAS prediction suggests that CDSSTR significantly overestimates % helicity of His$_6$-VanS$_{SC}$ in DPC, and underestimates in LMPG. The loss of the positive peak at 190 nm may explain the underestimation of helicity in LMPG; the source of the error in DPC is unclear.

As a further analysis of secondary structure, the maximum helical content of each protein was calculated from mean residue molar ellipticity at 222 nm (Ysselstein et al., 2015). This method offers an alternative interpretation of CD measurements, relying only

on recorded ellipticity at a single wavelength. Mean residue molar ellipticity (θ_{MR}) is calculated from circular dichroism in millidegrees (θ), using Equation 3.2:

$$\theta_{MR} = \frac{\theta}{10 \times C \times N_A \times l} \tag{3.2}$$

where C is the protein concentration in M, N_A is the residue length of the protein, and l is the pathlength in cm. % helicity is then calculated using Equation 3.3:

$$H = 100\% \times \frac{\theta - \theta_{coil}}{\theta_\alpha - \theta_{coil}} \tag{3.3}$$

where

$$\theta_\alpha = -40000(1 - 2.5/N_A) + 100t$$

and

$$\theta_{coil} = 640 - 45t,$$

and t is temperature (25 °C for these experiments).

Using this method, His_6-$VanS_A$ is estimated to be 29% helical in DPC, and 31% helical in LMPG; lower estimates than those given by CDSSTR, and further from the prediction provided by SAS. However, this method estimates the helicity of His_6-$VanS_{SC}$ in DPC as 32%, and in LMPG as 36%, much closer to the value predicted by SAS.

Since the method for estimating maximal helical content from ellipticity at 222 nm takes only a fraction of the gathered data into account, it is a simpler method of estimating helicity. This presents both benefits and drawbacks; the method does not take into account ellipticity at 190 nm, so high HT(V) at lower wavelengths does not pose a problem. However, errors at 222 nm cannot be accommodated by reference to other datapoints.

High tension exceeded 600 V in CD data of His_6-$VanS_A$ only in the range 180-190 nm. Truncation of the dataset left sufficient data for CDSSTR to perfom analysis of the secondary structure of the protein in DPC and LMPG micelles. Estimated helicity of His_6-$VanS_A$ in both DPC (38%) and LMPG (36%) agrees well with the predicted % helicity from

SAS (42%).

High tension exceeded 600 V below 200 nm in data acquired of His_6-$VanS_{SC}$ in LMPG; CDSSTR requires data in the range 190 to 240 nm, so truncation of the data could not be completed. CDSSTR struggled to analyse CD data of His_6-$VanS_{SC}$ in LMPG, likely leading to underestimation of % helicity. CDSSTR apparently overestimates % helicity of His_6-$VanS_{SC}$ in DPC, although the source of this error is unclear. Estimation of % helicity from mean residue molar ellipticity at 222 nm gives estimates of 32% in DPC, and 36% in LMPG, in close agreement with the predicted value of 36% helicity from SAS. It is likely therefore that His_6-$VanS_{SC}$ is also correctly folded in these detergents.

3.9 Measuring the Specific Activity of Autophosphorylation in VanS with an ADP Release Assay

The ADP release assay (Figure 3.10) is a coupled enzymatic assay popularly used to assay the specific activities of kinases (Wampler and Westhead, 1968). During phosphorylation, a phosphate group is transferred from ATP to the target protein (*i.e.* VanS), resulting in the release of an ADP molecule. ADP is a substrate for the enzyme pyruvate kinase (PK), which transfers a phosphate group from phosphoenol pyruvate (PEK) to this free ADP, producing ATP and pyruvate. Pyruvate, in turn, is converted to lactate by the enzyme lactate dehydrogenase (LDH), which also catalyses the oxidation of NADH to NAD+. The conversion of NADH to NAD+ may be measured spectrophotomerically, as NADH absorbs light at 340 nm while NAD+ does not. Therefore, the release of ADP may be measured by proxy, through the change in absorbance at 340 nm. A reduction in absorbance indicates an increase in concentration of ADP, and thus the autophosphorylation of VanS.

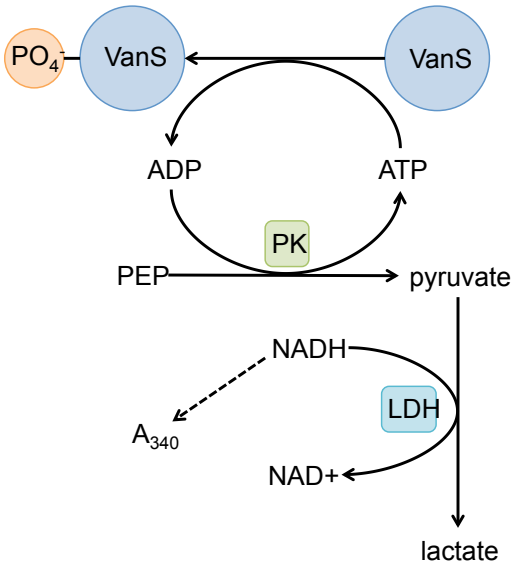

Figure 3.10: Schematic breakdown of reactions taking place during a continuous ADP release assay; also shown in Figure 2.2. The target protein VanS undergoes autophosphorylation, releasing ADP to which another phosphate group is transferred by pyruvate kinase (PK). This results in the conversion of phosphoenol pyruvate (PEP) to pyruvate. Lactate dehydrogenase (LDH) catalyses the oxidation of NADH to NAD+, converting pyruvate to lactate. The concentration of NADH can be measured spectrophotomerically at 340 nm; a reduction in absorbance at this wavelength corresponds to an increase in ADP concentration, and thus indicates autophosphorylation by VanS.

Autophosphorylation of VanS_A has been observed by this method in dodecylmaltoside (DM) (Quigley, 2010). Autophosphorylation of both VanS_A and VanS_{SC} has also been observed in DPC micelles (Edwards, 2014).

STD-NMR experiments were conducted in LMPG micelles, as this detergent has a low CMC resulting in a lower concentration of detergent monomers in solution. It was desirable therefore to assay VanS activity in this detergent. Assays were carried out as described in Section 2.8. Stock solutions of VanS were diluted in order that for the first minute of the assay, the change in absorbance over time was linear. Gradients of these lines were then determined, and initial rates of reaction were calculated. In 1.15 mM LMPG, His_6-$VanS_A$ was found to have a specific activity of 3.0 μmol mg^{-1} min^{-1}, and His_6-$VanS_{SC}$ was found to have a specific activity of 8.0 μmol mg^{-1} min^{-1} (Figure 3.11).

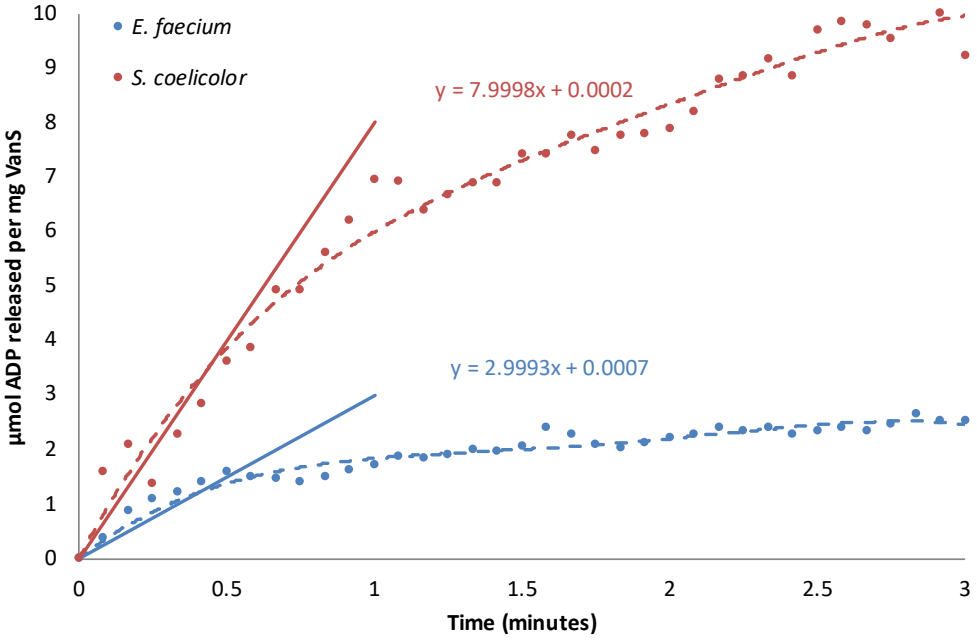

Figure 3.11: Turnover of ADP by His_6-$VanS_A$ (blue) and His_6-$VanS_{SC}$ (red) over the course of a 3 minute continuous photometric kinase activity assay. μmol ADP released is estimated from the chance in absorbance of the solution at 240 nm, caused by the conversion of NADH to NAD+. The specific activities of His_6-$VanS_A$ and His_6-$VanS_{SC}$ in 1.15 mM LMPG are calculated respectively as 3.0 and 8.0 μmol ADP released per mg VanS per minute.

While the constitutive autophosphorylation activity of VanS has been demonstrated in the literature and has been assayed under various conditions to confirm the native fold of the protein, the rate of autophosphorylation of VanS has not yet been discussed in the literature in terms of *specific activity*. It is therefore difficult to make comparisons

between the specific activities of VanS reported here, and qualitative findings of VanS activity reported in the literature. However, the specific activities of a number of kinase enzymes have been reported in the literature, ranging from as low as 1 to as high as 59 μmol ADP released per mg enzyme per minute (Wampler and Westhead, 1968). The calculated specific activities of His_6-$VanS_A$ and His_6-$VanS_{SC}$ (3 and 8 μmol ADP per mg enzyme per minute, respectively) fall safely within this range, towards the lower end of the spectrum. This may be due to the constitutive nature of VanS autophosphorylation; in the absence of vancomycin, VanS is expressed at low levels and exhibits both autokinase activity, and phosphatase activity against VanR (Hutchings et al., 2006). The presence of vancomycin induces VanS kinase activity against VanR, leading to upregulation of *van* genes and vancomycin resistance. VanS kinase activity is the "switch" which induces antibiotic resistance; autokinase activity is constitutive and may occur at relatively low levels in the absence of vancomycin.

3.10 Discussion

3.10.1 Overexpression of VanS in *E. coli*, and Solubilisation into Detergent Micelles

The expression of His_6-$VanS_A$ was achieved through the utilisation of a protocol optimised by Richard Edwards (2014); expression of His_6-$VanS_{SC}$ was achieved following an expression trial to screen conditions including cell line, incubation temperature, and IPTG concentration. BL21 (DE3) pStar.Rosetta was identified as an appropriate cell line in which to express His_6-$VanS_{SC}$, following overnight incubation at 16 °C with 200 μM IPTG.

A solubility trial identified LMPG and LPPG as low-CMC detergents capable of solubilising VanS from isolated *E. coli* cell membranes. Another low-CMC detergent, DM, was determined to be less efficient in solubilising VanS. A low-CMC detergent was desirable for STD-NMR experiments, to minimise the concentration of monomeric detergent in solution.

3.10.2 Purification of VanS

His_6-$VanS_A$ and His_6-$VanS_{SC}$ were purified by immobilised metal ion affinity chromatography (IMAC). Following purification, protease inhibitors which interfere with the BCA concentration assay were removed from protein samples. Removal of these inhibitors resulted in degradation of His_6-$VanS_{SC}$, suggesting the presence of a contaminant protease.

To avoid degradation, inhibitors were left in His_6-$VanS_{SC}$ samples following IMAC purification, and a further purification step by size-exclusion chromatography was added to remove the contaminant protease. Following purification by size exclusion chromatography, protease inhibitors could be removed from His_6-$VanS_{SC}$ samples without protein degradation occurring.

The addition of a size exclusion chromatography purification step negatively impacted the purification yield of His_6-$VanS_{SC}$; as protease inhibitors could not be removed from samples of IMAC-purified His_6-$VanS_{SC}$, it was not possible to quantify the protein yield at this point. However, visual analysis of equivalent SDS-PAGE gels indicates that

the concentration of His_6-$VanS_{SC}$ in IMAC eluates was perhaps half of the concentration of His_6-$VanS_A$; this would suggest a yield of approximately 0.7 mg His_6-$VanS_{SC}$ per litre of cell culture. Following size exclusion chromatography, protease inhibitors could be removed and protein concentration could be measured by BCA assay; the protein yield at this point was approximately 0.01 mg per litre of cell culture, less than 10% of the yield of His_6-$VanS_A$ following IMAC purification.

To improve the yield of His_6-$VanS_{SC}$, it may be desirable to investigate alternative purification methods. Since the contaminant protease co-elutes from the IMAC column, alternative affinity tags could be explored by which $VanS_{SC}$ could be purified without the use of an IMAC column. Other chromatography techniques, for instance ion exchange chromatography, might separate His_6-$VanS_{SC}$ from the contaminant protease while retaining more of the target protein than was achieved by size exclusion chromatography.

3.10.3 Analysis of VanS Secondary Structure by CD Spectroscopy

The secondary structures of the proteins were assessed by circular dichroism spectroscopy. The presence of LMPG detergent resulted in a high signal:noise ratio in the 180-200 nm region for both proteins, but more significantly in data acquired of His_6-$VanS_{SC}$. Ellipticity data with high signal:noise were truncated where possible, but CDSSTR requires data at least in the range 190-240 nm, so the 190-200 nm region of the His_6-$VanS_{SC}$:LMPG dataset could not be discarded. This caused CDSSTR to underestimate the % helicity of His_6-$VanS_{SC}$ in LMPG.

The Sequence Annotated by Structure (SAS) tool of EMBL-EBI (Milburn et al., 1998) was used to predict the secondary structures of His_6-$VanS_A$ and His_6-$VanS_{SC}$ from their amino acid sequences, giving predictions of 42% and 36%, respectively. CDSSTR analysis of His_6-$VanS_A$ in DPC and LMPG estimated % helicities of 38% in DPC, and 36% in LMPG, in good agreement with the SAS prediction. CDSSTR analysis of His_6-$VanS_{SC}$ in DPC and LMPG estimated helicities of 52% in DPC, and 18% in LMPG, respectively. CDSSTR appears to overestimate % helicity in DPC, and underestimate % helicity in

LMPG.

% helicity of His_6-$VanS_{SC}$ in DPC and LMPG was estimated from acquired data using the mean residue molar ellipticity at 222 nm (Ysselstein et al., 2015). Using this method, % helicity of His_6-$VanS_{SC}$ was estimated as 32% in DPC, and 36% in LMPG, in good agreement with the SAS prediction of 36%.

3.10.4 Assaying The Specific Activity of VanS Autophosphorylation

VanS is a receptor histidine kinase exhibiting constitutive autophosphorylation activity (Hutchings et al., 2006). When properly folded and active, this activity may be measured through the use of an appropriate kinase activity assay.

A range of techniques have previously been used to measure VanS autophosphorylation. Wright et al. (1993) expressed and purified a fusion protein of maltose binding protein (MBP) and the cytosolic domain of $VanS_A$ (residues 95-374), incubated this fusion protein with [γ-^{32}P]-ATP, and examined the protein by SDS-PAGE to investigate the exchange of labelled phosphate from ATP to the protein. Transfer of the labelled phosphate group from ATP to the fusion protein was observed, and the initial rate of reaction found to be first-order with respect to ATP concentration.

Similarly, Hutchings et al. (2006) expressed and purified the cytosolic domain of $VanS_{SC}$ (residues 85-364) with incorporated polyhistidine tag, without a large fusion protein to enhance solubility. A similar [γ-^{32}P]-ATP transfer assay was performed, and autophosphorylation of cytosolic $VanS_{SC}$ was observed under these conditions.

Radiolabelling is a popular method by which kinase activity may be assayed, and attempts were made to assay autophosphorylation of full-length VanS by this method. Andrew Quigley (2010) observed autophosphorylation of cytosolic truncates of $VanS_A$ by this method, but could not observe autophosphorylation of full-length $VanS_A$ purified in detergent micelles. However, an alternative kinase activity assay monitoring ADP release did allow autophosphorylation of full-length VanS in DM detergent micelles to be measured. This assay was also employed by Richard Edwards (2014) to measure the activity of $VanS_A$

and VanS$_{SC}$ in DM and DPC detergent micelles.

Autophosphorylation activity of full-length VanS has been measured through another spectrophotometric assay, a phosphate release assay, by Hughes et al. (2017). However, as this assay measures the concentration of inorganic phosphate in solution, it is incompatible with sodium phosphate buffers and therefore could not be explored in this work.

The ADP release assay was utilised to investigate the constitutive autophosphorylation activity of VanS in LMPG micelles. Both His$_6$-VanS$_A$ and His$_6$-VanS$_{SC}$ were observed to be constitutively active in this mimetic, with specific activities or 3.0 and 8.0 μmol ADP released per mg VanS per minute, respectively. These rates are within the range of 1 to 59 μmol ADP per mg enzyme per minute reported in the literature (Wampler and Westhead, 1968). Both His$_6$-VanS$_A$ and His$_6$-VanS$_{SC}$ were therefore found to be appropriately folded and active in LMPG, and suitable for further study by solution-state NMR.

Chapter 4

Analysis of Protein-Ligand Interactions by Affinity Chromatography

4.1 Introduction

Affinity chromatography is an important technique in biochemistry which allows the separation of a protein from a mixture, depending on the tendency of that protein to interact with a particular ligand (Hage, 1999). Affinity chromatography is frequently used as a tool to purify proteins; the target protein is expressed with an attached affinity tag, such as hexahistidine or maltose binding protein, and the specific ligand to which the tag displays an affinity (metal ions or amylose respectively, in these examples) is bound to a resin such as Sepharose. A mixture of proteins in solution, such as a cell lysate, is exposed to the resin, and the target protein is selectively retained due to the interaction between the affinity tag and the specific ligand. Unbound proteins are washed away, and the target protein is eluted from the resin through application of some complimentary material in solution (imidazole or maltose, here), which competes either with the affinity tag or with the ligand to disrupt the interaction and allow the bound protein to dissociate from the resin.

Affinity chromatography may also be used as an analytical technique. By exposing a mixture of proteins to a likely ligand, proteins within the mixture with an affinity for that ligand may be identified. Roy et al. (2001) used affinity chromatography to analyse proteins solubilised from *E. coli* cell membranes. A putrescine linker was attached to the C-terminus of a semisynthetic vancomycin derivative, and this linker was coupled to *N*-hydroxysuccinimide (NHS)-activated Sepharose 4B. This resulted in a sepharose-based resin with a covalently bound vancomycin derivative as a putative ligand to *E. coli* membrane proteins. Proteins solubilised into Triton X-100 from *E. coli* membranes were applied to this resin, and several were observed to bind to the vancomycin derivative.

Construction of a vancomycin affinity column by this technique presents some difficulties, including the chemical modification of vancomycin to facilitate binding to the sepharose resin, and the cost of NHS-activated Sepharose 4B. Proteins were eluted from the resin by the application of free vancomycin, representing a further significant cost.

Vancomycin is known to interact with copper (Pfeiffer, 1981) and zinc ions (Zarkan et al., 2016). The region of vancomycin involved in these interactions is shown in Figure 4.1 (From Zn^{2+} binding studies conducted by Zarkan et al. (2016); consistent with Kucharczyk et al. (2008) who identify three nitrogens in this region as being involved in Cu^{2+} binding); the metal ion affinity of vancomycin involves the N-terminus of the peptide component, rather than the C-terminus utilised by Roy et al. (2001). Since metal ion affinity columns are cheap and readily available, and may be recharged with a number of different metal ions, this represents an alternative route by which vancomycin might be incorporated into a chromatography column (Figure 4.2).

If a protein interacts with a region of vancomycin which is occluded in the process of attaching the molecule to a chromatography resin (*i.e.* the C-terminus following covalent binding as outlined by Roy et al. (2001), or the N-terminus following interaction with metal ions) then interactions between the protein and this region of the antibiotic might not be observed. These two approaches could therefore be used in tandem to investigate interactions between proteins and vancomycin in two orientations, so that interactions blocked in one experimental setup might be observed in the other (Figure 4.2, inset).

If vancomycin is bound to a metal ion affinity column, and proteins are then to be applied to this column to investigate their affinity for vancomycin, then it is essential that these proteins should not also display an affinity for metal ions. Specifically, the ligand-binding characteristics of VanS are the focus of this study. It was therefore necessary to express and purify VanS without a hexahistidine affinity tag. An alternative affinity tag must be inserted into the plasmid by site-directed mutagenesis, removing the existing hexahistidine tag in the process. Because it is small, relatively polar, does not require that the protein be exposed to harsh conditions during purification, and is therefore judged to

be unlikely to interfere with the fold of VanS or to occlude itself within a detergent micelle, the StrepII tag (sequence WSHPQFEK; Section 2.1.2) was selected for substitution into His_6-$VanS_A$ (Lichty et al., 2005).

Following successful purification of StrepII-$VanS_A$ by StrepTactin affinity chromatography, the affinity of this protein for metal ions - particularly Cu^{2+} - must be assessed by metal ion affinity chromatography prior to exposure to the vancomycin-copper affinity column. Interactions between StrepII-$VanS_A$ and vancomycin may then be investigated by sequential application of vancomycin and StrepII-$VanS_A$ to the Cu^{2+} affinity column, elution by the application of imidazole, and analysis of eluates by SDS-PAGE.

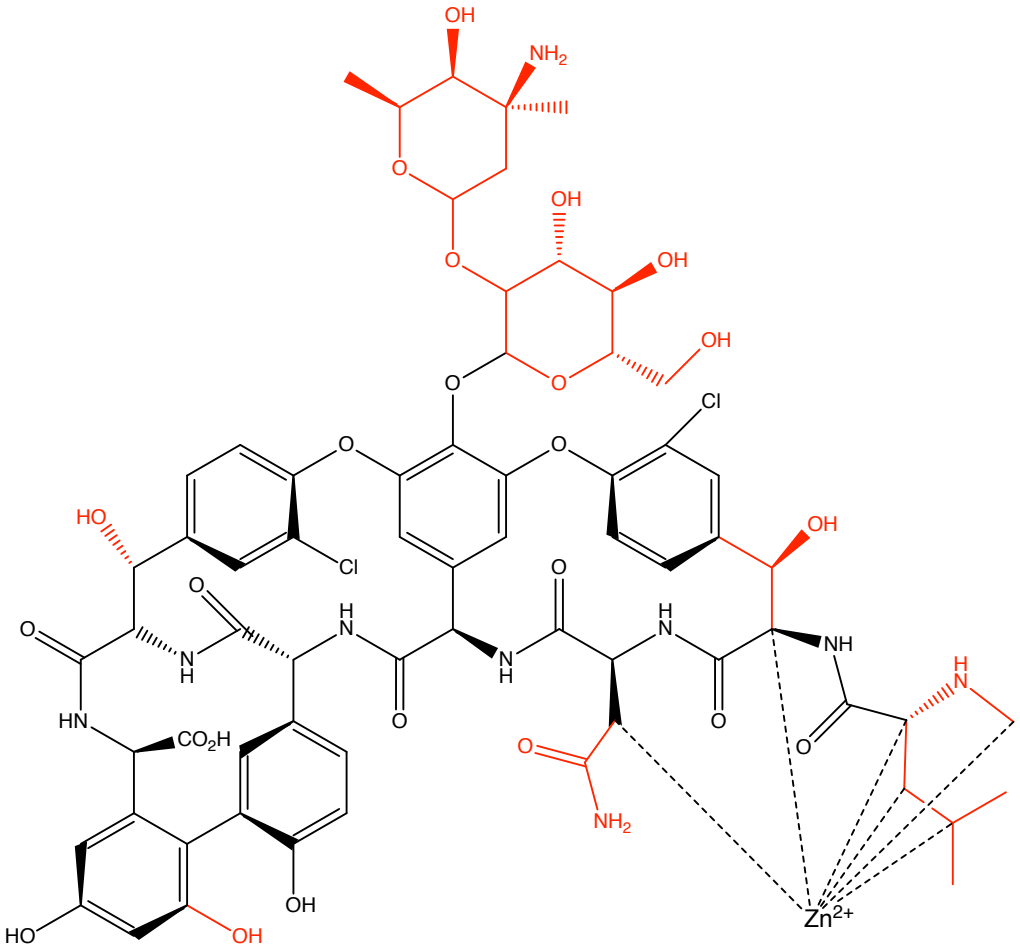

Figure 4.1: Adapted from Zarkan et al. (2016). The chemical structure of vancomycin. Regions conserved between vancomycin and teicoplanin are shown in black; regions unique to vancomycin are highlighted in red. Zarkan et al. (2016) used ^{1}H NMR to analyse the interaction between vancomycin and Zn^{2+}; protons whose chemical environments are altered by Zn^{2+} binding are indicated. The C-terminus of the peptide component, utilised by Roy et al. (2001) to link vancomycin to a Sepharose resin, is shown in the lower-left of the diagram.

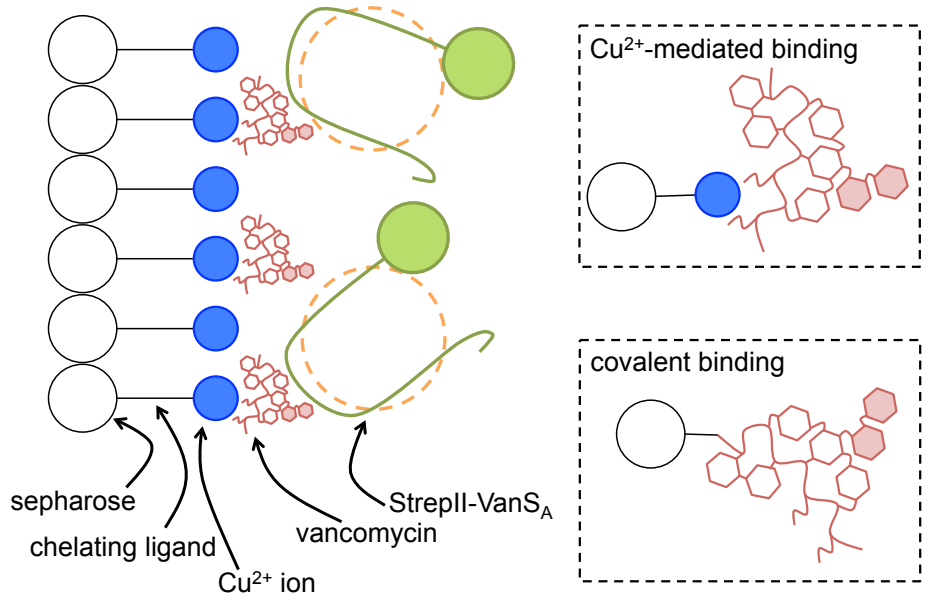

Figure 4.2: A schematic outlining the structure of a Cu^{2+}-mediated vancomycin affinity column. A commercial rechargable sepharose resin (HisTrap FF, GE Healthcare, Illinois) is charged with Cu^{2+} ions (blue), to which vancomycin (red) reversibly binds. Proteins with an affinity for vancomycin will be retained by the resin when applied to the column. Vancomycin, and interacting proteins, are co-eluted with the application of imidazole to the column. Inset: construction of a vancomycin resin via metal ion affinity, and via a covalent linker (Roy et al., 2001), expose different regions of the molecule to proteins in solution. A combination of both approaches would allow a more thorough investigations of interactions between proteins and vancomycin.

4.2 Aims

1. To construct a vancomycin affinity column by reversibly but stably binding vancomycin to a metal ion affinity chromatography column;
2. To replace the existing hexahistidine tag on His_6-$VanS_A$ with an appropriate alternative affinity tag;
3. To optimise the expression and purification of $VanS_A$ without a hexahistidine tag;
4. To confirm that $VanS_A$ lacking a hexahistidine tag possesses no intrinsic metal ion affinity;
5. To apply the modified $VanS_A$ to the vancomycin affinity column and investigate whether an interaction between VanS and vancomycin results in retention of the protein in the column.

4.3 Constructing a Vancomycin Affinity Column

To generate the vancomycin affinity column, a 1 mL prepacked HisTrap FF metal ion affinity column (GE Healthcare, Illinois) was stripped and recharged with Cu^{2+} as per manufacturer's instructions. A pH of 7.4 was maintained throughout the experiment, as this is recommended in the HisTrap user manual and consistent with the buffer requirements for StrepTag purification. 20 mM sodium phosphate buffer (pH 7.4) was prepared and used as a wash buffer, and 50 mM imidazole was added to this to prepare an elution buffer. Buffers were applied to the column at a flowrate of 2 mL min^{-1} using a P1 peristaltic pump. Outputs from the column were collected in 1 mL fractions, and the absorbance at 282 nm (A_{282}) of each fraction was measured. The peptide backbone of proteins absorbs light at this wavelength, so an increase in absorbance indicates the presence of protein in solution.

The process of binding and eluting vancomycin to the Cu^{2+} ion affinity column is outlined in Figure 4.3. The column was first equilibrated with 5 mL wash buffer. Then, to

establish the A_{282} of the elution buffer, and to confirm that this is not affected by passage through the column (for instance, by the accumulation of Cu^{2+} ions picked up from the column), 5 mL elution buffer was applied to the column. The column was then washed with a further 10 mL wash buffer. 150 μL 10 mM vancomycin HCl dissolved in wash buffer was then applied to the column, illustrated by a dashed black line in Figure 4.3, and the column was washed with a further 24 mL wash buffer. A large peak in absorbance was observed as unbound vancomycin was washed from the column. When A_{282} was observed to stabilise, elution buffer was applied to elute bound vancomycin. A smaller peak in absorbance is observed before A_{282} stabilises again, indicating that bound vancomycin has been eluted from the column.

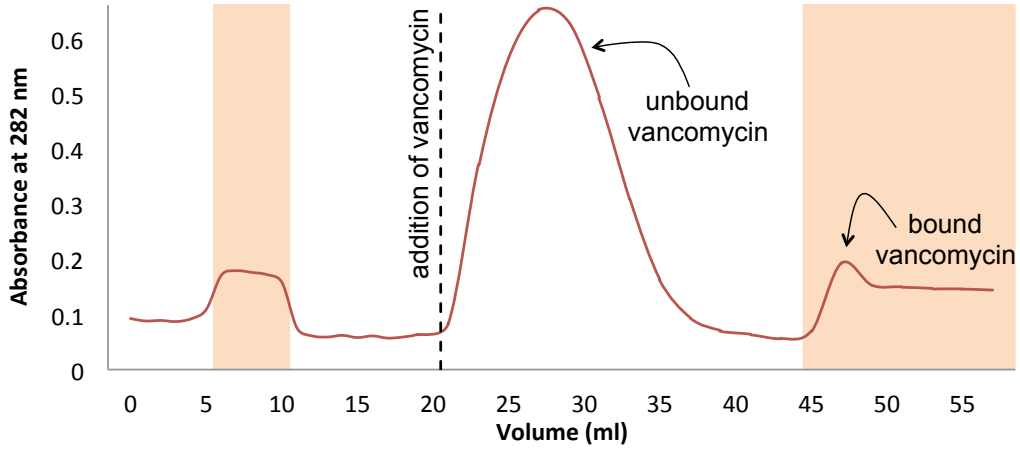

Figure 4.3: Absorbance at 282 nm (A_{282}) of 1 mL fractions collected from a HisTrap FF 1 mL prepacked column, stripped and recharged with Cu^{2+} ions. Orange shading indicates the application of 50 mM imidazole to the column; the black vertical line indicates the point at which 150 μL 10 mM vancomycin was applied to the column. A large peak in absorbance following application of vancomycin represents unbound vancomycin being washed from the column. A smaller peak following application of imidazole represents the elution of bound vancomycin.

4.4 Cloning to generate a StrepII-VanS$_A$ expression construct

A pProEx HTa plasmid encoding full-length VanS$_A$ with N-terminal His$_6$ tags was kindly provided by Dr Richard Edwards. This plasmid encodes a hexahistidine (His$_6$) tag and TEV protease cleavage site fused to the N-terminus of VanS.

In order to conduct experiments using a vancomycin affinity column, the His$_6$ tag must be removed and replaced with an alternative affinity tag that would not confer metal ion affinity to the target protein. The ideal replacement affinity tag would not embed in the bacterial membrane or mimetic, or interfere with the native fold of the protein. The tag must also not require exposing the protein to a suboptimal environment in order to achieve purification. For instance, a penta-arginine (R$_5$) tag requires pH >8.0 for purification (Terpe, 2002), which is outside the buffering range of sodium phosphate buffer and not ideal for solution-state NMR studies. The affinity tag StrepII, which confers affinity for streptavidin, was selected for its short length of 8 amino acids, and its mild purification conditions (Lichty et al., 2005).

The StrepII tag was inserted in place of the His$_6$ tag by site-directed mutagenesis, as outlined in 2.1.2. Correct insertion of the desired sequence was confirmed by LIGHTRUN Sanger sequencing (GATC Biotech, Germany).

4.5 Overexpression of StrepII-VanS$_A$

A similar expression trial as described in Section 3.3 was carried out to screen expression conditions for StrepII-VanS$_A$. Competent C41 (DE3) pRIL, BL21 (DE3), and BL21 (DE3) Star.pRosetta cells were transformed with the pProEx::StrepII-VanS$_A$ plasmid and starter cultures were grown at 37 °C, 180 rpm, overnight. LB was innoculated from these starter cultures and incubated at 37 °C, 180 rpm, to an optical density at 600 nm of 0.6. Expression of the target protein was induced with 200 μM IPTG, as this concentration successfully induces expression of His$_6$-VanS$_A$, and expression of His$_6$-VanS$_{SC}$ does not appear to be

dependent on IPTG concentration. Cultures were incubated overnight at 180 rpm and 16 or 25 °C, as neither His_6-$VanS_A$ nor His_6-$VanS_{SC}$ has been expressed successfully following overnight incubation at 37 °C.

In order to detect the presence of StrepII-$VanS_A$ in cell lysates, a modified Western blot protocol was followed (IBA Life Sciences, Germany). Following transfer of proteins from an SDS-PAGE gel to a PVDF membrane as described in Section 2.6.3, the membrane was incubated with 3% (w/v) BSA in TBST overnight at 4 °C with gentle agitation. The blot was then washed twice for 5 minutes in 20 mL TBST. A 1:1000 dilution of biotin blocking buffer (IBA Life Sciences) in 10 mL TBST was applied to the blot for 10 minutes. 10 μL of 1:100 diluted Streptactin-HRP conjugate was then added to the same 10 mL blocking buffer/TBST, and the blot was incubated for 1 hour with gentle agitation at room temperature. The blot was then washed twice for 5 minutes in 10 mL TBST and twice for 5 minutes in TBS. Exposure to HRP substrate and visualisation of the blot was performed as described in Section 2.6.3.

A consequence of probing for the StrepII tag is that proteins native to *E. coli* which are biotinylated will also be detected by the Streptactin-HRP conjugate. The effect of this is minimised by the use of biotin blocking buffer, but this did not completely prevent interactions between Streptactin-HRP conjugate and native biotinylated proteins. Therefore, several bands appear on the Western blot, many of which will correspond to proteins native to *E. coli*. In particular, relatively intense bands of approximately 35 and 17 kDa appear in both pre- and post-induction lanes of all three screened cell lines. In *E. coli*, the AccB subunit of acetyl-CoA carboxylase is a 17 kDa protein which exists as a homodimer and is biotinylated by the biotin protein ligase BirA (Choi-Rhee et al., 2004); this may explain the intrusive bands appearing in the Western blot. It was necessary to overexpose these bands, in order to clearly visualise less intense bands on the blot including those corresponding to StrepII-$VanS_A$.

As shown in Figure 4.4, following overnight incubation at 16 °C, a band corresponding to a protein of approximately 46 kDa (the molecular weight of $VanS_A$) appears in the

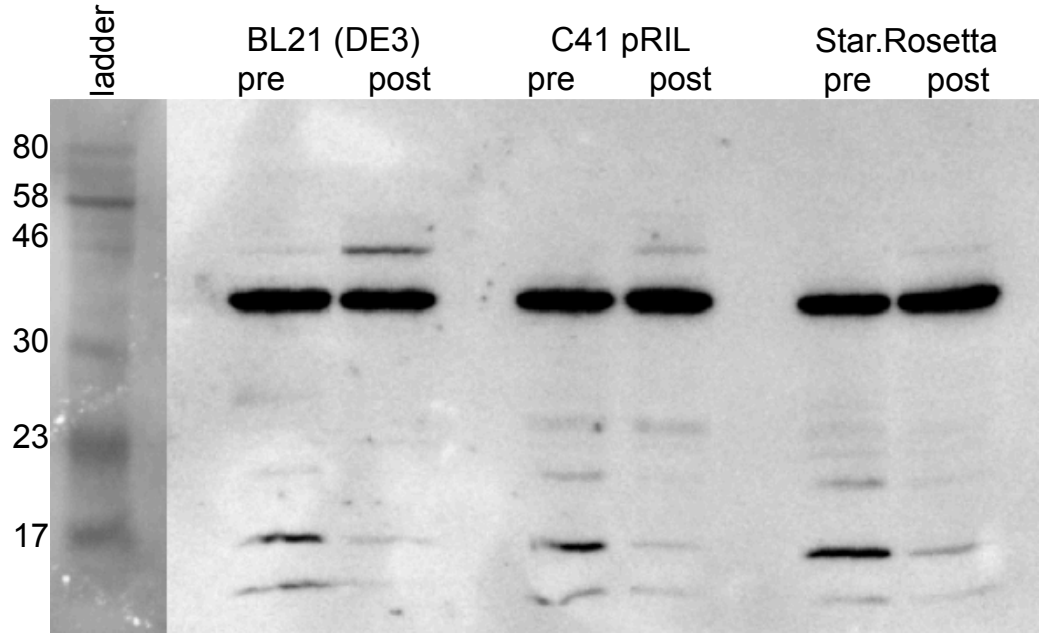

Figure 4.4: StrepII-VanS$_A$ (46 kDa, indicated by arrow) is expressed most efficiently in the BL21 (DE3) cell line, at 16 °C and 180 rpm overnight in the presence of 200 μM IPTG.

post-induction cell lysates of all three cell lines, with the most intense band corresponding to the BL21 (DE3) cell line. This cell line and set of expression conditions was therefore selected for StrepII-VanS$_A$ expression.

The StrepTrap HP prepacked column user manual (GE Healthcare, Illinois) recommends binding buffers with pH greater than 7; Zarkan et al. (2016) demonstrated that vancomycin could be reversibly bound to a range of metal ion affinity chromatography resins at pH 7.4. Therefore, pH 7.4 was selected for StrepII-VanS$_A$ purification and subsequent vancomycin affinity studies. Cells grown in litre cultures of LB were pelleted as described in Section 2.3.1 and resuspended in 25 mM sodium phosphate buffer (pH 7.4), 300 mM NaCl, 10% (v/v) glycerol, and 2 μM leupeptin, 2 μM pepstatin to prevent protein degradation.

4.6 Purification of StrepII-VanS$_A$ by StrepTactin Affinity Chromatography

Preparation of native membranes and solubilisation of membrane proteins into 10 mM DPC were carried out as described in Sections 2.3.2 and 2.3.3, with a pH of 7.4 maintained throughout.

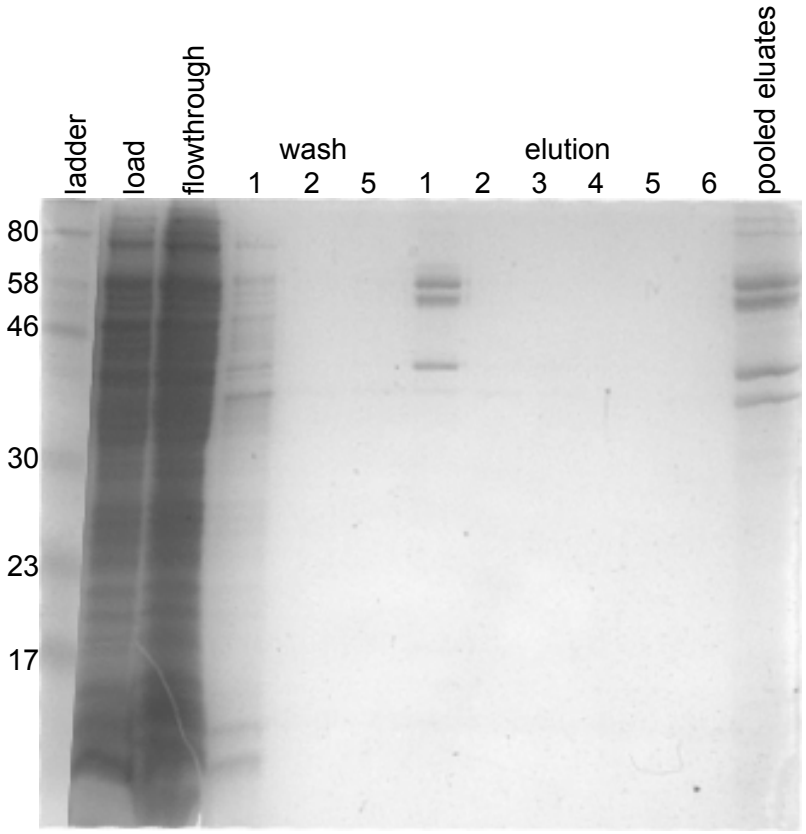

Figure 4.5: Coomassie-stained polyacrylamide gel. Biotinylated proteins are bound to, and subsequently eluted from, a StrepTrap 5 mL prepacked column (GE Healthcare, Illinois). StrepII-VanS$_A$ (46 kDa) is not observed in the eluate.

As a preliminary purification trial, a standard protocol was followed as outlined in the StrepTrap HP user manual (GE Healthcare, Illinois). A 5 mL StrepTrap prepacked column was equilibrated with 25 mL binding buffer (25 mM sodium phosphate buffer pH 7.4, 25 mM NaCl, 2 mM DPC) at a flowrate of 5 mL min^{-1}. Solubilised proteins were applied to the column using a syringe and luer adapter. The column was washed with 25

mL binding buffer, and flowthrough was collected in 1 mL fractions. Proteins were eluted with 30 mL elution buffer (binding buffer with 2.5 mM desthiobiotin), also collected in 1 mL fractions. All 30 fractions of eluate were pooled and concentrated to a volume of 200 μL, in order that very small quantities of protein should be observable.

Fractions were analysed by SDS-PAGE to investigate the presence of StrepII-VanS$_A$ (Figure 4.5). Since the column volume is 5 mL, 1 mL fractions were grouped in clusters of 5, and the first fraction in each investigated cluster was analysed; "Wash 1" is the first 1 mL fraction to be washed from the column, but "Wash 2" is the sixth (the first 1 mL fraction of the second cluster of fractions), and so on. Several proteins were observed in the pooled, concentrated eluate, but none correspond to StrepII-VanS$_A$, which is 46 kDa in size.

The user manual suggests that the target protein may be prevented from binding to the column when biotinylated proteins are present in the sample. The presence of biotinylated proteins has been established in this case (Figure 4.4). It is recommended under these conditions that 2-3 nmol of avidin is added per litre of cell culture, to prevent binding of biotinylated proteins to the column.

Protein-containing washes and eluates were returned to the flowthrough from the initial purification trial, along with 2 nmol avidin to inhibit binding of biotinylated proteins. The protocol was repeated as above, and fractions analysed by SDS-PAGE (Figure 4.6). Proteins of inappropriate mass to be StrepII-VanS$_A$ are still observed in the concentrated eluate, but at lower concentrations.

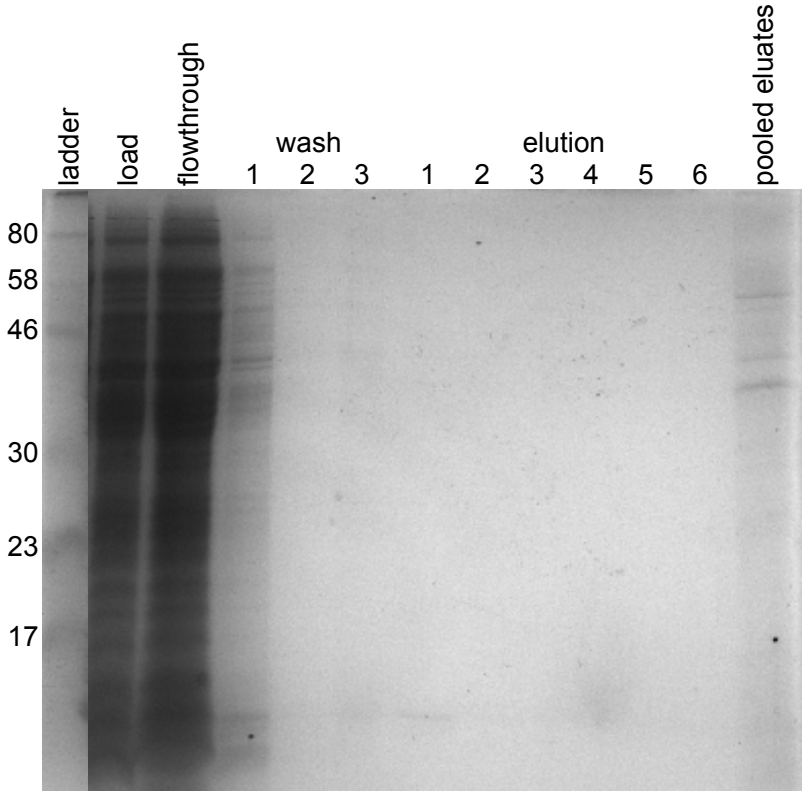

Figure 4.6: Coomassie-stained polyacrylamide gel. The addition of avidin to the solubilised protein mixture reduces the extent to which biotinylated proteins bind to the StrepTrap column. StrepII-VanS$_A$ is still not observed in the eluate.

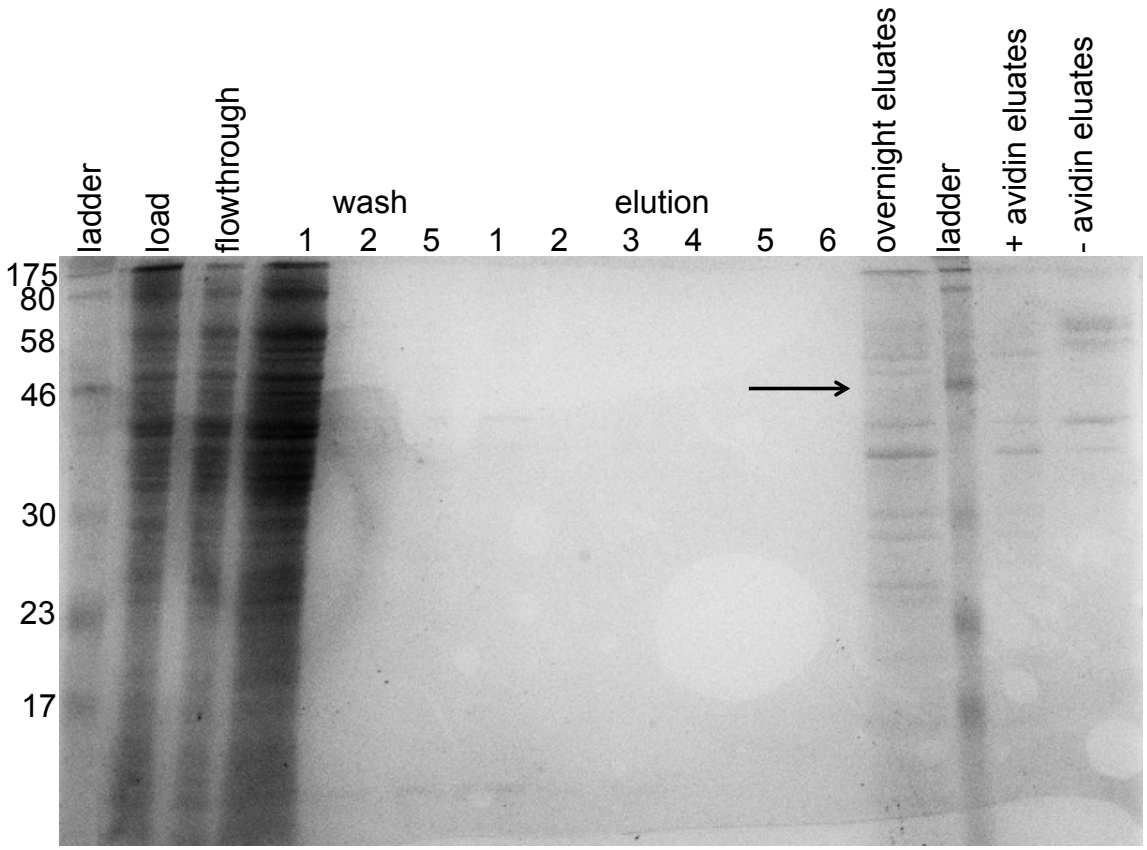

Figure 4.7: Coomassie-stained polyacrylamide gel. Overnight application of avidin-containing solubilised protein mixture resulted in further binding of biotinylated proteins, compared to a single application of the sample to the StrepTrap column. A faint band of 46 kDa is apparent (highlighted), and may correspond to StrepII-VanS$_A$.

A third attempt was made to bind StrepII-VanS$_A$ to the StrepTrap column. Protein-containing washes and eluates from the second trial were returned to the flowthrough, and this was applied to the column at a rate of 5 mL min^{-1} overnight. The purification procedure was then repeated as above. Fractions were analysed by SDS-PAGE, alongside concentrated eluates from the previous two trials, to allow a side-by-side comparison of the three methods (Figure 4.7).

Compared to the second trial in which avidin-containing protein solution was applied once to the column, more extensive binding of proteins is observed following overnight application. Several prominent bands are visible which do not correspond to StrepII-VanS$_A$. However, a faint band at 46 kDa is also visible (highlighted), and may represent StrepII-VanS$_A$ at low concentration, in an eluate mostly comprised of other proteins which have bound to the column.

4.7 Discussion

4.7.1 Construction of a Vancomycin Affinity Column

Under the conditions presented by Zarkan et al. (2016), vancomycin was successfully bound to Cu^{2+} ions in a HisTrap FF 1 mL prepacked column (GE Healthcare, Illinois). This interaction was observed to be reversible by the application of 50 mM imidazole to the column (Figure 4.3). It should therefore be possible to elute bound proteins from the vancomycin affinity column with imidazole; eluates would then contain both vancomycin, and the interacting protein. The presence of protein in these eluates could be analysed by SDS-PAGE.

4.7.2 Generation of a StrepII-VanS Expression Construct

The hexahistidine tag of His_6-$VanS_A$ was successfully replaced by a StrepII tag by site-directed mutagenesis. The presence of the StrepII tag was confirmed by LIGHTRUN Sanger sequencing (GATC Biotech, Germany).

Similar substitution of the StrepII tag for the existing His_6 tag of His_6-$VanS_{SC}$ should be readily achievable using the same approach.

4.7.3 Overexpression of StrepII-$VanS_A$ in *E. coli*

Expression of StrepII-$VanS_A$ was attempted in three *E. coli* cell lines, and achieved in the BL21 (DE3) *E. coli* strain following overnight incubation at 16 °C, 180 rpm, with 200 μM IPTG. The presence of StrepII-$VanS_A$ in cell lysates was investigated by a modified Western blot protocol, in which Streptactin-HRP conjugate was applied to the membrane following overnight blocking in 3% (w/v) BSA in TBST at 4 °C. Even with the use of biotin blocking buffer (IBA Life Sciences) to limit the interaction between Streptactin and biotinylated proteins in the cell lysate, the most intense bands corresponded to biotinylated proteins in both pre- and post-induction cell lysates; the band corresponding to StrepII-$VanS_A$ was of relatively low intensity, although visible. This indicates that biotin blocking buffer is not

entirely effective in preventing interactions between Streptactin and biotinylated proteins in the lysate.

4.7.4 Further Optimisation of a Purification Protocol for StrepII-VanS$_A$

Three methods of purifying StrepII-VanS$_A$ by application to a StrepTrap HP prepacked column (GE Healthcare, Illinois) were trialed. A mixture of proteins solubilised from *E. coli* cell membranes into DPC detergent micelles was applied to the column in the presence and absence of avidin, to prevent natively biotinylated proteins from binding to the column. The avidin-containing protein mixture was also applied to the resin overnight with a P1 peristaltic pump at a flowrate of 5 mL min^{-1}. Following overnight application of the protein sample, and subsequent washing and elution from the column, a faint band which might correspond to StrepII-VanS$_A$ was observed by analysis of eluates by SDS-PAGE. Eluates also contained significant levels of contaminating, natively biotinylated proteins.

Further optimisation of the protocol will be necessary in order to achieve purification of StrepII-VanS$_A$. An appropriate sample need not be fully pure, but should predominantly contain StrepII-VanS$_A$ with minimal contamination by other proteins. This will reduce the impact which contaminating proteins might have on interactions between StrepII-VanS$_A$ and a glycopeptide antibiotic affinity column. Contaminating proteins might have an affinity for glycopeptides, or for metal ions, potentially complicating interpretation of results from glycopeptide affinity experiments.

When purification of StrepII-VanS$_A$ is achieved, it will first be necessary to investigate this protein's affinity for Cu^{2+} ions. This may be achieved by applying the purified protein sample to a metal ion affinity column charged with Cu^{2+} ions. It is essential that the protein should not bind to this column, otherwise later observations of interactions between the protein and the vancomycin-copper affinity column will be unreliable.

If StrepII-VanS$_A$ is shown to possess no affinity for Cu^{2+} ions, then vancomycin may be applied to the metal ion affinity column. Vancomycin will bind, and is not removed until imidazole is applied to the column. StrepII-VanS$_A$ may then be applied to the column with

vancomycin still bound. If the protein interacts with vancomycin, it may be retained in the column. Following sufficient washing of the column to remove unbound protein, imidazole may be applied to elute vancomycin. Any bound StrepII-VanS$_A$ will co-elute with the vancomycin. The presence of StrepII-VanS$_A$ in the eluate can be analysed by SDS-PAGE.

4.7.5 Towards Construction of Teicoplanin Affinity Column

Teicoplanin is a glycopeptide antibiotic with significant structural similarities to vancomycin. One significant difference between the two antibiotics is that teicoplanin possesses a lipid chain, which allows it to become anchored into cell membranes (Beauregard et al., 1995). However, there are several other regions of structural dissimilarity (Figure 4.1). Zarkan et al. (2016) observed ^{1}H chemical shift perturbations in vancomycin with increasing concentrations of Zn^{2+}, and suggest that these regions of vancomycin constitute the binding site for Zn^{2+}. As shown in Figure 4.1, while some of these regions are conserved between vancomycin and teicoplanin, others are unique to vancomycin.

An interaction takes place between teicoplanin and Cu^{2+} ions, but fewer coordinations are formed than form with vancomycin (Brzezowska et al., 2010). There is therefore a question as to whether teicoplanin will display a sufficient affinity for metal ions, including copper, and whether a similar technique as described above may be applied to teicoplanin in order to construct a teicoplanin affinity column.

Both vancomycin and teicoplanin are glycopeptide antibiotics, and the peptide component is largely conserved between the two antibiotics. Therefore teicoplanin is expected to absorb light at 282 nm, as does vancomycin, owing to the presence of aromatic amino acid side chains in the structure. Construction of an affinity column as described above may be investigated quickly and cheaply, and examined through absorbance measurements at this wavelength. If this method of constructing a teicoplanin affinity column is found not to be suitable, other approaches may need to be considered by which a teicoplanin affinity column may be constructed.

Roy et al. (2001) constructed a vancomycin affinity column by adding a putrescine

linker to the C-terminus of vancomycin, a region conserved in teicoplanin. This linker was then coupled to *N*-hydroxysuccinimide-activated Sepharose 4B, and packed into a column with 1 mL bed volume. Since the region is conserved in teicoplanin, this approach may be utilised to produce a teicoplanin affinity column. One limitation to this approach would be occlusion of the peptide's C-terminus in the process of binding teicoplanin to the sepharose resin. This would likely interfere with interactions between VanS and this region of teicoplanin. It may be possible to construct a similar teicoplanin-sepharose resin by targetting a second region of teicoplanin, exposing the C-terminus of the peptide to proteins in solution.

4.7.6 Other Approaches to Constructing a Vancomycin Affinity Column

Since binding of vancomycin to the Cu^{2+} affinity column occludes the N-terminus of the peptide component of vancomycin, it will be desirable to also construct a vancomycin affinity column covalently as described by Roy et al. (2001). This method involves linking the C-terminus of the peptide component of vancomycin to NHS-activated Sepharose 4B, via a putrescinyl liner. This leaves the N-terminus of the peptide component free, so any interactions between StrepII-VanS$_A$ and this region of vancomycin that were blocked in the vancomycin-copper affinity column might be observable under these conditions.

Chapter 5

Analysis of VanS-Ligand Interactions by Saturation Transfer Difference NMR

5.1 Introduction

Saturation transfer difference (STD) NMR is a solution-state NMR method well-suited to the study of interactions between small ligands and large proteins (Section 2.9.6). A selective saturation pulse irradiates protons in a large, slowly-tumbling protein, and this saturation is allowed to spread via the Nuclear Overhauser Effect (NOE) to other protons in a distance-dependent manner, including to protons in a reversibly bound ligand molecule. When the small ligand molecule dissociates and tumbles freely in solution, saturation accumulated during the interaction may be observed and quantified, allowing the binding epitope to be mapped.

In this study, STD-NMR was used to investigate the binding of potential ligands to both His_6-$VanS_A$ (47 kDa) and His_6-$VanS_{SC}$ (42 kDa). The two proteins were solubilised and purified in LMPG micelles (26 kDa; yielding effective molecular weights for His_6-$VanS_A$ and His_6-$VanS_{SC}$ of 73 and 68 kDa, respectively). These larger molecular weights place these two proteins outside of the viable range for solution-state NMR characterisation, but well within the range of larger molecular weights to which STD-NMR is suited.

5.2 Aims

1. To identify potential ligands amenable to STD-NMR studies;
2. To acquire and assign high-quality 1D and 2D ^{1}H NMR data of potential ligands in solution;
3. To prepare appropriate samples of VanS and potential ligands, suitable for study by STD-NMR;
4. To acquire high-quality STD-NMR data investigating the transfer of saturation from VanS to potential ligands, indicating an interaction between the two molecules;
5. To map the binding epitope of any ligand for which binding is observed by STD-NMR;
6. To estimate the dissociation constant, K_D, of the interaction between VanS and any ligand for which binding is observed by NMR.

5.3 Selection and Suitability of Potential Ligands for STD-NMR

The first ligand selected for investigation was the glycopeptide antibiotic vancomycin (1.5 kDa), as both proteins are sensitive to it. A second glycopeptide antibiotic, teicoplanin, was also selected for investigation - the kinase activity of $VanS_A$ is known to be induced by exposure to this antibiotic, which $VanS_{SC}$ does not respond to its presence (Koteva et al., 2010; Arthur and Jr., 2001).

The pentapeptide component of the peptidoglycan precursor lipid II, Ala-D-γ-Glu-Lys-D-Ala-D-Ala (0.5 kDa), a well-known cell wall degradation product accumulated *in vivo*, was chosen as a potential ligand for VanS. This peptide was selected because it is readily available to purchase, it is small and soluble, and it lacks the lipid chain of the insoluble lipid II molecule (Vollmerhaus et al., 2003). which would complicate interpretation of these studies performed in detergent micelles.

In order to conduct an STD-NMR experiment, it is first necessary to identify the "on-resonance" frequency which saturates only protons within the protein, and leads to no direct saturation of ligand resonances. To identify these "on-resonance" frequencies for the selected ligands, 200 μL samples were prepared for each potential ligand, consisting 1 mM ligand in 25 mM sodium phosphate buffer (pD 6.8), 25 mM NaCl, 1.15 mM LMPG, 100% D_2O. LMPG was included in ligand samples at this point to ensure that selected saturation frequencies would saturate neither ligand nor LMPG protons. Saturation pulses were applied to each ligand sample across a range of frequencies between -3290 and -5390 Hz (between 0 and -2 ppm, where protein signals are found). When a frequency was identified which did not irradiate any protons within the ligand or detergent, the same saturation pulse was applied to a sample of protein to confirm that the frequency was capable of irradiating protons in the protein.

Figure 5.1 shows the results for selection of appropriate on-resonance frequencies for both vancomycin-VanS and pentapeptide-VanS binding studies. An on-resonance frequency

corresponding to 2 ppm led to no excitation of vancomycin (Figure 5.1 A), while yielding excitation of protons within both His_6-$VanS_A$ and His_6-$VanS_{SC}$ (Figures 5.1 B-C). Vancomycin was therefore found to be suitable for STD-NMR studies of both VanS proteins, with -2 ppm used as the on-resonance saturation frequency. This on-resonance frequency was not suitable for the pentapeptide, however, as small amounts of irradiation were detected in the difference spectrum (Figure 5.1 D). Therefore, an alternative on-resonance frequency had to be identified. An on-resonance frequency of 1400 Hz (corresponding to 6.7 ppm) lead to no irradiation of protons in the pentapeptide (Figure 5.1 E), while effectively irradiating protons in His_6-$VanS_A$ (Figure 5.1 F). This frequency was therefore used in STD-NMR studies of this receptor/ligand pair. In all STD-NMR experiments, 24720 Hz (40 ppm) was used as the off-resonance saturation frequency. This frequency is at least 30 ppm away from the furthest downfield protons in the sample, and does not irradiate any protons.

Unfortunately, no saturation frequency could be identified which could selectively irradiate VanS protons without irradiating any protons in teicoplanin. The potential for teicoplanin to interact with VanS was therefore not studied by STD-NMR.

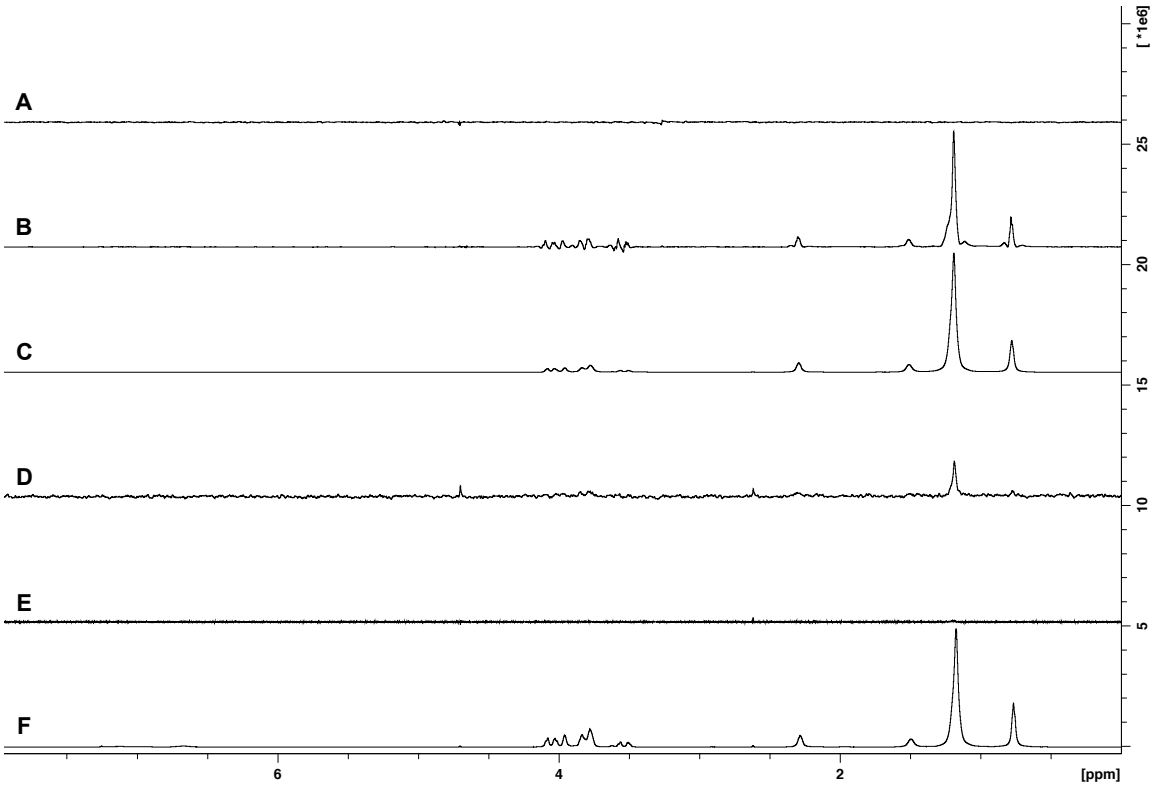

Figure 5.1: Selection of appropriate on-resonance frequencies. Difference spectra of: **A**, 1 mM vancomycin saturated at -2 ppm; **B**, 20 μM His_6-$VanS_A$ saturated at -2 ppm; **C**, His_6-$VanS_{SC}$ saturated at -2 ppm; **D**, lipid II pentapeptide saturated at -2 ppm; **E**, lipid II pentapeptide saturated at 6.7 ppm; **F**, His_6-$VanS_A$ saturated at 6.7 ppm.

5.4 Assignment of 1D and 2D ^{1}H NMR Spectra of Selected Ligands

The output of an STD-NMR experiment is a ^{1}H 1D spectrum in which signal "intensity" (peak area) represents a spatial relationship between a proton in the ligand and selectively irradiated protons in the protein. Ligand protons which experience signal attenuation are closely spatially associated with the protein during a binding event. In order to identify which ligand protons have experience signal attenuation, it is first necessary to generate assigned ^{1}H 1D spectra of each potential ligand.

To this end, 200 μL samples were prepared for each potential ligand, consisting of

1 mM ligand in 25 mM sodium phosphate buffer (pD 6.8), 25 mM NaCl, 100% D_2O. ^1H 1D and 2D (TOCSY and NOESY) spectra were acquired for each sample, as described in Sections 2.9.5 and 2.9.8, and chemical shift assignment was achieved through reference to published chemical shift lists (Convert et al., 1980; Pearce and Williams, 1995; McDonald and Phillips, 1969).

5.4.1 ^1H Assignment of Vancomycin

^1H assignment of vancomycin has previously been completed at 0.25 mM in CD_3COOD-NaOD, 99.8% deuterium, pD 5.5 at 318K (Convert et al., 1980), and at 50 mM in $(CD_3)_2SO$, 99.96% deuterium, pD 6.0 at 298K Pearce and Williams (1995). To assign the protons in vancomycin under the conditions used here, specifically 25 mM sodium phosphate buffer (pD 6.8), 25 mM NaCl, 99.99% D_2O, NOESY, TOCSY (Figure 5.2) and ^1H 1D spectra were acquired. The experimentally obtained chemical shifts and coupling patterns were used alongside values obtained from the literature and from chemical shift prediction in ChemDraw (PerkinElmer Informatics, Massachussets), to obtain complete assignment of ^1Hs in the antibiotic as shown in Table 5.1.

The annotation scheme from Convert et al. (1980) was adapted for this study; as in Pearce and Williams (1995), protons are identified in the structure of vancomycin in Figure 5.3. Assignments were established from 2D spectra and then mapped onto the 1D spectrum for comparison to STD-NMR data (Figure 5.4).

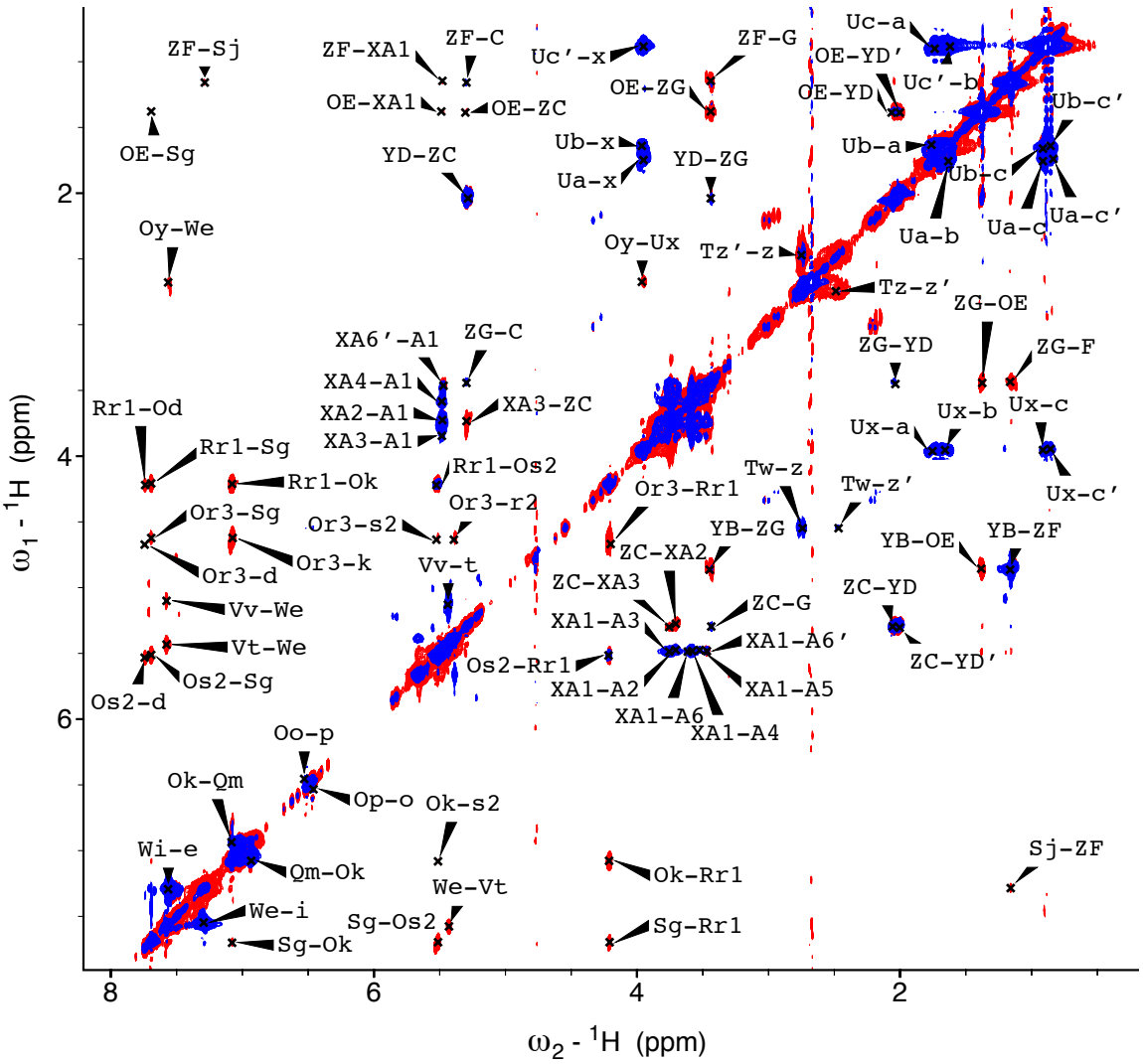

Figure 5.2: Overlaid 70 ms TOCSY (blue) and 80 ms NOESY (red) spectra of vancomycin in 25 mM sodium phosphate buffer (pD 6.8), 25 mM NaCl, 100% D_2O. Assignment was completed in Sparky.

Proton	δ (ppm)	Proton	δ (ppm)	Proton	δ (ppm)	Proton	δ (ppm)
d	7.74	r4	5.86	w	4.54	y	2.68
g	7.71	s1	5.80	r1	4.22	z'	2.46
e	7.58	u	5.65	x	3.95	D	2.03
f	7.58	s2	5.53	A3	3.75	D'	2.00
j	7.29	A1	5.48	A2	3.70	a	1.73
i	7.28	t	5.43	A6	3.57	b	1.68
k	7.09	v	5.38	A4	3.55	E	1.39
l	7.03	C	5.28	A5	3.52	F	1.17
m	6.84	B	4.85	A6'	3.47	c	0.90
p	6.52	r3	4.64	G	3.45	c'	0.86
o	6.47	r2	4.62	z	2.76		

Table 5.1: Assigned chemical shifts for protons in vancomycin, at 298 K in 25 mM sodium phosphate buffer (pD 6.8), 25 mM NaCl, 100% D_2O.

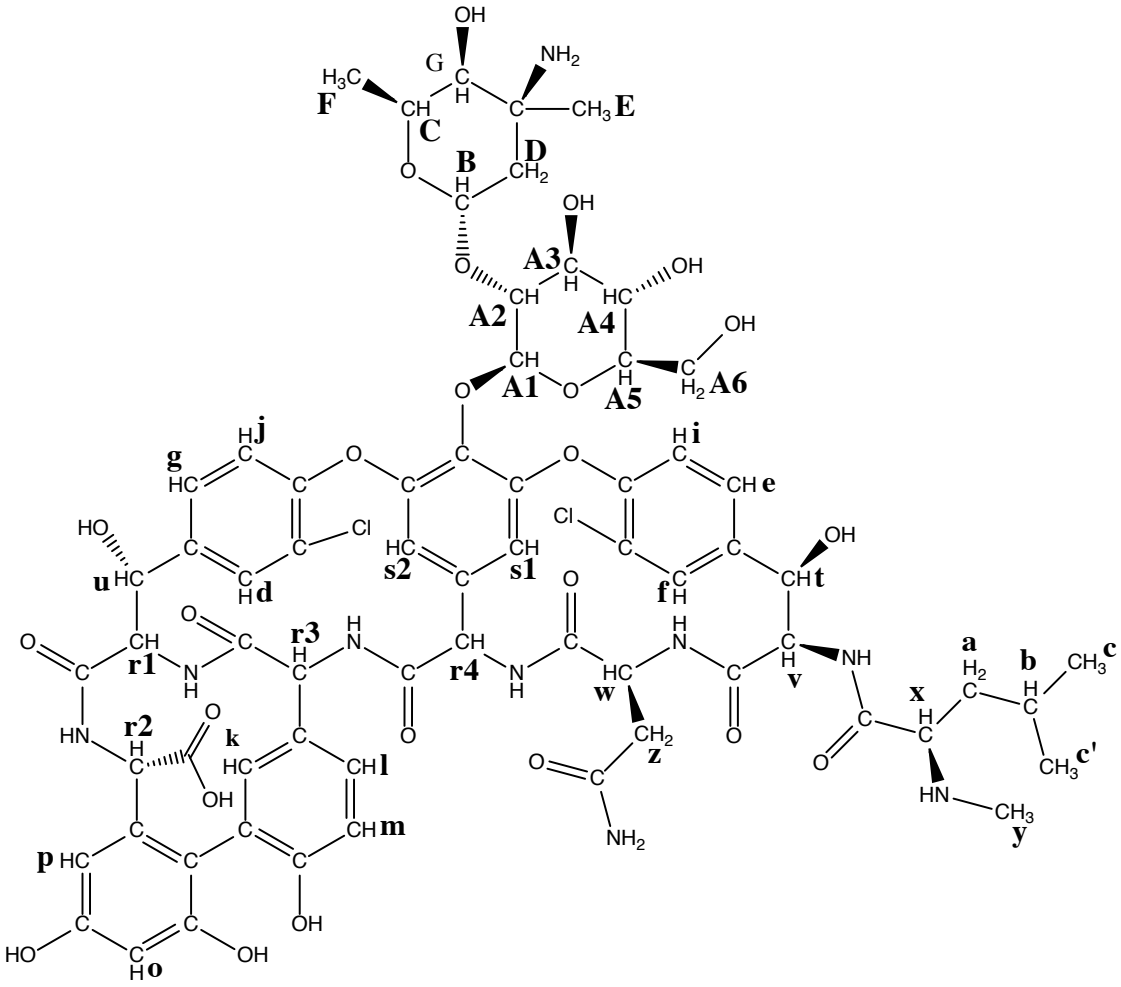

Figure 5.3: The structure of vancomycin, with assignable protons annotated. Annotation scheme adapted from Convert et al. (1980) and Pearce and Williams (1995).

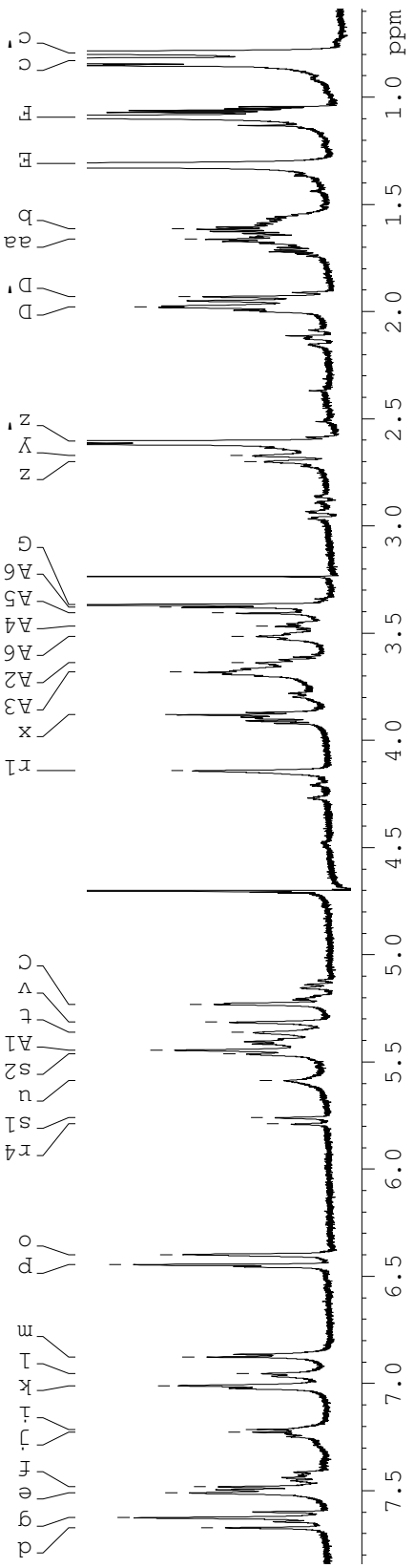

Figure 5.4: Fully assigned ^{1}H 1D NMR spectrum of 1 mM vancomycin, at 298 K in 25 mM sodium phosphate buffer (pD 6.8), 25 mM NaCl, 100% D_2O.

5.4.2 ^{1}H Assignment of Lipid II Pentapeptide

^{1}H assignment of the lipid II pentapeptide (Figure 5.6) dissolved in 25 mM sodium phosphate buffer (pD 6.8), 25 mM NaCl, 99.99% D_2O was achieved through acquisition of NOESY and TOCSY spectra (Figure 5.5) and ^{1}H 1D spectra. Protons in each residue type were assigned (with reference to published values of ^{1}H chemical shifts for amino acids in random coil structures (McDonald and Phillips, 1969)) from the TOCSY spectrum, and crosspeaks connecting residues along the peptide backbone were identified in the NOESY spectrum so that the three alanines could be distinguished. The complete assignment of ^{1}Hs in the pentapeptide is shown in Table 5.2. Assignments were then mapped onto the 1D spectrum for comparison to STD-NMR data (Figure 5.7).

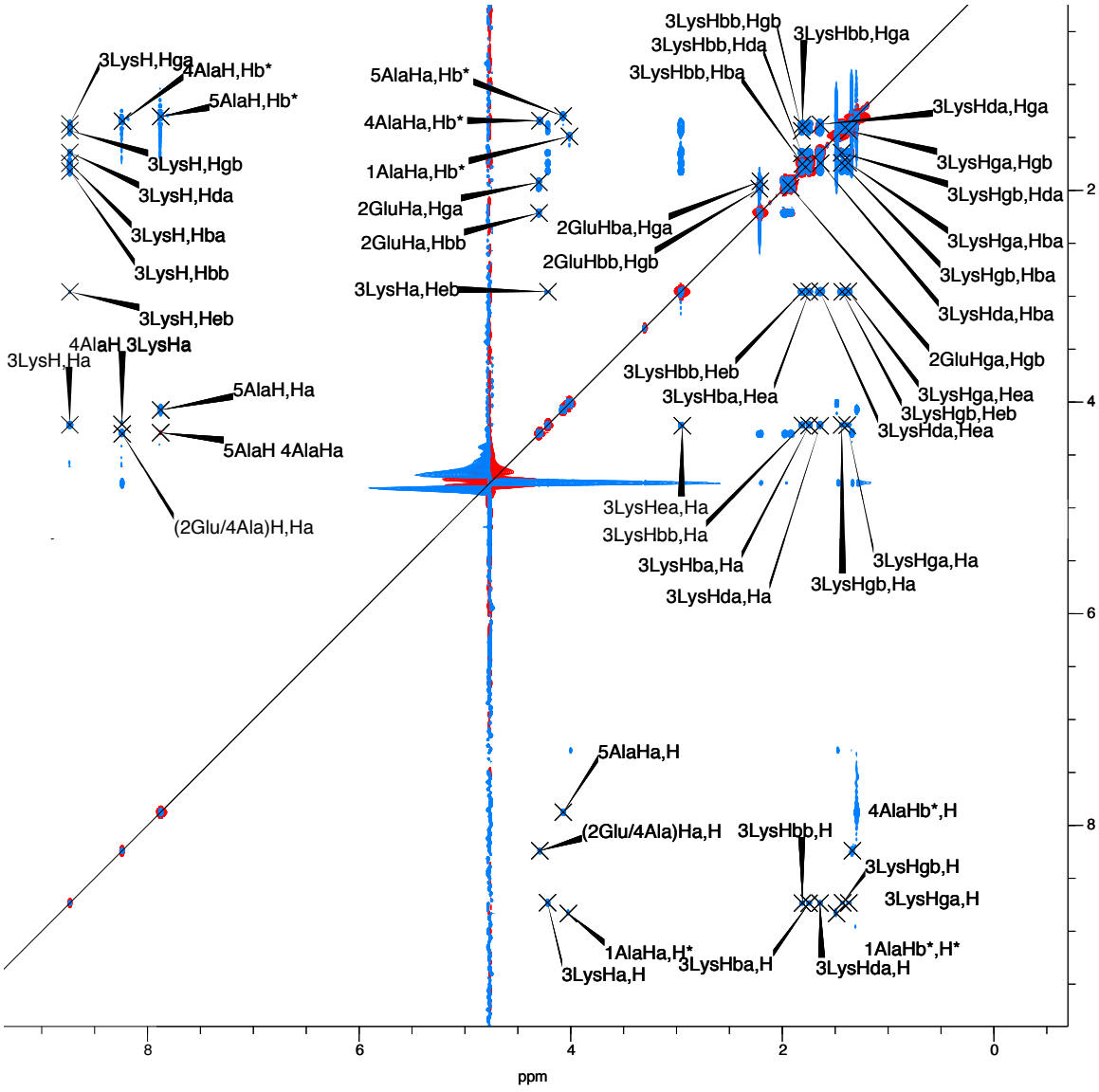

Figure 5.5: Overlaid TOCSY (blue) and NOESY (red) spectra of lipid II pentapeptide in 25 mM sodium phosphate buffer (pD 6.8), 25 mM NaCl, 100% D_2O. Assignment was completed in CCPN.

	δ (ppm)								
Residue	HN	Hα	Hβ		Hγ		Hδ	Hϵ		
A1	8.833	4.017	1.488							
Q2	8.239	4.301	2.217	2.203	1.976	1.919				
K3	8.732	4.219	1.815	1.745	1.436	1.377	1.643	2.962	2.952	8.402
A4	8.239	4.294	1.341							
A5	7.875	4.072	1.300							

Table 5.2: Assigned chemical shifts for protons in the lipid II pentapeptide, at 298 K in 25 mM sodium phosphate buffer (pD 6.8), 25 mM NaCl, 100% D_2O.

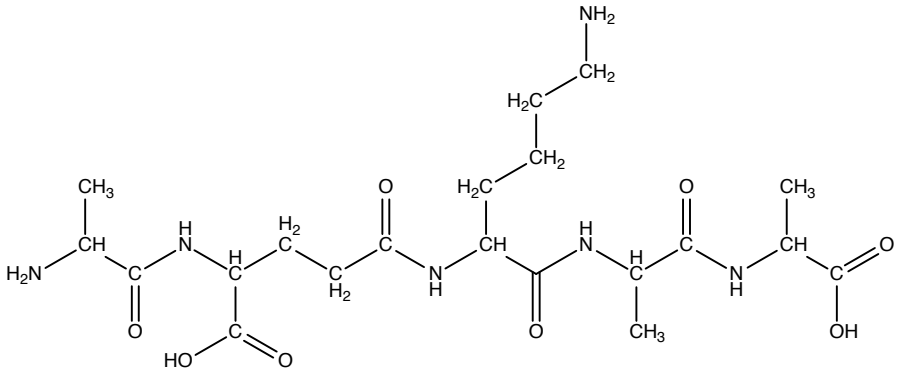

Figure 5.6: From Sigma Aldrich (Montana). The structure of the lipid II pentapeptide Ala-D-γ-Glu-Lys-D-Ala-D-Ala.

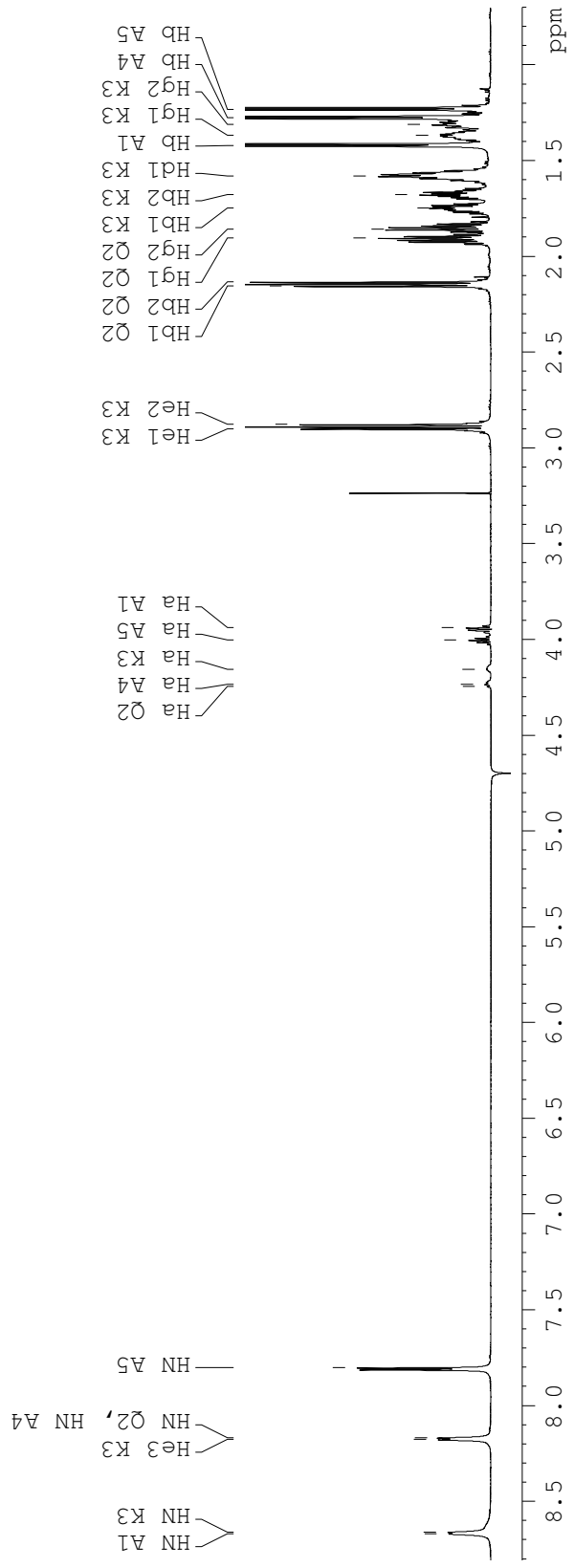

Figure 5.7: Fully assigned ^{1}H 1D NMR spectrum of 1 mM lipid II pentapeptide, at 298 K in 25 mM sodium phosphate buffer (pD 6.8), 25 mM NaCl, 100% D_2O.

5.5 STD NMR Studies of VanS Exposed To Potential Ligands

5.5.1 Sample Preparation and Data Acquisition

A limitation in studying integral membrane proteins is the need to include an appropriate membrane mimetic in purified protein samples. VanS has been determined to be soluble in a number of different detergents (Section 3.5), which form spherical micelles consisting of hydrophobic cores with a hydrophilic external shell. Every detergent has a critical micellar concentration (CMC), a population of detergent molecules which maintain a monomeric state rather than assembling into micelles. This population of monomeric detergent molecules is observable in ^{1}H NMR spectra; the higher a detergent's CMC, the more intrusive the NMR signals from the fast-tumbling monomeric detergent molecules.

Some deuterated detergents, which do not yield ^{1}H NMR signals, are available. Deuterated *n*-dodecylphosphocholine (DPC-d_{38}) can be purchased at a cost of approximately £1,000 per 500 mg (Avanti Polar Lipids, Alabama; August 2017). The process of solubilising VanS from native membranes, and then purifying the protein by chromatography, requires approximately 300 mg of detergent per 200 μL NMR sample. To prepare VanS in deuterated detergent was therefore deemed too costly, and other options were explored.

DPC also has a CMC of 1.25 mM (Lazaridis et al., 2005), resulting in significant intrusion of detergent signals on ^{1}H NMR spectra. A number of lower-CMC detergents were screened (Section 3.5) in order to identify a detergent which would minimise the concentration of monomeric detergent molecules in solution. LMPG and LPPG were found to be similarly effective in solubilising VanS as was DPC (Section 3.5); due to considerations of cost and availability, LMPG was selected as a low-CMC detergent suitable for NMR studies.

Proteins were prepared as described in Sections 2.3.3 - 2.4. STD-NMR samples contained 300 μL of 10 μM VanS in 25 mM sodium phosphate buffer (pD 6.8), 25 mM NaCl, 100% D_2O. Increasing the concentration of receptor protein in an STD-NMR sample

results in larger apparent K_D values (Angulo et al., 2010). Protein concentrations of 5-20 μM are often reported in the literature (Viegas et al., 2011; Fielding, 2007); a concentration of 10 μM was therefore selected for this study. Increasing concentrations of ligand were then titrated into the protein sample, using a highly concentrated ligand stock solution (25 mM ligand dissolved in 100% D_2O), to minimise dilution of the protein sample.

STD-NMR spectra were acquired at each ligand concentration and processed as described in Section 2.9.6.

5.6 Mapping the Binding Epitopes of Vancomycin to His_6-VanS Proteins

The STD experiment yields ^1H 1D spectra of a sample acquired with and without the application of a selective saturation pulse targeting receptor protons (on-resonance and off-resonance spectra, respectively). Signals from ligand protons spatially associated with the receptor during a binding event are attenuated in the on-resonance spectrum. In an STD-NMR experiment, the attenuation of a ligand proton signal due to the proximity of the (saturated) protein is expressed as a fraction of peak intensity in the off-resonance spectrum. In this way, the extent to which each proton experiences saturation transfer may be quantified to identify those protons in closest proximity to (and most likely involved in the interaction with) the receptor.

The difference in signal intensities is small, relative to overall signal intensity. It is difficult to accurately quantify these differences. The signal:noise ratio increases as the saturation time is increased (Angulo et al., 2010), but so does the impact of ligand re-binding, which leads to overestimation of apparent K_D. It is desirable to identify the minimum saturation time which yields sufficient signal:noise ratio to allow differences in peak intensity to be reliably measured, while minimising the affect of ligand re-binding.

$$I_{STD} = I_0 - I_{sat} \tag{5.1}$$

$$\mathrm{A}_{STD} = \frac{\mathrm{I}_{STD}}{\mathrm{I}_0} \times \frac{[L]}{[P]} \tag{5.2}$$

At each saturation time, the STD amplification factor, A_{STD}, is calculated as described in Section 2.9.6 for each ligand proton with a clearly resolved signal, using Equations 5.1 and 5.2. Despite utilisation of a low-CMC detergent, signals from LMPG crowd the spectrum above 5 ppm (Figure 5.8), so that only ligand peaks in the range 5 - 8 ppm were resolvable. Fortunately, approximately half of vancomycin's assignable protons have chemical shifts in this region of the spectrum (Figure 5.9).

Protons in the 6-8 ppm range were positively identifiable, and saturation to these protons is quantified below. In both datasets, saturation is also observed to transfer to three protons with chemical shifts in the range 5-6 ppm. However, tight clustering of vancomycin protons in this region of the spectrum precludes positive identification of these three protons. Candidate protons with chemical shifts in this range are shown in Figure 5.9.

Note that vancomycin proton pairs d/g and e/f have very similar chemical shifts and overlapping signals in the high resolution ^{1}H 1D NMR spectrum. These protons are near neighbours within the structure. The purpose of STD NMR, which outluts lower-resolution spectra, is to identify regions of the molecule which are involved in a binding event. It was not possible to distinguish between protons d and g, or between e and f, so they are considered together.

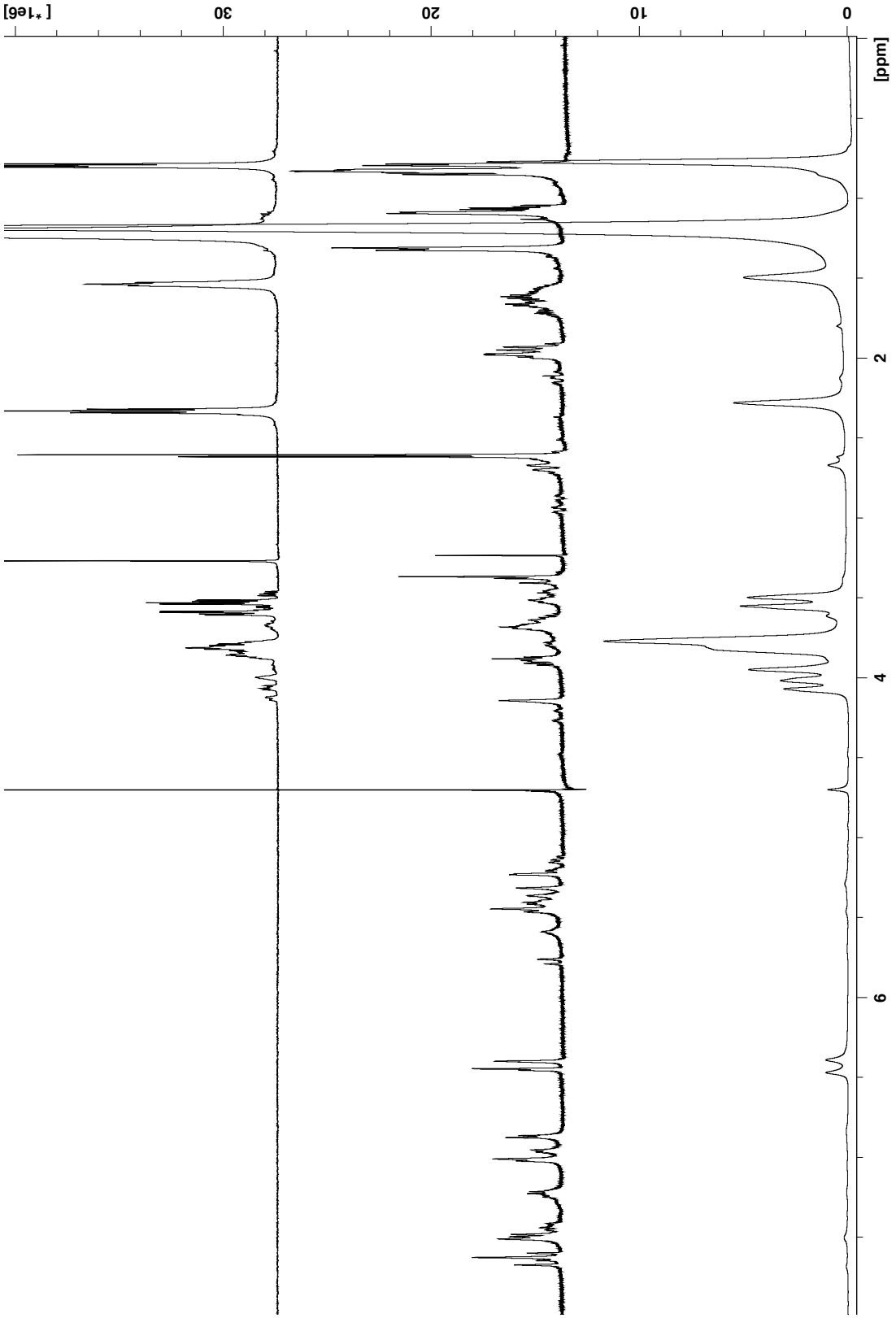

Figure 5.8: ^{1}H 1D NMR spectra of LMPG (top) and vancomycin (middle), and STD difference spectrum of vancomycin and His_6-$VanS_{SC}$ (bottom). Upfield of 5 ppm, LMPG peaks in the difference spectrum obscure vancomycin peaks, impeding quantification of saturation transfer.

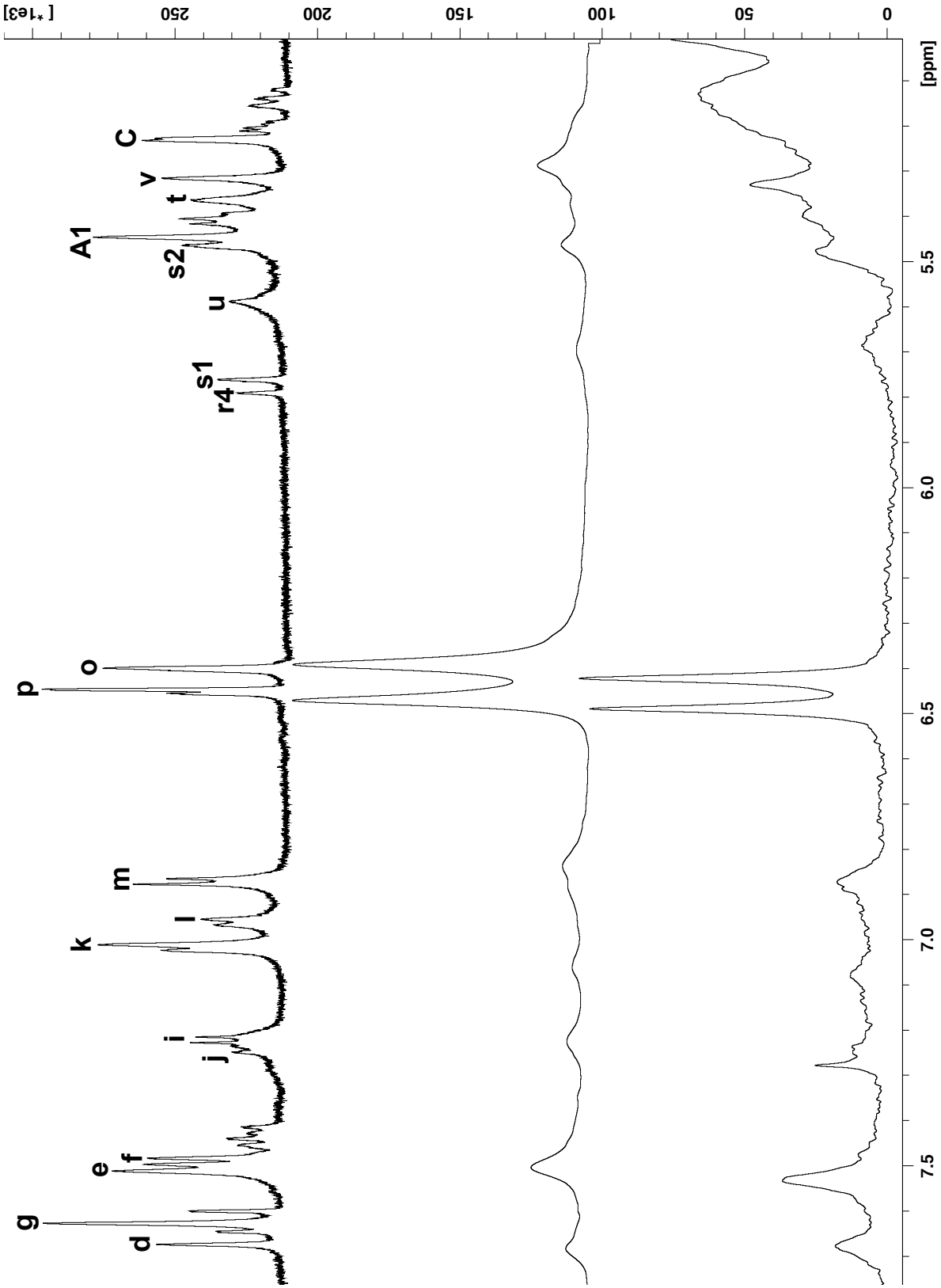

Figure 5.9: In the 5-8 ppm chemical shift range; assigned ^{1}H 1D NMR spectrum of vancomycin (top), and STD-NMR difference spectra of vancomycin and His_6-$VanS_{SC}$ (middle) or His_6-$VanS_A$ (bottom).

5.6.1 The Vancomycin Epitope Binding to His_6-$VanS_A$

For samples containing 20 μM His_6-$VanS_A$ and 1 mM vancomycin (50-fold molar excess of ligand), saturation times ranging from 0.5 sec to 5 sec were tested in the acquisition of STD-NMR data to determine the optimal value. A relaxation delay of 3.5 sec was used for saturation times below 3.5 sec. For saturation times above this threshold, a relaxation delay of 0.5 sec greater than the saturation time was needed.

Data were processed as described in Section 2.9.6. Baselines were manually corrected in each on-resonance and off-resonance spectrum by fitting a polynomial function. The pair of spectra for each saturation time were overlaid to confirm that differences in peak intensities were due to signal attenuation, and not due to differences in spectral baselines. By comparison to a ^{1}H 1D spectrum of vancomycin in equivalent buffer conditions, peaks representing vancomycin protons are identified in the key to Figure 5.10; their positions within the vancomycin molecule are shown in Figure 5.3. Positively identified peaks were integrated using the interactive integration function of NMR software package TopSpin (Bruker, Massachussetts). Integral regions were kept consistent for on- and off-resonance spectra at all saturation times. A_{STD} was then calculated for each proton at each saturation time, and the data are shown in Figure 5.10.

As expected, the data form a logarithmic curve indicating that the impact of saturation time on signal attenuation reaches a limit at around 3 seconds. There is no need to exceed 3 second saturation times in titration experiments; this value will yield sufficient signal:noise, while minimising the impact of ligand re-binding.

LMPG signals crowd the spectrum below 5 ppm, and vancomycin peaks observable between 6 and 5 ppm could not be distinguished due to crowding in the vancomycin 1D spectrum. Between 9 and 5 ppm, vancomycin peaks are resolvable. 11 vancomycin protons possess chemical shifts in this region, and 9 signals are observed in the on- and off-resonance spectra. Protons d and g, and e and f, have very similar chemical shifts and cannot be distinguished from one another in STD spectra. All nine of the visible signals were attenuated to some degree during the STD-NMR experiment.

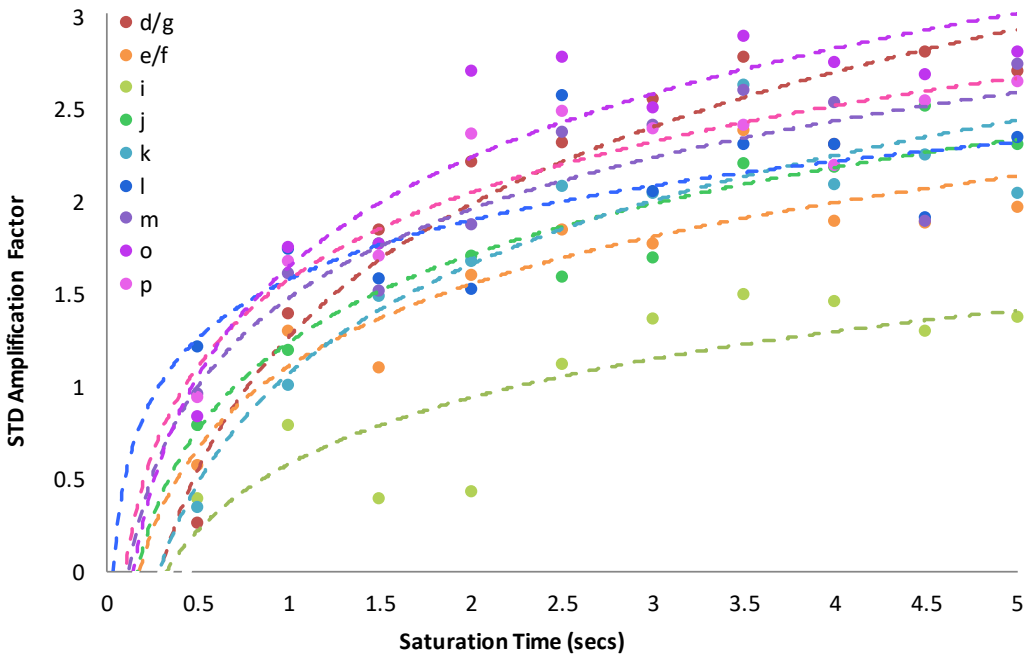

Figure 5.10: STD amplification factor as a function of saturation time, for protons within vancomycin titrated into a sample of His_6-$VanS_A$. Proton identities in the legend correspond to those in Figure 5.3.

It is difficult to accurately measure signal attenuation, due to the relatively small differences between signal intensities in on- and off-resonance spectra. To account for inaccuracies in signal intensity measurements, the data were fit to logarithmic curves with the Equation 5.3:

$$A_{STD} = M\log_{10}(\text{saturation time}) + N \tag{5.3}$$

where M and N are constants. Fit lines were used to map the binding epitope (Figure 5.11).

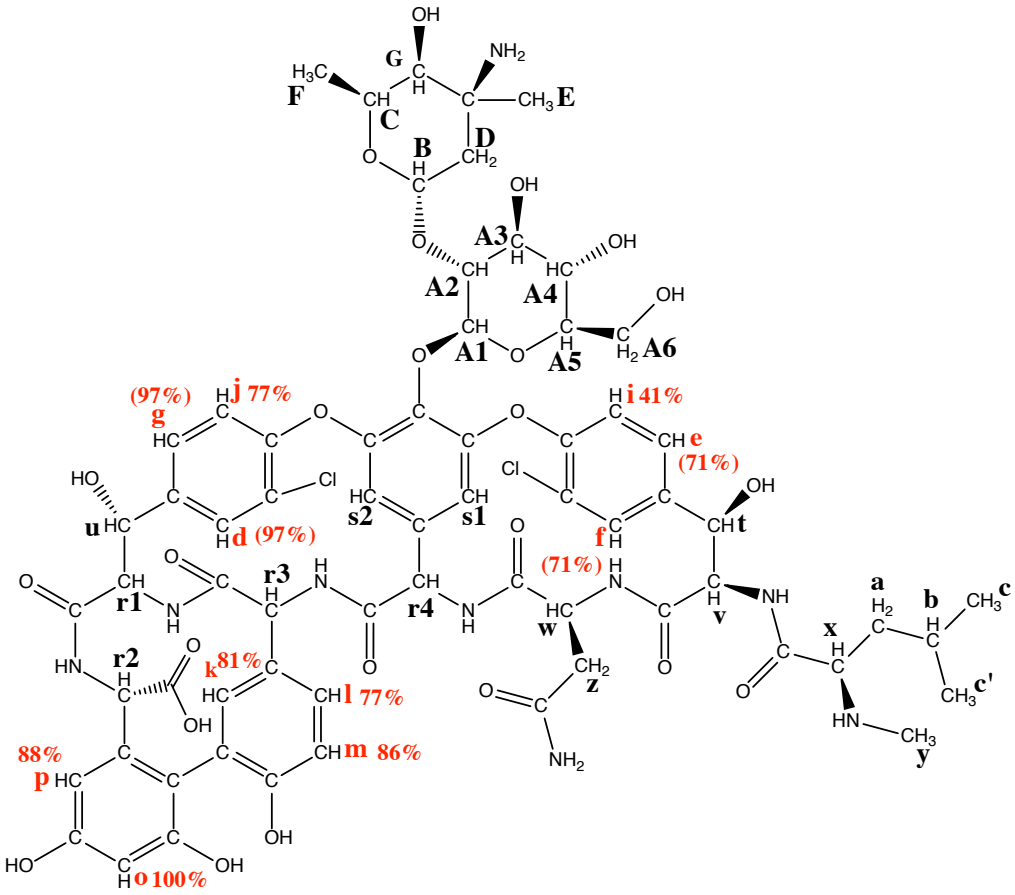

Figure 5.11: The vancomycin epitope binding His_6-$VanS_A$; vancomycin protons accumulating saturation in the presence of His_6-$VanS_A$ are highlighted in red. Signal attenuation is expressed as a percentage of maximum signal attenuation, in this case experienced by proton o. NMR signals from protons d/g and e/f could not be distinguished; signal attenuation is observed for a peak in each of these regions of the spectrum, but the exact proton involved cannot be elucidated. Relative signal attenuations in these cases are shown in parentheses.

When mapped onto the structure of vancomycin, patterns in levels of signal attenuation begin to emerge. Proton o experiences the greatest level of signal attenuation, and attenuation of each proton is scaled relative to that experienced by proton o. Near neighbours k, l, m, and p all also experience >75% of the signal attenuation of proton o, suggesting this region of the molecule is in close contact with His_6-$VanS_A$ during the interaction.

The two rings incorporating protons d/g/j and e/f/i are similar in structure and in

chemical environment. It is important to note that signal attenuation of proton d could not be distinguished from attenuation of proton g, and similarly for protons e and f. Attenuation levels displayed in the figure represent average attenuations between each pair of protons. Overall, signals from protons d/g/j are more attenuated than signals from protons e/f/i, suggesting the former ring is more closely associated with His_6-$VanS_A$.

Together, this suggests that His_6-$VanS_A$ may interface with the region of vancomycin encompassing the C-terminus of the peptide component, involving the three hydrocarbon rings housing protons d/g, j, k, l, m, o, and p.

5.6.2 The Vancomycin Epitope Binding to His$_6$-VanS$_{SC}$

Data was acquired from a sample of 9.9 μM His$_6$-VanS$_{SC}$ containing 934.4 μM vancomycin (94.2× molar excess of ligand), and processed as described above to ensure comparable baselines between spectra. STD amplification factor as a function of saturation time is shown in Figure 5.12 for identifiable vancomycin ^{1}Hs. 3.5 sec was selected as the appropriate saturation time in this experiment, as previously, because amplification factors did not increase significantly beyond this point.

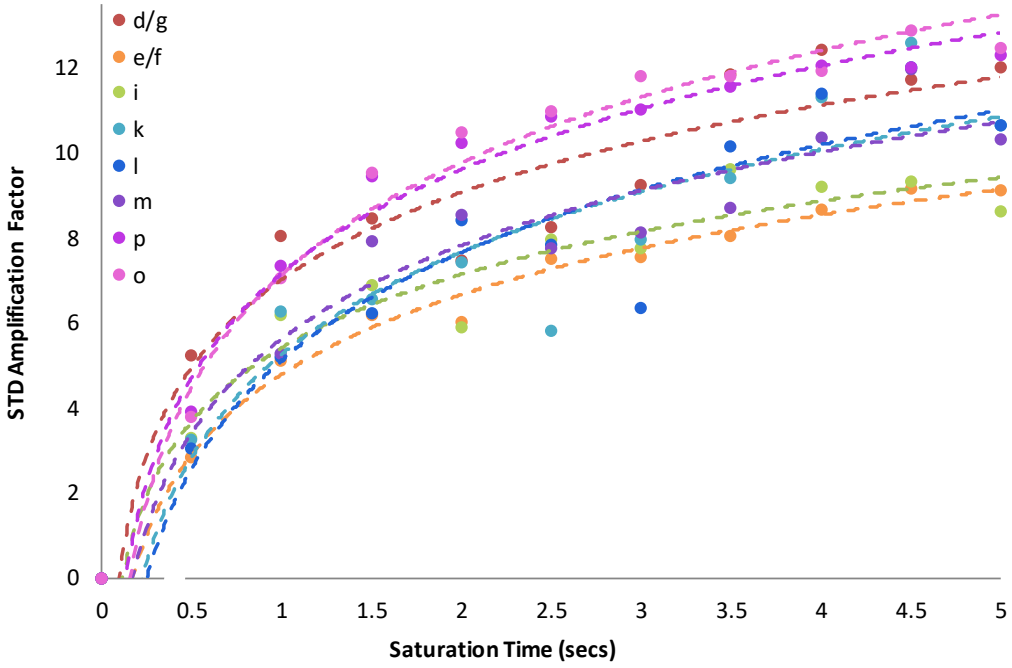

Figure 5.12: STD amplification factor as a function of saturation time, for vancomycin and His$_6$-VanS$_{SC}$.

The binding epitope of vancomycin in the presence of His$_6$-VanS$_{SC}$ is shown in Figure 5.13.

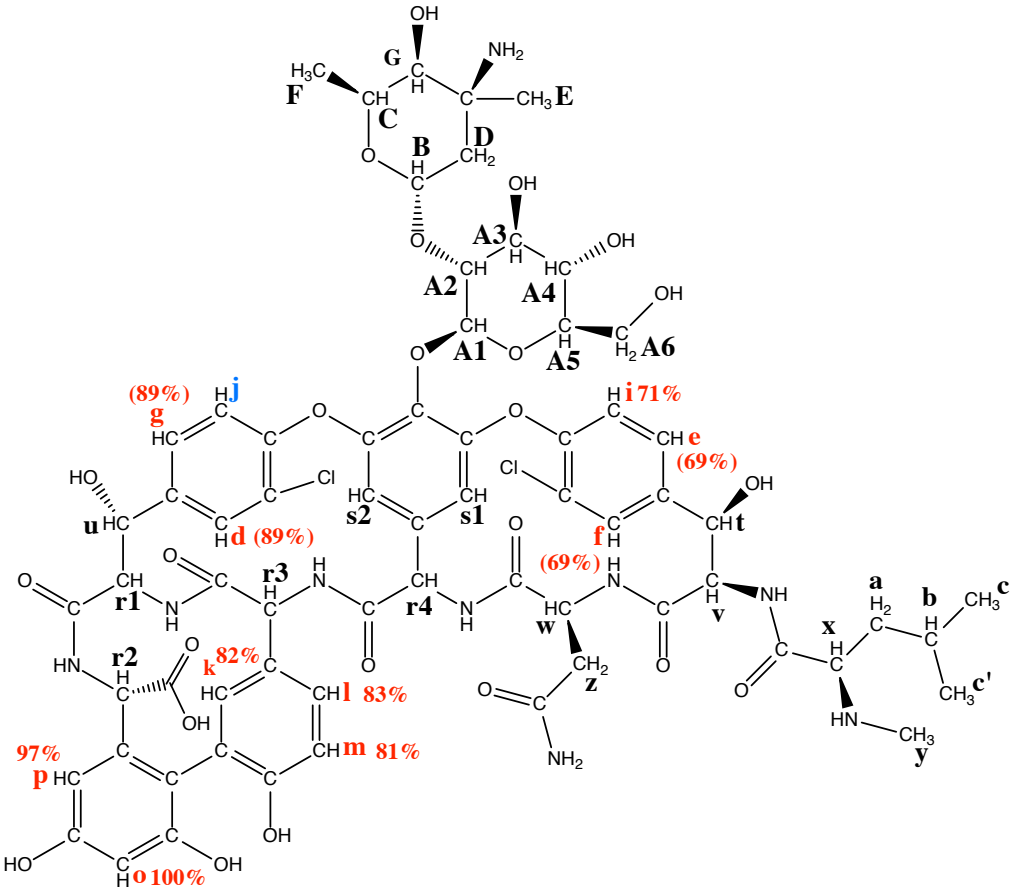

Figure 5.13: The vancomycin epitope binding His$_6$-VanS$_{SC}$; vancomycin protons accumulating saturation in the presence of His$_6$-VanS$_{SC}$ are highlighted in red. Signal attenuation is expressed as a percentage of maximum signal attenuation, experienced by proton o. The NMR signal from proton j (blue) is absent in both on- and off-resonance spectra during this titration series, suggesting a change in the chemical environment of this proton. NMR signals from protons d/g and e/f could not be distinguished; signal attenuation is observed for a peak in each of these regions of the spectrum, but the exact proton involved cannot be elucidated. Relative signal attenuations in these cases are shown in parentheses.

The most significant difference between these datasets and those discussed in Section 5.6.1 is that signals from vancomycin proton j (Figure 5.3) were not visible in His$_6$-VanS$_{SC}$ on- or off-resonance spectra (Figure 5.9). This may suggest that the chemical environment for proton j is different in these two contexts, such that a chemical shift perturbation is observed. Possibly the peak has moved so as to overlap with the peak of another proton. The chemical shifts of other protons in this region are consistent between datasets.

Other differences in the interaction between vancomycin and His_6-$VanS_A$, and His_6-$VanS_{SC}$, are also apparent. Proton i experiences a similar level of signal attenuation with respect to saturation time as protons e/f. This may be explained if signals from protons j and i are overlapping, so that the level of signal attenuation observed is the product of those of two contributing protons. Protons d/g and m experience less signal attenuation, and protons l and p experience more signal attenuation, when vancomycin interacts with His_6-$VanS_{SC}$ than with His_6-$VanS_A$.

The same general pattern in levels of signal attenuation across the structure of vancomycin is observed when interacting with either VanS protein. The interaction appears to involve the C-terminus of the peptide component, particularly the three hydrocarbon rings in that region, with the fourth ring towards the N-terminus of the peptide experiencing a lesser degree of signal attenuation. Perturbation of the chemical shift of proton j may indicate a change in chemical environment of this proton.

5.7 Estimation of Dissociation Constants from Michaelis Menten-Like Titration Curves

Using a saturation time of 3 seconds, STD-NMR data were acquired at increasing vancomycin concentrations for both His_6-$VanS_A$ and His_6-$VanS_{SC}$. Vancomycin peak intensities in difference spectra were observed to increase as vancomycin was titrated into each sample (Figures 5.14 and 5.15). Integral regions were kept constant for on- and off-resonance spectra for each titration point, but had to be varied between titration points. The chemical environment of protons in vancomycin changes over the course of the titration series, so that the exact chemical shift of each proton is different in each dataset). Since A_{STD} represents signal attenuation as a fraction of off-resonance signal intensity, so long as integration regions are consistent at each titration point, it is possible to compare A_{STD} between datasets.

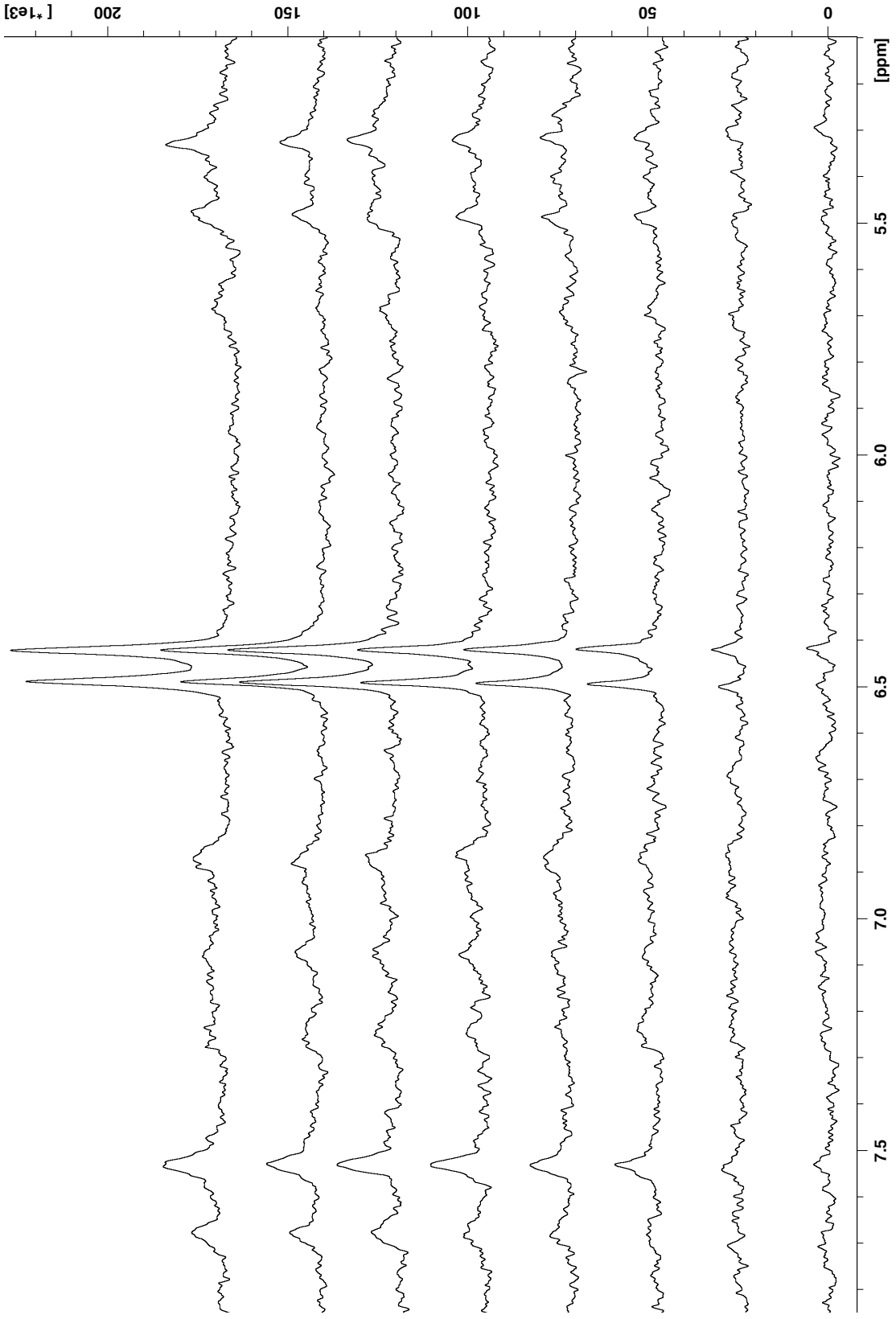

Figure 5.14: Comparison of STD difference spectra acquired of a sample of 20 μM His_6-$VanS_A$ in 25 mM sodium phosphate buffer (pD 6.8), 25 mM NaCl, 1.15 mM LMPG, and increasing concentrations of vancomycin, up to 3.4 mM.

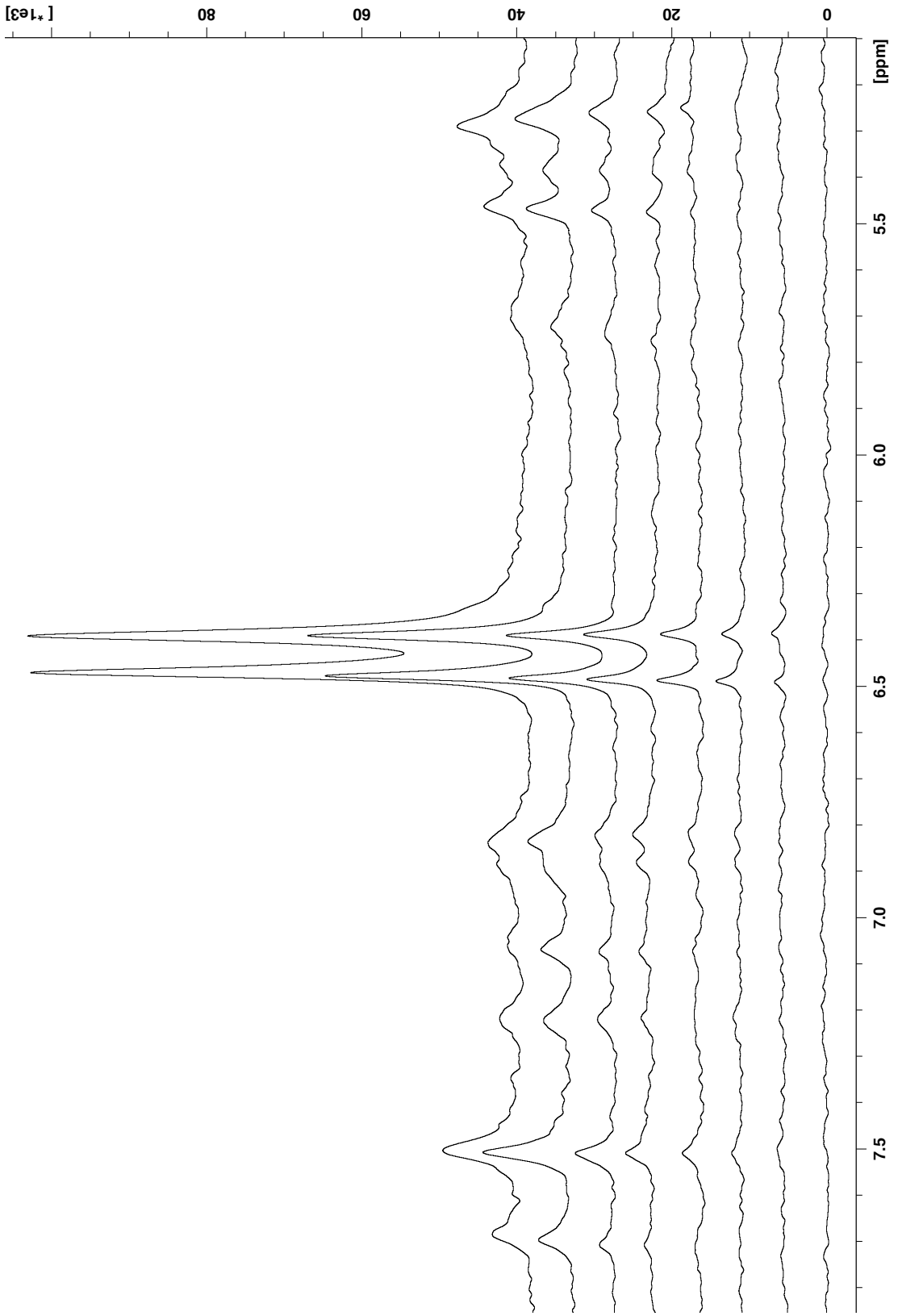

Figure 5.15: Comparison of STD difference spectra acquired of a sample of 9.9 μM His_6-$VanS_{SC}$ in 25 mM sodium phosphate buffer (pD 6.8), 25 mM NaCl, 1.15 mM LMPG, and increasing concentrations of vancomycin, up to 4.0 mM.

5.7.1 Estimating Dissociation Constants for Interactions between His$_6$-VanS and Vancomycin

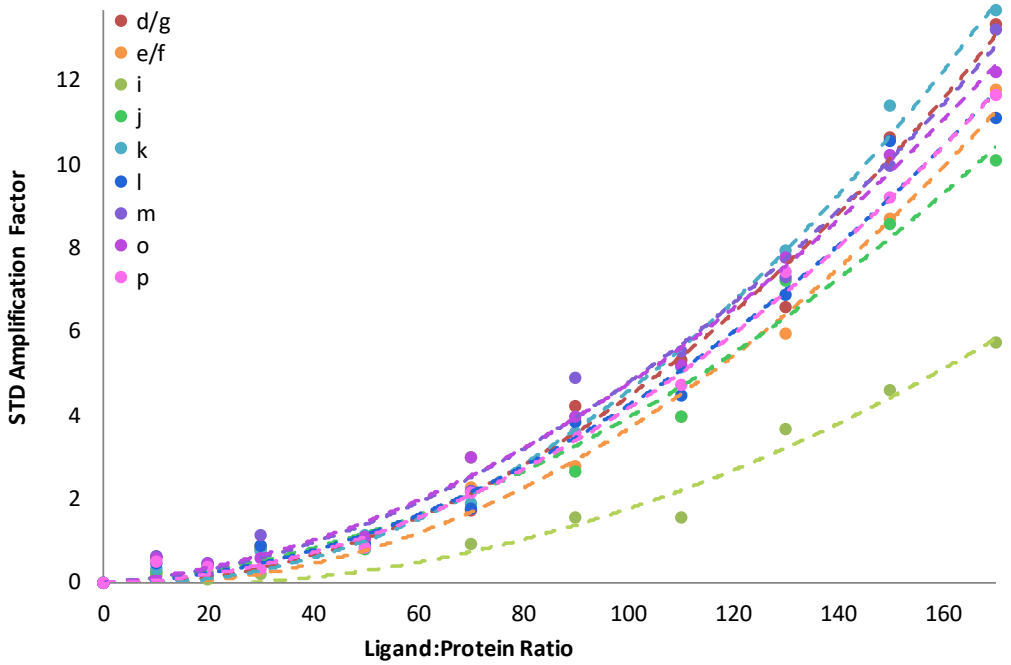

Figure 5.16: STD amplification factor as a function of ligand:protein ratio, for vancomycin and His$_6$-VanS$_A$.

Vancomycin was added in stages to a sample of 20 μM His$_6$-VanS$_A$ until a 170-fold molar excess of ligand was reached in the final sample. As ligand concentration increased, A_{STD} was observed to increase for all protons. A_{STD} is quantified in Figure 5.16. For strongly bound ligands, this relationship will follow the Michaelis Menten equation (Equation 5.4, below), and a dissociation constant (K_D) for each proton can be estimated.

$$v_0 = \frac{V_{MAX}[L]}{K_M + [L]}, \quad A_{STD} = \frac{\alpha_{STD}[L]}{K_D + [L]} \tag{5.4}$$

Obtaining a reliable value for K_D relies on saturation of the interaction, reaching a maximum amplification factor α_{STD}. K_D estimates for each proton can be averaged to give an apparent dissociation constant ($K_{D(app)}$) (Viegas et al., 2011).

However, as shown in Figure 5.16, while an increase in vancomycin concentration

does lead to increasing A_{STD}, we were unable to saturate this interaction. It is apparent from the A_{STD} curve that significantly higher concentrations of vancomycin would be required to reach the α_{STD} plateau. The data acquired indicate that the dissociation constant for this interaction is very high, thus the interaction is very weak. Vancomycin proton i shows an even weaker interaction, with a slower increase in A_{STD} with respect to vancomycin concentration than the other observable protons.

STD-NMR data were also acquired for increasing concentrations of vancomycin and 9.9 μM His$_6$-VanS$_{SC}$. A 400-fold molar excess of vancomycin was reached in this case.

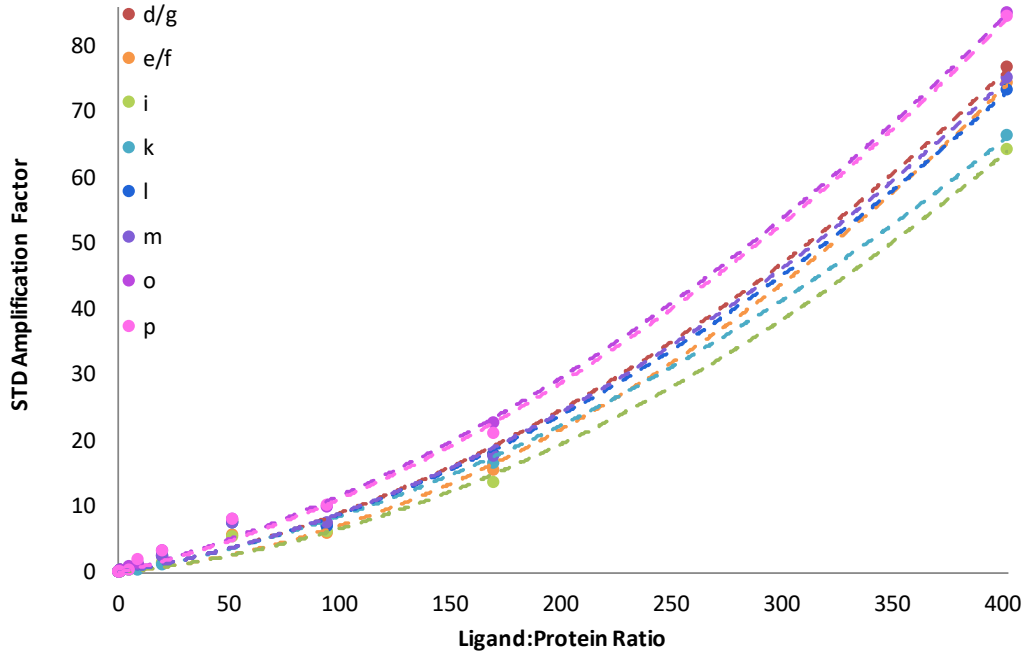

Figure 5.17: STD amplification factor as a function of ligand:protein ratio, for vancomycin and His$_6$-VanS$_{SC}$.

As with the interaction between vancomycin and His$_6$-VanS$_A$ (Figure 5.16), the data form an exponential curve representing the early stages of a Michaelis-Menten binding curve. Although a 400-fold molar excess of ligand is achieved in this case, a plateau at α_{STD} is not reached. The dissociation constant for this interaction is very high, representing a very weak interaction.

Unlike in the interaction with His$_6$-VanS$_A$, in this case, all involved protons exhibit

similar changes in A_{STD} with respect to ligand concentration. Vancomycin proton j does not appear in on- or off-resonance spectra in this experiment, although it is prominent in the presence of His_6-$VanS_A$ (Figure 5.9). This may indicate that vancomycin interacts differently with the two proteins, exposing proton j to a different chemical environment in each case.

5.8 Investigation of Saturation Transfer from His_6-$VanS_A$ to the Lipid II Pentapeptide

As a preliminary investigation into an interaction between His_6-$VanS_A$ and the lipid II pentapeptide, data was acquired of a mixed sample of His_6-$VanS_A$ and pentapeptide as described in Section 5.6.1 across a range of saturation times. Observation was limited to protons in the downfield region of the spectrum - the amide protons of each residue - due to intrusion of LMPG NMR signals.

No transfer of saturation to pentapeptide protons is observed (Figure 5.18).

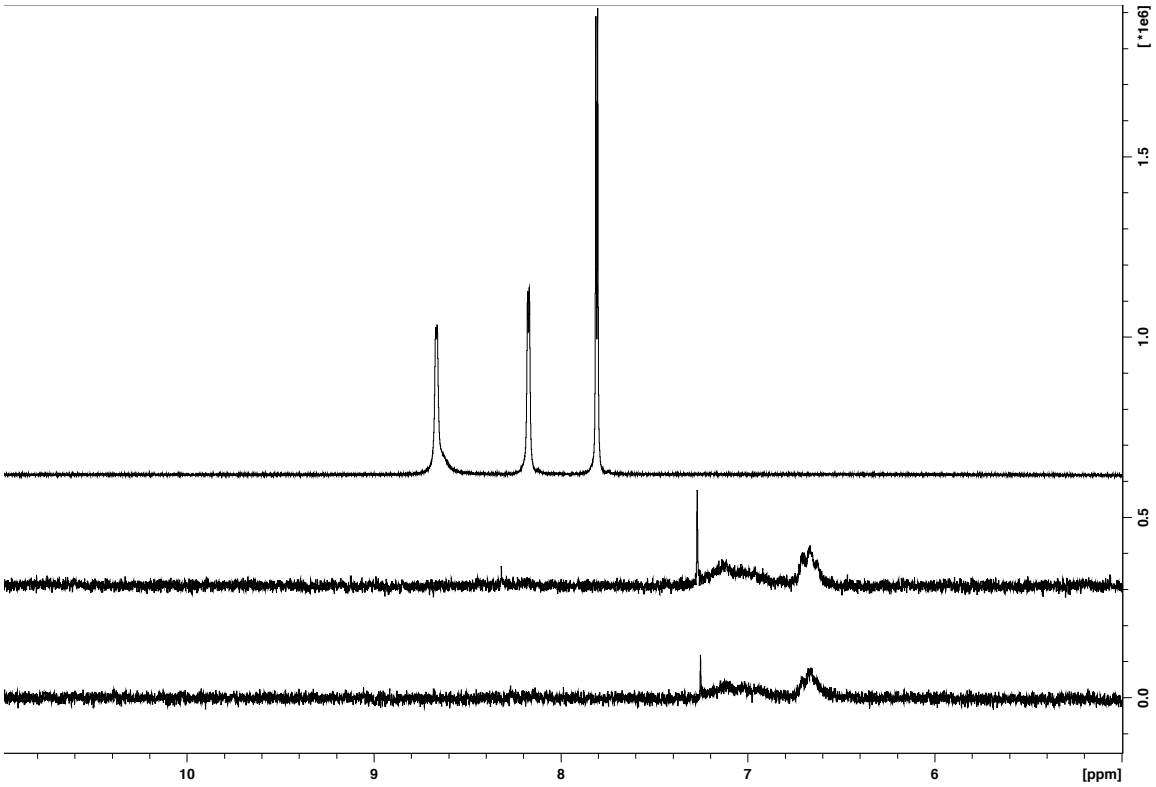

Figure 5.18: ^{1}H 1D NMR spectrum of the lipid II pentapeptide (top), and difference spectra of 10 μM His_6-$VanS_A$ in the absence (middle) and presence (bottom) of 1 mM pentapeptide, saturated for 5 seconds at an on-resonance frequency of 6.7 ppm to excite protons in His_6-$VanS_A$ while avoiding protons in the pentapeptide. No transfer of saturation from the protein to the peptide is observed, indicating that binding does not occur.

5.9 Discussion

5.9.1 STD-NMR as a Technique for Studying VanS Ligand Binding

STD-NMR is a method suited to systems in which a relatively small ligand interacts with a relatively large protein. Since larger molecules tumble more slowly, resulting in reduced signal intensity and peak broadening, solution-state NMR is generally poorly suited to the study of larger molecules. STD-NMR bypasses the size limit to the study of large molecules in solution, by focusing on protons within small ligands in solution, rather than on protons within the protein itself.

STD-NMR has been used to investigate the binding of one receptor to several potential ligands at once; if the ligands contain sufficiently few observable protons, so that their ^{1}H 1D spectra do not overlap, then a mixed samples of several potential ligands and the receptor may be prepared and analysed. Saturation will transfer from protons of the protein to protons of the ligand, but not to protons of the other small molecules in the sample. The ligand may then be identified by comparison of the STD-NMR difference spectrum to appropriate reference spectra of each ligand screened. STD-NMR may therefore represent a fast method of identifying a protein's ligand from a mixed sample of several molecules of interest.

In the case of VanS ligand binding, multiple ligands could not be screened simultaneously. Potential ligands to VanS include vancomycin, teicoplanin, moenomycin, and lipid II; these molecules, while under 2 kDa in mass and therefore small enough to study by solution state NMR, are sufficiently large that their ^{1}H 1D spectra overlap - particularly in the case of vancomycin and teicoplanin, which share significant structural similarities. Each potential ligand was therefore investigated separately.

A disadvantage of the STD-NMR technique is the need to identify suitable on-resonance frequencies to selectively saturate particular protons within a system, while avoiding others. On-resonance frequencies were identified by which protons in VanS could be selectively saturated, without affecting protons in vancomycin or in the lipid II pentapeptide.

However, an appropriate on-resonance frequency could not be identified for teicoplanin. STD-NMR is therefore not an appropriate technique to investigate interactions between teicoplanin and VanS.

However, STD-NMR was successful in studying the interactions of VanS with both vancomycin and the lipid II pentapeptide. STD-NMR offers a straightforward solution-state NMR approach to the study of ligand-binding, requiring only small quantities of receptor and ligand, and avoiding the need for costly preparative steps such as isotopic labelling.

5.9.2 The Lipid II Pentapeptide Does Not Appear to Bind to VanS

STD-NMR data was acquired for the lipid II pentapeptide in the presence of His_6-$VanS_A$. While saturation transfer was observed from both proteins to vancomycin, saturation was not observed to transfer from His_6-$VanS_A$ to the lipid II pentapeptide. The absence of an observable interaction between VanS and the pentapeptide supports the validity of the observed interactions with vancomycin, since this suggests that saturation transfer to vancomycin was not an artifact of the experimental design.

$VanS_{SC}$ is sensitive only to vancomycin, while $VanS_A$ is sensitive to vancomycin, related glycopeptide antibiotics, and moenomycin. While moenomycin is not structurally related to vancomycin, its presence could also result in an accumulation of lipid II as its mode of activity is to inhibit transglycosylase, an enzyme involved in integrating the disaccharide-pentapeptide component of lipid II into the peptidoglycan cell wall. If lipid II, or a related degradation product, is a ligand to any VanS protein, therefore, $VanS_A$ is a likely candidate.

Since an interaction between $VanS_A$ and the pentapeptide was not observed, further investigation into the interaction between $VanS_A$ and lipid II could focus on other regions of the lipid II molecule. Lipid II consists of a pentapeptide, a dissacharide, and a lipid chain. The terminal D-Alanyl-D-Alanine of the pentapeptide is crucial for the interaction between lipid II and vancomycin. If the lipid II/vancomycin complex is the ligand to $VanS_A$, then the terminal dipeptide is likely to be occluded during binding to vancomycin, so is unlikely to be involved in an interaction with $VanS_A$.

5.9.3 Weak Binding of Vancomycin to VanS Is Observed

Interactions were observed between vancomycin and both His_6-$VanS_A$ and His_6-$VanS_{SC}$ by STD-NMR. The interaction appears to involve the C-terminus of the peptide component of vancomycin, as signals of protons in the three hydrocarbon rings in this region of the molecule are more attenuated than signals from protons in the fourth hydrocarbon ring, nearer the N-terminus of the peptide. Other protons within vancomycin could not be probed by STD-NMR due to the intrusion of upfield NMR signals from LMPG.

Dissociation constants for the interactions between vancomycin and either VanS protein could not be calculated; These values are expected to be very high. A 200-fold molar excess of ligand is typically sufficient to reach a maximal STD amplification factor for interactions with K_D between 10^{-8} and 10^{-3} M (Viegas et al., 2011); a 400-fold molar excess of vancomycin was applied to His_6-$VanS_{SC}$ without approaching the maximal STD amplification factor, suggesting the K_D for each interaction exceeds this range.

Koteva et al. (2010) report an interaction between His_6-$VanS_{SC}$ and a modified vancomycin photoprobe. Phillips-Jones et al. (2017) report indirect observation of an interaction between His_6-$VanS_A$ and vancomycin, via changes in protein conformation and analytical ultracentrifugation sedimentation rate of the protein on exposure to the antibiotic. Thus, while there exists evidence in the literature to support vancomycin as the ligand to VanS, this STD-NMR study represents the first time that a direct observation has been made of an interaction between VanS and vancomycin.

Chapter 6

Structural and Ligand-Binding Characterisation of the VanS Extracellular Domain

6.1 Introduction

VanS is an integral membrane protein, comprised of two transmembrane helices flanking a short extracellular domain, and a C-terminal catalytic domain of approximately 30 kDa (Figure 6.1A). The extracellular domain is expected to contain the site at which any ligand, such as vancomycin, could bind. Therefore, a structural understanding of this extracellular domain is a required first step to understanding the mechanism of ligand-binding, and downstream antibiotic resistance. Previous studies have identified the upstream end of the extracellular domain of $VanS_{SC}$, and in particular, the short sequence D38-W41, as having an affinity for a modified vancomycin photoprobe (Koteva et al., 2010).

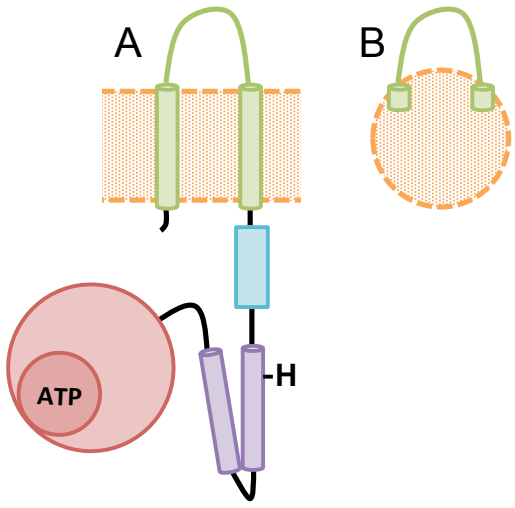

Figure 6.1: A: Schematic showing VanS inserted into a membrane, with predicted structural components: transmembrane helices flanking extracellular sensor domain (green); HAMP domain (blue), DHp domain (purple); ATPase domain (red); adapted from Bhate et al. (2015). B: the hypothesised insertion of a 40meric peptide, comprising extracellular domain and transmembrane "anchors", into a detergent micelle.

In Chapter 5, a ligand-focused binding study was carried out. STD-NMR experiments identified vancomycin as a weak binding partner to both His_6-$VanS_A$ and His_6-

$VanS_{SC}$. Protons within vancomycin which came into close spatial proximity (<5 Å) with VanS were identified; however, the binding site on either protein was investigated by this method.

VanS is a large protein and has a propensity to assemble into dimer (Koteva et al., 2010), so that the final protein mass is in excess of 80 kDa. This makes structural investigation of the protein binding site intractable by methods such as solution-state NMR, where the slow molecular tumbling of the full-length protein leads to broadening of NMR peaks and negatively impacts the resolution of NMR spectra. Likewise, methods such as circular dichroism can be used to characterise the secondary structure of a protein, but the whole protein is considered at once; individual regions of a protein cannot be studied independently by this technique. Therefore, within a large protein, it is difficult to assess the secondary structure of a small domain because the structures of larger neighbouring domains will contribute significantly to the overall signal.

For these reasons, it is frequently desirable to divide a large protein into smaller domains, and characterise these separately. The division of large proteins, including membrane proteins, into their constitutive domains for detailed study is established in the literature (Bordan and Keller, 2010). This "divide and conquer" approach does introduce the possibility that removal of regions from the intact protein might lead to destabilisation of structure. However, this must be weighed against the significant advantage of working with protein regions of a size that is readily studied by a full range of methods including NMR, and has proved particularly popular in the study of transmembrane helices (Nash et al., 2015), and membrane-associated amphipathic helices (Breeze et al., 2016).

To build on the STD-NMR results presented in Chapter 5, and on the work of Koteva et al. (2010) who propose that phosphorylation activity of VanS is induced by direct binding of vancomycin to the N-terminus of the $VanS_{SC}$ extracellular domain, we take a divide and conquer approach to investigation of the structure and vancomycin-binding properties of this domain of $VanS_{SC}$. To achieve this, synthetic peptides representing this domain were purchased, purified, and reconstituted in a range of membrane mimetics. The structures of

the peptides under various conditions were characterised using circular dichroism and NMR. Ligand-binding studies identified residues in this region which are affected by exposure to vancomycin. Simultaneously, solution-state NMR studies of vancomycin allowed regions of the ligand which are affected by exposure to the synthetic peptide to be identified.

6.2 Aims

1. To rationally design synthetic peptides corresponding to portions of the extracellular domain of VanS_{SC};
2. To purify these peptides by HPLC;
3. To investigate the secondary structures of these peptides under various solution conditions, using circular dichroism spectroscopy and solution state NMR;
4. To investigate interactions between these peptides and the glycopeptide antibiotic vancomycin.

6.3 Sequence Selection of VanS$_{SC}$ Extracellular Domain Synthetic Peptides

The transmembrane and extracellular domains of VanS$_{SC}$ are shown in Figure 6.2, alongside the sequences of two synthetic peptides which were acquired for study.

```
VanS_SC
LTLSYAGFLTLAGVLLLVAVGVFLLDQGWLLTNERGAVRATPGTVFLRSFAPTAAWVMAFLLVFGLVGGWFLAG

VSC_EC-40
                    VAVGVFLLDQGWLLTNERGAVRATPGTVFLRSFAPTAAWV

VSC_EC-25
                              DQGWLLTNERGAVRATPGTVFLRSF
```

Figure 6.2: Sequence alignment of the transmembrane and extracellular domains of VanS$_{SC}$ (top) and two synthetic peptides (middle and bottom). Transmembrane domains, predicted by TMHHM, are highlighted in blue. The 40mer VSC$_{EC-40}$ includes transmembrane "anchors" comprised of the distal ends of each transmembrane domain, intended to encourage interaction between the peptide and membrane mimetics. The 25mer VSC$_{EC-25}$ represents the core extracellular domain, beginning with the region D38-W41 proposed by Koteva et al. (2010) to form a vancomycin binding site.

The first peptide, referred to here as VSC$_{EC-40}$, corresponds to the extracellular domain of VanS$_{SC}$, and the six residues flanking either end of the domain. These residues represent the outer portions of each transmembrane helix, and were included in order to encourage the peptide to associate with membrane mimetics (Figure 6.1B). A second peptide, referred to as VSC$_{EC-25}$, contains the core 25 residues that comprise the extracellular domain, and begins with the sequence D38-W41 previously suggested to form a potential binding site for vancomycin (Koteva et al., 2010).

6.4 Purification of Synthetic Peptides by HPLC, and MALDI-TOF Analysis of Peptide Purity

Peptides were purchased in both crude and purified states. It was frequently necessary to purify peptides by HPLC, either to isolate the peptide from the crude sample purchased from the supplier, or to retrieve peptide from previously prepared samples. 1 mg crude peptide, or several pooled lyophilised samples containing up to 0.5 mg peptide in total, was solubilised in 200 μL Buffer B (Table 2.6) and purified on a Luna C5 Reversed Phase 10 $\times$ 250 mm HPLC column (Phenomenex, California) as outlined in Section 2.5. The absorbance at 280 nm (A_{280}) of the column eluate was monitored throughout, and is shown in Figure 6.3. Aromatic amino acids absorb light at this wavelength, and both peptides contain a number of such residues. An increase in absorbance therefore indicates the presence of protein in the column eluate. 1 mL fractions were collected from the column, and fractions corresponding to peaks in A_{280} were analysed by MALDI-TOF mass spectrometry (Section 2.6.5) for the presence and relative purity of the desired peptide. Typically, purified peptide would be present in 2-3 fractions around the major peak of the chromatogram (outlined in figure), with smaller quantities of contaminated peptide present in other fractions. Pure peptide fractions were pooled and lyophilised, then resolubilised in a minimum volume of 50% acetonitrile. Peptide concentration was calculated from absorbance at 280 nm, using extinction coefficients ϵ_{280} = 11000 M^{-1} cm^{-1} for VSC_{EC-40} and ϵ_{280} = 5500 M^{-1} cm^{-1} for VSC_{EC-25}. Solutions were separated into aliquots each containing 0.2 mg peptide, and these aliquots were then lyophilised and stored at -20 °C.

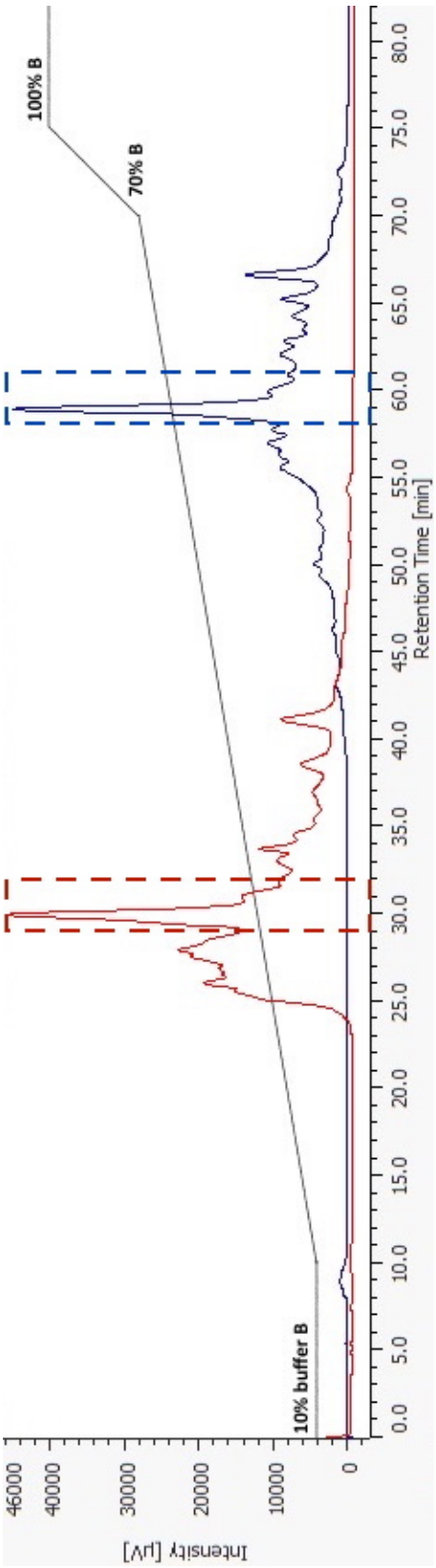

Figure 6.3: Chromatogram showing the absorbance at 280 nm (A_{280}) of eluate from a Luna C5 HPLC column (Phenomenex, California) following injection of 1 mg crude VSC_{EC-25} (red) or VSC_{EC-40} (navy). After an initial application of 10 mL 10% buffer B to clear the column void volume, a gradient was applied at a flowrate of 1 mL min^{-1} increasing % B by 1% every minute until 70% B was reached. At this point, all material was eluted from the column. % B was increased to 100% over 5 minutes and the column was washed at 100% B for 20 minutes. 1 mL fractions were collected and analysed by MALDI-TOF. Fractions containing purified peptide are highlighted in the figure. VSC_{EC-25} eluted at 29% buffer B, while VSC_{EC-40} eluted at 58% buffer B.

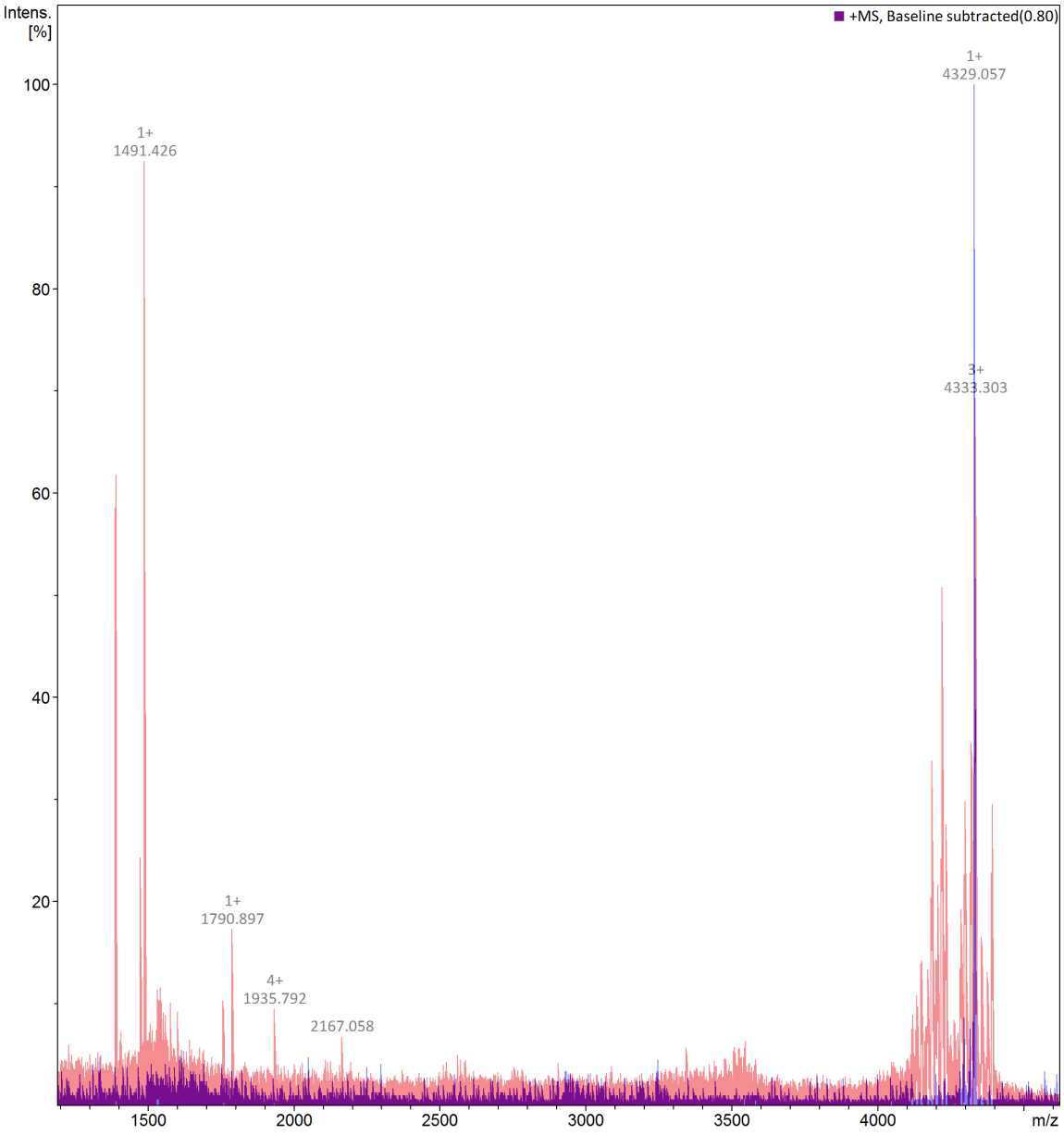

Figure 6.4: Overlaid MALDI-TOF spectra of crude (red) and HPLC-purified (blue) VSC_{EC-40}, with an expected molecular weight of 4329.07 Da. Spectra are scaled to relative intensity. Significant contamination of species with molecular weights around 1500 or 4200 Da are removed by HPLC purification.

6.5 Circular Dichroism Analysis of Peptide Fold in the Presence of Different Membrane Mimetics

Purified, lyophilised peptide samples were solubilised into minimal volumes of 25 mM sodium phosphate buffer (pH 6.8), 25 mM NaCl. This produced concentrated stocks of approximately 2-3 mg mL^{-1} peptide. Samples were centrifuged at 7,000 $\times$ g for 3 minutes to remove any precipitate. Stocks were diluted in appropriate solutions of detergent micelles, to yield samples for CD spectrometry consisting of approximately 1 mg mL^{-1} peptide and 100 mM of a chosen detergent.

In CD, the required protein concentration decreases linearly with respect to the pathlength of the cuvette used. Acquisition of CD spectra in a 0.1 cm pathlength cuvette typically requires a protein solution of approximately 0.1 mg mL^{-1}, although the exact optimal concentration must be determined experimentally as it depends upon the protein and the solution conditions. Acquisition in a 0.02 cm pathlength cuvette requires an approximately 5-fold increase in protein concentration from that used in a 0.1 cm pathlength cuvette. When the secondary structure of VSC_{EC-25} was characterised by circular dichroism spectroscopy, a 0.02 cm pathlength cuvette was used to minimise the effects of scattering, which increases high tension voltage during acquisition of CD data. In order to acquire CD data in a cuvette of this narrow pathlength, the peptide concentration was subsequently increased.

6.5.1 Secondary Structure Analysis of VSC_{EC-40} by Circular Dichroism

VSC_{EC-40} was found to be insoluble in aqueous buffers; the secondary structure of this peptide could therefore not be assessed in the absence of membrane mimetics. Jpred4 (Drozdetskiy et al., 2015), a secondary structure prediction tool, predicted the peptide to be 15% helical with 23% β-strands. CD spectra were acquired of VSC_{EC-40} in a 0.1 cm pathlength cuvette, at a concentration of 0.1 mg mL^{-1} in 100 mM DPC and 100 mM LMPG detergent micelles (as described in Section 2.7) and results are shown in Figure 6.5. The resulting spectra were fit using the CDSSTR (Sreerama and Woody, 2000) analysis program in Dichroweb (Whitemore and Wallace, 2007), which estimates the secondary structure of the peptide to be 52% helical, 10% β-strands, and 12% turns in DPC micelles (NRMSD = 0.017), and 28% helical, 16% β-strands, and 19% turns in LMPG micelles (NRMSD = 0.016).

In both cases, high tension exceeded 600 V below 190 nm, so datasets were truncated to exclude data collected below this wavelength.

The high level of α-helical secondary sturucture in the 40 mer peptide was surprising. Based on the known secondary structure characteristics of this region of $VanS_{SC}$, we expect to observe approximately 30% α-helicity, localised to the exterior ends of the two transmembrane helices flanking the extracellular domain. Helicity greater than 30% indicates that some portion of the extracellular domain may also be adopting a helical conformation in the presence of a membrane mimetic. Overall helicity of 53% in DPC micelles suggests that a further 23% of the peptide, equivalent to approximately 9 residues within the extracellular domain, is adopting a helical conformation in the presence of DPC micelles.

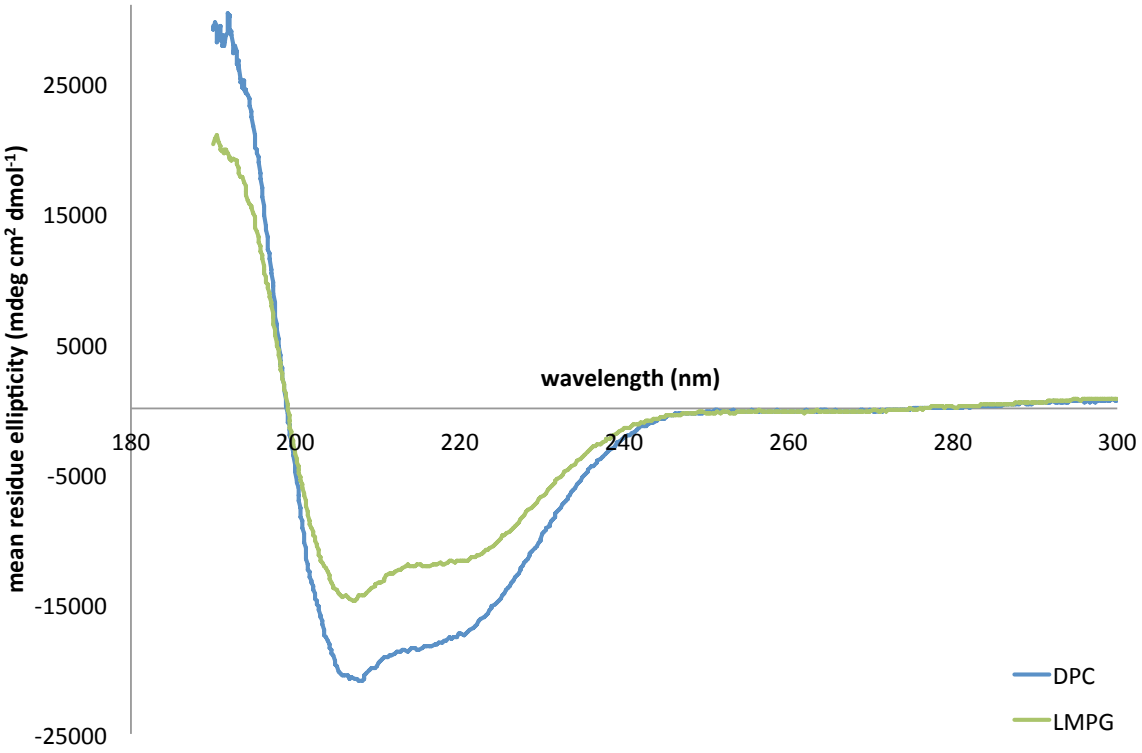

Figure 6.5: Circular dichroism spectra of VSC_{EC-40} in 100 mM DPC micelles (blue) and 100 mM LMPG micelles (green). Data were acquired as described in Section 2.7. CDSSTR estimates the peptide to be 53% α-helical in DPC (NRMSD = 0.017), and 38% α-helical in LMPG (NRMSD = 0.016).

6.5.2 Secondary Structure Analysis of VSC_{EC-25} by Circular Dichroism

To further investigate the structure of the VanSSC extracellular domain, as well as any intrinsic ability of this region to associate with membrane mimetics independent of the transmembrane helices, a synthetic peptide was acquired containing only the sequence of the core 25 residues. The shorter peptide lacked flanking transmembrane "anchors", whilst retaining residues D38-W41 suggested to form a potential binding site for Vancomycin (Koteva et al., 2010).

VSC_{EC-25} was soluble aqueous buffers, so its structure in the absence of membrane mimetics was measured using CD (Figure 6.6). From the amino acid sequence, Jpred4 predicts VSC_{EC-25} to be 0% helical with 40% β-strands. CDSSTR fitting of the spectrum estimated that the secondary structure of VSC_{EC-25} is 7% α-helical, 33% β-strands, and

22% turns when solubilised in sodium phosphate buffer (NRMSD = 0.051).

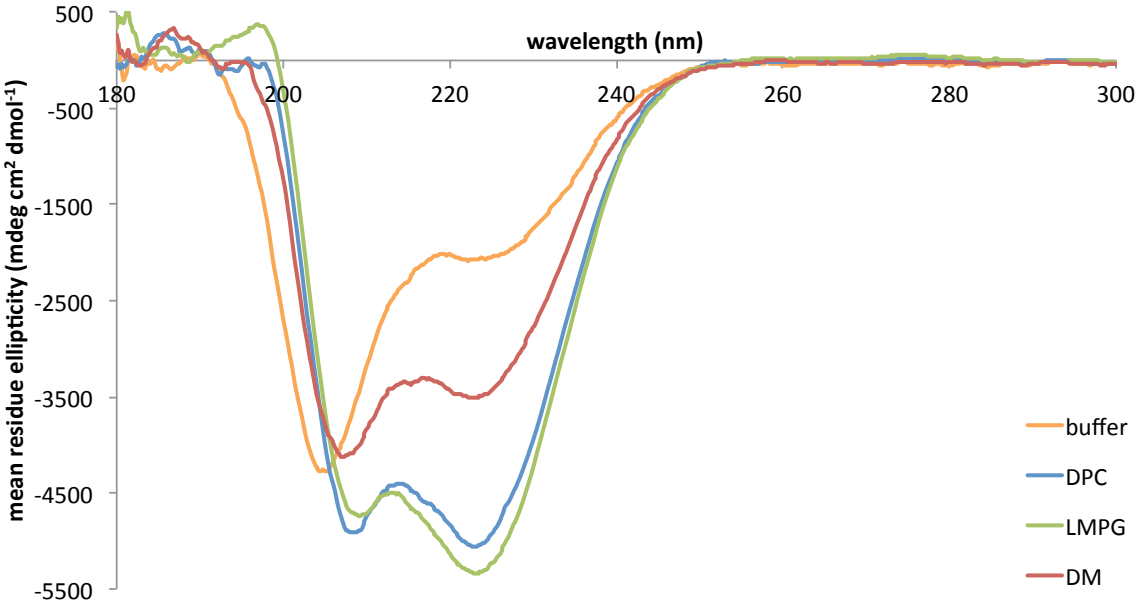

Figure 6.6: Circular dichroism of VSC_{EC-25} in the absence of a membrane mimetic (orange), and in 100 mM DPC (blue), 100 mM LMPG (green), or 100 mM DM (red). Data acquired as in Section 2.7. CDSSTR estimates the peptide is 7% helical in buffer (NRMSD = 0.051), 11% helical in DPC (NRMSD = 0.048), 11% helical in LMPG (NRMSD = 0.047), and 9% helical in DM (NRMSD = 0.047).

The secondary structures of VSC_{EC-25} exposed to micelles of various detergents were also analysed by CD (Figure 6.6). Qualitatively, it is obvious from the spectra that addition of any of the three detergents causes a dramatic change in the CD spectrum. A positive peak in the vicinity of 190 nm was not recorded for the peptide in the presence of any mimetic. Though spectra in this region appear noisy, high tension never exceeded 600 V, suggesting the absence of 190 nm peak is real and not an artifact of poor signal:noise. Unlike in datasets acquired of full-length $VanS_{SC}$ (Section 3.8) or of VSC_{EC-40} (Section 6.5.1), no datapoints in spectra acquired from VSC_{EC-25} were discarded as a result of excessive high tension.

CDSSTR estimates of secondary structures (Sreerama and Woody, 2000), and estimates calculated from ellipticity at 222 nm (Ysselstein et al., 2015), are outlined in Table 6.1. There is poor agreement between the two prediction methods, although general trends

are consistent; the peptide is more helical in DPC and LMPG than in DM, and more still than in the absence of a mimetic. These trends are supported by visual analysis of the spectra, and suggest that the presence of a membrane mimetic stimulates a measurable change in the secondary structure of the extracellular domain.

		CDSSTR Estimate			
Membrane Mimetic	% α-helix$_{222}$	% α-helix	% β-strand	% turn	NRMSD
none	5	7	33	22	0.051
100 mM DPC	14	11	32	25	0.048
100 mM LMPG	15	11	31	25	0.047
100 mM DM	9	9	35	25	0.047

Table 6.1: Estimations of secondary structure content of VSC$_{EC-25}$ in 25 mM sodium phosphate buffer (pH 6.8), 25 mM NaCl, and a number of detergent micelles, from CD spectra acquired at 25 °C as described in Section 2.7.

6.6 Solution State NMR Analysis of Peptide Fold in DPC-d_{38} Micelles

To characterise the fold of the 25 mer peptide in DPC micelles at atomic resulution, and thus gain a molecular level understanding of how the membrane mimetic is changing the peptide fold, solution-state NMR was used. The small size of the peptide was amenable for use of 1H detected NMR, thus circumventing the requirement for isotopic labeling in the first instance. This approach did require use of a fully deuterated membrane mimetic, so that signals from the detergent would not obscure signals from the peptide. Since DPC micelles were used throughout this study, fully deuterated DPC (DPC-d_{38}) micelles were used for this part of the work.

6.6.1 Partial ^{1}H Assignment of VSC_{EC-25}

A 200 μL NMR sample was prepared, containing 1 mM VSC_{EC-25} dissolved in 25 mM sodium phosphate buffer (pH 6.8), 25 mM NaCl, 100 mM DPC-d_{38} (equivalent to 1.4 mM micelles), and 10% D_2O. To assign the proton signals in VSC_{EC-25} under these conditions, two-dimensional ^{1}H-^{1}H 80 ms TOCSY and 80 ms NOESY spectra were acquired at multiple mixing times ranging from 70 ms for TOCSY and 80 ms for NOESY spectra (as described in Section 2.9.3). An overlay of the fingerprint region of TOCSY and NOESY spectra for the peptide in DPC micelles is shown in Figure 6.7. Spectra were assigned with reference to published ^{1}H chemical shift values for amino acids in random coil structures (McDonald and Phillips, 1969), however only partial assignment of these spectra was possible because fewer NMR signals were resolvable in the spectra than would account for every proton within the peptide. In particular, NMR signals corresponding to amino acid sidechain protons were absent in TOCSY spectra even following significant optimisation of experimental parameters. Chemical shift assignments are tabulated in Table 6.2.

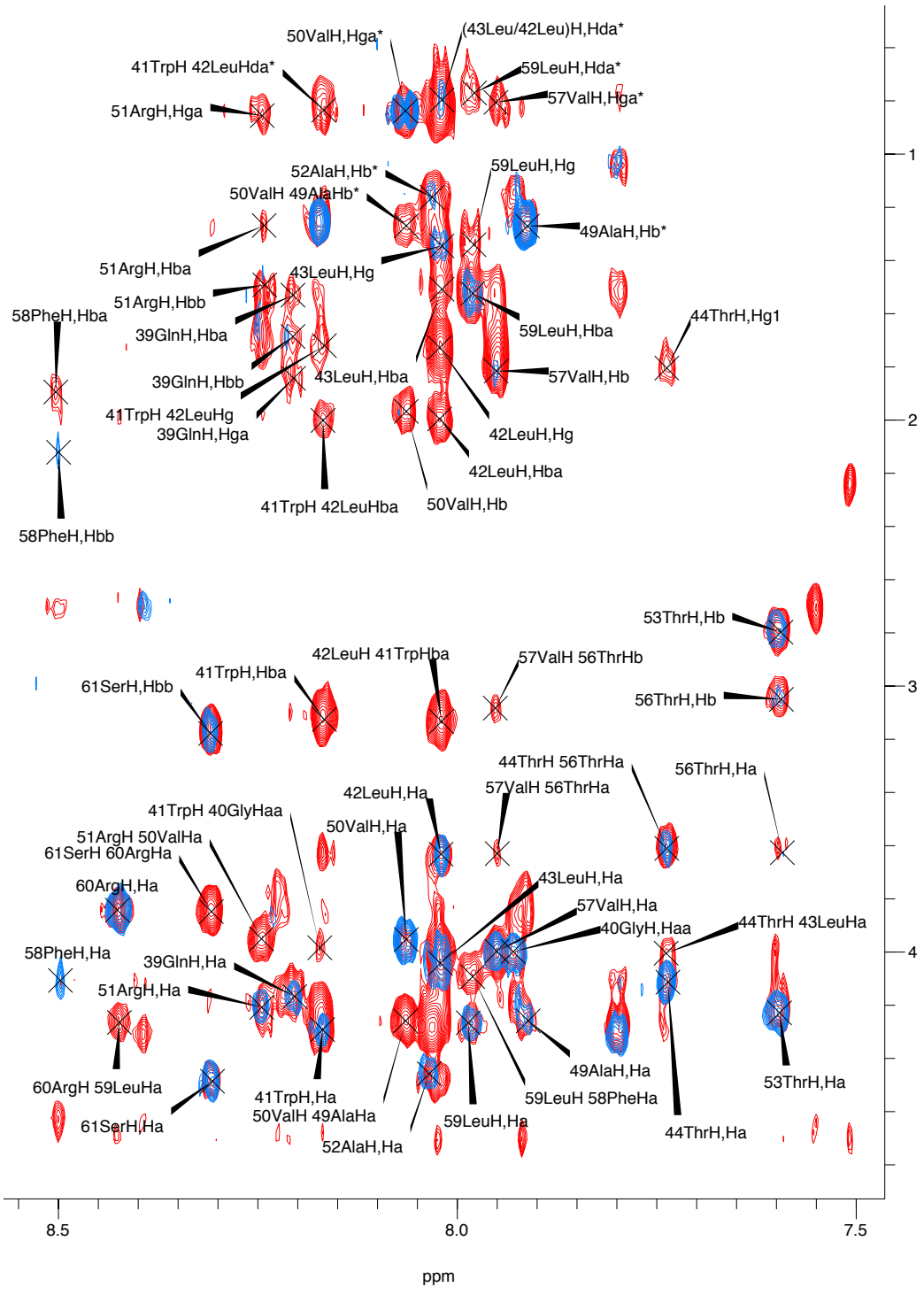

Figure 6.7: Fingerprint region of overlaid 80 ms TOCSY (blue) and 80 ms NOESY (red) spectra acquired for VSC_{EC-25} solubilised into 100 mM DPC-d_{38}, 25 mM sodium phosphate buffer (pH 6.8), 25 mM NaCl, 10% D_2O, showing crosspeaks between amide and sidechain protons. The spectra are partially assigned; there are insufficient peaks present in the spectrum to account for all protons in the peptide. In particular, signals from (upfield) sidechain protons are underrepresented in TOCSY spectra.

	δ (ppm)															
Residue	HN	Hα	Hβ		Hγ		Hδ		Hϵ		Hη		Hζ	
D38														
Q39	8.205	4.174	1.528	0.687	1.827									
G40	7.940	3.996												
W41	8.170	4.298	3.124				7.254		10.533	7.432	6.908		7.370	6.950
L42	8.022	3.635	2.001		1.724		0.809							
L43	8.016	4.200	1.504		1.346		0.805							
T44	7.739	4.111			1.805									
N45														
E46														
R47														
G48														
A49	7.916	4.257	1.270											
V50	8.066	3.958	1.967		0.839	0.844								
R51	8.235	4.226	1.269	1.499	0.855									
A52	8.031	4.465	1.157											
T53	7.597	4.232	2.794											
P54														
G55														
T56	7.593	3.612	3.062											
V57	7.951	4.004	1.801		0.812									
F58	8.500	4.116	1.898	2.132										
L59	7.986	4.268	1.521		1.340		0.768							
R60	8.425	3.846												
S61	8.311	4.491	3.164											
F62														

Table 6.2: Assigned chemical shifts for protons of VSC_{EC-25}, at 298 K in 100 mM DPC-d_{38}, 25 mM sodium phosphate buffer (pH 6.8), 25 mM NaCl, 10% D_2O. White cells indicate assignable protons in an ideal spectrum.

6.6.2 Secondary Structure Analysis of VSC_{EC-25} by NMR

The secondary structure of VSC_{EC-25} in 100 mM DPC-d_{38} was assessed on a residue-by-residue basis using the chemical shift index method (Wishart et al., 1992). Assigned α^1H chemical shifts were compared to published ranges considered to be indicative of a random coil structure. Residues for which the assigned α^1H has a chemical shift downfield (higher ppm) of the published range of random coil chemical shifts for that residue are assigned a value of +1, while residues for which the assigned α^1H has a chemical shift upfield (lower ppm) of the published range of random coil chemical shifts are assigned a value of -1. Residues for which the assigned α^1H chemical shift falls within the published range of shifts for random coil are assigned an index of 0. Strings of four or more sequential residues of +1, -1, or 0 index indicate regions of β strand, α helix, or random coil, respectively.

The chemical shift indices of assigned residues in VSC_{EC-25}, in 100 mM DPC-d_{38}, are shown in Figure 6.8. Indices of value zero are represented as having a CSI of 0.05, so that they are displayed in the figure. Residues for which no CSI is rendered were not assigned. Above the graph is a schematic representing the secondary structure elements along the length of the peptide; breaks in the schematic indicate regions of the peptide which were not assigned.

CSI analysis of the partially assigned ^{1}H NMR data indicates that the majority of the peptide adopts a random coil conformation, which is the predominant conformation predicted from analysis of the sequence (60% coil predicted by Jpred4) and in keeping with the accepted model that this region is an unstructured loop. However, these data suggest that the region W41-T44 of the peptide adopts a helical conformation in the presence of DPC-d_{38}. This constitutes 16% of the total peptide sequence, bringing these NMR results into close agreement with those obtained from CD (estimated 11-14% helicity; Table 6.1). There is a possibility that the N-terminal helix could extend to G48, and the lack of assignment in this region means we cannot verify this, but the agreement between CD and NMR suggests that we have identified the entire helical region within the residues assigned. A helical region at the N-terminus of the extracellular loop has not been predicted either

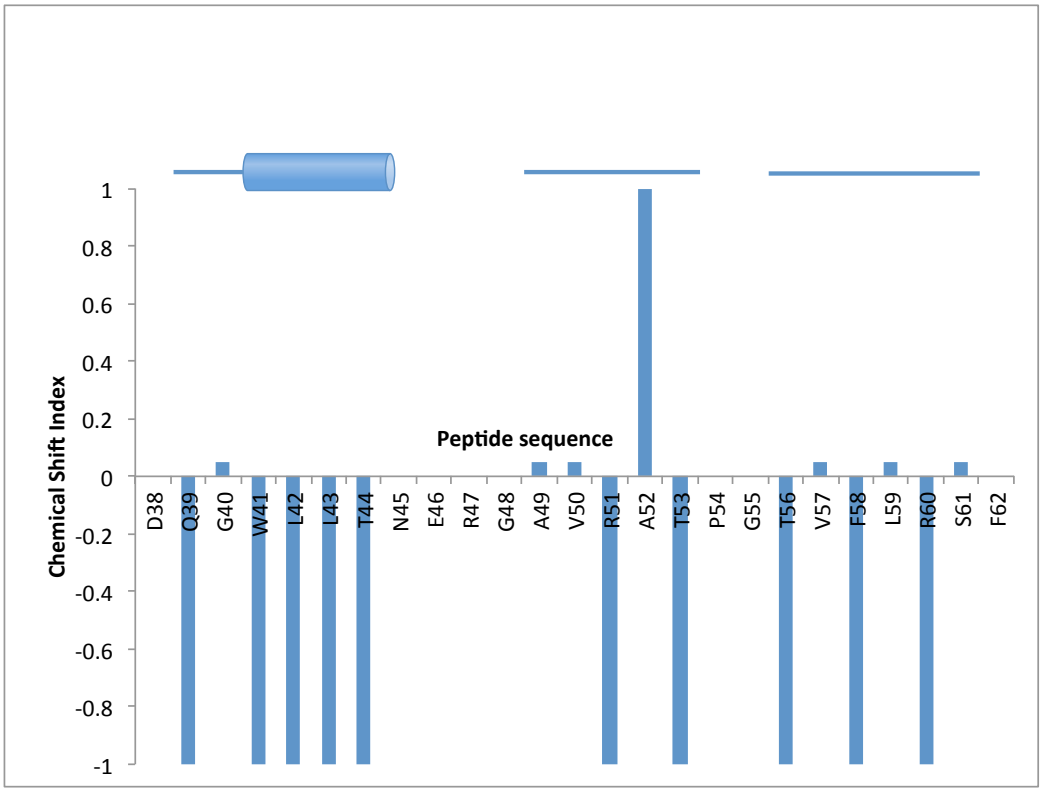

Figure 6.8: Chemical Shift Indices for assigned residues in VSC_{EC-25}, with respect to published random coil values. Series of four or more residues with negative CSI indicate regions of helicity. CSI analysis of the peptide in 100 mM DPC-d_{38} estimates that 16% of residues in the peptide, or 23% of assigned residues, adopt a helical conformation in this environment.

from sequence or in any previous published work. NMR data also suggest a notable lack of β-sheet content in the peptide. Given that sequence analysis using Jpred4 yielded a prediction of 40% β-strand in this peptide, and fitting of CD data using CDSSTR yielded an estimate of 30% β-sheet content in every membrane mimetic tested, this lack of β-sheet content from NMR analyses was unexpected and suggests that β-sheet secondary structure estimates from CD data should be interpreted with caution and validated using a complimentary method.

6.7 Solution State NMR Analyses of Interactions between the Extracellular Domain Peptide and Vancomycin

Having acquired and assigned solution-state NMR data of both VSC_{EC-25} (Section 6.6.1) and vancomycin (Section 5.4.1) in 25 mM sodium phosphate buffer (pH 6.8) containing 25 mM NaCl, further data was acquired for mixed samples containing both components. NMR signals from protons in both molecules were monitored, and changes in chemical shifts and signal intensities were recorded - these changes in NMR signals indicate changes in the chemical environments of the source protons, and suggest an interaction between the two molecules.

6.7.1 Loss of Signals from Peptide Protons in the Presence of Vancomycin

Vancomycin was titrated into a sample of 1 mM VSC_{EC-25} solubilised in 25 mM sodium phosphate buffer (pH 6.8), containing 25 mM NaCl, 10% D_2O, and 100 mM DPC-d_{38}. Since neither the peptide nor vancomycin was deuterated, ^1H signals of both vancomycin and the VSC_{EC-25} peptide appeared in spectra acquired from mixed samples. In many regions of the spectra, vancomycin signals quickly obscured signals from the peptide; however, in the "fingerprint" region (7-9 ppm in F2, 2-4 ppm in F1) of TOCSY and NOESY spectra, HN-Hα crosspeaks from the peptide were clearly resolved as vancomycin peaks do not populate this region of the spectrum. These signals were monitored to observe the impact of increasing vancomycin concentrations on the chemical environment of the peptide backbone (Figure 6.9).

Only very small changes in ^1H chemical shifts of VSC_{EC-25} were observed as the vancomycin concentration was increased from 50 M 1 mM. Much more significant was the decrease in peptide signal intensity upon addition of vancomycin. Relative signal intensities of VSC_{EC-25} HN-Hα crosspeaks in the presence and absence of an equimolar quantity of vancomycin vancomycin were used to evaluate the degree of signal attenuation, and a summary is shown in Figure 6.10. Signal intensity was attenuated for all H protons in the

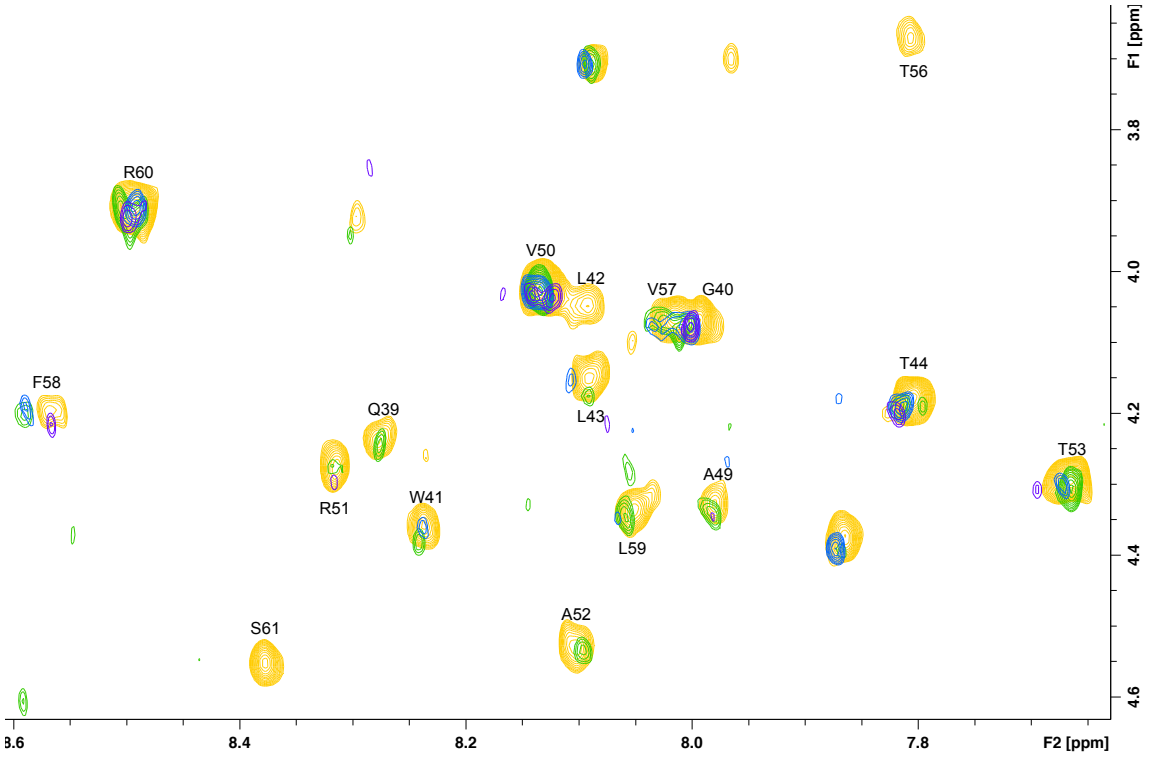

Figure 6.9: The HN-Hα region of an 80 ms TOCSY acquired for 1 mM VSC_{EC-25}, 100 mM DPC-d_{38}, 25 mM sodium phosphate buffer (pH 6.8), 25 mM NaCl, 10% D_2O, and 0 μM (yellow), 50 μM (green), 100 μM (blue), and 1 mM (purple) vancomycin. Signal intensities are normalised with respect to the peptide-only spectrum.

peptide; however, this attenuation varied along the peptide chain. In Figure 6.10, residues in which the HN-H crosspeak was lost entirely are highlighted in red, with 100% signal attenuation. Residues experiencing more than 80% attentuation are highlighted in orange, and residues experiencing less than 80% attenuation are shown in green. Variation in signal attenuation between residues may identify regions of the peptide which are involved in an interaction with vancomycin.

The region of the peptide which we have identified as helical, W41-T44, also experiences significant signal attenuation in the presence of vancomycin. NMR signals from L42 and L43 are lost entirely, while W41 and T44 experience 81% and 86% signal attentuation, respectively. Koteva et al. (2010) examined tryptic digests of His_6-$VanS_{SC}$ and found that a modified vancomycin photoprobe interacts with the N-terminal peptide terminating with

Figure 6.10: The extent to which HN-Hα crosspeaks of VSC$_{EC-25}$ are attenuated by the addition of an equal quantity of vancomycin. Signal attenuation is heterogenous across the peptide sequence. Since the receiver gain decreased over the course of the titration series, some signal attenuation is expected for all protons; more extreme attenuation may suggest an interaction with vancomycin.

W41. Since the transmembrane helix exits the membrane at approximately residue L37, only residues D38-W41 are expected to be exposed to the extracellular environment. If this region interacts with unmodified vancomycin, and the helical portion of VSC$_{EC-25}$ identified here also interacts with vancomycin, then the adjoining W41 residue is likely to be very important in this interaction.

6.7.2 Chemical Shift Perturbations in Vancomycin in the Presence of the Peptide

^{1}H TOCSY and NOESY solution state NMR spectra were acquired for 1 mM vancomycin in 25 mM sodium phosphate buffer (pH 6.8), 25 mM NaCl, 10% D_2O, and in the presence of 1 mM VSC$_{EC-25}$ peptide. Signals corresponding to vancomycin protons were identified in the mixed spectrum by comparison to the fully assigned spectrum in Section 5.4.1. Note was made of any differences between the spectra, including changes in chemical shift for any vancomycin protons, or the emergence of any previously unrecorded crosspeaks which could not be attributed to the peptide.

NOESY spectra acquired for 1 mM vancomycin in the presence (orange) and absence (red) of 1 mM VSC$_{EC-25}$ are shown in Figure 6.11. Changes in the chemical environments of vancomycin protons were observed in the form of chemical shift perturbations, calculated by subtracting chemical shifts shown in Table 5.1 from re-measured values in the presence of VSC$_{EC-25}$. The mean chemical shift perturbation was -0.02 ppm. In Figure 6.12, two sets of vancomycin protons are identified; in red, protons for which the difference in chemical shifts is greater than one standard deviation from the mean difference (Tomlinson et al.,

2015), and in blue, protons for which the difference is greater than 0.5 of one standard deviation from the mean difference.

In Chapter 5, saturation transfer difference NMR identified the three hydrocarbon rings near the C-terminus of the vancomycin peptide component as being in close proximity to His_6-$VanS_{SC}$ at the time of an apparent binding event. STD-NMR investigation was limited to protons with chemical shifts in the 6-8 ppm range, due to the presence of obtrusive NMR signals in the spectra originating from the LMPG detergent. In this Chapter, by monitoring chemical shift perturbations of vancomycin protons in the presence of the extracellular loop of $VanS_{SC}$, we identify protons u, v, w, and z as being *significantly* affected by the presence of VSC_{EC-25} (Tomlinson et al., 2015), with perturbations greater than one standard deviation from the mean perturbation of -0.02 ppm. These protons could not be studied by STD-NMR, as they possess chemical shifts upfield of 5 ppm, so their NMR signals were obscured by signals from LMPG.

When considering vancomycin protons with perturbations of greater than 0.5 of one standard deviation from the mean, it becomes apparent that the bulk of the vancomycin molecule experiences a change in chemical environment when exposed to VSC_{EC-25}. It is difficult to elucidate which protons are involved in the interaction, and which are simply affected by changes in environment as a result of the interaction. In Chapter 7, investigations were carried out to investigate the extent to which chemical shift perturbations in vancomycin in the presence of VSC_{EC-25} are explained by the presence of 100 mM DPC-d_{38}.

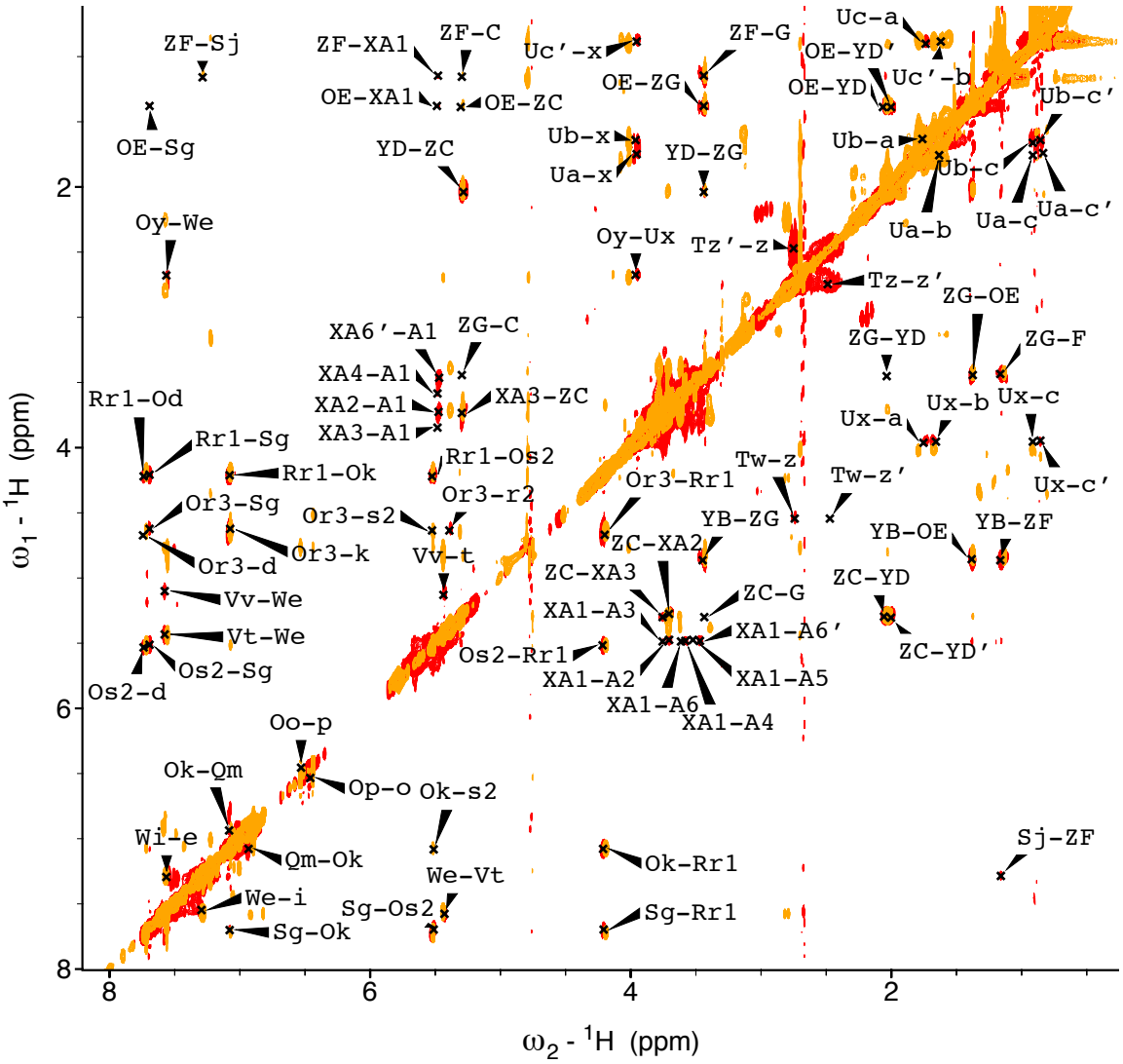

Figure 6.11: A comparison of equivalent NOESY spectra acquired for 1 mM vancomycin in the presence (orange) and absence (red) of 1 mM VSC_{EC-25} peptide. Where crosspeaks do not overlap exactly, the chemical shift of one or both of the relevant protons has been perturbed. These perturbations are quantified in Figure 6.12.

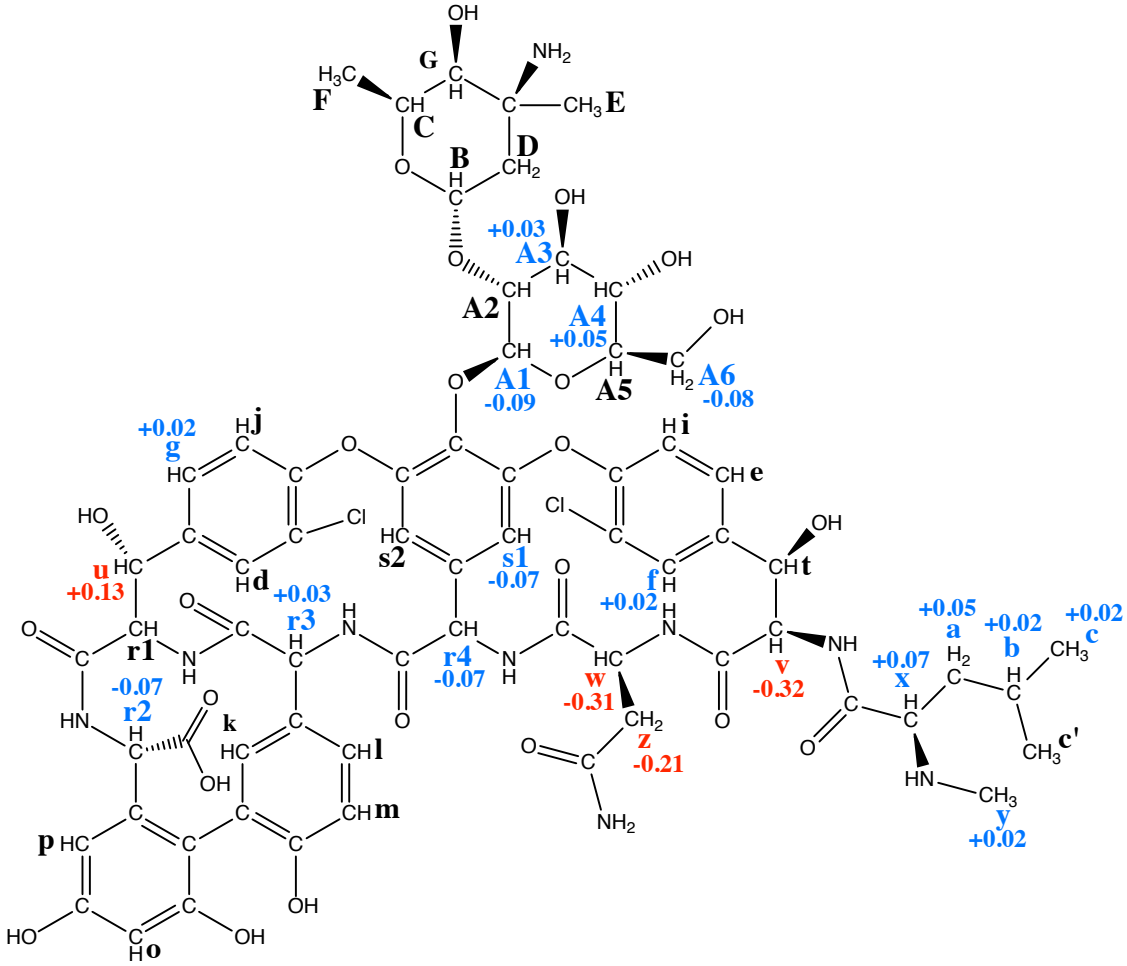

Figure 6.12: Chemical shift perturbations (expressed in units of ppm) of vancomycin protons on exposure to VSC_{EC-25}. The chemical shifts of protons highlighted in red are perturbed to an extent that is greater than one standard deviation from the mean of -0.02 ppm; for protons highlighted in blue, this magnitude is greater than 0.5 of one standard deviation from the mean (Tomlinson et al., 2015).

6.8 Discussion

6.8.1 The Structures of Peptides Corresponding to the Extracellular Domain of VanS$_{SC}$ Are Mimetic-Dependent

CD spectra acquired for VSC$_{EC-40}$ (Figure 6.5) in different detergent micelles are visually different; analysis by CDSSTR estimates helicity at 53% in DPC, and at 38% in LMPG; this is supported by visual analysis of the spectra. The peptide sequence is derived from the sequence of VanS$_{SC}$; the corresponding region of the protein is predicted to be 30% helical by SAS (Milburn et al., 1998), corresponding to the truncated transmembrane helices flanking the extracellular domain. CD estimation of 53% helicity indicates that the extracellular domain adopts a partially helical structure.

CD spectra acquired for VSC$_{EC-25}$ (Figure 6.6) indicate that, in detergent micelles, VSC$_{EC-25}$ adopts a partially helical structure. This is quantified by CDSSTR as 9% helicity in DM, and 11% helicity in DPC and LMPG. Visual inspection of the spectra suggest that the peptide is more helical in LMPG and DPC than in DM, and this is supported by estimations of helicity from ellipticity at 222 nm (Ysselstein et al., 2015), which yields estimates of 9% in DM, and 14 and 15% in DPC and LMPG respectively.

Constitutive ATPase activity of VanS$_{SC}$ has been demonstrated in DM (Quigley, 2010), DPC (Edwards, 2014), and LMPG (Section 3.9). CD data acquired of VSC$_{EC-40}$ and VSC$_{EC-25}$ indicate that the secondary structure of the VanS$_{SC}$ extracellular domain varies depending on the mimetic in which it is solubilised. Constitutive ATPase activity is localised to the cytosolic C-terminal domains of the peptide (Figure 6.1) and operates independently of the sensor domain (Wright et al., 1993); it is phosphorylation of VanR which is inducible by vancomycin. The influence of membrane composition on sensor domain architecture may therefore represent a further layer of complexity in the problem of identifying the activating ligand to VanS.

We have discussed the possibility that lipid II, accumulating in the local area as a result of vancomycin activity, could serve as a ligand to VanS. Lipid II remains anchored

in the cell membrane until it is integrated into the cell wall, at which point the anchoring lipid tail is cleaved. An accumulation of lipid II could therefore cause local changes in the characteristics of the cell membrane (affecting, for instance, its fluidity or curvature) which might either directly induce signal transduction in VanS, or facilitate adoption of an appropriate sensor domain architecture to allow binding of vancomycin.

To gain a deeper understanding of the role of membrane composition in VanS sensor loop architecture, this domain should be studied in a wide range of mimetics including detergent micelles and lipid vesicles. By varying characteristics such as polar head group identity, lipid chain length or saturation, and surface curvature, it may be possible to derive a model by which sensor domain structure may be predicted. Mixed lipid vesicles, or lipid/detergent bicelles, might more closely mimic the heterogeneous lipid composition of the membranes in which VanS natively functions.

6.8.2 Peptide Helicity Is Consistent When Measured by Circular Dichroism and by Solution-State NMR, but β-Sheet Content Is Inconsistent

The secondary structure of VSC_{EC-25}, corresponding to the core extracellular domain of $VanS_{SC}$, was studied by CD and by solution-state NMR. Chemical shift index analysis indicates that 4 of the peptide's 25 residues adopt a helical conformation in DPC-d_{38} micelles. This corresponds to 16% of the peptide and is in good agreement with helicity estimates from CD ellipticity at 222 nm. We can conclude that the peptide is approximately 15% helical in DPC, and that residues W41-T44 make up this helical region.

A helical secondary structure in the N-terminal end of the extracellular domain of $VanS_{SC}$ has not yet been proposed in the literature. However, this region of the protein has been identified as having some involvement in the interaction between $VanS_{SC}$ and a modified vancomycin photoprobe (Koteva et al., 2010). This suggests that the helical motif identified here plays an important role in vancomycin binding. It would be very interesting to characterise the secondary structure of the extracellular domain in the presence of vanco-

mycin, to see whether this helical region is maintained or destabilised. Unfortunately, NMR signals from the peptide were lost in the presence of vancomycin, so the secondary structure could not be characterised by CSI analysis. As a glycopeptide, vancomycin produces a CD signal, complicating interpretation of CD data acquired of mixed samples. Complete deuteration of vancomycin would facilitate structural characterisation of the peptide in a mixed sample.

CDSSTR predicts from CD data that a large portion of the remainder of the peptide adopts a β-strand conformation in DPC. However, this characterisation is not supported by the NMR data, which suggests that the peptide is mostly random coil in structure aside from the short helical region described above. A maximum of 16\$ β-strand could be conferred to the peptide by unassigned residues N45-G48; this still would not explain CD estimates of over 30% helicity in all three detergents, and in aqueous buffer.

6.8.3 An Interaction is Observed Between VSC_{EC-25} and Vancomycin

Intensities of HN-Hα crosspeaks of VSC_{EC-25} were attenuated in the presence of vancomycin (Figure 6.13). The extent to which signals were attenuated varied between residues. Peptide segment W41-T44, corresponding to the predicted α-helical portion of the peptide, experienced significant signal attenuation including the complete loss of the HN-Hα crosspeaks of L42 and L43. The region D38-W41 has been proposed by Koteva et al. (2010) to be involved in an interaction between vancomycin and $VanS_{SC}$; this is supported by the apparent interaction between vancomycin and the region G3-T44 presented here.

Complete signal attenuation is also seen in five residues towards the C-terminus. Since the remainder of the peptide is unstructured, it may be that these attenuated regions are closely associated with the helical region W41-T44 in space.

Chemical shift perturbations were observed in vancomycin in the presence of VSC_{EC-25}. The chemical shifts of protons u, v, w, and z experienced chemical shift perturbations greater than one standard deviation from the mean perturbation of -0.02. As these protons all possess chemical shifts in the 2-6 ppm range, they were not measurable in

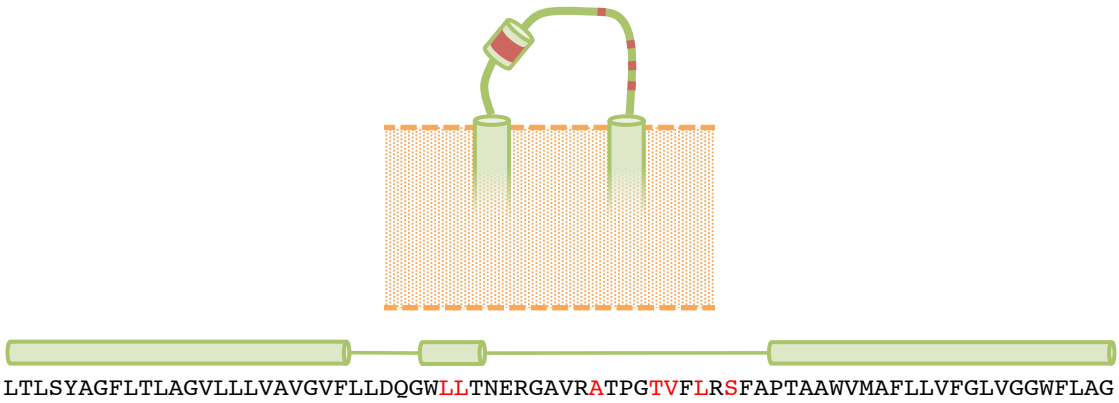

Figure 6.13: A schematic outlining the structural features of the VanS$_{SC}$ extracellular domain identified in this Chapter; a short helical region comprising residues W38-T41, in an otherwise unstructured extracellular domain. Residues for which HN-Hα crosspeaks were fully attenuated in the presence of 1 mM vancomycin are highlighted in red.

STD-NMR experiments in Chapter 6. However, protons v, w, and z are in close proximity to the hydrocarbon ring towards the N-terminus of the vancomycin peptide, to which saturation is transferred from His$_6$-VanS$_{SC}$ during STD-NMR experiments. Proton u is close to the N-terminus of the vancomycin peptide, situated close to the other three hydrocarbon chains to which saturation transferred during STD-NMR.

In conjunction with the attenuation of peptide NMR signals in the presence of vancomycin, this suggests an interaction between the peptide and antibiotic, which may represent an interaction between vancomycin and the extracellular domain of VanS$_{SC}$ *in vivo*.

Chapter 7

Interactions between the Glycopeptide Antibiotic Vancomycin and Various Membrane Mimetics

7.1 Introduction

Vancomycin is a glycopeptide antibiotic first isolated from *Streptomyces orientalis* in 1956 (McCormick et al., 1956; Dutton and Elmes, 1959). Its mode of action involves binding to the D-Alanyl-D-Alanine terminus of the pentapeptide component of lipid II, after it is exported through the bacterial membrane, but before it is integrated into the peptidoglycan cell wall. Binding of vancomycin to the peptide terminus inhibits the activity of transpeptidase enzymes which catalyse essential crosslinking reactions. The activity of vancomycin takes place in the immediate periphery of the bacterial cell membrane. Its target lipid II remains anchored to the membrane by its lipid tail, which is cleaved from the disaccharide-pentapeptide component only after the latter has been integrated into the cell wall.

Vancomycin is a member of the glycopeptide class of antibiotics. Members of this class exhibit various mechanisms by which they become localised to the cell membrane (Beauregard et al., 1995). Teicoplanins are lipoylated, and these lipid chains embed into cell membranes to anchor the antibiotic in the vicinity of cell wall production. Other glycopeptide antibiotics including vancomycin are not lipoylated, but undergo dimerisation (MacKay et al., 1993) at the peptide backbone such that an initial binding of one antibiotic molecule to lipid II will result in the localisation of a second antibiotic molecule to the membrane. This second antibiotic molecule therefore binds a second lipid II molecule more efficiently than had its localisation depended upon diffusion alone.

The interaction between teicoplanins and cell membranes is documented, and is mediated by the presence of a lipid chain in the teicoplanin molecule. However, we find

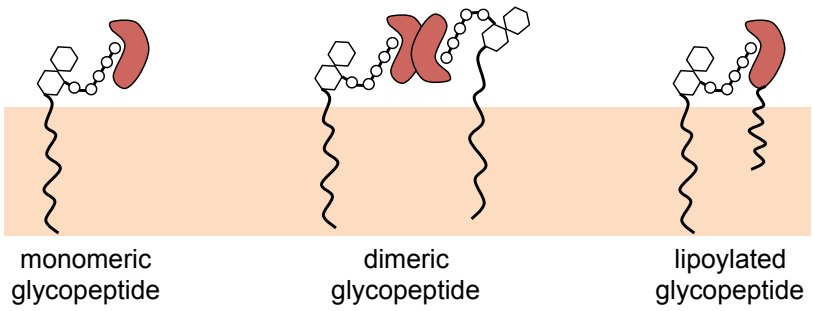

Figure 7.1: Schematic outlining the binding advantage of dimeric or lipoylated glycopeptide antibiotics, versus monomeric glycopeptides in solution. Adapted from Beauregard et al. (1995).

no reports in the literature of interactions between vancomycin and a cell membrane or membrane mimetic. It is not immediately clear whether any biochemical characteristics of vancomycin would mediate such an interaction, but since this would offer a selective advantage to the source organism (*i.e. Streptomyces orientalis*), it is plausible that such an interaction might take place. This interaction between vancomycin and membranes forms the hypothesis which is explored in this chapter.

Experiments conducted in Chapters 5 and 6 have identified regions of vancomycin which appear to be involved in an interaction with VanS. However, as VanS must necessarily be encapsulated within a membrane or appropriate membrane mimetic to maintain its native fold, interactions between vancomycin and VanS cannot be properly characterised without first accounting for possible interactions between vancomycin and the membrane mimetic.

7.2 Aims

1. To biophysically investigate interactions between vancomycin and a range of membrane mimetics;

2. To critically review data acquired in previous Chapters in the context of interactions between vancomycin and membrane mimetics, and assess the extent to which the membrane mimetic might explain observed interactions between vancomycin and VanS.

7.3 Interactions Between Vancomycin and LMPG Micelles

As outlined in Chapter 5, transfer of saturation from VanS to vancomycin indicated that protons within the antibiotic were held in close proximity (>5 Å) to the protein for a sustained amount of time. However, an interaction between the antibiotic and LMPG micelles might also result in the observed transfer of saturation to the antibiotic via the micelle, without any direct interaction with the protein taking place (Figure 7.2). To rule out this possibility, or account for these vancomycin-micelle interactions in the interpretation of the data, it was therefore important to investigate such an interaction in the absence of VanS.

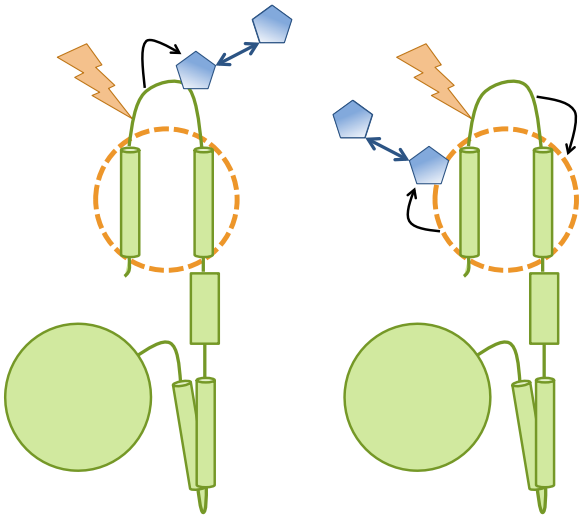

Figure 7.2: Schematic outlining the potential for saturation to be transferred to vancomycin via the LMPG micelle (right), as opposed to directly from VanS (left).

7.3.1 Saturation Transfer Difference NMR

Interactions between vancomycin and LMPG micelles were first probed by STD-NMR. Since protons of both LMPG and vancomycin populate the NMR spectrum upfield of 5 ppm, no on-resonance frequency could be identified which would selectively saturate LMPG protons without saturating vancomycin protons. However, a frequency was identified (8.5 ppm) which saturated protons in vancomycin while causing minimal saturation of protons in LMPG. STD-NMR experiments were carried out for a sample containing 1 mM vancomycin and 1.15 mM LMPG. Saturation of a sample containing 1 mM vancomycin (middle spectrum, Figure 7.3) yields peaks in the difference spectrum corresponding to many vancomycin protons. Saturation of a sample of 1.15 mM LMPG (top spectrum) results in a difference spectrum in which just two proton signals are observed. Saturation of a mixed sample results in more intense saturation of LMPG signals than is achieved with saturation of the LMPG-only sample, indicating that saturation is transferred to these LMPG protons from vancomycin protons, and an interaction takes place.

A limitation of STD-NMR in this context is that no distinction is made between the monomeric and micellar populations of LMPG molecules. Transfer of saturation from vancomycin to LMPG may indicate that the antibiotic interacts with the micelle; alternatively, this may represent an interaction between the antibiotic and monomeric LMPG molecules in solution.

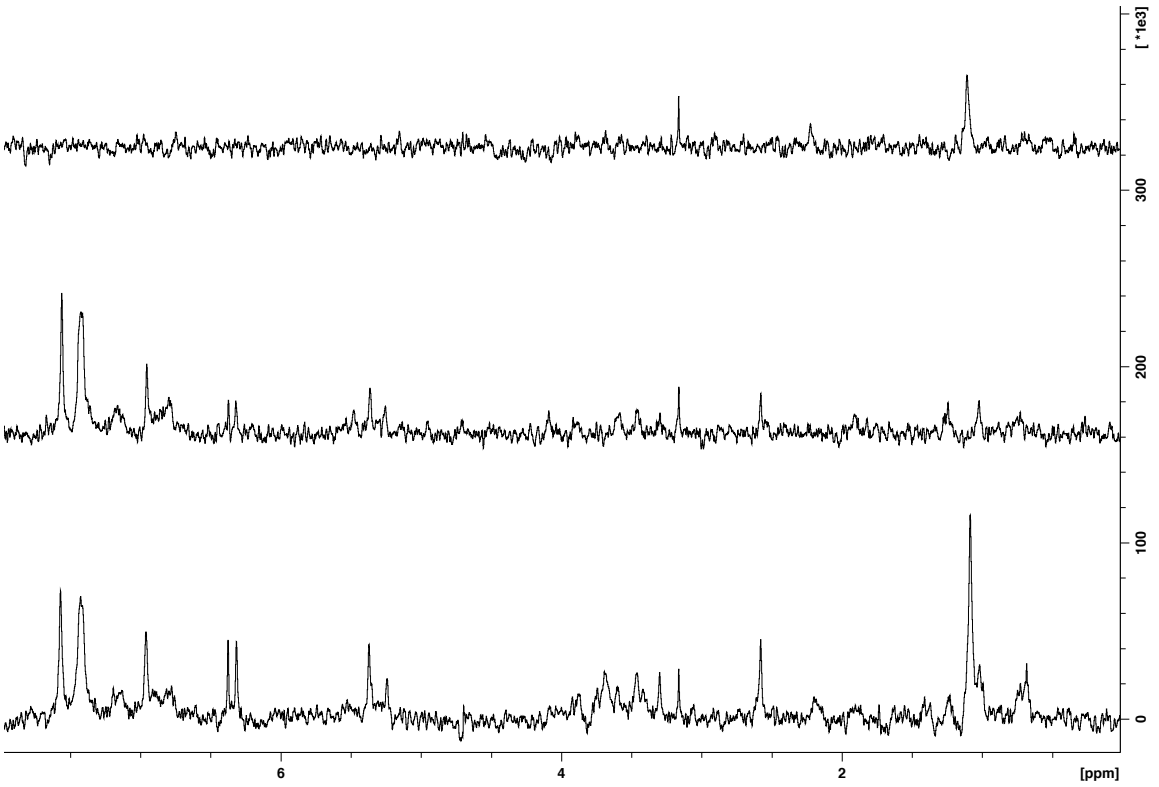

Figure 7.3: Saturation transfer difference spectra acquired at an on-resonance frequency of 8.5 ppm, of 1.15 mM LMPG (top), 1 mM vancomycin (middle), and a mixed sample of the two (bottom). Transfer of saturation from vancomycin peaks to LMPG peaks is observed.

7.3.2 Diffusion Ordered Spectroscopy

In order to distinguish between interactions with monomeric and micellar populations of LMPG, diffusion ordered spectroscopy (DOSY) was used. In DOSY, the diffusion coefficient of every proton in a sample is measured, and from these values the spherical diameters of molecules are estimated (Section 2.9.7). This allows the relative sizes of molecules within a sample to be compared. When two molecules interact, they form a complex with an overall larger size, and slower overall tumbling dynamics. This is seen as an increase in estimated spherical diameter, or decrease in diffusion coefficient, in DOSY measurements. DOSY can therefore be used to investigate interactions between molecules.

Figure 7.4 compares the resulting DOSY spectra of vancomycin and mixed vancomycin/LMPG samples using a diffusion delay time of 100 msec. In the absence of LMPG, the

diffusion coefficient of vancomycin was estimated as 3.606 $\times$ 10^{-6} cm^2 s^{-1} (-9.443 log[m^2 s^{-1}] in the y axis of Figure 7.4), which was the average of all diffusion coefficients obtained for protons in vancomycin. In a mixed sample of 1 mM vancomycin and 1.15 mM LMPG, the estimated average diffusion coefficient of vancomycin protons decreased only slightly to 3.133 $\times$ 10^{-6} cm^2 s^{-1} (-9.504 log[m^2 s^{-1}] in the y axis of Figure 7.4). The diffusion coefficient of LMPG was estimated as 0.948 $\times$ 10^{-6} cm^2 s^{-1} (-10.023 log[m^2 s^{-1}] in the y axis of Figure 7.4). We are unaware of any diffusion coefficients for LMPG micelles published in the literature.

If a significant population of vancomycin molecules were embedded in the available LMPG micelles during the DOSY experiment, the estimated diffusion coefficients for vancomycin and LMPG protons would be the same. Since they are not, this suggests that a population of vancomycin molecules interacts with LMPG while others remain free in solution. The fraction of bound vancomycin molecules can be calculated using Equation 7.1:

$$D_{obs} = D_{bound}F_{bound} + D_{free}F_{free} \tag{7.1}$$

where D_{obs} is the observed diffusion coefficient of vancomycin protons in the presence of LMPG, D_{bound} is the diffusion coefficient of LMPG protons (used as an estimate of the diffusion coefficient of a vancomycin/LMPG complex, as LMPG micelles are much larger than vancomycin), and D_{free} is the diffusion coefficient of vancomycin protons in the absence of LMPG.

Since $F_{free} + F_{bound} = 1$, Equation 7.1 can be rearranged to give Equation 7.2:

$$F_{bound} = \frac{D_{obs} - D_{free}}{D_{bound} - D_{free}} \tag{7.2}$$

Diffusion coefficients calculated from DOSY data indicate that in a sample of 1 mM vancomycin and 1.5 mM LMPG, only 10.5% of vancomycin molecules interact with LMPG micelles at a given time.

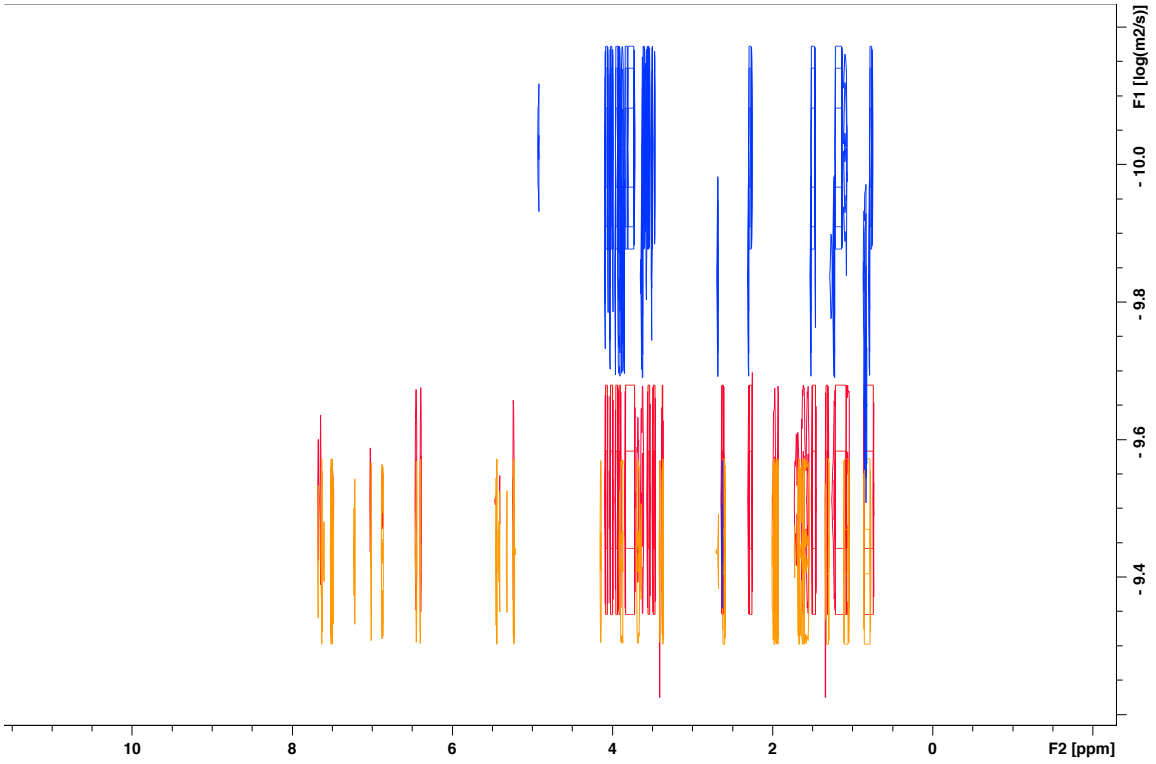

Figure 7.4: Overlaid DOSY spectra of 1 mM vancomycin in the absence of LMPG (yellow), with 1.15 mM LMPG (red), and with 20 mM LMPG (blue). The blue spectrum is scaled for clear visualisation of LMPG signals, so vancomycin signals are not shown. LMPG and vancomycin peaks populate the region of the spectrum upfield of 5 ppm; in DOSY spectra acquired at equimolar concentrations of vancomycin and LMPG, overlapping vancomycin and LMPG peaks in this region lead to averaging of diffusion coefficients for corresponding protons. Therefore, vancomycin diffusion coefficients are calculated from signals downfield of 5 ppm, and the diffusion coefficient for LMPG is calculated from data acquired of a sample in which a large molar excess of LMPG is present. Upfield, the difference in diffusion coefficients of free vancomycin (yellow) and LMPG micelles (blue) is clear. Downfield, the diffusion coefficients of vancomycin protons (red) appear to decrease slightly, possibly due to interactions with more slowly-diffusing LMPG micelles.

7.3.3 Chemical Shift Perturbations

To identify vancomycin protons whose chemical environment was changed by the presence of LMPG micelles, a series of ^{1}H 1D experiments were conducted in which increasing concentrations of LMPG (0.1 - 20.0 mM) were added to samples containing 1 mM vancomycin in 25 mM sodium phosphate buffer (pD 6.8) containing 25 mM NaCl. As was observed in Section 5.6, since LMPG is not deuterated, intrusive ^{1}H NMR signals obscured the spectrum upfield of 5 ppm. Therefore, vancomycin protons with chemical shifts downfield of 5 ppm were monitored for chemical shift perturbations upon addition of LMPG. Figure 7.5 shows the 5-8 ppm region of these spectra, with vancomycin proton signals annotated at three points in the titration series. Chemical shift perturbations were first observed for vancomycin protons g, o, t, and v at an LMPG concentration of 1.15 mM LMPG, and further purturbations arose in protons d, i, k, and p as further LMPG was titrated into the sample.

The protons within the vancomycin structure which showed significant chemical shift perturbations in the presence of either 1.15 mM or 20 mM LMPG are summarized in Figure 7.6. Significance has been defined previously as discussed in Section 6.7.2 (Tomlinson et al., 2015). It is worth noting that STD-NMR experiments described in Chapter 5 were carried out in 1.15 mM LMPG. At this LMPG concentration, minimal perturbation of vancomycin protons was observed. At 20 mM LMPG, more significant perturbation of vancomycin protons was observed, but even at this high concentration, LMPG micelles do not perturb the chemical environment of every vancomycin proton to which saturation was transferred from either VanS molecule. Although an interaction between vancomycin and LMPG may contribute to the observed interaction with VanS, the antibiotic-protein interaction cannot be fully explained by the presence of the membrane mimetic. This suggests that the interaction between vancomycin and VanS reported in Chapter 5 is genuine, and not a consequence of the presence of LMPG micelles in the system.

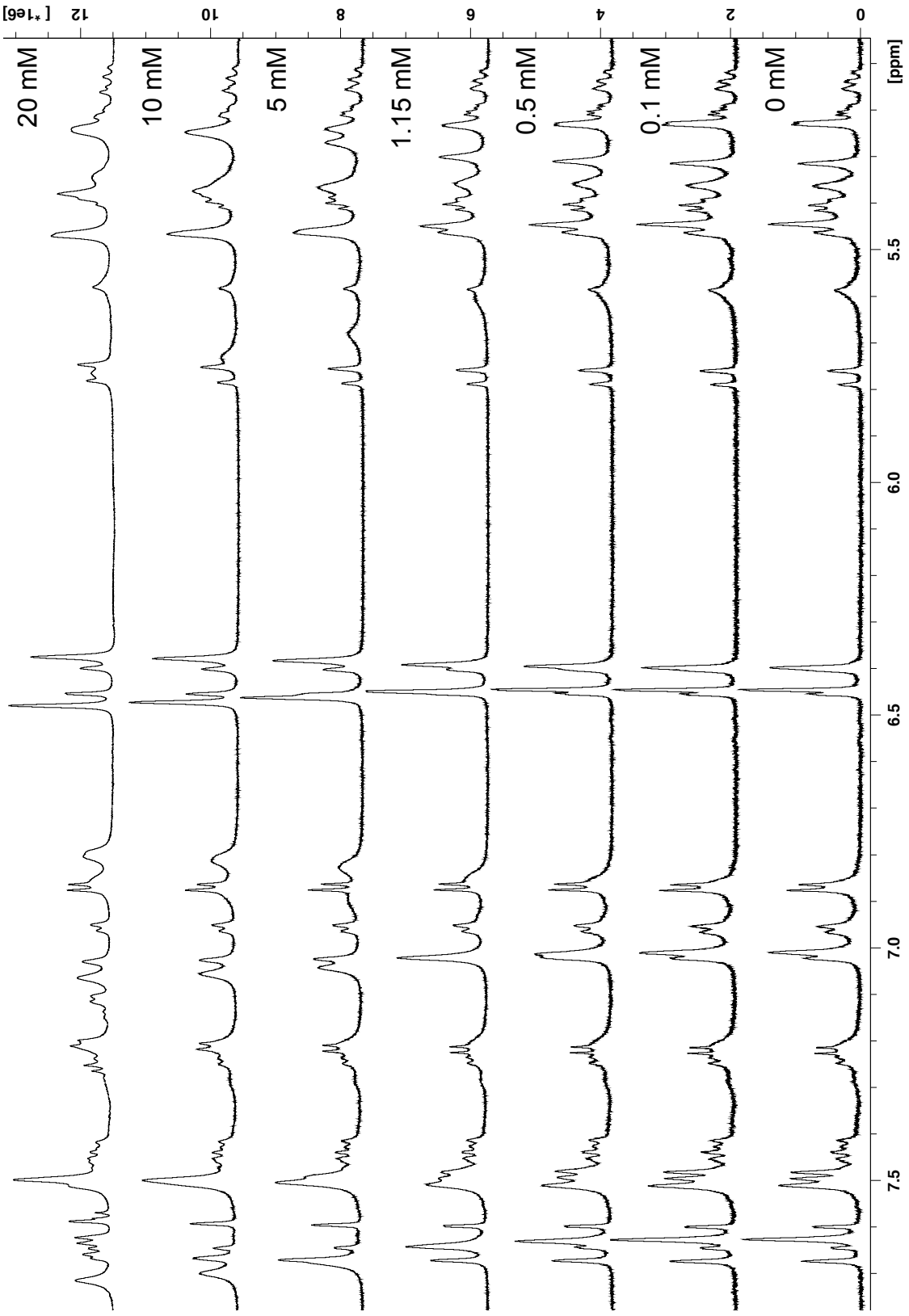

Figure 7.5: A series of ^{1}H 1D NMR spectra acquired of 1 mM vancomycin and increasing concentrations of LMPG. Chemical shift perturbations begin to emerge in the presence of 1.15 mM LMPG; the magnitudes of these perturbations increases as further LMPG is added.

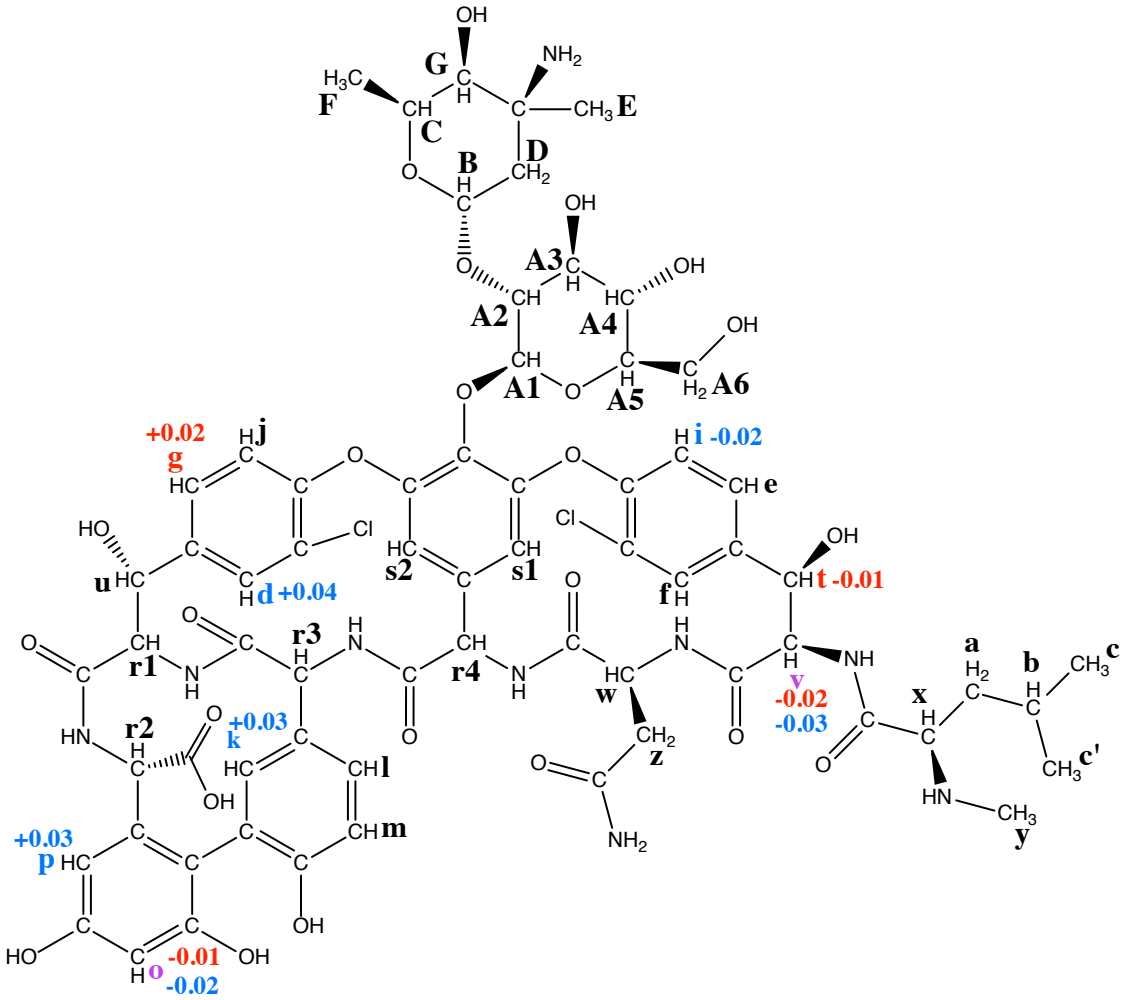

Figure 7.6: Protons of vancomycin which experience significant perturbation of chemical shift in the presence of 1.15 mM (red) or 20 mM (blue) LMPG. Protons which are affected under both conditions are shown in purple.

7.4 Interactions Between Vancomycin and DPC Micelles

The data presented in Chapter 6 suggest a sustained interaction between vancomycin and a synthetic peptide representing the extracellular domain of $VanS_{SC}$. This peptide was solubilised in 100 mM DPC-d_{38} to encourage adoption of the native fold of the VanS extracellular domain. By the same rationale presented in Section 7.3, it was necessary to investigate interactions between vancomycin and DPC-d_{38} to assess the extent to which this interaction might explain apparent interactions with the peptide.

7.4.1 Diffusion Ordered Spectroscopy

DOSY measurements were once again utilised to assess the change in diffusion coefficient of vancomycin in the presence of DPC-d_{38} micelles. Figure 7.7 shows an overlay of DOSY spectra acquired for vancomycin in the absence (orange) and presence of 100 mM DPC-d_{38} (red).

The diffusion coefficient for vancomycin decreased from 3.606×10^{-6} cm^2 s^{-1} (-9.443 $\log[m^2\ s^{-1}]$ in the y axis of Figure 7.7) to 0.826×10^{-6} cm^2 s^{-1} (-10.083 $\log[m^2\ s^{-1}]$ in the y axis of Figure 7.7) in 100 mM DPC-d_{38}. Since DPC-d_{38} is fully deuterated and does not produce ^{1}H NMR signals, a diffusion coefficient for the micelle could not be estimated from acquired data. However, diffusion coefficients of DPC micelles have been published in the literature. Values of 0.72×10^{-6} cm^2 s^{-1} (-10.143 $\log[m^2\ s^{-1}]$ in the y axis of Figure 7.7) are reported by Dixon et al. (2002) for 250 mM DPC at 298 K, and by Kallick et al. (1995) for 228 mM DPC at 310 K. The good agreement in diffusion coefficients between these two studies indicates that this is a reliable measurement, which we can use to assess the interaction between vancomycin and DPC. Substituting these diffusion coefficients into Equation 7.2 we find that in a sample of 1 mM vancomycin and 100 mM DPC-d_{38}, 91% of vancomycin molecules interact with DPC micelles at a given time.

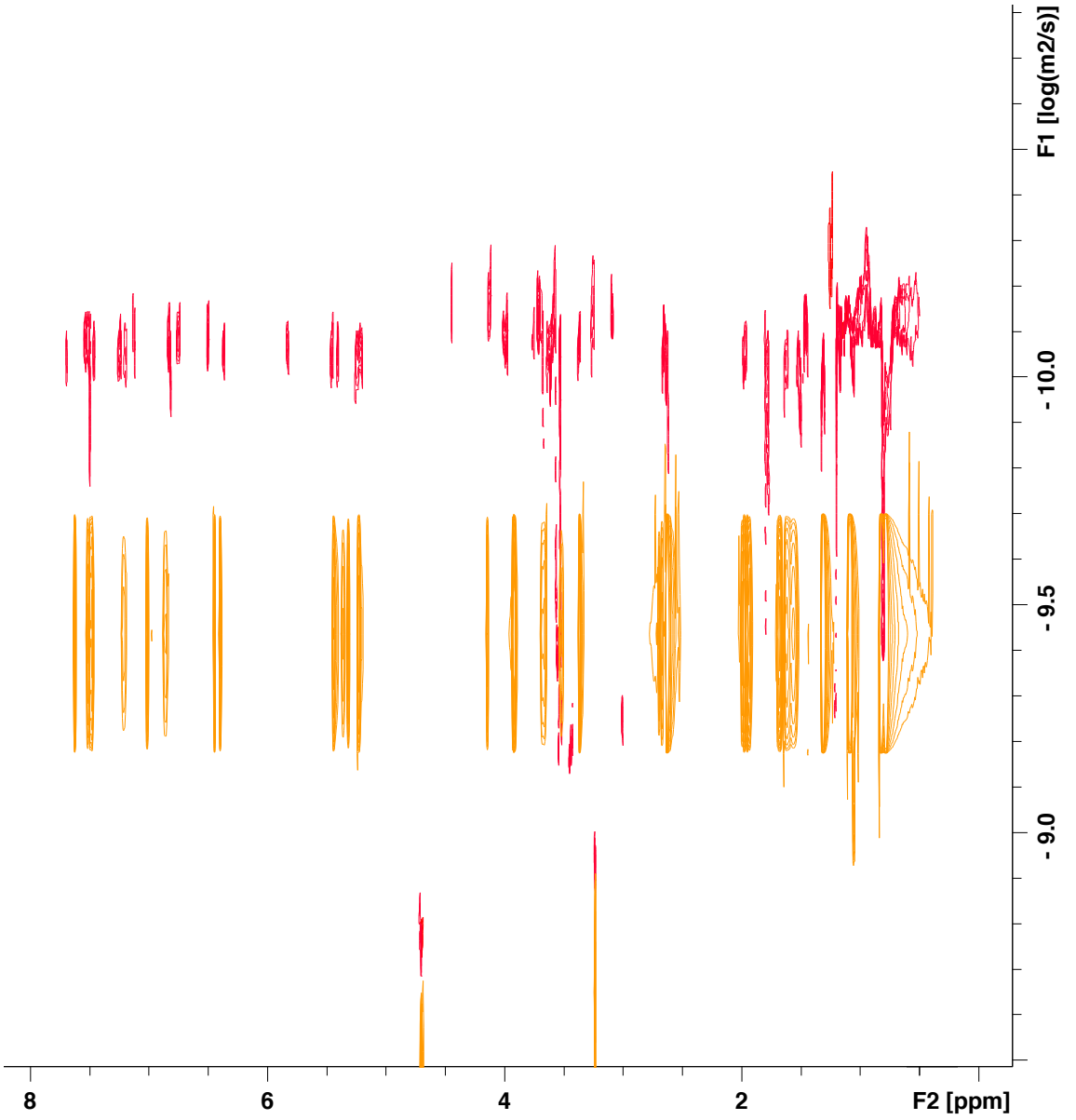

Figure 7.7: Overlaid DOSY spectra of 1 mM vancomycin in the absence (yellow) and presence (red) of 100 mM DPC-d_{38}. Protons are separated by diffusion coefficient in the Y axis; larger species diffuse more slowly, yielding smaller diffusion coefficients. Diffusion coefficients for vancomycin protons decrease in the presence of DPC-d_{38}, indicating that vancomycin diffuses more slowly under these conditions.

7.4.2 Chemical Shift Perturbations

^{1}H 1D and 2D NMR spectra were acquired for a 1 mM vancomycin sample containing 100 mM DPC-d_{38} to observe any changes in the chemical environment of protons in vancomycin upon exposure to the micelle. Since DPC-d_{38} is fully deuterated, NMR signals do not intrude upon the spectrum. By comparison to equivalent spectra acquired for vancomycin in aqueous buffer, protons were identified for which chemical shifts were perturbed in the presence of the detergent. Overlaid NOESY spectra of vancomycin in these two environments are shown in Figure 7.8 and chemical shift perturbations are quantified in Figure 7.9.

When 1 mM vancomycin was exposed to an equimolar quantity of VSC_{EC-25} and 100 mM DPC-d_{38}, chemical shift perturbations indicated that the chemical environments of protons u, v, w, and z were affected, in comparison to their environments in aqueous buffer. It is interesting that a broader profile of vancomycin protons is identified as being affected by DPC-d_{38} in the absence of VSC_{EC-25}. DPC-d_{38} alone appears to significantly change the chemical environments of protons A6, a, l, x, and y, which are not perturbed by DPC-d_{38} in the presence of the peptide. What appears to be happening here is that DPC-d_{38} alters the chemical environments of some vancomycin protons, but subsequently, the peptide alters the environments further in such a way that the net changes in chemical shifts of these protons appear insignificant. In fact, two significant perturbations have taken place, but observed simultaneously, they mask one another. The chemical environments of protons w and z are similar in the presence and absence of DPC-d_{38}, but perturbed in the presence of VSC_{EC-25}.

With the aim of investigating chemical shift perturbations of vancomycin protons in the presence and absence of VSC_{EC-25}, we have compared chemical shift perturbations of vancomycin protons in the presence and absence of DPC-d_{38} *versus*, and in the presence and absence of VSC_{EC-25} and DPC-d_{38}. It is more sensible to directly measure chemical shift perturbations in vancomycin in DPC-d_{38}, in the presence and absence of VSC_{EC-25}. In this way, the impact of the peptide may be assessed while discounting the impact of the

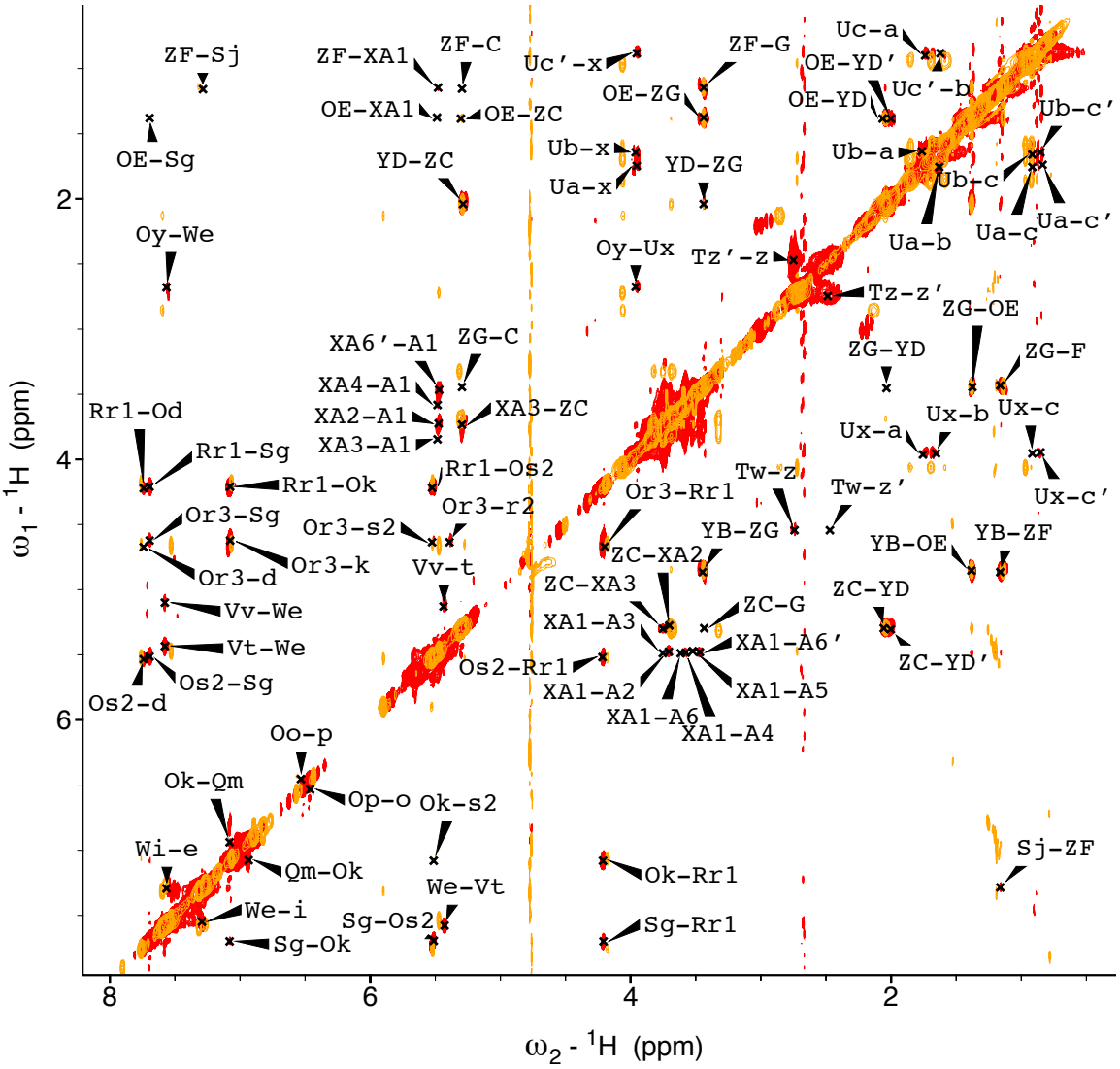

Figure 7.8: Overlaid NOESY spectra of 1 mM vancomycin in the absence (red) and presence (orange) of 100 mM DPC-d_{38}. Perturbations are observable in the chemical shifts of some vancomycin protons. These perturbations are quantified in Figure 7.9.

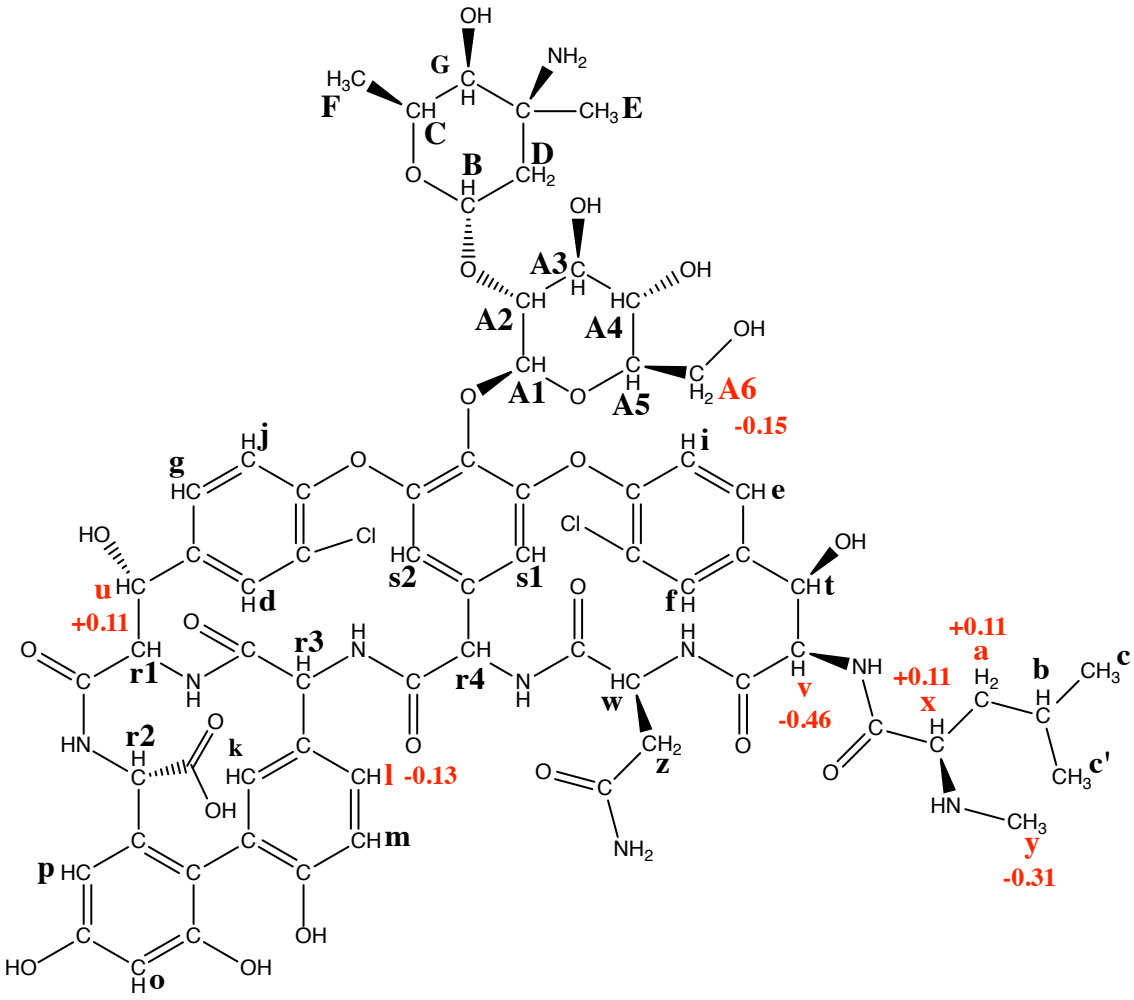

Figure 7.9: Vancomycin protons whose chemical shifts are perturbed in the presence of 100 mM DPC-d_{38}, with respect to chemical shifts in aqueous buffer.

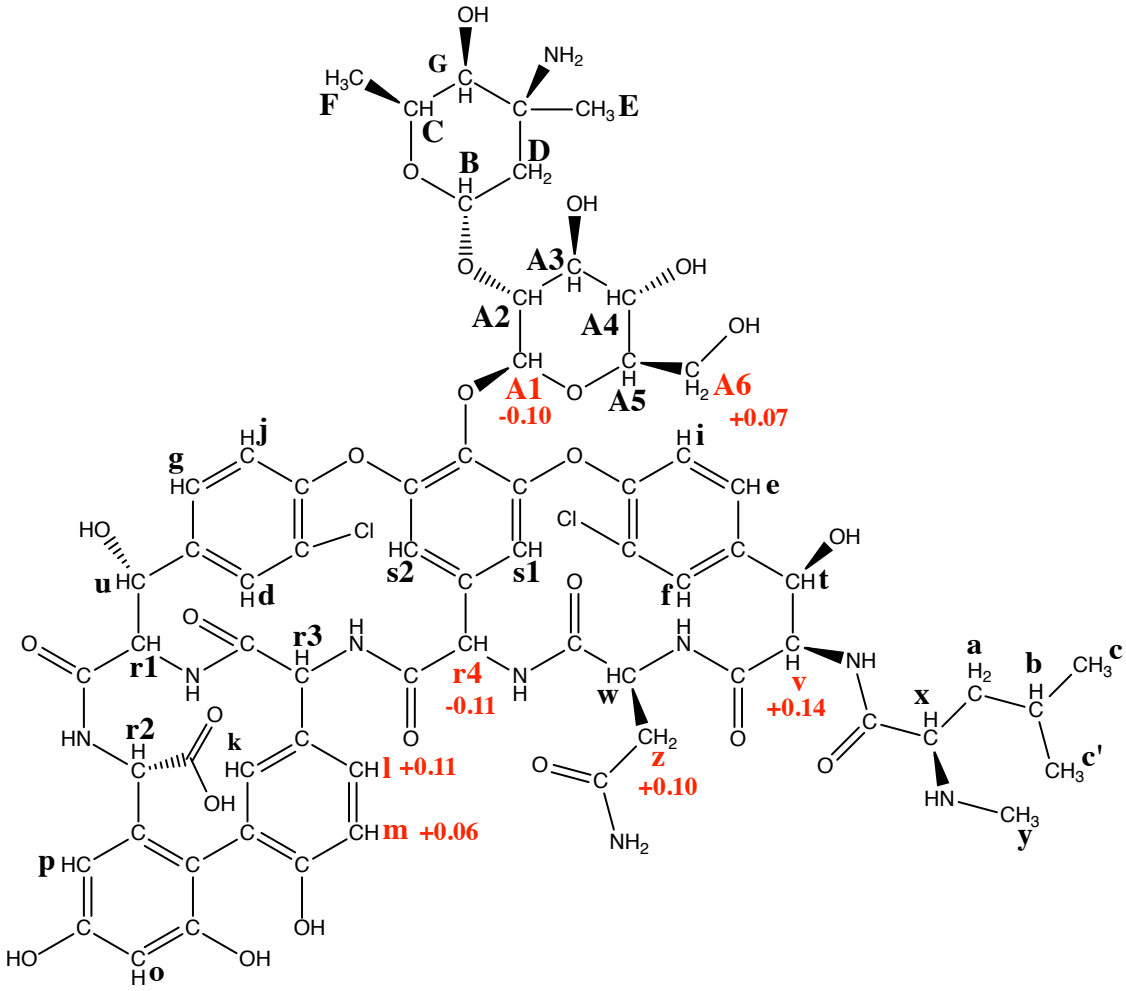

Figure 7.10: Vancomycin protons whose chemical shifts are perturbed in the presence of 1 mM VSC_{EC-25}. The impact of 100 mM DPC-d_{38} is accounted for in this dataset, in contrast to Section 6.7.2, which compared against chemical shifts measured in aqueous buffer.

detergent micelle. Figure 7.10 quantifies these chemical shift perturbations.

These analyses reveal that the chemical environment of proton u is affected by DPC-d_{38}, but not by VSC_{EC-25}. This is also true for protons a, x, and y located towards the N-terminus of the peptide component of vancomycin. Protons v and z are affected by the peptide, as are neighbouring protons l, m, and r4. Glucose protons A1 and A6 are also affected by VSC_{EC-25}.

7.5 Discussion

7.5.1 Vancomycin does not Interact Strongly with LMPG Micelles

A very weak interaction between vancomycin and LMPG is apparent from DOSY experiments, and from chemical shift perturbations observed in vancomycin in the presence of LMPG. The presence of 1.15 mM LMPG affects the chemical shifts of four vancomycin protons (Figure 7.6, red), but since these protons are isolated from one another within the structure of vancomycin, they do not identify a region which might be interacting with LMPG micelles. These results increase our confidence that the direct interaction between VanS and vancomycin indicated by STD-NMR experiments in Chapter 5 is genuine, and not an artifact of indirect saturation transfer via LMPG micelles.

However, a number of vancomycin protons accumulated saturation during STD-NMR experiments which do not experience chemical shift perturbations in the presence of LMPG micelles. This suggests that a separate interaction takes place between vancomycin and VanS, such that saturation is transferred directly to these protons.

7.5.2 Vancomycin Interacts with DPC Micelles More Strongly than with LMPG Micelles

DOSY data indicate that a significant proportion (91%) of 1 mM vancomycin molecules interact with DPC micelles in a sample of 100 mM DPC-d_{38}. Chemical shift perturbations identify a number of vancomycin protons whose chemical shifts are perturbed in the presence of 100 mM DPC-d_{38}, with respect to shifts in aqueous buffer, which indicate the presence of a DPC binding site within the structure of vancomycin. The chemical shifts of protons a, v, x, and y towards the N-terminal end of the peptide, and protons l and u towards the C-terminal end, are perturbed by DPC. These protons are broadly located around the "rim" of the D-Alanyl-D-Alanine binding pocket. While an interaction was not observed between vancomycin and LMPG (phosphoglycerol headgroup), this interaction with DPC (phosphocholine headgroup) may represent a propensity for vancomycin to interact with

bacterial cell membranes. Further investigation will be required before definite conclusions can be drawn as to the biological significance of this finding.

The DPC binding site appears to be distinct from the region where vancomycin bound to the $VanS_{SC}$ extracellular domain embedded in DPC micelles. In Chapter 6, chemical shift perturbations were recorded for vancomycin in the presence of 1 mM $VanS_{SC}$ extracellular domain and 100 mM DPC-d_{38}. When chemical shift perturbations in the presence of the extracellular domain are considered with reference to shifts in DPC alone, rather than in aqueous buffer, two regions of vancomycin are identified as being affected by the presence of the extracellular domain. In the region of vancomycin which binds lipid II (Figure 1.4), protons l, m, r4, v, and z experience chemical shift perturbations in the presence of the $VanS_{SC}$ extracellular loop. Glucose protons A1 and A6 also experience chemical shift perturbations. It is difficult to comment on similarities or differences between the $VanS_{SC}$ binding site identified in Chapter 5, and the VSC_{EC-25} binding site identified here, because STD-NMR investigations were limited to protons with chemical shifts downfield of 5 ppm *i.e.* those within hydrocarbon rings in amino acid sidechains. However, protons l and m which experienced chemical shift perturbations from VSC_{EC-25} also acquired saturation from $VanS_{SC}$, and proton r4 neighbours this region of the antibiotic; perturbed protons v and z neighbour the hydrocarbon ring housing saturated protons e, f, and i.

Chapter 8

Discussion and Future Work

8.1 Project Background and Aims

Vancomycin is a glycopeptide antibiotic that is frequently used in the treatment of methicillin-resistant *Staphylococcus aureus* (MRSA) infections. Its mode of action is to bind to D-Alanyl-D-Alanine-terminating peptides in lipid II, inhibiting binding of penicillin-binding proteins (PBPs) which catalyse transglycosylation and transpeptidation crosslinking reactions to integrate lipid II into the peptidoglycan cell wall.

Vancomycin resistance was first reported in the late 1980s (Leclercq et al., 1988), and has emerged in *S. aureus* following intergeneric transfer of genes from a vancomycin-resistant *Enterococcus faecalis* (Chambers and DeLeo, 2010). The mechanism by which vancomycin resistance is achieved is well-characterised; on exposure to vancomycin, the integral membrane protein VanS phosphorylates VanR, increasing its affinity for the promoter regions of transcription elements within the *van* gene cluster. The *vanHAX* transcription element encodes three enzymes which subvert the cell's normal peptidoglycan synthesis machinery, resulting in the substitution of D-Alanyl-D-Alanine with D-Alanyl-D-Lactate at the terminus of the lipid II pentapeptide. Vancomycin cannot bind D-Alanyl-D-Lactate, but PBPs can, so crosslinking reactions are allowed to take place.

Within this well-characterised system, details pertaining to the structure and function of VanS remain to be elucidated. There is evidence in the literature to suggest that VanS binds either glycopeptide antibiotics, peptidoglycan precursors, or a complex of the two. The extracellular domain and putative ligand binding site of VanS has yet to be structurally characterised. Sequence homology between the extracellular domains of VanS proteins of different species is low (Table 1.2), even when antibiotic sensitivity profiles are similar, as in *E. faecalis* VanS_B and *S. coelicolor* VanS_{SC}.

This study aimed to structurally characterise the extracellular domain of a VanS protein, and to investigate the ligand binding capabilities of that extracellular domain and of two full-length VanS proteins.

8.2 Progress Towards a Glycopeptide Affinity Column

Affinity chromatography allows for the isolation of proteins with a binding affinity for a particular substance. Metal ion affinity chromatography is frequently used to purify proteins with inserted hexahistidine (His_6) tags. The glycopeptide antibiotic vancomycin also has an affinity for metal ions, and particularly for copper (Pfeiffer, 1981).

In this work, we have demonstrated that vancomycin can be bound to a copper ion affinity column, and following washing to remove unbound vancomycin, the bound portion does not elute until imidazole is applied to disrupt the interaction (Section 4.3). The column can therefore be "charged" with vancomycin, which will not be dislodged when buffer is subsequently applied.

A His_6-tagged VanS protein could not be applied to this vancomycin affinity column, because interactions between the His_6 tag and the copper ions would result in retention of the protein regardless of any interaction with vancomycin. Therefore, the His_6 tag of His_6-$VanS_A$ was replaced with a StrepII tag by site-directed mutagenesis (Section 4.4). The modified protein was successfully expressed (Section 4.5) but could not be purified using a standard StrepTactin affinity chromatography protocol (Section 4.6). Further optimisation of this purification protocol will be necessary before sufficiently pure StrepII-$VanS_A$ can be obtained to facilitate a binding study.

An interaction between teicoplanin and Cu^{2+} has been documented (Brzezowska et al., 2010), but it is unclear whether this interaction will be sufficient to retain teicoplanin within a Cu^{2+} affinity column when buffer is passed through the resin. The plausibility of constructing a teicoplanin affinity column as has been achieved for vancomycin remains to be determined.

Attachment of a covalent linker to the C-terminus of vancomycin has been exploited by Roy et al. (2001) to construct a vancomycin affinity column in the past. This approach occludes a different region of vancomycin than is occluded by Cu^{2+} interactions, and could be adopted in tandem with the Cu^{2+} approach to allow for a more flexible investigation of protein-vancomycin interactions. The covalent linker might also be attached to teicoplanin, as its attachment targets the carboxyl group common to peptide termini.

8.3 VanS-Ligand Binding Studies

8.3.1 Active, Folded Full-length VanS proteins

His_6-$VanS_A$ (from *E. faecium*) and His_6-$VanS_{SC}$ (from *S. coelicolor*) were expressed in *E. coli*, purified to homogeneity, and demonstrated to be properly folded (Section 3.8) and to possess constitutive ATPase activity (Section 3.9). Saturation transfer difference NMR experiments were conducted, and interactions were observed between vancomycin and both VanS proteins (Section 5.5). Conversely, no interaction between His_6-$VanS_A$ and the pentapeptide of lipid II was observed.

^{1}H 1D and 2D (TOCSY and NOESY) NMR spectra acquired for vancomycin were fully assigned (Section 5.4.1), so that protons involved in the interaction observed by STD-NMR could be identified. Investigation by STD-NMR was limited to protons of hydrocarbon rings in the sidechains of residues in the peptide component of vancomycin, due to intrusion of NMR signals from LMPG detergent in the upfield region of the spectrum. We show that, among observable protons, those at the C-terminal end of the peptide component of vancomycin accumulate a greater degree of saturation from both $VanS_A$ and $VanS_{SC}$ than those at the N-terminus of the peptide component (Sections 5.6.1 - 5.6.2). We do not expect every proton accumulating saturation from VanS to be actively involved in an interaction; saturation is transferred in a distance-dependent manner, so protons accumulating a greater degree of saturation are physically closer to the binding interface than protons accumulating a lesser degree of saturation. We also report a change in chemical environment of vancomycin

proton j in the presence of $VanS_{SC}$, as opposed to $VanS_A$ or in the absence of VanS protein.

For STD-NMR experiments, both VanS proteins were encapsulated in LMPG micelles to maintain their native folds as integral membrane proteins. To investigate the influence of the micelle on the results of STD experiments, we investigated the propensity of vancomycin to interact with the LMPG micelle in the absence of VanS (Section 7.3). DOSY and STD-NMR data indicate an interaction between vancomycin and the micelle. Monitoring chemical shift perturbations in vancomycin protons, we find that a concentration of 1.15 mM LMPG (as used in STD-NMR) perturbs a subset of vancomycin protons accumulating saturation from VanS during STD-NMR. Unlike STD-NMR data, chemical shift perturbations do not clearly indicate a preference towards the C-terminal end of the vancomycin peptide component. This suggests that the interaction between vancomycin and LMPG does not explain the observed interactions with VanS presented in Chapter 5. We report with confidence that saturation is transferred from VanS to vancomycin in a manner which indicates binding of residues at the C-terminus of the peptide component.

8.3.2 The $VanS_{SC}$ Extracellular Domain

A synthetic peptide VSC_{EC-25} was acquired with sequence D38-F62, corresponding to the core extracellular domain of $VanS_{SC}$ and beginning with the sequence DQGW, which has previously been suggested to be involved in an interaction with vancomycin (Koteva et al., 2010). Exposed to an equimolar quantity of vancomycin, VSC_{EC-25} HN-Hα NMR crosspeaks were heterogeneously attenuated (Section 6.7.1). Crosspeaks from L42 and L43 were lost entirely, as were crosspeaks from A52, V57, L59, and S61. Heterogeneous attenuation of peptide NMR signals indicates a change in chemical environments of these peptide protons, suggesting an interaction between this region of $VanS_{SC}$ and vancomycin.

NMR data acquired of vancomycin in DPC-d_{38} micelles and in the presence and absence of VSC_{EC-25} led to the identification of vancomycin protons, the chemical shifts of which are perturbed by the $VanS_{SC}$ extracellular domain (Section 7.4.2). Unlike in STD-NMR, all protons within vancomycin were observable in this experiment. Vancomycin

protons identified as being involved in an interaction with either full-length VanS (orange) or VSC_{EC-25} (blue) are highlighted in Figure 8.1.

A number of vancomycin protons perturbed by the presence of VSC_{EC-25} could not be monitored during STD-NMR in Chapter 5, due to their upfield chemical shifts. The majority of protons to which saturation was observed to transfer from His_6-$VanS_{SC}$ do not experience chemical shift perturbations in the presence of VSC_{EC-25}; exceptions are protons l and m which are affected in both experiments. Perturbed protons r4, v, and z are within or near to the peptide backbone, and perturbation of these protons may result from the same interaction that transferred saturation to protons in hydrocarbon ring sidechains. Protons A1 and A6 are in a sugar moiety to which saturation transfer could not be monitored during STD-NMR.

STD-NMR identifies protons in close proximity to the binding interface of an interaction; chemical shift perturbations identify protons whose chemical environments are altered in the presence of an introduced molecule. Further investigation will facilitate interpretation of the results acquired here, however it is possible that chemical shift perturbations in vancomycin caused by VSC_{EC-25} represent the binding site of the interaction, while saturation transfer describes the overall orientation of the vancomycin molecule at the time of binding.

STD-NMR investigation of interactions between VanS and vancomycin was limited by intrusive NMR signals from LMPG protons. In the future, to facilitate comparison of binding studies of $VanS_{SC}$ and VSC_{EC-25}, it would be valuable to identify a membrane mimetic in which His_6-$VanS_{SC}$ could be reconstituted which would not contribute invasive NMR signals to STD spectra. This would allow all protons within vancomycin to be monitored for saturation accumulation. It is prohibitively expensive to solubilise and purify heterologously expressed VanS into deuterated detergents. However, it is possible to purify membrane proteins in a detergent micelle, and then extract proteins from micelles into lipid vesicles. Lipid vesicles sufficiently large to far exceed the upper size limit of solution-state NMR, so protons in lipid vesicles - including protons of encapsulated proteins - do not

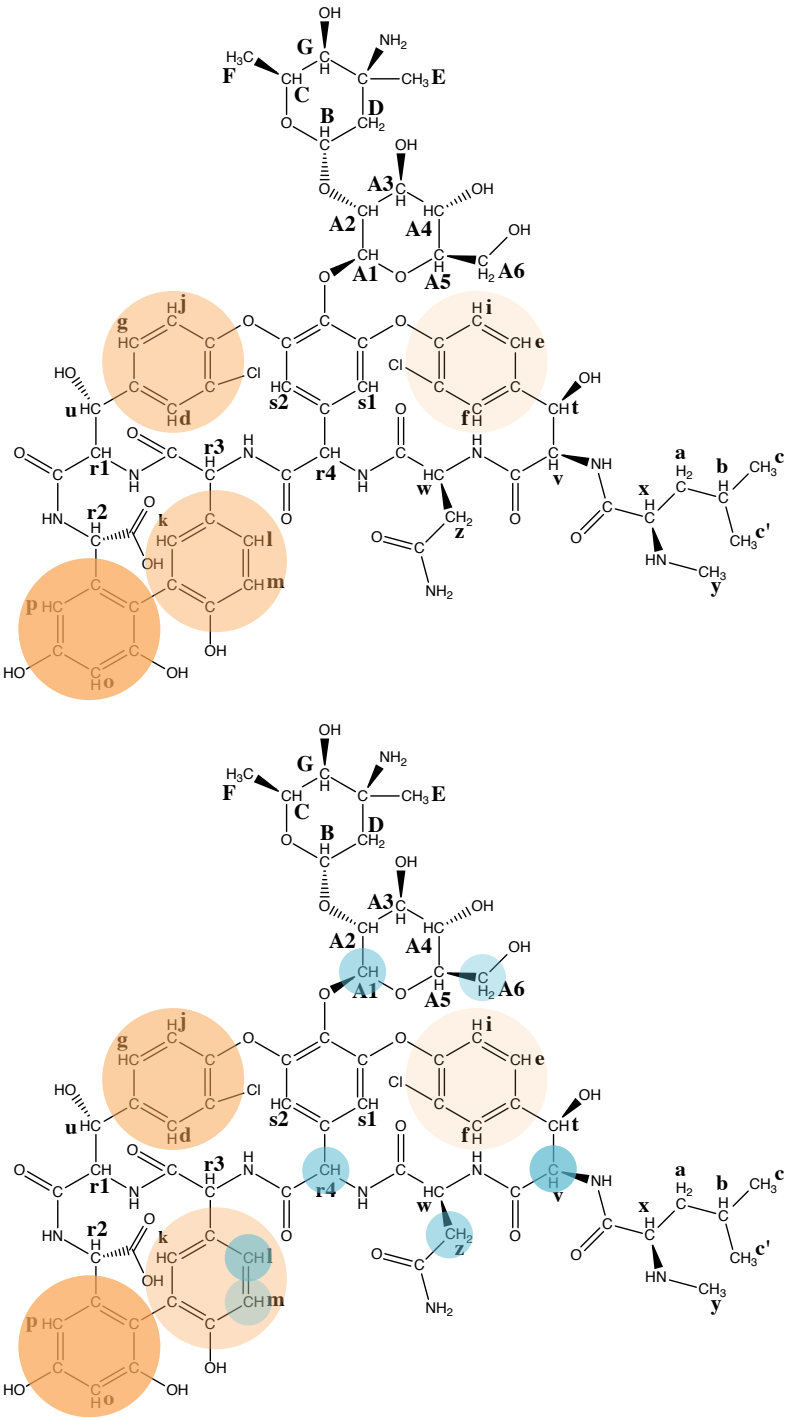

Figure 8.1: Top: vancomycin, with hydrocarbon rings accumulating saturation from His_6-$VanS_A$ highlighted in orange. Intensity of orange colour approximates degree to which saturation accumulates. Bottom: vancomycin, with hydrocarbon rings accumulating saturation from His_6-$VanS_{SC}$ highlighted in orange and protons whose chemical shifts are perturbed by VSC_{EC-25} highlighted in blue. Intensity of blue colour indicates magnitude of chemical shift perturbation.

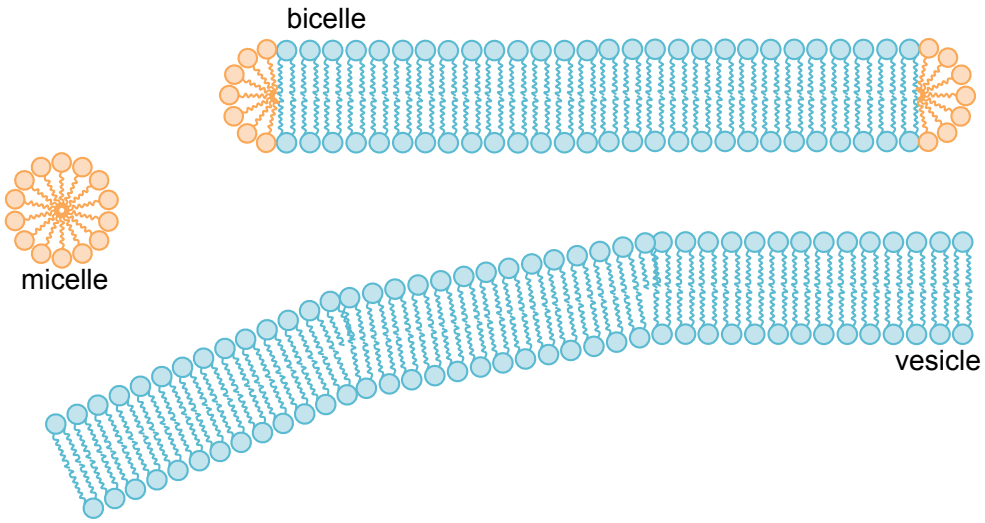

Figure 8.2: Three types of membrane mimetic used in the study of integral membrane proteins: detergent micelles, lipid vesicles (a section of which is shown), and mixed detergent/lipid vesicles in which a disc of lipid bilayer is enclosed inside a ring of detergent molecules.

contribute to NMR spectra.

When selecting an appropriate lipid vesicle for VanS reconstitution, it will be preferable to avoid vesicles for which vancomycin has an affinity. Therefore, an extended investigation of vancomycin/mimetic interactions should be carried out. A range of different lipid headgroups should be examined, as should mimetic structures of different curvatures - *i.e.* detergent micelles, lipid vesicles of different dimeters (achieved by extrusion of vesicles in solution), and mixed detergent/lipid bicelles. Bicelles are relatively large disc-shaped structures comprising a lipid bilayer, with a ring of detergent around the perimeter providing more extreme curvature than is seen in a lipid vesicle (Figure 8.2). Cell membranes are heterogeneous mixtures of lipids; mixed lipid vesicles and bicelles should also be investigated, to examine whether certain proportions of charged/uncharged/zwitterionic headgroups impact on vancomycin's propensity to interact with a mimetic.

The propensity for VanS to bind other ligands could also be investigated, including a range of peptidoglycan precursors. The actions of both glycopeptide and β-lactam antibiotics prevent transpeptidation of lipid II; glycopeptides also prevent transglycosylation,

which is allowed to occur in the presence of β-lactam antibiotics. Since β-lactams do not induce vancomycin-type resistance, if a lipid II precursor is the ligand to VanS, that precursor is unlikely to be transglycosylated. Monomeric lipid II is a rational starting point for ligand-binding studies; however, interactions between the lipid tail and any membrane mimetic are expected to be significantly intrusive. Since the lipid itself is inserted into the membrane it is unlikely that it binds to the extracellular domain of VanS; it may be appropriate to truncate or remove this lipid tail, and study interactions between VanS and GlcNAc-MurNAc-pentapeptide in its absence. However, this would preclude the study of interactions between the lipid tail and the transmembrane domains of VanS, or the impact of lipid on membrane fluidity and the downstream effects of this on VanS signal transduction.

A popular technique in the investigation of ligand-binding is surface plasmon resonance spectroscopy (SPR). In this technique, one component of an interaction is immobilised on a surface, and a solution of the other component is allowed to flow over this surface. Binding is detected as a change in the adsorptive properties of molecules on the surface (Forest et al., 2016). One limitation of the technique is the need to immobilise a component of the interaction without denaturing it, or otherwise disabling the desired interaction (Fischer and Mol, 2010). This is similar to the limitation of the vancomycin affinity column, and might be overcome by similar means - using several different anchor points within the vancomycin structure to immobilise it to the surface, ultimately exposing every face of the antibiotic to VanS proteins in solution.

Analytical ultracentrifugation has been used to study the interaction between VanS_A and vancomycin (Phillips-Jones et al., 2017). VanS_A was studied in the absence of a membrane mimetic, raising questions about the fold of the extracellular (ligand binding) domain of the protein. However, the reported significant increase in the sedimentation coefficient of VanS_A in the presence of vancomycin is interesting. This technique could be applied to other VanS proteins, ideally solubilised within membrane mimetics in order that the native fold of the extracellular domain be maintained. It might also be possible to cleave VanS proteins, or to express truncations representing the cytosolic catalytic domains of VanS.

A cytosolic truncation of $VanS_A$ has previously been expressed as an MBP fusion protein (Wright et al., 1993). The cytosolic domain of VanS could be used as a negative control; changes in the sedimentation coefficient of this truncated form of VanS in the presence of vancomycin would suggest that the previously reported interaction does not involve the extracellular, putative ligand-binding domain.

8.4 Structural Characterisation of the Extracellular Domain

Analysis of the secondary structure of the VSC_{EC-25} peptide by circular dichroism (Section 6.5.2) and solution-state NMR (Section 6.6.2) indicates that in the presence of DPC and LMPG micelles, this peptide contains a small, N-terminal helical region spanning residues W41-T44, and that the peptide is otherwise random coil in structure. The helical region incorporates residue W41, suggested to be involved in the vancomycin-$VanS_{SC}$ interaction (Koteva et al., 2010). While the domain appears to adopt no further secondary structure beyond this short helical region, the tertiary structure of the domain has yet to be described. Attenuation of HN-Hα NMR crosspeaks by vancomycin extended to several residues towards the C-terminus of VSC_{EC-25}; if these residues form part of the vancomycin binding site, this suggests a possible doubling-back of the peptide backbone towards the N-terminus to bring these residues into close proximity with the helical region. One such tertiary structure is shown in Figure 8.3; close association of the helix with section T56-F62 would bring together residues experiencing complete signal attenuation in the presence of vancomycin.

We have demonstrated that the structure of the peptide is changed in the presence of DM micelles, suggesting that the structure of the extracellular domain of VanS may be dependent on local membrane composition. The extended mimetic study proposed above could also be used to further characterise the structure of VSC_{EC-25}. We have demonstrated that the secondary structure of this peptide is different in DM than in DPC or LMPG. It would be interesting to investigate whether membrane mimetics of particular chemical or structural characteristics induce particular structures in the peptide. This may translate

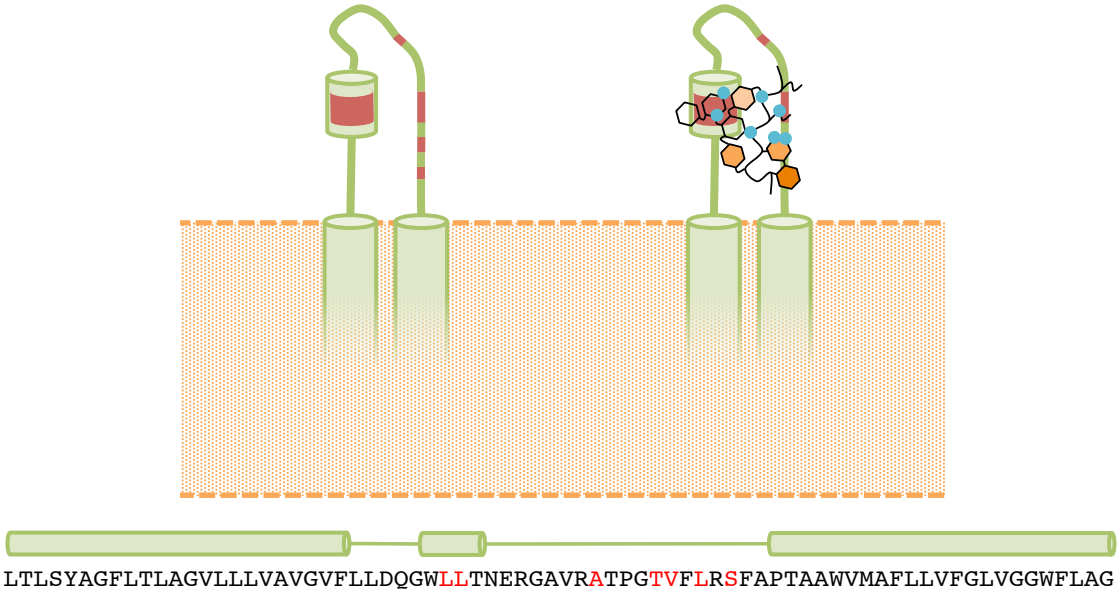

Figure 8.3: Left: A possible tertiary structure of the VanS$_{SC}$ extracellular domain, bringing together residues which experienced complete HN-Hα NMR signal attenuation in the presence of vancomycin (red) to form a possible binding site. Right: Vancomycin (Figure 8.1) is depicted in an orientation such that the C-terminus of the peptide component is in closer proximity to the protein than the N-terminus, consistent with STD data (orange), and vancomycin protons with chemical shifts perturbed by VSC$_{EC-25}$ (blue) are in close proximity to attenuated peptide residues.

to a biologically relevant finding; since bacterial cell membranes are heterogeneous and fluid, a change in membrane composition, perhaps due to the accumulation of lipid II as a result of vancomycin activity may induce a conformational change in the structure of the $VanS_{SC}$ extracellular domain. Lipid II can therefore be thought of both as a ligand and as a component of an appropriate membrane mimetic when studying VanS. Investigation of the structure of VSC_{EC-25} in lipid vesicles of differing fluidities might shed light on the significance of this membrane characteristic. To investigate the native structure of the $VanS_{SC}$ extracellular domain, it would be most appropriate to study it in the presence of *S. coelicolor* cell membranes. *S. coelicolor* is nonpathogenic, so it may be possible to culture a non-resistant strain and extract the lipid content of the cells. Total lipid extracts of a number of organisms, including Gram-negative *E. coli*, are available for purchase.

The extracellular domains of other VanS proteins could be isolated as synthetic peptides and studied in this same manner. To achieve full sequential assignment of NMR spectra acquired of these peptides, it is preferable to select shorter peptides, to minimise difficulties arising from overlapping peaks in NMR spectra. Alternatively, peptides could be isotopically labelled. This would facilitate sequential assignment, and avoid the issue of vancomycin NMR signals overwhelming spectra.

It would be of particular value to solve the structure of the extracellular domain of VanS within the full, natively-folded protein, rather than extracting this region as a synthetic peptide. If the structure of this domain of the protein could be solved, this would provide a valuable reference point for ligand-binding studies of VanS (including truncations and synthetic peptides) in the future. Reliance on the constitutive ATPase activity of VanS as an indicator of native fold is problematic, because this activity has been demonstrated in a cytosolic truncation of VanS (Wright et al., 1993), indicating that integrity of the extracellular domain is not required for this catalytic activity to take place. At this time, constitutive ATPase activity remains the benchmark by which the integrity of VanS is assessed in the literature (Phillips-Jones et al., 2017).

We have presented here evidence that vancomycin binds to both $VanS_A$ from *En-*

terococcus faecium and $VanS_{SC}$ from *Streptomyces coelicolor*, and that in the latter case, this interaction involves a short helical region W41-T44 in the extracellular domain of the protein, in agreement with the findings of Koteva et al. (2010). Further optimisation of the methods recommended in this Chapter would lead to a fuller understanding of these interactions, and allow similar interactions between other VanS proteins and other potential ligands to be characterised. When the ligand-induced activation of VanS is fully understood, it might be undermined perhaps through the design of novel inhibitors to prevent this binding from taking place. This would allow vancomycin-resistant pathogens, including VRSA, to be resensitised to the antibiotic.

Bibliography

Addinall, Johnson, Dafforn, Smith, Rodger, Gomez, Sloan, Blewett, Scott, and Roper. Expression, purification and crystallization of the cell-division protein YgfE from Escherichia coli. *Acta Crystallogr Sect F Struct Biol Cryst Commun*, 61(3):305–307, 2005.

Angulo, Enriquez-Navas, and Nieto. Ligand-Receptor Binding Affinities from Saturation Transfer Difference (STD) NMR Spectroscopy: The Binding Isotherm of STD Initial Growth Rates. *Chem. Eur. J.*, 16(1):7803–7812, 2010.

Aravind and Ponting. The cytoplasmic helical linker domain of receptor histidine kinase and methyl-accepting proteins is common to many prokaryotic signalling proteins. *FEMS Microbiology Letters*, 176(1):111–116, 1999.

Arthur and Quintiliani Jr. Regulation of VanA- and VanB-Type Glycopeptide Resistance in Enterococci. *Antimicrobial Agents and Chemotherapy*, 45(1):375–281, 2001.

Arthur, Depardieu, Molinas, Reynolds, and Courvalin. the *vanZ* gene of Tn*1546* from *Enterococcus faecium* BM4147 confers resistance to teicoplanin. *Gene*, 154(1):87–92, 1995.

Arthur, Depardieu, Cabanié, Reynolds, and Courvalin. Requirement of the VanY and VanX D,D-peptidases for glycopeptide resistance in 'textitEnterococci. *Molecular Microbiology*, 30(1):819–830, 1998.

Baptista, Depardieu, and Courvalin. Specificity of Induction of Glycopeptide Resistance Genes in *Enterococcus faecalis*. *Antimicrob Agents Chemother*, 40(1):2291–2295, 1996.

Baptista, Depardieu, Reynolds, Courvalin, and Arthur. Mutations Leading to Increased Levels of Resistance to Glycopeptide Antibiotics in VanB-type Enterococci. *Molecular Microbiology*, 25(1):93–105, 1997.

Baptista, Rodrigues, and Depardieu. Single-cell analysis of glycopeptide resistance gene

expression in teicoplanin-resistant mutants of a VanB-type *Enterococcus faecalis*. *Mol Microbiol*, 32(1):17–28, 1999.

Barna and Williams. The Structure and Mode of Action of Glycopeptide Antibiotics of the Vancomycin Group. *Ann. Rev. Microbiol.*, 38(1):339–357, 1984.

Barreteau, Kovac, Boniface, Sova, Gobec, and Blanot. Cytoplasmic Steps of Peptidoglycan Biosynthesis. *FEMS Microbiology Reviews*, 32(1):168–207, 2008.

Bateman, Holden, and Yeats. The G5 domain: a potential *N*-acetylglucosamine recognition domain involved in biofilm formation. *Bioinformatics*, 21(8):1301–1303, 2005.

Beauregard, Williams, Gwynn, and Knowles. Dimerization and membrane anchors in extracellular targeting of vancomycin group antibiotics. *Antimicrobial Agents and Chemotherapy*, 39(3):781–785, 1995.

Beltrametti, Consolandi, Carrano, Bagatini, Rossi, Leoni, Zennaro, Selva, and Marinelli. Resistance to Glycopeptide Antibiotics in the Teicoplanin Producer is Mediated by *van* Gene Homologue Expression Directing the Synthesis of a Modified Cell Wall Peptidoglycan. *ANtimicrob. Agents Chemother.*, 51(4):1135–1141, 2007.

Bertani. Lysogeny at Mid-Twentieth Century: P1, P2, and Other Experimental Systems. *Journal of Bacteriology*, 186(3):595–600, 2004.

Bertino. Cost burden of viral respiratory infections: Issues for formulary decision makers. *Disease-a-Month*, 49(3):225–239, 2003.

Bhate, Molnar, Goulian, and DeGrado. Signal Transduction in Histidine Kinases: Insights from New Structures. *Structure*, 23(1):981–994, 2015.

Boeckel, Brower, Gilbert, Grenfell, Levin, Robinson, Teillant, and Laxminarayan. Global trends in antimicrobial use in food animals. *PNAS*, 112(18):5649–5654, 2015.

Bordan and Keller. Helical transmembrane peptides: A "Divide and Conquer" approach to membrane proteins. *Chemistry and Physics of Lipids*, 163(1):1–26, 2010.

Breeze, Dzimitrowicz, Kierchbaumer, Brooks, Botchway, Prady, Hawes, Dixon, Schnell, Fricker, and Frigerio. A C-terminal amphipathic helix is necessary for the *in vivo* tubule-shaping function of a plant reticulon. *PNAS*, 113(39):10902–10907, 2016.

Breukink and de Kruijff. Lipid II as a Target for Antibiotics. *Nature Reviews Drug Discovery*, 5(1):321–323, 2006.

Brotz, Bierbaum, Reynolds, and Sahl. The lantibiotic mersacidin inhibits peptidoglycan biosynthesis at the level of transglycosylation. *European Journal of Biochemistry*, 246(1): 193–199, 1997.

Brzezowska, Kucharczyn-Klaminska, Bernardi, Valensin, Gaggelli, Gaggelli, Valensin, and Jezowska-Bojczuk. Cu(II) ion interaction with teicoplanin - vancomycin's analog. *Journal of Inorganic Chemistry*, 104(2):193–198, 2010.

Bugg, Wright, Dutka-Malen, Arthur, Courvalin, and Walsh. Molecular Basis for Vancomycin Resistance in *Enterococcus faecium* BM4147: Biosynthesis of a Depsipeptide Peptidoglycan Precursor by Vancomycin Resistance Proteins VanH and VanA. *Biochemistry*, 30(1):10408–10415, 1991.

Bush, Courvalin, Dantas, Davies, Eisenstein, Huovinen, Jacoby, Kishony, Kreiswirth, Kutter, Lerner, Levy, Lewis, Lomovskaya, Miller, Mobashery, Piddock, Projan, Thomas, Tomasz, Tulkens, Walsh, Watson, Witkowski, Witte, Wright, Yeh, and Zgurskaya. Tackling antibiotic resistance. *Nature reviews Microbiology*, 9(12):894–896, 2011.

Chambers and DeLeo. Waves of Resistance: *Staphylococcus aureus* in the Antibiotic Era. *Nat Rev Microbiol.*, 7(9):629–641, 2010.

Choi-Rhee, Schulman, and Cronan. Promiscuous protein biotinylation by *Escherichia coli* biotin protein ligase. *Protein Sci.*, 13(11):3043–3050, 2004.

Chung, Kim, Manglik, Alvarez, Kobilka, and Prosser. Role of Detergents in Conformational

Exchange of a G Protein-coupled Receptor. *The Journal of Biological Chemistry*, 287(1): 36305–30311, 2012.

Clardy and Walsh. Lessons from Natural Molecules. *Nature*, 432(1):829–837, 2004.

Convert, Bongini, and Feeney. A ^{1}H Nuclear Magnetic Resonance Study of the Interactions of Vancomycin with *N*-Acetyl-D-alanyl-D-alanine and Related Peptides. *J. Chem. Soc., Perkin Transactions*, 8(1):1262–1270, 1980.

Courvalin. Vancomycin Resistance in Gram-Positive Cocci. *Clinical Infectious Diseases*, 42 (1):S25–S34, 2006.

D'Costa, King, Kalan, Morar, Sung, Schwarz, Froese, Zazula, Calmems, Debruyne, and Golding. Antibiotic resistance is ancient. *Nature*, 477(7365):457–462, 2011.

Depardieu, Courvalin, and Kolb. Binding sites of VanR$_B$ and σ_{70} RNA polymerase in the *vanB* vancomycin resistance operon of *Enterococcus faecium* BM4524. *Molecular Microbiology*, 57(2):550–564, 2005.

Dixon, Venable, Pastor, and Bull. Micelle-Bound Conformation of a Hairpin-Forming Peptide: Combined NMR and Molecular Dynamics Study. *Biopolymers*, 65(4):284–298, 2002.

Drew, Lerch, Kunji, Slotboom, and de Gier. Optimization of membrane protein overexpression nd purification using GFP fusions. *Nature Methods*, 3(4):303–313, 2006.

Drozdetskiy, Cole, Procter, and Barton. JPred4: a protein secondary structure prediction server. *Nucleic Acids Research*, 43(W1):W389–W394, 2015.

Duncan, van Heijenoort, and Walsh. Purification and Characterisation of the D-Alanyl-D-Alanine-Adding Enzyme from *Escherichia coli*. *Biochemistry*, 29(1):2379–2386, 1990.

Dutton and Elmes. Vancomycin: report on treatment of patients with severe staphylococcal infections. *British Medical Journal*, 1(5130):1144–1149, 1959.

Edwards. *An Investigation into the Structure and Function of VanS proteins involved in the Two-Component VanS/VanR Regulatory System controlling Antibiotic Resistance*. PhD thesis, The University of Warwick, Coventry, Sept 2014.

Enright, Day, Davies, Peacock, and Pratt. Multilocus Sequence Typing for Characterization of Methicillin-Resistant and Methicillin-Susceptible Clones of Staphylococcus aureus. *J Clin Microbiol*, 38(1):1008–1015, 2000.

Fang, Tiyanont, Zhang, Wanner, Boger, and Walker. The mechanism of action of ramoplanin and enduracidin. *Molecular Biosystems*, 2(1):69–76, 2006.

Fielding. NMR Methods for the Determination of Protein-Ligand Dissociation Constants. *Progress in Nuclear Magnetic Resonance Spectroscopy*, 51(1):219–242, 2007.

Fischer and Mol. Amine Coupling Through EDC/NHS: A Practical Approach. *Methods in Molecular Biology (Methods and Protocols)*, 627(1), 2010.

Fleming. Nobel lecture: penicillin, 1945.

Forest, Breault-Turcot, Chaurand, and Masson. Surface plasmon resonance imaging-MALDI-TOF imaging mass spectrometry of thin tissue sections. *Analytical Chemistry*, 88(4), 2016.

Gasteiger, Hoogland, Gattiker, Duvaud, Wilkins, Appel, and Bairoch. Protein Identification and Analysis Tools on the ExPASy Server. In *The Proteomics Protocols Handbook*. Humana Press, 2005.

Grant, Jessee, Bloom, and Hanahan. Differential plasmid rescue from transgenic mouse DNAs into *Escherichia coli* methylation-restriction mutants. *PNAS*, 87(1):4645–4649, 1990.

Hage. Affinity chromatography: a review of clinical applications. *Clinical Chemistry*, 45 (5):593–615, 1999.

Haldimann, Fisher, and Daniels. Transcriptional Regulation of the *Enterococcus faecium* BM4147 Vancomycin Resistance Gene Cluster by the VanS-VanR Two-Component Regulatory System in *Escherischia coli* K-12. *J Bacteriol*, 179(1):5903–5913, 1997.

Hanahan. Studies on Transformation of Escherichia coli with Plasmids. *J. Mol. Biol.*, 166 (1):557–580, 1983.

Handwerger and Kolokathis. Induction of vancomycin resistane in *Enterococcus faecium* by inhibition of transglycosylation. *FEMS Microbiology Letters*, 70(2):167–170, 1990.

Hiramatsu, Hanaki, Ino, Yabuta, Oguri, and Tenover. Methicillin-resistant *Staphylococcus aureus* clinical strain with reduced vancomycin susceptibility. *J Antimicrob Chemother*, 40(1):135–136, 1997.

Holman, Wu, Wanner, and Walsh. Identification of the DNA-Binding Site for the Phosphorylated VanR Protein Required for Vancomycin Resistance in *Enterococcus faecium*. *Am Chem Soc*, 33(1):4625–4631, 1994.

Hong, Hutchings, and Neu. Characterisation of an Inducible Vancomycin Resistance System in 'textitStreptomyces coelicolor Reveals a Novel Gene (*vanK*) Required for Drug Resistance. *Mol Microbiol*, 52(1):1107–1121, 2004.

Hong, Hutchings, and Buttner. Vancomycin Resistance VanS/VanR Two-Component Systems. In *Bacterial Signal Transduction: Networks and Drug Targets*. Landes Bioscience and Springer Science+Business Media, 2008.

Hughes, Longo, Phillips-Jones, and Hussain. Characterisation of the Selective Binding of Antibiotics Vancomycin and Teicoplanin by the VanS Receptor Regulating Type A Vancomycin Resistance in the Enterococci. *BBA - General Subjects*, 1861(1):1951–1959, 2017.

Hulko, Berndt, Gruber, Linder, Truffault, Schultz, Martin, Schultz, Lupas, and Coles. The

HAMP Domain Structure Implies Kelic Rotation in Transmembrane Signaling. *Cell*, 126 (8):929–940, 2006.

Hutchings, Hoskisson, Chandra, and Buttner. Sensing and responding to diverse extracellular signals? Analysis of the sensor kinases and response regulators of *Streptomyces coelicolor* A3(2). *Microbiology*, 150(1):2795–2806, 2004.

Hutchings, Hong, and Buttner. The Vancomycin Resistance VanRS Two-Component Signal Transduction System of *Streptomyces coelicolor*. *Molecular Microbiology*, 59(3):923–935, 2006.

Hwang and Shaka. Water Suppression That Works. Excitation Sculpting Using Arbitrary Waveforms and Pulsed Field Gradients. *Journal of Magnetic Resonance*, 112(1):275–279, 1995.

Kahan, Kahan, Cassidy, and Kropp. The mechanism of action of fosfomycin (phosphonomycin). *Annals of the New York Academy of Sciences*, 235(1):364–386, 1974.

Kallick, Tessmer, Watts, and Li. The use of dodecylphosphocholine micelles in solution NMR. *Journal of Magnetic Resonance*, 109(1):60–65, 1995.

Yuri Kazakevich and Rosario Lobrutto. *HPLC for Pharmaceutical Scientists*. Wiley-Interscience, first edition, 2007.

Kelly, Jess, and Price. How to study proteins by circular dichroism. *Biochimica et Biophysica Acta*, 1751(1):119–139, 2005.

Koteva, Hong, Wang, Nazi, Hughes, Naldrett, Buttner, and Wright. A Vancomycin Photoprobe Identifies the Histidine Kinase as a Vancomycin Receptor. *Nature Chemical Biology*, 6(1):327–329, 2010.

Kucharczyk, Brzezowska, Maciag, Lis, and Jezowska-Bojczuk. Structural features of the Cu^{2+}-vancomycin complex. *Journal of Inorganic Biochemistry*, 102(1):936–942, 2008.

Kwun, Novotna, Hesketh, Hill, and Hong. *In Vivo* Studies Suggest that Induction of VanS-Dependent Vancomycin Resistance Requires Binding of the Drug to D-Ala-D-Ala Termini in the Peptidoglycan Cell Wall. *Antimicrobial Agents and Chemotherapy*, 57(1): 4470–4480, 2013.

Lai and Kirsch. Induction Signals for Vancomycin Resistance Encoded by the vanA Gene Cluster in *Enterococcus faecium*. *Antimicrobial Agents and Chemotherapy*, 40(7):1645–1648, 1996.

Lambert. Bacterial resistance to antibiotics: Modified target sites. *Advanced Drug Delivery Reviews*, 57(1):1471–1485, 2005.

Lazar and Walker. Substrate analogues to study cell-wall biosynthesis and its inhibition. *Current Opinion in Cell Biology*, 6(6):786–793, 2002.

Lazaridis, Mallik, and Chen. Implicit Solvent Simulations of DPC Micelle Formation. *J. Phys. Chem. B.*, 109(31):15098–15106, 2005.

Leclercq, Derlot, Duval, and Courvalin. Plasmid-mediated resistance to vancomycin and teicoplanin in *Enterococcus faecium*. *New England Journal of Medicine*, 319(1):157–161, 1988.

Lichty, Malecki, Agnew, Michelson-Horowitz, and Tan. Affinity chromatography: a review of clinical applications. *Protein Expression and Purification*, 41(1):98–105, 2005.

Liu, Mao, Ye, Huang, Nicholson, and Linden. Improved WATERGATE Pulse Sequences for Solvent Suppression in NMR Spectroscopy. *Journal of Magnetic Resonance*, 132(1): 125–129, 1998.

Lyons. Penicillin Therapy of Surgical Infections in the U.S. Army. *Journal of the American Medical Association*, 123(16):1007–1018, 1943.

MacKay, Gerhard, Beauregard, Maplestone, and Williams. Dissection of the Contributions

toward Dimerization of Glycopeptide Antibiotics. *J. Am. Chem. Soc.*, 116(1):4573–4580, 1993.

McComas, Crowley, and Boger. Partitioning the Loss in Vancomycin Binding Affinity for D-Ala-D-Lac into Lost H-Bond and Repulsive Lone Pair Contributions. *JACS*, 125(1): 9314–9315, 2003.

McCormick, McGuire, Pittenger, Pittenger, and Stark. Vancomycin, a New Antibiotic. *Antibiot Annu*, 3(1):606–611, 1956.

McDonald and Phillips. Proton Magnetic Resonance Spectra of Proteins in Random-Coil Configurations. *J. Am. Chem. Soc.*, 91(6):1513–1521, 1969.

Milburn, Laskowski, and Thornton. Sequences annotated by structure: a tool to facilitate the use of structural information in sequence analysis. *Prot. Eng.*, 11(1):855–859, 1998.

Millan, Depardieu, Godreuil, and Courvalin. VanB-Type *Enterococcus faecium* Clinical Isolate Successively Inducibly Resistant to, Dependent on, and Constitutively Resistant to Vancomycin. *Antimicrobial Agents and Chemotherapy*, 53(5):1974–1982, 2009.

Miroux and Walker. Over-production of Proteins in Escherichia coli: Mutant Hosts that Allow Synthesis of some Membrane Proteins and Globular Proteins at High Levels. *J. Mol. Biol.*, 260(1):289–298, 1996.

Moffat and Studier. T7 lysozyme inhibits transcription by t7 rna polymerase. *Cell*, 49(2): 221–227, 1987.

Nash, Notman, and Dixon. *De novo* design of transmembrane helix-helix interactions and measurement of stability in a biological membrane. *Biochimica et Biophysica Acta - Biomembranes*, 1848(5):1248–1257, 2015.

Nicolaou, Boddy, Braase, and Winssinger. Chemistry, Biology, and Medicine of the Glycopeptide Antibiotics. *Angewandte Chemie*, 38(1):2096–2152, 1999.

Novotna, Hill, Vincent, Liu, and Hong. A novel membrane protein, VanJ, conferring resistance to teicoplanin. *Antimicrobial agents and chemotherapy*, AAC:05869–11, 2012.

Ortega-Roldan, Ossa, Amin, and Schnell. Solution NMR studies reveal the location of the second transmembrane domain of the human sigma-1 receptor. *FEBS letters*, 589(1): 659–665, 2015.

Ostash, Saghatelian, and Walker. A Streamlined Metabolic Pathway for the Biosynthesis of Moenomycin A. *Chemistry Biology*, 14(1):257–267, 2007.

Patel. *Development of Nuclear Magnetic Resonance Methods for Determination of Membrane Protein Structure*. PhD thesis, The University of Warwick, Coventry, Sept 2012.

Pearce and Williams. Complete Assignment of the ^{13}C NMR Spectrum of Vancomycin. *J. Chem. Soc., Perkin Transactions*, 1(1):153–157, 1995.

Pfeiffer. Structural features of vancomycin. *Reviews of Infectious Diseases*, 3(2):205–209, 1981.

Phillips-Jones, Channell, Kelsall, Hughes, Ashcroft, Patching, Dinu, Gillis, Adams, and Harding. Hydrodynamics of the VanA-type VanS histidine kinase: an extended solution conformation and first evidence for interactions with vancomycin. *Nature Scientific Reports*, 7(41680):1–12, 2017.

Piddock. Multidrug-resistance efflux pumps–not just for resistance. *Nature reviews Microbiology*, 4(8):629–636, 2016.

Pootoolal, Thomas, Marshall, Neu, Hubbard, Walsh, and Wright. Assembling the glycopeptide antibiotic scaffold: the biosynthesis of A47934 from *Streptomyces toyocaensis* NRRL15009. *PNAS*, 99(13):8962–8967, 2002.

Quigley. *The Two-Component System Controlling Inducible Glycopeptide Resistance in Enterococci*. PhD thesis, The University of Warwick, Coventry, February 2010.

Reynolds. Structure, Biochemistry and Mechanism of Action of Glycopeptide Antibiotics. *Eur. J. Clin. Microbio. Infect. Dis.*, 8(1):943–950, 1989.

Reynolds, Depardieu, Dutka-Malen, Arthur, and Courvalin. Glycopeptide resistance mediated by enterococcal transposon Tn*1546* requires production of VanX for hydrolysis of D-alanyl-D-alanine. *Molecular Microbiology*, 13(6):1065–1070, 1994.

Roy, Yang, Kodali, Xiong, Kim, Griffin, Onishi, Kohler, Silver, and Chapman. Direct interaction of a vancomycin derivative with bacterial enzymes involved in cell wall biosynthesis. *Chemistry & Biology*, 8(1):1095–1106, 2001.

Rule and Hitchens. *Fundamentals of Protein NMR Spectroscopy.* Springer, fifth edition, 2006.

Ruzin, Singh, Severin, Yang, Dushin, Sutherland, Minnick, Greenstein, May, Shlaes, and Bradford. Mechanism of Action of the Mannopeptimycins, a Novel Class of Glycopeptide Antibiotics Active agaisnt Vancomycin-Resistant Gram-Positive Bacteria. *Antimicrobial Agents and Chemotherapy*, 48(3):728–738, 2004.

Sauvage, Kerff, Terrak, Ayala, and Charlier. The Penicillin-Binding Proteins: Structure and Role in peptidoglycan Biosynthesis. *Nature*, 432(1):829–837, 2004.

Schmidt and Sesler. Development of Resistance to Penicillin by Pneumococci. *Experimental Biology and Medicine*, 52(4):343–347, 1943.

Sigalov and Hendricks. Membrane binding mode of intrinsically disordered cytoplasmic domains of T cell receptor signaling subunits depends on lipid composition. *Biochem Biophys Res Commun.*, 389(2):388–393, 2009.

Sreerama and Woody. Estimation of protein secondary structure from CD spectra: Comparison of CONTIN, SELCON and CDSSTR methods with an expanded reference set. *Anal Biochem*, 287(2):252–260, 2000.

Stafford, Fanni, and Dennis. Interfacial Properties and Critical Micelle Concentration of Lysophospholipids. *Biochemistry*, 28(1):5113–5120, 1989.

Steinkraus, White, and Friedrich. Vancomycin MIC creem in non-vancomycin-intermedia *Staphylococcus aureus* (VISA), vancomycin-susceptible clinical methicillin-resistant *S. aureus* (MRSA) blood isolates from 2001-05. *Journal of Antimicrobial Chemotherapy*, 60(4):788–794, 2007.

Stone and Strominger. Mechanism of Action of Bacitracin: Complexation with Metal Ion and C55-Isoprenyl Pyrophosphate. *PNAS*, 68(12):3223–3227, 1971.

Terpe. Overview of tag protein fusions: from molecular and biochemical fundamentals to commercial systems. *Appl Microbiol Biotechnol*, 60(1):525–533, 2002.

Tomlinson, Thompson, Kalverda, Zhuravleva, and O'Neill. A target-protection mechanism of antibiotic resitance at atomic resolution: insights into FusB-type fusidic acid resistance. *Nature Scientific Reports*, 6(19524):1–12, 2015.

Uttley, Collins, Naidoo, and George. Vancomycin-resistant enterococci. *Lancet*, 1(1):57–58, 1988.

van Heijenoort. Recent advances in the formation of the bacterial peptidoglycan monomer unit. *Nat. Prod. Rep.*, 18(1):503–519, 2001.

van Heijenoort, Derrien, and van Heijenoort. Polymerization by transglycosylation in the biosynthesis of the peptidoglycan of *Escherichia coli* K 12 and its inhibition by antibiotics. *FEBS Letters*, 89(1):141–144, 1978.

Viegas, Manso, Nobrega, and Cabrita. Saturation-Transfer Difference (STD) NMR: A Simple and Fast Method for Ligand Screening and Characterization of Protein Binding. *Journal of Chemical Education*, 88(1):990–994, 2011.

Vollmerhaus, Breukink, and Heck. Getting Closer to the Real Bacterial Cell Wall Target:

Biomolecular Interactions of Water-Soluble Lipid II with Glycopeptide Antibiotics. *Chem. Eur. J.*, 9(7):1556–1565, 2003.

Wainwright and Swan. C. G. Paine and the Earliest Surviving Clinical Records of Penicillin Therapy. *Medical History*, 30(1):42–56, 1986.

Walsh. *Antibiotics: actions, origins, resistance*. American Society for Microbiology, first edition, 2003.

Wampler and Westhead. Two Aspartokinases from *Escherichia Coli*: Nature of the Inhibition and Molecular Changes Accompanying Reversible Inactivation. *Biochemistry*, 7(5): 1661–1671, 1968.

Weigel, Clewell, Gill, Clarl, McDougal, Flannagan, Kolonay, Shetty, Killgore, and Tenover. Genetic Analysis of a High-Level Vancomycin-Resistant Isolate of *Staphylococcus aureus*. *Science*, 302(1):1569–1571, 2003.

Whitemore and Wallace. Protein Secondary Structure Analyses from Circular Dichroism Spectroscopy: Methods and Reference Databases. *Biopolymers*, 89(5):392–400, 2007.

Wiechelman, Braun, and Fitzpatrick. Investigation of the Bicinchoninic Acid Protein Assay: Identification of the Groups Responsible for Color Formation. *Anal Biochem*, 175(1):231–237, 1988.

Wilke, Francis, and Carlson. Activity-Based Probe for Kistidine Kinase Signaling. *JACS*, 134(1):9150–9153, 2012.

Wishart, Sykes, and Richards. The chemical shift index: a fast and simple method for the assignment of protein secondary structure through NMR spectroscopy. *Biochemistry*, 31 (6):1647–1651, 1992.

Wright, Holman, and Walsh. Purification and Characterization of VanR and the Cytosolic Domain of VanS: A Two-Component Regulatory System Required for Vancomycin Resistance in *Enterococcus faecium* BM4147. *Biochemistry*, 32(1):5057–5063, 1993.

Wu, Wright, and Walsh. Overexpression, Purification, and Characterisation of VanX, a D-,D-Dipeptidase which is Essential for Vancomycin Resistance in *Enterococcus faecium* BM4147. *Biochemistry*, 34(1):2455–2563, 1995.

Xu, Li, Zhu, Zhao, Chen, Huang, and Yang. Characterization of plasmid pXL100 from *Amycolatopsis orientalis* HCCB10007 and construction of a shuttle vector. *J. Basic Microbiol.*, 55(1):247–254, 2015.

Yildiz, Kang, and Sinner. Biomimetic membrane platform containing hERG potassium channel and its application to drug screening. *Analyst*, 138(1):2007–2012, 2013.

Ysselstein, Joshi, Mishra, Griggs, Asiago, McCabe, Stanciu, Post, and Rochet. Effects of impaired membrane interactions on α-synuclein aggregation and neurotoxicity. *Neurobiology of Disease*, 79(1):150–163, 2015.

Zarkan, Machlyne, Truman, Hesketh, and Hong. The frontline antibiotic vancomycin induces a zinc starvation response in bacteria by binding to Zn(II). *Nature Scientific Reports*, 6(19602):1–9, 2016.